A STUDY OF SOIL NAILING IN SAND

by

Kouji Tei

Thesis submitted for the
degree of Doctor of Philosophy
at the University of Oxford

Magdalen College

Trinity Term, 1993.

A Study of Soil Nailing in Sand

Kouji Tei
Magdalen College, University of Oxford

A Thesis submitted for the Degree of Doctor of Philosophy.
Trinity Term, 1993.

ABSTRACT

This dissertation is concerned with a study of soil nailing, in particular the interaction mechanism between the soil and a nail and the failure mechanism and suitable design procedure for nailed slopes in sand.

The interaction mechanism of a nail was studied by carring out a number of pull-out tests, direct shear tests of nailed sand and interface tests using two uniform sands. Major parameters of the tests were flexibility, surface roughness and diameter of a nail. From the tests, it was found that:
(1) flexibility of a nail significantly influences the interaction mechanism. Both the interaction parameter k_i and apparent friction coefficient f^* differ between a flexible and a stiff nail. Theoretical consideration indicates that the mobilization of nail forces is dominated by the relative stiffness between soil and nail.
(2) a smooth-surface nail produces smaller bond friction than the critical state friction angle ϕ_{cv} and mineral-to-mineral angle ϕ_u of the soil. This is due to the very thin rupture surface developed around the nail. On the other hand, a rough-surface nail was observed to produce two to four times larger bond friction than the direct shear friction angle ϕ_{ds} of sand, due to the thick rupture surface developed and the dilatancy of the soil.
(3) increasing the diameter of a nail produces a smaller apparent friction coefficient f^*. Restrained dilatancy was found to play an important role.
(4) the pull-out test, direct shear test of nailed sand and interface test produce different values of apparent friction coefficient f^*, due to the different amount of restrained dilatancy effect around the nail (or reinforcement).

The overall behaviour of nailed slopes was studied by carring out a comprehensive series of centrifuge tests. Excavation of soil was simulated by draining water from two rubber bags in front of the facing wall. The centrifuge tests have provided much useful information on the mechanics of soil nailing. From the tests, it was found that:
(1) draining of the water significantly influences both the earth pressure on the facing wall and the displacements of the nailed slope. Horizontal displacements of the facing wall were decreased by increasing the length and/or friction (bond) of the nail.
(2) earth pressures on the facing wall do not exhibit a simple hydrostatic distribution. The deviations of the earth pressure are not negligible especially near the top and bottom of the facing wall.
(3) roughness and bending stiffness of the facing wall considerably influence the stability and displacement of the nailed slope, respectively.
(4) the observed failure surfaces were well described by a logarithmic spiral passing through the toe of the facing wall.

(5) fairly good predictions for the failure acceleration were made using stability analysis of the nailed slopes based on the limit equilibrium method, provided an accurate friction angle for the sand and pull-out resistance of each nail could be determined. The factor of safety F_s of the nailed slopes was estimated by comparing the *total available force* and the *total required force* based on the observed failure surfaces.

CONTENT

ACKNOWLEDGEMENTS

I wish to express my sincere gratitude to Tokyu Construction Co.,Ltd in Japan for their financial support and leave of absence to pursue the research.

There are many people who have contributed to the accomplishment of this thesis.

First and foremost, I would like to express sincere gratitude to my supervisor, Dr. George Milligan. Without his thoughtful guidance, input and advice I could hardly have completed this research. I am also greatly indebted to Dr. Neil Taylor at the City University, London, for his countless suggestions and ideas in carrying out the centrifuge tests; I have been fortunate to work closely with them.

I am also grateful to Professor Guy Houlsby for his comments, and his kind permission to use the BITPAD program.

Gratitude is extended to Dr. Gilliane Sills and Mr. Chris Waddup for their help in using the X ray facility, and to Mr. Bob Earl and Mr. Bob Sawala who made several pieces of test apparatus.

Many thanks go to Mr. Harvey Skinner in the centrifuge laboratory at the City University, for his co-operation and excellent assistance throughout the centrifuge test programme.

I am also grateful to Dr. Richard Jewell for his comments during the early stage of the research.

Appreciation is extended to Professor Toru Konda at the Tokyo Metropolitan University and Professor Fumio Tatsuoka at the University of Tokyo for their continuous encouragement during the pursuit of the research. Further, I would like to thank Mr. Masaaki Terashi for his comments on the centrifuge tests.

On a personal note I would like to express thanks to past and present members of the Soil Mechanics research group for providing an excellent social environment which allowed me some escape from the frustrations associated with the research.

Finally, but not least, I would like to express my sincere gratitude to my wife and two children for their constant support, understanding and encouragement, and to them I dedicate this thesis.

NOMENCLATURE

α	Relative stiffness between soil and nail, or magnitude of acceleration
α_i	Angle of failure surface from horizontal
β	Inclination of slope or facing wall from horizontal
γ	Unit weight of soil or shear strain in sand
γ_{yx}	Shear strain of sand
Γ	Inclination of nail from horizontal
δ	Displacement of slope
δ_b	Angle of bond friction of nail
δ_h	Horizontal displacement of facing wall
$(\delta_h)_{base}$	Horizontal displacement of facing wall at base
δ_v	Vertical displacement of upper ground surface
δ_w	Friction angle of facing wall
ε_0	Axial strain at the head of a nail
ε_1, ε_3	Maximum and minimum normal strains of sand
ε_y	Yield strain of material
ε_s	Normal strain of soil
ε_{yy}	Normal strain of sand in y direction
$\Delta\varepsilon$	Increment of circumferential strain of soil
η	Displacement of soil when nail is pulled out
θ	Inclination of failure surface from horizontal, or direction of nail from vertical direction in direct shear test, or deflection of facing wall from verical direction
θ_0, θ_f	Angles of radius of logarithmic spiral from horizontal
θ_1, θ_2, θ_3	Angles of failure surfaces from horizontal in two part wedge analysis
θ_α	Direction of resultant acceleration
θ_{sc}	Inclination of stress characteristics from horizontal
θ_{vc}	Inclination of velocity characteristics from horizontal
θ^*	Direction of minimum strain ε_3 from vertical direction
$\Delta\theta$	Deviation of angle of failure surface from frictionless facing wall at the toe
κ	Horizontal distance of centroid of weight dA from pole O
λ	Angle of failure surface to horizontal at upper ground surface
μ^*	Friction coefficient of nail
Ξ	Angle of total reaction force of logarithmic spiral from horizontal
ξ	Pull-out displacement of nail
ξ_0	Pull-out displacement at the head of nail
ξ_p	Pull-out dispacement of nail required to mobilize the peak force
ρ	Flexibility number of wall, or horizontal distance of centroid of surcharge loads from pole O
ρ_x	Horizontal distance of centroid of soil mass W from pole O
σ	Normal stress
σ_0	Axial stress at the head of nail
$\sigma_{m\theta}$	Avarage normal stress on a nail in direct shear test
σ_i	Principal stress (i = 1, 2 or 3)
σ_m	Mean normal stress on a nail
σ_p	Yield stress
σ_v	Vertical stress

$(\sigma_v)_{ave}$	Average vertical stress of soil in centrifuge test
$\sigma(x)$	Axial stress distribution of nail
σ_{yy}	Normal stress of soil in y direction
$\Delta\sigma_m$	Increment of mean normal stress on a nail
τ	Shear stress
τ_0	Shear stress at the head of nail
τ_{EXT}	Extra shearing resistance due to a nail
τ_{max}	Maximum shear stress
$\tau(x)$	Shear stress distribution on a nail
τ_{yx}	Shear stress of soil in direct shear test
ϕ	Friction angle of sand
$\phi_{\chi i}$	Friction angle of sand taking into account the direction of principal stress
ϕ_{cv}	Critical state friction angle of soil
ϕ_{ds}	Direct shear friction angle
ϕ_{ps}	Plane strain friction angle
ϕ_u	Angle of mineral-to-mineral friction of soil
χ	Direction of principal stress σ_1 from horizontal
ψ	Angle of dilation
Ω_r, Ω_t	Dimensionless parameters for nail
ω	Angular velocity of centrifuge, or angle of logarithmic spiral
a, b	Interaction parameters or interface stiffness for hyperbola
A	Cross sectional area of nail
A_r	Total surface area of a nail
A_s	Plane area of sand in direct shear test
B	Distance B from centre line in centrifuge model
c_{ds}	Cohesion of soil in direct shear
c_{ps}	Cohesion of soil in plane strain
C	Point of failure surface in two part wedge analysis
dH	Vertical distance of two β-characteristics
dV	Velocity increment
D	Diameter of nail
D_e	External diameter of tube
D_h	Diameter of borehole
D_i	Internal diameter of tube
D_{50}	Mean particle size of sand
ΔD	Additional thickness of nail due to sand layer
e_0	Initial void ratio of sand
E_a	Elastic modulus of nail
f_s	Tensile strength of reinforcement
f^*	Apparent friction coefficient between soil and nail
F	Pull-out force of nail
F_p	Peak pull-out force of nail
F_s	Factor of safety
$(F_s)_{ave}$	Average safety factor
$(F_s)_{lower}$	Safety factor assuming lower bound pull-out force of nails
$(F_s)_{upper}$	Safety factor assuming upper bound pull-out force of nails
$(F_s)_{36}$	Safety factor assuming $\phi = 36°$
$(F_s)_{41}$	Safety factor assuming $\phi = 41°$

g	Acceleration due to gravity
G	Shear modulus of sand
h	Thickness of rupture zone around nail, or depth of model in centrifuge test
Δh	Increment of thickness of rupture zone
H	Height of slope or facing wall
I	Moment of inertia
I_D	Relative density of sand
J	Material stiffness of reinforcement
k_i	Interface stiffness or interface parameter between soil and nail
K_0	Earth pressure coefficient at rest
K_{a_*}	Active earth pressure coefficient
K_a	Apparent earth pressure coefficient
K_{req}	Earth pressure coefficient correponding to required force
$(K_{req})_h$	Horizontal earth pressure coefficient
K_s, K_n	Shear and normal stiffnesses of soil
l	Current length of nail embedded in sand
Δl	Elastic displacement of nail in free part
l_i	Initial length of nail embedded in sand
L_i	Length of nail beyond failure surface (i = 1 ~ 5)
m	Constant equal to critical state shearing resistance (in Chapter 2)
M_w	Moment of soil mass W
n	Number of reinforcement in cross section
n_H	Location of centroid of horizontal earth pressures
N	Centrifuge acceleration or scaling factor of model
N_f	Failure acceleration
N_i	Ultimate pull-out force per unit length of nail
O	Pole of logarithmic spiral
ΔP	Additional shear resistance for soil due to nail forces
p	Measured horizontal earth pressure
p'	Surcharge load on upper ground surface
p_0	Horizontal earth pressure at rest
P_A	Axial nail force
P_D	Pole of direction in Mohr's circle
P_h	Horizontal earth pressure on facing wall
P_R	Limiting nail force due to friction
P_S	Shear force of nail
r_0, r_f	Radii of logarithmic spiral
R	Radius of centrifuge or reaction force in logarithmic spiral
R'	Representative radius
R_a	Radius of nail
R_s	Radius of unstressed upper surface
S	Applied shear load in direct shear test
S_v, S_h	Vertical and horizontal spacing of nails
t	Thickness of tube
T	Nail forces
T_0	Axial nail force at facing wall
T_{ava}	Available force in limit equilibrium analysis
$(T_{ava})_{lower}$	Lower bound available force of nails

$(T_{ava})_{upper}$	Upper bound available force of nails
$(T_m)_i$	Ultimate mean pull-out force obtained from *in - situ* tests
T_{max}	Maximum axial force of nail
T_{req}	Required force in limit equilibrium analysis
T_{ult}	Ultimate tensile force of reinforcement
w	Horizontal distance of failure surface from facing wall at upper ground surface
W	Weight of soil mass
(x, y)	Co-ordinate system
X	Shear displacement in x direction
(X_c, Y_c)	Location of pole of logarithmic spiral
y_0	Vertical distance of β-characteristics from the point of upper ground surface
Y	Vertical displacement or dilation in Y direction

Subscripts and Superscript

max	Maximum value
min	Minimum value
mob	Mobilised
*	Apparent coefficient

Chapter 1

Introduction

The major objective of the research described in this dissertation is the study of soil nailing, in particular the pull-out of an individual nail in sand, and the behaviour of nailed model slopes under increased acceleration in a centrifuge. The work forms a part of continuing research of soil reinforcement at Oxford University, which has included pull-out and direct shear tests of several types of reinforcement using a large scale direct shear apparatus, investigations of the analysis and design theory of unpaved roads on soft soil, and a study of the role of bending stiffness of nails on the stability of nailed slopes.

The most important feature of soil nailing as opposed to the ground anchor technique is that the nail force is passively generated by the displacement of the soil, and the displacement is in turn due to the nail force. The construction sequence of placing the nails and facing walls, and the stiffness and continuity of facing walls on the excavation surface may also affect the behaviour of nailed slopes. There is thus a complex interaction between a nail, facing wall and the surrounding soil, and for this reason, any complete solution for the mechanics of soil nailing, if it exists, should take account of the displacements of both nails and the soil.

In this research programme, rather than trying to consider all the numerous parameters which may affect the performance of soil nailing, it was decided to concentrate on relatively

simple models using ideal soils, nails and facing walls in the experiments, in the hope of understanding the fundamental mechanics and developing an appropriate design theory of soil nailing. It will then be possible to investigate full scale earth structures constructed with more complex soils and boundary conditions.

1.1 Overview of soil nailing

In recent years soil nailing has come into widespread use in geotechnical engineering as a means to stabilize cut slopes and natural slopes in granular soil with some cohesion, stiff clays and rocks. The term "soil nailing", after Jewell (1990b), refers to the use of relatively small diameter bars (typically 20 *mm* to 30 *mm*) inserted into the ground directly or more usually by drilling and grouting, and oriented to develop the tensile (rather than compressive) axial force. There is a great deal of debate on the contribution of the shear force generated in nails to the slope stability, stemming from the confusion between soil nailing and soil dowelling.

The distinctive features of soil nailing compared to other existing methods of stabilising slopes are:

(1) unlike the ground anchor technique in which the post tension of tendons has a major effect in stabilising a soil mass, nail forces are generated by the relative displacement between a nail and the surrounding soil; displacements of soil due to excavation of the slope, increase of pore water pressure and surcharge load on the slope play an important role in generating the forces and effect of the nail.

(2) unlike the more widely known reinforced soil wall (Vidal, 1969) which is constructed "bottom - up", the construction of soil nailing is "top - down" with excavation followed by covering of the new surface with facing walls or shotcrete, and systematic inserting

of the nails; the resulting differences in the stress paths to which soil elements are subjected cause the different mechanical behaviour of two types of the earth structure, as shown in Fig.1.1 (Jones, 1990).

(3) unlike grout injection and soil improvements, soil nailing does not increase the strength of the soil itself; nail forces perpendicular to the failure surface increase the shear resistance of soil, and those parallel to the failure surface decrease the shear force on the soil.

Although steel bars or rock bolts have been used for more than forty years to support excavation surfaces and portals in tunnelling, the application of and vigorous research on soil nailing were started in the 1970s in Germany, France and the United States. Since then, soil nailing has been used successfully in temporary and permanent applications under a wide variety of ground conditions. Recently, several new techniques to decrease the displacements of nailed slopes due to the excavation have been proposed, where especially in urban areas the excessive displacements as well as problems with ground water were regarded as the major shortcomings in applying soil nailing. Extensive reviews of the historic evolution and major features of soil nailing are summarized by Bruce and Jewell (1986 / 1987) and Gassler (1990).

1.2 Previous research on soil nailing

From a mechanical point of view, a nailed slope may be regarded as a composite structure with elements of nails, grout, facing walls and soil. Because the difficulty of research on soil nailing comes from the complex interactions among those four elements, most of the previous research work has concentrated on one or some of the elements. In this section the characteristics and mechanics of soil nailing are briefly described with respect to those

elements, along with the design theories proposed so far.

1.2.1 Nail

A nail is the fundamental element in soil nailing, and estimation of the quantity of nails (lengths and spacing) forms the major part of the design procedure for soil nailing. It is widely known that a nail force, by friction or bond to the surrounding soil, can decrease the principal tensile strain ε_3 of the soil, and hence improve the stability and decrease the displacements of the soil (Mc Gown *et al.*, 1978). The axial tension in the nail generated by the relative displacement between the nail and the soil is then transmitted back into the soil at the nail / soil interface. It is, therefore, of great importance that the interaction mechanism between soil and nail are understood, and the effects of the interaction on improving the slope stability are fully clarified.

Jewell (1980) carried out a series of direct shear tests of reinforced soil to study how a wide range of reinforcements modified the mechanical response of the soil to the applied stresses. He showed that the reinforcement modifies locally the stress and strain of the soil, and the most efficient use of the reinforcement is achieved when the direction of the reinforcement coincides with that of the minimum normal strain ε_3 (tensile strain) in the soil. Basset *et al.* (1978) reported that because a reinforcement restricts anisotropically the normal strain ε_s of the soil, it is important to know the strain of the soil. The normal strain increment in a direction parallel to the nail $\dot{\varepsilon}_s$ of soil in a steep slope is estimated from the Mohr's circle of strain increment, as shown in Fig.1.2(a), assuming that the direction of the failure surface coincides with that of a zero - extension line in the soil (Roscoe, 1970, and Wroth, 1972), as

$$\dot{\varepsilon}_s = -\frac{\dot{\gamma}}{2}\{\sin\psi + \sin(2\Gamma + 2\theta - \psi)\} \qquad ...(1.1)$$

in which $\dot{\gamma}$ is the maximum shear strain increment of the soil, ψ is the angle of dilation of the soil, and Γ and θ are the angles of a nail and of a failure surface from horizontal, respectively. In Fig.1.2 (a), P_D is the pole of direction. Fig.1.2 (b) shows the relationship between the normalized normal strain increment $\dot{\varepsilon}_s /(\dot{\gamma}/2)$ and the direction Γ of a nail from equation (1.1), with angles of failure surface $\theta = 50°$, $60°$ and $70°$ and the angles of dilation $\psi = 0°$ and $20°$. When direction of the maximum strain increment $\dot{\varepsilon}_1$ of the soil is assumed to be vertical, the angle θ equals to $45° + \psi/2$. From the figure, it is easily understood that both the angle of dilation ψ and direction Γ of the nail play a very important role in determining the amount of normal strain increment $\dot{\varepsilon}_s$ in the nail. Generally, a larger angle of dilation ψ produces a larger normalized normal strain increment $\dot{\varepsilon}_s /(\dot{\gamma}/2)$ in the soil.

The interaction mechanism between a nail and soil, or a relationship between strain of the soil and the axial stress in a nail, has been investigated mostly using pull-out test and direct shear test apparatus (*e.g.* Chang *et al.*, 1977, Shen *et al.*, 1979, Jewell, 1980, and Irsyam and Hryciw, 1991). Dyer (1985) visually observed the stress transfer between a reinforcement and soil using a photoelastic technique. Palmeira and Milligan (1989) showed the influence of longitudinal stiffness of a reinforcement and progressive failure of soil along the reinforcement in developing the full interaction mechanism. When a nail is pulled out in dense sand, restrained dilatancy of the sand will occur, and the normal stress acting on the nail may be increased, as in the constant volume direct shear test of sand. Wernic (1977), Guilloux *et al.* (1979), Plumelle (1984), Boulton *et al.* (1986) and Heymann *et al.* (1992) reported increased normal stress in dense sand when a reinforcement with rough surface is pulled out, and consequently, a larger apparent friction coefficient f^* than the direct shear

resistance of the soil was observed, as

$$f^* = \frac{\tau_{max}}{\sigma_m} \geq \tan\phi_{ds} \qquad ...(1.2)$$

where τ_{max} and σ_m are the maximum shear stress and the initial normal stress on the nail respectively, and ϕ_{ds} is the direct shear friction angle of the soil. It should be noted that the difinition σ_m is different for different types of test and boundary conditions, as shown in the pull-out test of a nail (equation (3.12)) and the direct shear test of nailed sand (section 3.5). The estimate of the increased normal stress due to the dilatancy is, however, still not clear, and in these circumstances Jewell (1990b) suggested that the effect of dilatancy should not be relied upon in safety design, unless suitable pull-out tests on nails are carried out.

Adib (1988), Whittle *et al.* (1992) and Mitachi *et al.* (1992) formulated the relationship between shear stress τ on a nail and pull-out displacement ξ of the nail, as

$$\tau = k_i \xi \qquad ...(1.3)$$

where k_i is usually called the interface stiffness. Adib (1988), Jaber (1989) and Farmer (1975), from model tests and finite element analyses, showed that in a pull-out test of a nail the maximum shear stress τ_{max} or the maximum pull-out force and the shear stress distribution of the nail are greatly influenced by the interface stiffness k_i.

In order to investigate the characteristics of the interface stiffness k_i of a nail, consider a simple circular nail / soil model in the pull-out test, as shown in Fig.1.3. When it is assumed that both the nail and soil are elastic and the surrounding soil is subjected only to shearing in the x - direction, (Farmer, 1975),

$$\frac{d\sigma(x)}{dx} = -\frac{2}{R_a}\tau(x),$$

$$\sigma(x) = -E_a \frac{d\xi(x)}{dx} \qquad \text{...(1.4)}$$

in which R_a is the radius of the nail, $\tau(x)$ and $\sigma(x)$ are the shear and axial stresses in the nail, E_a is the elastic modulus of the nail, and $\xi(x)$ is the pull-out displacement of the nail. When the displacement $\xi(x)$ of the nail is small and the surface of the nail is assumed to be rough, then the displacement $\eta(x)$ of the soil contacting with the nail surface may be regarded as equal to that of the nail (Jewell, 1980), then

$$\xi(x) = \eta(x) = \int_{R_a}^{R_a+h} \gamma(y)\,dy = \int_{R_a}^{R_a+h} \frac{\tau(x,y)}{G(\gamma)}\,dy \qquad \text{...(1.5)}$$

where h is the current thickness of the deforming (or rupture) zone and G and γ are the shear modulus and shear strain of the sand, respectively. Assuming that the shear stress $\tau(x,y)$ varies with $1 / y$ in the moving zone of the "thick - walled" cylinder of soil,

$$\tau(x,y) = \{\tau(x)\}_{y=R_a} \frac{R_a}{y}, \qquad R_a \le y \le R_a + h \qquad \text{...(1.6)}$$

Thus, the interface stiffness k_i is derived by combining equations (1.3), (1.5) and (1.6),

$$k_i = \frac{1}{R_a} \frac{1}{\int_{R_a}^{R_a+h} \frac{dy}{G(\gamma)y}} \qquad \text{...(1.7)}$$

If it is assumed that the shear modulus G of the soil is constant irrespective of the shear strain γ, namely $G = G(\gamma) = \textit{constant}$, then equation (1.7) is simplified, as

$$k_i = \frac{1}{R_a} \frac{G}{\ln\left(1 + \frac{h}{R_a}\right)} \qquad \text{...(1.8)}$$

Fig.1.4 shows the relationship between k_i / G and the radius R_a of a nail estimated from equation (1.8), with the thickness of the deforming zone h = 0.50 *cm*, 0.75 *cm*, 1.00 *cm* and 1.50 *cm*. It is seen from the figure that as the radius R_a and the thickness h increase, the magnitude of k_i / G becomes smaller. While large changes of k_i / G are observed for smaller values of R_a, k_i / G is nearly constant in a range of $R_a \geq 3$ *cm*. In design of pipe lines, for which the radius R_a of the pipe line is usually larger than that of a nail, a range of k_i / G = 1 ~ 3 has been proposed by several researchers (*e.g.* Hmadi *et al.*, 1988), and this range of k_i / G is consistent with the results shown in Fig.1.4.

Herrmann and Al-Yassin (1978) and Adib (1988) formulated the interface stiffness k_i considering an axial equilibrium of a two dimensional reinforced soil element, where the soil was assumed to be linear isotropic elastic material, as

$$k_i = \frac{8G}{S_v^2\left(\ln\frac{4}{S_v} - \frac{3}{4}\right)} \qquad \text{...(1.9)}$$

in which S_v (unit: ft) is the vertical spacing of the reinforcement. It is, however, difficult to imagine that the interface stiffness k_i is a function of the spacing S_v in equation (1.9), except in the case of very close spacing S_v of the reinforcement which causes mutual interaction in the soil.

Although the interface stiffness k_i is simply modelled as equation (1.8) or (1.9) in idealized conditions, the difficulty of obtaining the thickness h of the deforming zone in equation (1.8) and the shear modulus G of the soil in equations (1.8) and (1.9) still remains. Therefore, the interface stiffness k_i should be more reliably determined by experiment. In a pull-out test of a stiff nail, the interface stiffness k_i can simply be calculated using equation (1.3) since the shear stress τ and the pull-out displacement ξ are almost constant along the nail. For a flexible nail, on the other hand, an estimate of the interface stiffness k_i from a

pull-out test is not straightforward, as shown in Chapter 3.

When nail forces on the failure surface, such as the axial force P_A and shear force P_S (Fig.1.2 (a)), are known, the contribution of those nail forces to the stability analysis of the slope is straightforward in the context of the limit equilibrium analysis, as

$$\Delta P = \{P_A \sin(\Gamma + \theta) - P_S \cos(\Gamma + \theta)\}\tan\phi + \{P_A \cos(\Gamma + \theta) + P_S \sin(\Gamma + \theta)\} \quad ...(1.10)$$

where ΔP is an additional shear resistance due to the nail forces P_A and P_S. The first term of equation (1.10) denotes the increase in shear resistance of the soil and the second term denotes the decrease of shear force (driving force) on the soil.

1.2.2 Grout

The grout, which is usually made of cement or cement mortar, is injected directly into the borehole not only to ensure a good bond between the soil and a nail but to protect the nail from corrosion in the case of a permanent structure. The diameter of the borehole is usually 40 *mm* up to 150 *mm* or 200 *mm* depending on the required pull-out force of a nail in design and drilling efficiency. Snyder (1979) showed that the ratio of the diameters of the borehole and of a nail directly affects the maximum pull-out force of the nail. Plumelle (1987) reported that considerably larger *in - situ* pull-out forces can be obtained by increasing the pressure of grout injection.

It is well known that the maximum pull-out force of a nail in the field is not proportional to the vertical depth of the nail from the upper ground surface possibly because the dilatancy of the soil decreases with the surcharge pressures (Schlosser and Juran, 1983), or because the initial confining stress of the soil has already been released by drilling of the borehole. Gassler (1988) showed that beyond a maximum depth of about 2.5 *m*, the value of the limit

bond stress is nearly constant. Cartier and Gigan (1983) also observed a similar result.

1.2.3 Facing

Currently, shotcrete and prefabricated facings have been mainly used for ensuring the stability of the local soil and protection from soil erosion. The thickness of the shotcrete facing is usually 8 *cm* to up to 25 *cm* depending on the soil properties, height of the facing wall and the expected service life (Gassler, 1988). Several researchers reported that a stiff facing firmly connected to the reinforcement improves the stability of slopes and walls. Jaber (1989) showed in centrifuge model tests that the failure accelerations of full height facing panel walls are 25% to 50% higher than those of segmented facing walls. Tatsuoka (1992) and Gutierreg and Tatsuoka (1988) reported that a facing wall reduces the strain of the soil near the slope surface, and increases the slope stability by increasing the force in the reinforcement above that of a slope without a facing wall. Tubouchi *et al.* (1990) investigated the influence of size of a facing wall on soil nailing from plane strain tests of nailed sand and finite element analysis. It is, however, mentioned that in order to make full use of the facing walls on the slope stability, each nail should have sufficient pull-out capacity to resist the increased nail forces.

1.2.4 Design theories of soil nailing

There are some design theories proposed for soil nailing and most of these are based either on limit equilibrium analyses, which do not take account of the displacements of the soil and nail, or on finite element analyses. In the limit equilibrium analyses, several assumptions have been made regarding the shape of the potential failure surfaces and possible nail forces at failure.

Stocker *et al.* (1979) and Gassler and Gudeus (1981), observed failure surfaces of nailed slopes in model and full scale tests, and suggested that the most critical failure mechanism consisted of two wedge failure surfaces whose shape and location are determined by angles θ_1 and θ_2 and a point C, as shown in Fig.1.5. They evaluated the global safety factor F_s of nailed slopes, as

$$F_S = \frac{Z_a}{Z_e} \qquad ...(1.11)$$

In which Z_a denotes the total available nail force determined from the maximum pull-out force of the nails and the total nail length in the resistance zone, and Z_e the total required nail force to obtain equilibrium in the slope. Consequently, they showed that the length of nails is usually 50% to 60% of the height of the slope and the reinforcement ratio should be at least 1 nail per 2.25 m^2. In Fig.1.5 a hodograph of velocity vectors (Smith, 1977) indicates that the soil block *DCE* moves downward related to the soil block *BCDA* provided $\theta_2 \geq \theta_1$. Romstad *et al.* (1978) also observed a two wedge failure mechanism in reinforced soil walls. Jewell (1990), in addition to the overall stability analysis, suggested checking whether individual nails can provide sufficient local resistance; that is called an internal stability analysis.

Juran *et al.* (1990) proposed a kinematic limit analysis which considers the effects of shear resistance of nails as well as an axial tension. Shen *et al.* (1981), Long *et al.* (1992), Matsui *et al.* (1990), Guilloux *et al.* (1983), Carton (1983), Bridle and Barr (1990) and Bernardi *et al.* (1992) assumed hyperbolic, logarithmic spiral or circular failure surfaces and the latter four methods take into account both the axial and shear resistance of nails. There is, however, a controversy as to whether the axial force P_A and shear force P_S of a nail can be expected to work simultaneously in equation (1.10), as reported by Jewell and Pedley

(1990) and Gassler (1990). They recommended that the effect of shear resistance of nails should be ignored in the design of soil nailing, though not in soil dowelling, because the shear forces P_S are negligibly small up to the point of failure of the slope.

Another conventional method for the design of reinforced soil walls is to assume composite properties for the reinforced soil mass, or anisotropic cohesion in the soil (Long *et al.*, 1972). While this method is rather simpler than those which assume the individual reinforcement force, the unrealistic approach caused some critisisms (Mc Gown *et al.*, 1989).

There are few proposed methods for estimating the displacement of a nailed slope. This is attributed mainly to the difficulty of simulating the construction sequence and of correctly modelling the nails in the analysis, and of investigating the properties of the *in - situ* soil. Jewell and Milligan (1989) proposed a method for predicting the displacements of a reinforced soil wall with extensible reinforcement by assuming that perfect adherence is maintained between soil and reinforcement, and the displacement of facing wall is equal to the total extension of the reinforcement in the soil. Jarret and McGown (1988) applied several methods in the recent NATO wall prediction excercise, and almost all methods determine the displacement of the facing wall from the axial force of the reinforcement assumed in the designs.

Although there is no theoretical basis, it is empirically well known that the typical horizontal displacement δ_h on the top of a nailed slope is approximately 0.1% to 0.3% of the total slope height H (Tatsuoka, 1992). A number of published *in - situ* data for the displacement ratio δ_h / H are shown in Fig.1.6. While most of the displacement ratios remain within a range of δ_h / H = 0.1% to 0.3%, it is observed that as the slope height H increases, the ratio δ_h / H becomes less. This may partly be due to the fact that there is a tendency for greater conservatism adopted, both in design and construction on the site, as the height H of

the nailed slope increases. Schlosser *et al.* (1992), from a full scale test of soil nailing, reported that the horizontal displacement δ_h of the facing wall depended on the global safety factor F_s of the nailed slope, and that the displacement ratio δ_h / H decreased as F_s increased. Details of the displacement of nailed slopes in centrifuge tests will be shown in Chapter 6.

The finite element method is an effective tool both in design work and in the fundamental study of soil nailing and reinforced soil walls, (Murray, *et al.*, 1989). The advantages of the finite element method are the ability to:

(1) take into account the strain and strain compatibility between soil and nail,

(2) estimate the nail forces and slope displacements, and

(3) simulate the construction sequence and the initial and boundary conditions in design.

Usually, a nail is modelled as a beam or truss element in the analysis. In order to allow slip between the soil and nail, an estimate of the interface stiffness k_i in equation (1.3) is necessary in the finite element analysis.

1.3 Outline of this dissertation

The aims of the current research programme into soil nailing are to make a study of the interaction between a nail and soil, the mechanical behaviour of a nailed slope, and especially to study the failure mechanism and effect of the nails on the slope stability. The proposed failure mechanism should be based on the observed failure surface and the type of failure, *e.g.* breakage or pull-out of the nails or overturning of the reinforced soil block. The prediction of slope displacements is also important for practical reasons.

In soil nailing, an earth pressure p, nail force T and slope displacement δ are not independent parameters but are closely related to each other, as shown schematically in Fig.1.7. It is, therefore, most appropriate for such a study to perform a number of laboratory

tests with relatively small samples which can be controlled and repeated under almost the same sample conditions.

The thesis is divided into two parts:

Part 1 Pull-out tests of a nail and direct shear tests of nailed sands

Part 2 Centrifuge tests of nailed slopes

The results obtained in the tests will be used to evaluate and, if necessary, to provide a basis for changes to the existing theory and design methods. Cohesionless sands were used in all of the tests because soil nailing has been adopted for sandy soils in practice due to the larger pull-out forces than can be mobilized in clays.

In part 1, dominant factors which affect the interaction between a nail and sand are investigated by carrying out a number of pull-out tests of a nail, direct shear tests of nailed sand and interface tests between soil and reinforcement. Comparisons are made of bond friction of a nail (or reinforcement) as measured by the three types of tests. These results are also compared with results of direct shear tests carried out by other research workers. Some considerations of the dilatancy of the soil and extensibility of the nail are given.

In part 2, centrifuge model tests were performed to investigate the effect of self weight of soil on the behaviour of nailed slopes. Excavation of the slope was simulated by gradually draining water from two sets of rubber bags located in front of the facing wall, after a centrifuge acceleration $N = 30g$ was reached in the model. Earth pressures on the facing wall and displacements of the facing wall and upper ground surface were measured. The main variables of the tests were lengths and bond conditions of the nails, flexibility and roughness of the facing walls, and angle of the facing walls to the horizontal. Limit equilibrium analysis,

based on the observed failure mechanisms, was carried out and the failure accelerations N_f of the centrifuge tests were compared with those from the limit equilibrium analysis. Data from a field test carried out in Germany were also compared with those of the centrifuge tests to verify the analysis for soil nailing.

Finally, the main conclusions from the tests are drawn together in a final Chapter, where recommendations for future research are also made.

Chapter 2

Pull-out tests of a nail and direct shear tests of nailed sand

---

2.1 Introduction

In soil nailing as well as reinforced soil walls the friction between a reinforcing element and the surrounding soil plays a major role in improving the stability of earth structures. Since the axial force in a nail is generated by the relative displacement between the nail and the soil, as shown in Chapter 1, a full understanding of soil nailing requires an understanding of the interaction mechanism between them. It is not, however, an easy task to achieve because the interaction is influenced by several factors, such as the properties of the soil, roughness and stiffness of the nail and the boundary conditions of the test apparatus, as reported by Palmeira and Milligan (1989). Furthermore, the change in stress on the nail due to dilatancy of the soil, when a nail is pulled out, makes the interaction mechanism very complicated and difficult to analyse (Schlosser and Guilloux, 1979).

From this point of view, the apparent friction coefficient f^*, obtained from the pull-out test of a nail and defined by equation (1.2), may not be regarded as a characteristic index representing the interaction mechanism because the initial mean normal stress σ_m acting on the nail used for estimating f^* is assumed to be unchanged throughout the test. As pointed out by Dunham (1976) and Bolton (1990), pull-out tests of reinforcement tend to cause non - uniform strain and stress conditions both in the soil and the reinforcement, and hence require

very careful interpretation of the pull-out test data. This non - uniformity of the stress and strain may be significant, especially for flexible nails in which the displacement and shear stress on the nail cannot be assumed constant along the nail.

It should be also mentioned that although the pull-out test has been one of the most convenient and popular means of obtaining a maximum pull-out force of a nail for both *in - situ* and model tests, as shown by Chang *et al.* (1977), Ingold and Templeman (1979) and Murray *et al.* (1979), no standard methods and configurations have been established. As the pull-out test of reinforcement is very sensitive to the test procedure and the test boundary conditions, care should be taken when comparing the data obtained between tests. However, when pull-out tests are carried out under well - controlled and similar conditions, the pull-out curves and peak pull-out forces from these tests may provide fundamental and useful information regarding the interaction mechanism. At the same time, for a practical reason, index tests (Giroud, 1989) should be developed for ordinary projects.

A great deal of research investigating the interaction mechanisms of reinforcement, mainly using pull-out test or direct shear test apparatus, has been reported. In soil nailing, the latter apparatus has been used much less than the former because of the difficulty of modelling a nail of circular bar across a 2 - dimensional shear surface in the shear box. It is also widely known that the apparent friction coefficient f^* of a nail or reinforcement obtained from these two types of tests are not usually the same, and a larger apparent friction coefficient f^* is commonly observed in the pull-out tests than in the direct shear tests (*e.g.* Schlosser, 1977, and Yoo, 1988). This is due to the different stress and boundary conditions for the reinforcement between these two types of tests, as will be discussed in following Chapter 3.

In this research programme a number of pull-out tests, direct shear tests of nailed sand and interface tests between soil and reinforcement were performed in order to:

(1) investigate the interaction mechanism between a nail or reinforcement and soil,

(2) compare the apparent friction coefficients f^* of a nail between these three types of tests, taking into account the direct shear friction angle ϕ_{ds} of the soil, and

(3) obtain basic data for analysing results of the centrifuge model tests of nailed slopes, as shown in Chapter 7.

In the remainder of this chapter a general description of the test programme and specific details of each test series are given, followed by some results of the unreinforced direct shear tests of three types of sands which were used in the current research programme.

2.2 Description of the direct shear tests of nailed sand and the interface tests

A medium size direct shear test apparatus made first by Jewell (1980) was used to carry out the direct shear tests of nailed sand. The box has a plan area of 254 *mm* × 153 *mm* and a sample depth of about 150 *mm*. The top platen of the shear box is fixed to the top half of the shear box, *i.e.* it has symmetrical upper and lower boundary conditions, which more or less eliminates the rotation of the shear box during shearing. The symmetrical direct shear test is preferable because it more closely conforms with simple shear deformation of the soil (Airey, 1987, Jewell, 1989). A diagram of the shear box is given in Fig.2.1.

The shear load S is applied by a ram driven at a constant speed of 0.08 *mm/min* by an electric motor, allowing sufficient time to read and record the measurements from dial gauges. The ram pushes the bottom half of the shear box which is free to run on bearings; the top half providing resistance to movement by reacting against a deflector bar. The deflection at the middle of the deflector bar is measured with a dial gauge, giving reading to an accuracy of about ±1 N, and is directly proportional to the applied shear load S transmitted through the soil.

Because of the relatively large plan area of the shear box and the use of a hanger system to apply the vertical surcharge load, the maximum vertical stress was limited to about σ_v = 60 kN/m^2. Generally, the sample was sheared to a displacement of 4 *mm* with readings being taken at regular intervals. The shear displacement X and the dilation Y during testing were measured by means of dial gauges with a sensitivity of ±0.01 *mm*.

Nails of circular cross section with several different diameters were made of mild steel, and these were roughened by glueing a thin layer of sand on the surface. The nails were of total length l = 127 *mm*, and of diameters excluding the thickness of sand layers D = 1.3 *mm*, 2.5 *mm*, 4.5 *mm*, 6.4 *mm* and 9.1 *mm* for 50/100 dense and medium dense sands, and D = 1.0 *mm*, 1.9 *mm*, 3.0 *mm*, 6.4 *mm* and 9.6 *mm* for 14/25 dense sand. Only one nail was placed in the sample in each test, and placed symmetrically both in plan and elevation of the shear box, as shown in Fig.2.2. The orientation of a nail from the vertical direction at the time of sample preparation was fixed at $\theta = 25°$ for all the tests, so that a comparison could be made between the current test and direct shear tests of nailed sand performed by Jewell (1980) and Pedley (1991). Nearly the most efficient use of a nail in order to increase the maximum shear load S_{max} could be acheived by placing reinforcement at $\theta \approx 30°$ in the tests, as reported by Jewell. Jewell also concluded that as a reinforcement was oriented toward the direction θ^* of the principal tensile strain ε_3 in the soil, as shown in Fig.1.2(b), the magnitude of the axial force of a nail increased and hence increased the maximum shear load S_{max}, namely

$$\theta^* = \frac{\pi}{4} - \frac{\psi}{2} \qquad \text{...(2.1)}$$

in which ψ is the angle of dilation of the soil and θ^* is the direction of the principal tensile strain ε_3 from vertical.

Before carrying out each pull-out test, the internal walls of the shear box were thoroughly cleaned to reduce the friction of the wall. Assadi (1975) and Johnston and Romstad (1989) pointed out that the shear resistance is increased by simply roughening the end - wall of the shear box. The upper and lower halves of the shear box were separated vertically by inserting two aluminium packing strips of 2 *mm* thickness, and then clamping them so that an even gap was formed. After a nail was supported in the specified position and oriented $\theta = 25°$ from the vertical in the empty shear box by several thin threads, a sand sample was prepared by raining, using a hopper with shutter plates located about 80 *cm* above the top of the box. The hopper covered the full plan area of the box. After a sufficient depth of sand had been deposited and the nail was fully embedded, the thin threads were cut carefully, and the sample preparation continued. Part of the thin threads were left in the sand because of the difficulty of removing all the threads from the box.

The sand was rained to a level slightly above that required and the surplus removed by an air vacuum device, a knife and a ruler to form a level sand surface. The top platen was placed onto the sample and the vertical surcharge stress $\sigma_v = 20.3\ kN/m^2$ applied by weights; the platen was then fastened to the top half of the shear box. The clamps fixing the upper and lower halves of the shear box together and the two packing aluminium strips were removed to leave a clear gap of 2 *mm*. A more detailed description of the apparatus and sample preparation is given in Jewell (1980) and Pedley (1991).

During the course of the test programme, the sample density was changed and this involved changing the perforated plates located in the base of the hopper. Three kinds of sand samples were prepared, using 50/100 dense and medium dense Yellow Leighton Buzzard Sands and 14/25 dense Yellow Leighton Buzzard Sand. The dense sand samples were prepared by raining the sand slowly, since the initial void ratio e_0 of the sand depends mainly

on the rate of sand raining, Cole (1967). The medium dense sand was prepared by raining the sand rapidly by moving the perforated plates. This method gave a reasonably uniform sample with nearly constant mean relative density I_D.

This medium size direct shear box was also used to perform interface tests by installing the interface to be investigated at the level of the shear plane, in the lower half of the shear box, as shown in Fig.2.3. In the test, an aluminium alloy plate, which has a plan area of 254 *mm* × 153 *mm* and a thickness of 3 *mm*, was used for the interface material. Care was taken when placing the interface on the sand in the lower half of the shear box so that no horizontal displacement of the interface occurred during the test. The top surface of the aluminium plate was placed flush with the top of the lower half of the shear box. The interface was made rough by glueing sand on the smooth surface of the aluminium plate. The upper half of the shear box was filled with the test sand and the interface test was carried out in a similar manner to a direct shear test of nailed sand.

2.3 Description of the pull-out tests of a nail in sand

The medium size direct shear box was modified to provide a displacement controlled pull-out test rig. A general view of the pull-out rig is shown in Fig.2.4. The pull-out box has a plan area of 254 *mm* × 153 *mm* and a sample depth of about 202 *mm*. After a sufficient depth of sand had been deposited using a hopper, in the same way as in the direct shear tests of nailed sand described in section 2.2, a nail was placed horizontally in the required position, 127 *mm* below the upper surface of the sand. The nail was not placed centrally in the box, so that the influence of surchage load σ_v on the upper sand surface was decreased. A hole of 6 *mm* diameter was made in the front wall of the box, through which the head of the nail was firmly connected to a load cell of 200 *N* maximum capacity manufactured by Tokyo Sokki

Kenkyujo Co.Ltd, allowing measurement of the pull-out force of a nail. The rest of the sand was again rained in to the test box. The method of sample preparation is, unless otherwise stated, similar to that used in the direct shear tests of nailed sand. The pull-out load was applied by a drive motor pulling the shear box on the roller bearings. This was opposite to the method of the conventional pull-out test in which the nail is pulled out while the test box remains stationary, but the relative displacement between soil and nail is the same in each system. Dial gauges allowed the measurements of horizontal displacement of the box.

To minimize the harmful influence of the front wall when a nail is pulled out, as pointed out by Palmeira *et al.* (1989), a small plastic tube which was 70 *mm* long and 6 *mm* diameter was firmly attached horizontally to the front wall of the box (Milligan, 1991), as shown in Fig.2.4. This tube enabled the nail in the box to be insulated from the surrounding sand near the front end - wall, so that there was no friction acting on that part of the length of the nail. It is also reported that the boundary problems exhibit themselves by reducing the surcharge pressure by 35%, due to friction developed between the front wall of the box and the soil, (Jonston and Romstad, 1989). Surcharge stresses of up to σ_v = 55 kN/m^2 were applied to the top of the soil sample by weight on a hanger. Great care was taken not to bring the nail into contact with either the front wall or the small plastic tube during the sample preparation. Thin threads were used to keep the nail exactly horizontal in the case of a longer nail. The threads were left in the sand sample. The same three types of sand sample, as used in the direct shear tests of nailed sand, were prepared for the pull-out tests.

Two types of nail, stiff and flexible, with several different lengths were prepared for the pull-out tests. Stiff nails were made of mild steel (Elastic modulus $E_a = 206 \times 10^6$ kN/m^2) with circular cross section, and of diameters D = 1.0 *mm*, 1.4 *mm*, 2.0 *mm*, 2.6 *mm*, 3.2 *mm*, 4.0 *mm* and 5.2 *mm*. Flexible nails were made of a rubber tube with external diameter D_e =

3.0 *mm* and internal diameter D_i = 2.0 *mm*. Elastic modulus of the rubber tube was measured as E_a = 0.02 kN/m^2, by carring out uniaxial tensile tests of the tube. The stiff nail was instrumented with 5 pairs of strain gauges along the nail to measure the axial strain distribution of the nail during pull-out tests. All of the strain gauges were covered by the sand coating. Radiographic techniques were also used to observe the location of the rupture surfaces in the sand after pulling out the nail. Details of the pull-out tests using radiography and the flexible nail are given in Chapter 3.

The term "flexible nails" and "stiff nails" are used here to describe the relative stiffness between soil and nail in a given stress condition. Mc Gown *et al.* (1978) and Bonaparte and Schmertmann (1988) clearly defined the concepts of "extensible reinforcement" and "in-extensible reinforcement", as

for the "extensible reinforcement" : $\varepsilon_{rein} \geq \varepsilon_{soil}$

for the " in-extensible reinforcement" : $\varepsilon_{rein} < \varepsilon_{soil}$

where ε_{rein} is the tensile strain of the reinforcement at peak stress and ε_{soil} is the horizontal strain required to develop an active state in the soil. In general, a steel nail is practically assumed to be "in-extensible reinforcement".

Three main parameters for the nail were varied in the pull-out tests; roughness (smooth surface and rough surface), extensibility (stiff and flexible) and diameter D of the nails. A rough nail was made by glueing sand on the surface of a corresponding smooth nail. The material properties of the stiff and flexible nails are given in section 3.3.

2.4 Properties of soils

Two Yellow Leighton Buzzard Sands, 14/25 and 50/100, were used for the standard soils in the pull-out tests, direct shear tests of nailed sand and the interface tests. These are quartz

laboratory sands composed of sub - angular particles. The reference numbers refer to two old British Standard sieve sizes; the sand passes the first but is retained by the second. The mean particle sizes are $D_{50} \approx 0.8\ mm$ for 14/25 sand and $D_{50} \approx 0.18\ mm$ for 50/100 sand, and properties of the two sands are compared in Table 2.1. The mechanical properties of 14/25 sand have been extensively investigated by several researchers, such as Cole (1967), Stroud (1971) and Jewell and Wroth (1987), while there are few data available for 50/100 sand.

A series of unreinforced direct shear tests was performed in the medium size direct shear apparatus for 50/100 dense and medium dense sands and 14/25 dense sand. The mean relative densities for these three sands are; $I_D \approx 90\% \sim 93\%$ for 14/25 dense sand, $I_D \approx 92\% \sim 94\%$ for 50/100 dense sand, and $I_D \approx 80\% \sim 83\%$ for 50/100 medium dense sand. The state of the maximum void ratio e_{max} was obtained by pouring the sand loosely in a cylinder through a funnel, maintaining the height of raining as zero. The state of the minimum void ratio e_{min}, on the other hand, was obtained by repeatedly hitting the outside of a steel box containing the deposited sand.

Fig.2.5 compares the behaviour of the three types of sand with applied vertical stress of $\sigma_v = 36\ kN/m^2$. The trends for 14/25 dense sand shown in Fig.2.5 are in good agreement with those observed by Jewell *et al.* (1987) and Pedley (1991) using the same direct shear box. The normalized shear stress (τ_{yx}/σ_v) shown on the left axis, plotted against shear displacement X shows that the 14/25 dense sand has a greater shear strength than that of 50/100 dense sand. The measurements of dilation Y shown on the right hand axis confirm the finding by showing the 14/25 dense sand to dilate more strongly than 50/100 dense and medium dense sands.

The measured peak shearing resistances for the tests with applied surcharge stress $\sigma_v = 36\ kN/m^2$ are shown in Table 2.2, where the angle of dilation ψ and the peak direct shear friction angle ϕ_{ds} of the soil are estimated, as

$$\tan\psi = -\frac{\dot{\varepsilon}_{yy}}{\dot{\gamma}_{yx}} = -\frac{dY}{dX}$$

$$\tan\phi_{ds} = \frac{\tau_{yx}}{\sigma_{yy}} \qquad \text{...(2.2)}$$

Although not shown in the figure, there was considerable scatter of data observed in the initial stages of shear displacements $0\ mm \le X \le 0.8\ mm$ for the tests at different applied vertical stresses σ_v. However, a high degree of repeatability was observed for the range of shear displacements $X \ge 0.8\ mm$, which included the peak mobilized direct shear friction angles ϕ_{ds} and the angle of dilation ψ.

Fig.2.6 shows the plots of energy correction from the direct shear data of Fig,2.5, where

$$\sin(\phi_{cv})_{ps} = \tan\phi_{ds} - \tan\psi = m \qquad \text{...(2.3)}$$

$(\phi_{cv})_{ps}$ is the critical state friction angle in the plane strain condition, which is considered as a material property of the soil irrespective of the initial density. Equation (2.3) is obtained from comparing Taylor's energy correction (1948), equation (2.2) and Mohr's flow rule (2.4) when constant volume shear is occuring in the soil. Theoretically, m in equation (2.3) should be constant throughout the test. It is seen from the figure, ignoring the data of initial stages, $m = 0.62$, giving $(\phi_{cv})_{ps} = 38°$ for 14/25 dense sand and $m = 0.56$, giving $(\phi_{cv})_{ps} = 34°$ for 50/100 dense and medium dense sands. The measured m for 14/25 dense sand is in good agreement with Jewell (1987), Palmeira (1987) and Pedley (1991), who reported a range of $m = 0.60 \sim 0.63$. On the other hand, $m = 0.56$ for 50/100 sands is less than that of 14/25 sand, and is nearly equal to $m = 0.57$ obtained by Stroud (1971) from simple shear tests on 14/25 dense sand.

Fig.2.7 shows the mobilized plane strain friction angle $(\phi_{ps})_{mob}$ with the shear

displacements X for 50/100 dense sand deduced from the test data in Fig.2.5 for all stages during the test, using Rowe's flow rule (1969), Mohr's circle analysis, Rowe's correlation (1962) and Bolton's flow rule (1986), as

$$\textit{Rowe's flow rule:} \quad \tan\phi_{ps} = \frac{\tan\phi_{ds}}{\cos\phi_{cv}}$$

$$\textit{Mohr's analysis:} \quad \sin\phi_{ps} = \frac{\tan\phi_{ds}}{\cos\psi(1 + \tan\phi_{ds}\tan\psi)} \qquad \text{...(2.4)}$$

$$\textit{Rowe's correlation:} \quad \sin\phi_{ps} = \frac{K - 1 + (K + 1)\tan\psi}{K + 1 + (K - 1)\tan\psi}, \quad K = \tan^2\left(\frac{\pi}{4} + \frac{\phi_{cv}}{2}\right)$$

$$\textit{Bolton's flow rule:} \quad \phi_{ps} = \phi_{cv} + 0.8\psi$$

In those analyses, the critical state friction angle was assumed to be $\phi_{cv} = 34°$ (Bolton, 1986). These four methods of analysis appear to exhibit good agreement with the plane strain friction angles $\phi_{ps} = 42° \sim 44°$, although in the initial loading stages the analyses were unable to provide any consistent result for the mobilized friction angles. This inconsistency and scatter of the test data in the initial stages of the direct shear tests may be attributed to the non - coaxiality of stress and strain (Stroud, 1971), and the re - arrangement of sand particles on the central plane.

Direct shear tests of unreinforced sand using a small Casagrande shear box were also carried out to compare the measured peak shearing resistances of the three types of sands as a function of applied vertical stress, over a range of $\sigma_v = 55\ kN/m^2 \sim 200\ kN/m^2$. The results of these tests are shown in Chapter 7.

Chapter 3

Results and analyses of pull-out tests and direct shear tests of nailed sand

---

A description of the pull-out test and direct shear test apparatus was given in Chapter 2. Great care was required during the preparation of the sand samples containing a nail or a reinforcement and in conducting the tests, because these tests were found to be very sensitive to the sample conditions and method of loading. In this chapter, results of the pull-out tests for different stiffness and roughness of the surface of a nail, and for different types of sands are shown, followed by considerations of the apparent friction coefficient f^* and the interaction parameter k_i of a nail. Comparison of the apparent friction coefficients f^* obtained from the results of the pull-out tests, direct shear tests of nailed sand and the interface tests are then presented, together with comparison of the data for direct shear tests of nailed sands reported in related literature.

3.1 Comments on the pull-out test of a nail

Out of the total of 51 tests for uninstrumented nails, 38 pull-out tests of a nail were performed on stiff - rough nails using the medium size direct shear box. Specific details, together with some results of the tests, are given in Table 3.1. In Table 3.1, μ^* is the friction coefficient, defined in equation (3.21). The values of σ_v include self weight of soil above the

nail in Table 3.1.

The correction of the current length l of a nail embedded in the sand during a pull-out test, which is necessary for the following analysis, was made as shown in Fig.3.1, as

$$\begin{aligned} l &= l_i - \xi + \Delta l \\ &= l_i - \xi + \frac{F l_f}{E_a A} \end{aligned} \qquad \ldots(3.1)$$

where l_i is the length of nail initially embedded in the sand before the test, ξ is the horizontal displacement of the test box, Δl is the elastic deformation of the nail in the free part l_f, F is the current pull-out force and $E_a A$ is the axial stiffness of the nail. However, elastic deformation of the nail currently embedded in the soil can be ignored in equation (3.1) because it was found to be very small and negligible when compared to the other components of deformation. The diameter D of a nail, unless otherwise stated, includes the thickness of the sand layer glued on the surface, as shown in Fig.3.2, which gives an additional diameter ΔD for each nail,

$\Delta D \approx 0.7$ *mm* for 50/100 Yellow Leighton Buzzard dense and medium dense sands, and

$\Delta D \approx 2.0$ *mm* for 14/25 Yellow Leighton Buzzard dense sand.

3.2 Pull-out tests of stiff nails

3.2.1 Rough surface nails

The typical load - pull out displacement results of stiff - rough surface nails for the three types of sand are shown in Fig.3.3(a), (b) and (c), together with results of unreinforced direct shear tests for the corresponding sands with nearly the same relative densities I_D as in the pull-out tests. As the parameters for the tests, the diameter D of a nail, its initial length l_i and

applied surcharge load σ_v were chosen. The pull-out displacement ξ is defined as the displacement with respect to the front face of the sand sample of a point on the nail. The important features of the results shown in Fig.3.3 are,

(1) ξ_p, the pull-out displacements of a nail required to mobilize the peak pull-out force F_p, were almost the same irrespective of diameters D, initial lengths l_i of the nails and the applied vertical surcharge stresses σ_v,

(2) excluding the post peak pull-out force, the pull-out curves are nearly approximated by hyperbolae, in which the trend is the same as that of the load - displacement curve for unreinforced direct shear tests of sand,

(3) the peak pull-out displacements ξ_p were also nearly equal to the horizontal displacement of the unreinforced direct shear tests of the corresponding sands at the peak stress ratio $(\tau_{yx} / \sigma_v)_{max}$, namely

$\xi_p \approx 2.0$ *mm* for 50/100 dense sand

≈ 2.2 *mm* for 50/100 medium dense sand, and

≈ 1.5 *mm* for 14/25 dense sand.

Schlosser (1990) and Bergado *et al.* (1992) pointed out that generally, a range of pull-out displacements $\xi_p = 1$ *mm* ~ 5 *mm* or $\xi_p = 1$ *mm* ~ 3 *mm* respectively, is required to mobilise the peak pull-out force F_p of the reinforcement and nail.

(4) the loss of the peak pull-out force F_p was observed to continue gradually, at least to the pull-out displacement $\xi < 4.0$ *mm*, which was the maximum range of pull-out displacement carried out in the current tests.

(5) peak pull-out force F_p increased as the shear strength of the soil increases, indicating that the friction angle ϕ of the sand plays an important role on the peak pull-out force F_p.

Fig.3.4 shows the axial stress distributions of a nail at the peak pull-out force F_p for 50/100 dense sand with the surcharge stresses σ_v = 5.6 kN/m^2, 11.0 kN/m^2 and 22.7 kN/m^2. Ten strain gauges were used to instrument the nail at different positions along the length of the nail. A pair of the strain gauges consisted of 2 strain gauges attached on exactly opposite sides of the nail surface. The nail was made of stainless steel tube, of total length l = 12.0 *cm* and external and internal diameters D_e = 2.0 *mm* and D_i = 1.9 *mm*, respectively, as shown in Plate 3.1. In order to minimize the possible influence of bending moment on a nail, the axial stresses σ of a nail during pull-out test were estimated as the mean of the two measured surface strains for both sides of the nail ε_1 and ε_2, as

$$\sigma = E_a \left(\frac{\varepsilon_1 + \varepsilon_2}{2} \right) \qquad ...(3.2)$$

where E_a ($\approx$ 210 kN/mm^2) is the elastic modulus of the nail. In Fig.3.4, fairly linear axial stress distributions $\sigma(x) / \sigma_0$ along the nail were observed in these pull-out tests, where σ_0 is the axial stress at the head of the nail (x =0) in the front wall. It is also found that the disturbance of the pull-out force caused by the soil near the front wall was very small, and this was probably due to the small plastic sleeve attached horizontally to the front wall.

The observed linear axial stress distributions for the stiff nails, Fig.3.4, may also be derived analytically. Combining equations (1.3) and (1.4) gives the following differential equation (Farmer, 1975), as

$$\frac{d^2\xi(x)}{dx^2} = \frac{2k_i}{R_a E_a} \xi(x) \qquad ...(3.3)$$

In the pull-out tests, the boundary conditions for equation (3.3) with regard to the axial stress of a nail are given at the head of nail (x = 0) and at the end of nail (x = l), namely

$$\sigma(x) = -E_a \frac{d\xi(x)}{dx}$$
$$= \sigma_0 \qquad : at\ x = 0$$
$$= 0 \qquad : at\ x = l \qquad ...(3.4)$$

The general solutions for equation (3.3) are then obtained, as

$$\frac{\sigma(x)}{\sigma_0} = \frac{\sinh\{\alpha(l - x)\}}{\sinh(\alpha l)},$$
$$\frac{\xi(x)}{\xi_0} = \frac{\cosh\{\alpha(l - x)\}}{\cosh(\alpha l)} \qquad ...(3.5)$$

where α is the parameter for the relative stiffness between soil and nail, as

$$\alpha = \sqrt{\frac{2k_i}{R_a E_a}} \qquad ...(3.6)$$

In equation (3.5), ξ_0 is the displacement of a nail at the head of nail ($x = 0$). Fig.3.5 shows the results of equation (3.5) with the different values of the relative stiffness $(0.1 / m) \leq \alpha \leq (10.0 / m)$. It is seen in the figure that as α decreases, or as the relative stiffness between a nail and soil increases for nails of the same diameter D, the axial stress distribution $\sigma(x) / \sigma_0$ becomes more linear and the shear stress distribution becomes more constant along the nail. Thus, for a stiff nail, from equations (1.3) and (3.5),

$$\frac{\tau(x)}{\tau_0} = \frac{\xi(x)}{\xi_0} \qquad ...(3.7)$$
$$\approx constant$$

where τ_0 is the shear stress at the head of the nail ($x = 0$). The interaction parameter k_i can be, therefore, directly estimated from the results of a pull-out test of a stiff nail using

equations (1.3) and (3.7) because the shear stress $\tau(x)$ and the displacement $\xi(x)$ of the nail are assumed almost constant along the nail, that is,

$$\begin{aligned} k_i(x) &= \frac{\tau(x)}{\xi(x)} \\ &\approx \frac{\tau_0}{\xi_0} \\ &= constant \end{aligned} \qquad ...(3.8)$$

From this point of view, the similarity observed between the results of pull-out tests of the stiff nails and those of the unreinforced direct shear tests of the corresponding sands, as shown in Fig.3.3, may be attributed to the fact that the direction along a nail is almost a direction of zero - extension in which the increment of axial strain $\varepsilon(x)$ is zero along the nail. Jewell and Wroth (1987) and Dyer (1985) reported that the single rupture band across the centre of a shear box appeared to coincide with the direction of zero - extension and not the plane of maximum stress obliquity. For a stiff nail of $E_a / k_i \gg 1$ (or $\alpha \ll 1$), equation (3.5) is simplified using Taylor's approximation ignoring terms α of degree 2, as

$$\begin{aligned} \xi(x) &\approx \xi_0 \\ &= constant\,, \\ \varepsilon(x) &= \frac{d\xi(x)}{dx} \\ &\approx \varepsilon_0\left(1 - \frac{x}{l}\right) \end{aligned} \qquad ...(3.9)$$

where ε_0 is the axial strain at the head of a nail ($x = 0$). Such a similarity with direct shear test was also observed by Tan (1990) by carrying out interface tests between a stiff - rough plate and sand. The pull-out force F of a nail is, therefore, more closely related to the direct shear friction angle ϕ_{ds} than the plane strain friction angle ϕ_{ps} of the sand. Randolph and

Wroth (1978) state that the behaviour of soil near a pile can be modelled as simple shear, in which the direction of the shearing is assumed to be that of zero - extension.

The relationships between friction angles ϕ_{ds} and ϕ_{ps}, and cohesions c_{ds} and c_{ps} may be derived by making Coulomb's active earth pressure P_a obtained from ϕ_{ds} and c_{ds} on velocity characteristics (obtained by direct shear test) equal to that from ϕ_{ps} and c_{ps} on stress characteristics (obtained by plane strain test) in a vertical and smooth wall (Jewell, 1989) in Fig.3.6, as

$$P_a = \frac{1}{2}\gamma H^2 \tan^2\left(\frac{\pi}{4} - \frac{\phi_{ps}}{2}\right) - 2c_{ps}H\tan\left(\frac{\pi}{4} - \frac{\phi_{ps}}{2}\right)$$

$$= \frac{1}{2}\gamma H^2 \frac{\tan\left(\frac{\phi_{ds}}{4} + \frac{\psi}{2} - \phi_{ds}\right)}{\tan\left(\frac{\pi}{4} + \frac{\psi}{2}\right)} - c_{ds}H\frac{\sin\left(\frac{\pi}{2} - \phi_{ds}\right)}{\sin\left(\frac{\pi}{4} + \phi_{ds} - \frac{\psi}{2}\right)\sin\left(\frac{\pi}{4} + \frac{\psi}{2}\right)} \qquad \text{...(3.10)}$$

Comparing the terms of two equations (3.10) which include the self weight γ of the soil or not, then

$$\tan\phi_{ds} = \frac{\sin\phi_{ps}\cos\psi}{1 - \sin\phi_{ps}\sin\psi},$$

$$c_{ds} = \frac{c_{ps}\cos\phi_{ds}\cos\psi}{1 - \sin\phi_{ps}\sin\psi} \qquad \text{...(3.11)}$$

These results in equation (3.11) are exactly the same as the solution obtained by Davis (1968) from a Mohr's circle analysis, as shown in Chapter 2.4. It is easily understood from equation (3.11) that the direct shear parameters (ϕ_{ds} and c_{ds}) are always less than or equal to the plane strain parameters (ϕ_{ps} and c_{ps}). Therefore, using direct shear strengths ϕ_{ds} and c_{ds} for the analysis of stress characteristics produces more conservative earth pressures than those from using plane strain strengths ϕ_{ps} and c_{ps}.

Radiographs were taken during pull-out tests of a reinforcement made of an aluminium alloy plate, which is 5 *mm* thick and of surface area 200 *mm* × 50 *mm* embedded in sand. The pull-out tests of a plate were carried out with either a smooth surface or a rough surface, where the rough surfaces were made by glueing sand layers onto the smooth surface. As with the pull-out tests of a nail, great care was required to make the roughness of the plate identical to the sand grains. Using a plate rather than a nail was necessary to get clear pictures in the radiographs. The *X* - ray head manufactured by Philips Co.Ltd was mounted rigidly on a stand in front of the apparatus, and the film to focus distance was about 90 *cm*. Fig.3.7 shows the schematic view of the arrangement for the radiograph and the pull-out box, which has a plan area of 200 *mm* × 50 *mm* and sample depth 200 *mm*. The plate was placed 110 *mm* below the upper surface with no vertical surcharge stresses (σ_v = 0 kN/m^2). 14/25 dense Yellow Leighton Buzzard and 50/100 dense Yellow Leighton Buzzard Sands were used in the tests.

Fig.3.8 (a), (b) and (c) are the photographic prints of the radiographs and show the development of rupture zones in the soil after a pull-out displacement ξ = 2.5 *mm*, which was thought to be a sufficient pull-out displacement to develop the rupture zone around the nail, as shown in Fig.3.3. It is observed that for the rough plate, the thickness h of the rupture zone gradually increased towards the front face, and the range of thickness observed is about h = 10 *mm* ~ 12 *mm* for 14/25 dense sand, and h = 5 *mm* ~ 8 *mm* for 50/100 dense sand. Those thicknesses h of the rupture zone are relatively close to those of a shear zone along failure surfaces in sands, in which a thickness of less than 20 times the mean sand particle size D_{50} is commonly observed, as reported by Muhlhaus and Vardoulakis (1987). Jewell (1980) reported that the observed thickness of the rupture zone was h = 17.5 *mm* when a stiff - rough bar was pulled out in 14/25 dense sand, which is the thickness of about 22 particles of the

mean particle size D_{50} ($\approx$ 0.8 *mm*) of the sand. For the smooth plate in 14/25 dense sand, on e other hand, a much thinner rupture zone, h = 1 *mm* ~ 3 *mm*, than that of the rough plates was observed, as shown in Fig.3.8 (b). This result is consistent with the smaller peak pull-out force F_p for a smooth nail than that for a rough nail in the tests, as will be shown in section 3.2.2.

Desrues (1984) observed in pull-out tests that initially there is a zone of high shear strain adjacent to the reinforcement, of thickness of the order of 10 to 20 D_{50}. Failure planes then develop as the displacement of the reinforcement relative to the soil increases. On the other hand, Lehane *et al.* (1993) reported that the rupture zone with shear and volume strains in the soil consists of a few grains of soil close to a steel pile, so that the slip occurs between the pile and soil. Bolton (1990) and Heymann *et al.* (1992) also stated that the thickness h of the rupture zone around a reinforcement is usually of a few grains of sand, which is much smaller than that of the rough reinforcement in dense sands observed in Fig.3.8. This discrepancy regarding the thickness h of rupture zone observed may be due to the difference of the roughness of a reinforcement surface; such as steel with a blasted surface, ribbed strip and rough nail with sand glued to the surface. For a ribbed strip and a geogrid, passive bearing resistance rather than the friction between soil and the strip dominates the interaction mechanism, and the observed thickness h of the rupture zone is usually larger, (Irsyam *et al.*, 1991).

It is interesting that while the influence of the surcharge load σ_v and the length l of a nail on the apparent friction coefficient f^* is small, as shown in Fig.3.9, f^* is not constant with the diameter D of the nail, Fig.3.15. It is, however, noted that in the following centrifuge tests, the relationship between f^* and σ_v is very important. The assumed mean normal stress σ_m on a nail in equation (1.2) is calculated from the vertical stress σ_v on the nail, as

$$\sigma_m = \frac{1 + K_0}{2}\sigma_v,$$
$$K_0 = 1 - \sin\phi_{ps} \qquad ...(3.12)$$

in which ϕ_{ps} is the plane strain friction angle of the soil obtained by flow rule and results of direct shear tests (see Table 2.2 and equation (2.4)), and K_0 is the earth pressure coefficient at rest, Jaky (1944). The result of Fig.3.15 contradicts the conventional assumption in the design of soil nailing, in which the peak pull-out force F_p is proportionally increased by simply increasing the diameter D of the nail. This point will be discussed in section 3.4.

As described before, the load - displacement curves shown in Fig.3.3 may be approximately modelled by a hyperbola up to the peak pull-out force F_p, as shown in Fig.3.10. In the figure, τ is the average shear stress on the stiff nail, calculated as

$$\tau = \frac{F}{\pi D l} \qquad ...(3.13)$$

The interaction parameter k_i for a range of pull-out displacements $0\ mm \le \xi \le \xi_p$ is then given from the hyperbola, as

$$k_i(\xi) = \frac{1}{a + b\xi} \qquad ...(3.14)$$

Parameters a and b in equation (3.14) are obtained from the load - displacement curves by plotting the pull-out data as ξ / τ versus ξ, as shown in Fig.3.10. From the pull-out tests and equation (1.8), both the interface stiffness k_i and the peak pull-out force F_p are found to be influenced by the diameter D of the nail. This is a somewhat similar trend to the modulus of subgrade reaction k_s of soil, in which k_s decreases with loaded area, Terzaghi (1955).

3.2.2 Smooth surface nails

Fig.3.11 shows the load - displacement results for stiff - smooth nails for 50/100 dense and 14/25 dense Yellow Leighton Buzzard Sand. For the tests of the smooth nails, the initial length of a nail was fixed as l_i = 200 *mm* and the applied vertical surcharge stress was σ_v = 22.7 kN/m^2. Compared with the pull-out test data with those of the stiff - rough nails in Fig.3.3, as expected, much smaller peak pull-out forces F_p were observed and the displacements required to mobilize F_p were about ξ_p = 0.8 *mm* ~ 0.9 *mm* irrespective of the type of sand, which is less than half of those for the rough nails. After the peak pull-out force F_p was achieved, a gradual reduction of the pull-out forces was observed and thereafter, those pull-out forces became nearly constant at a nail displacement of about ξ = 1.4 *mm* for 14/25 dense sand and ξ = 1.2 *mm* for 50/100 dense sand. The apparent friction coefficients and the angles of bond friction δ_b were f^* = 0.26 (δ_b = 14.5°) for 50/100 dense sand and f^* = 0.32 (δ_b = 17.7°) for 14/25 dense sand, where

$$\delta_b = \tan^{-1} f^* \qquad ...(3.15)$$

These f^* and δ_b observed are considerably smaller than the critical state friction angle of quartz sand ϕ_{cv} = 33° ~ 35° (Bolton, 1986), and further, even smaller than the angle of mineral - to - mineral friction angle ϕ_u estimated by Chen and Liu (1990) assuming ϕ_{cv} = 34°, as

$$\phi_u = \frac{(\phi_{cv} - 22.5°)}{0.9} + 15.0° = 26.7° \qquad ...(3.16)$$

In the design of reinforced soil walls using steel or concrete strips with smooth surfaces, Schlosser *et al.* (1979) suggested that the apparent friction coefficient of the reinforcement

is nearly equal to $f^* = 0.40$ ($\delta_b = 22°$). As the surfaces of the smooth nail used in the current pull-out tests are regarded as nearly "perfectly smooth", their suggestion for f^* is considered reasonable. The smaller apparent friction coefficient for the smooth nail compared with that of the rough nails is due to the very much thinner rupture zone of the soil developed around the nail when pulled out, and hence, much less energy dissipation in the soil, as shown in the results of the radiographs in Fig.3.8. A common belief is that in the pull-out of a smooth reinforcement, the discontinuity can be formed by the soil particles sliding on the reinforcement surface (Gourc and Beech, 1989).

It was also observed that unlike with the rough nails, the apparent friction coefficients f^* of the smooth nail were nearly constant irrespective of the diameter D of the nail, as shown in Fig.3.12. This result indicates that the apparent friction coefficient f^* of the stiff - smooth nail is not dominated by its geometric size.

3.3 Pull-out tests of flexible - rough nails

Fig.3.13 shows the load - displacement results of flexible - rough nails, which were made of a small rubber tube. Details of the tube were given in Chapter 2. In the tests, the initial length of a nail was fixed as $l_i = 200\ mm$ while the surcharge stress was $\sigma_v = 22.7\ kN/m^2$. As the model sands, 50/100 dense (*Test F1-1*), 50/100 medium dense (*Test F2-1*) and 14/25 dense (*Test F3-1*) Yellow Leighton Buzzard Sands were used. Compared with the results of the stiff - rough nails, as shown in Fig.3.3, it is clear that the longitudinal stiffness of a nail has a remarkable effect on the responses; the peak pull-out forces F_p for the flexible nail are smaller than those of stiff nails, and the pull-out displacements ξ_p required to mobilize F_p are two or three times larger than those of the stiff nail. The apparent friction coefficients are f^* = 1.88 and 2.10 for 50/100 dense and medium dense sands respectively, where an obvious

discrepancy in f^* was observed between these two sands. This discrepancy may be due to an experimental error in the pull-out tests of the flexible nail. For 14/25 dense sand $f^* = 2.47$ was obtained, which is larger than the values for 50/100 sands. The loss of pull-out force after achieving the peak pull-out force F_p was seen to be significant, and much greater than in the stiff - rough nails. It should be noted that the flexible nail may have suffered from a Poisson's ratio shrinkage effect, which may have caused some collapsing (or at least stress reduction) around the circumference as the nail was pulled.

It is predicted that the axial stress distribution in a flexible nail does not decrease linearly toward the end of the nail, as plotted in Fig.3.5, for a smaller relative stiffness between a nail and soil E_a / k_i. Further, the direction of the nail cannot to be assumed to be a direction of zero - extension, because the pull-out displacement $\xi(x)$ along a flexible nail is not constant any more. The pull-out displacement $\xi(x)$ and the strain $\varepsilon(x)$ of a flexible nail are obtained from equation (3.5), as

$$\xi(x) = \frac{\sigma_0}{\alpha E_a} \frac{\cosh\{\alpha(l - x)\}}{\sinh(\alpha l)} ,$$

$$\varepsilon(x) = \frac{d\xi(x)}{dx} \qquad \text{...(3.17)}$$

$$= \varepsilon_0 \frac{\sinh\{\alpha(l - x)\}}{\sinh(\alpha l)}$$

where ε_0 is the strain at the head of the nail ($x = 0$). Equations (3.5) and (3.17) indicate that the interaction parameter k_i cannot be directly estimated from the load - displacement curve of the flexible nails using equation (1.3), since the mobilizations of the interaction parameter k_i are different at different points along the flexible nail. For a flexible nail, therefore, the apparent friction coefficient f^* has little significance for generally describing the maximum pull-out force F_p of the nail, *e.g.* the peak pull-out force F_p for a flexible nail is not

proportional to the length l of the nail, because of the different mobilization of the shear stress τ and hence, the interaction parameter k_i along the nail.

Since the flexible nails were not instrumented with strain gauges because of technical difficulties, prediction of an axial stress distribution along a flexible nail was made here using the interaction parameter k_i estimated from the pull-out tests of the stiff - rough nails, section 3.2.1. It is now assumed that the interface parameter k_i of an element of a nail is a unique function of the property of the soil, geometry and roughness of the nail, and is not influenced by the stiffness of the nail itself, as shown in equation (1.7). This assumption may not be correct because in the flexible nail a direction of the nail is not a direction of zero - extension, as shown in equation (3.17). The results of the radiographs in Fig.3.8 suggest that the thickness h of the rupture zone around a nail is related to the mean sand particle size D_{50} and roughness of the surface. This also indicates that the interface stiffness k_i of a stiff nail is applicable to the analysis of the flexible nail, when the above conditions of the pull-out tests are maintained the same. From equations (1.3), (1.4) and (3.14) with an assumption that the load - displacement curves of the stiff nail in Fig.3.3 are modelled as hyperbolae with the parameters a and b, as shown in section 3.2.1, then

$$\frac{d^2\xi(x)}{dx^2} = \alpha^2 \xi(x) = \frac{4D_e \xi(x)}{E_a(D_e^2 - D_i^2)\{a + b\xi(x)\}} \qquad \text{...(3.18)}$$

where D_e = 0.3 *cm* and D_i = 0.2 *cm* are the external and internal diameters, and E_a = 0.02 kN/m^2 is the elastic modulus of the tubular nail made of rubber. In equation (3.18), the external diameter D_e excludes the additional thickness ΔD of the sand layers glued on the surface of the nail. Parameters a and b for the hyperbola for nearly the same diameter D of

the stiff - rough nails and the surcharge stress σ_v for the corresponding sand are obtained from the pull-out curves in Fig.3.3, these being,

$a = 0.022\ cm^3/N$ and $b = 0.120\ cm^2/N$: for 50/100 dense sand,

$a = 0.030\ cm^3/N$ and $b = 0.145\ cm^2/N$: for 50/100 medium dense sand, and

$a = 0.009\ cm^3/N$ and $b = 0.102\ cm^2/N$: for 14/25 dense sand.

Boundary conditions for equation (3.18), the pull-out forces F and the axial strains ε of nails estimated from the pull-out displacement ξ_0 at the head of nail $(x = 0)$ for three stages of the pull-out tests (stage A, B and C), are given in Fig.3.13. Namely,

for 50/100 dense sand,

$$\begin{aligned}
&at\ 1A: \quad \xi_0 = -2.0mm, \quad F = 50.2kN \rightarrow \frac{d\xi(x)}{dx} = -\frac{\sigma_0}{E_a} = -0.442 \\
&at\ 1B: \quad \xi_0 = -3.0mm, \quad F = 60.2kN \rightarrow \frac{d\xi(x)}{dx} = -0.529 \qquad ...(3.19a) \\
&at\ 1C: \quad \xi_0 = -5.0mm, \quad F = 65.0kN \rightarrow \frac{d\xi(x)}{dx} = -0.572
\end{aligned}$$

for 50/100 medium dense sand,

$$\begin{aligned}
&at\ 2A: \quad \xi_0 = -3.0mm, \quad F = 53.8kN \rightarrow \frac{d\xi(x)}{dx} = -\frac{\sigma_0}{E_a} = -0.476 \\
&at\ 2B: \quad \xi_0 = -5.0mm, \quad F = 70.0kN \rightarrow \frac{d\xi(x)}{dx} = -0.617 \qquad ...(3.19b) \\
&at\ 2C: \quad \xi_0 = -7.0mm, \quad F = 73.9kN \rightarrow \frac{d\xi(x)}{dx} = -0.652
\end{aligned}$$

for 14/25 dense sand,

$$
\begin{aligned}
&at\ 3A: \quad \xi_0 = -1.0mm, \quad F = 91.7kN \rightarrow \frac{d\xi(x)}{dx} = -\frac{\sigma_0}{E_a} = -0.487 \\
&at\ 3B: \quad \xi_0 = -3.0mm, \quad F = 101.3kN \rightarrow \frac{d\xi(x)}{dx} = -0.536 \\
&at\ 3C: \quad \xi_0 = -4.5mm, \quad F = 107.9kN \rightarrow \frac{d\xi(x)}{dx} = -0.573
\end{aligned}
\qquad ...(3.19c)
$$

Where in equations (3.19), the axial nail stresses σ_0 from the pull-out force F at the head of the nail ($x = 0$) are calculated considering a half of the additional thickness ΔD of the sand layers on the nail (because the sand layer was firmly glued on the nail surface), as

$$
\begin{aligned}
\sigma_0 &= \frac{F}{A} \\
&= \frac{4F}{\pi\left\{\left(D_e + \frac{\Delta D}{2}\right)^2 - D_i^2\right\}}
\end{aligned}
\qquad ...(3.20)
$$

where A is the area of the cross section of the flexible - rough nail. Fig.3.14(a), (b) and (c) compare the results of the normalized distributions of pull-out displacements of a nail ξ_0 / $\xi(x)$, estimated from equation (3.18) and the boundary conditions of ξ_0 and ε_0 from equations (3.19), using the Runge - Kutta method for the numerical solutions of the differential equations. Another boundary condition for equation (3.18) is that the pull-out displacement should always be negative (tension) or zero on the nail, such as $\xi(x) \leq 0$. Unlike the results of the stiff - rough nails shown in Fig.3.3, the distributions of pull-out displacement for the flexible nails are not constant ($\xi_0 \neq \xi(x)$) nor decreasing linearly from the head of the nail ($x = 0$) to the end of the nail ($x = l$). A great deal of the pull-out displacement $\xi(x)$ and shear stress $\tau(x)$ is generated near the head of the nail ($x = 0$), while at small pull-out forces, such

as stage A, there are negligible displacements ξ of the nail generated deeper into the soil. As the pull-out displacement ξ_0 or pull-out force F increases, the displacement distributions $\xi(x)$ are observed to be gradually transmitted to the nail deeper in the soil, as pointed out by Gourc and Beech (1989) for the case of pull-out of a geotextile in sand. Burd (1986) presented a very similar result from finite element analysis for the tensile force distribution in a reinforced unpaved road under a loaded footing, as the footing displacement increases. It is also noticed that a considerable pull-out displacement ξ_0 at the head of nail (x = 0) will be needed to mobilize the friction along the full length l of the flexible nail. The results from Fig.3.14 imply that for a pull-out test of a flexible nail, as already mentioned, the peak pull-out force F_p is not directly proportional to the length l of the nail, in contrast to the stiff - rough nail shown in Fig.3.9; mobilisation of the shear stress τ of a nail is strongly related to that of the tensile strain ε of a nail. It is, however, to be remembered that since the hyperbola with parameters a and b cannot exactly model the post peak pull-out curves, (*e.g.* reduction of the pull-out force F after the peak), the analysis based on equation (3.18) tends to overestimate the shear stress τ on the flexible nail, particularly near the head of the nail (x = 0). This may lead to a discrepancy in the pull-out curves in Fig.3.14. For example, when peak pull-out forces F_p are observed in the tests, the analysis predicts that nail friction is only mobilised along half the length l of the nail. From this point of view, it is important for the analysis of friction of a flexible nail to formulate correctly the pull-out curve of the stiff nail to include the post peak behaviour.

It is easily predicted from Fig.3.14 that the mobilization of shear stress τ along a nail is progressive from the head of nail (x = 0), and such a phenomenon is similar to the pull-out of a grid material in dense sand, as observed by Palmeira (1987). In practice, since a nail is regarded as neither "ideally stiff" nor "ideally flexible" material, pull-out of a nail would

exhibit an intermediate behaviour between the stiff and flexible nails. This implies that caution should be exercised about the compatibility between the apparent friction coefficient f^* of the nail and the friction angle ϕ of the soil in design of soil nailing. It may be reasonable to use the critical state friction angle ϕ_{cv} in the case of flexible reinforcement because of the large pull-out displacement ξ_p required to mobilize the peak pull-out force F_p.

3.4 Considerations for peak pull-out force F_p of stiff - rough nails

It is common practice to interpret the peak pull-out force F_p of a nail or strip reinforcement using the apparent friction coefficient f^* (*e.g.* Schlosser, 1982, Juran, 1991, and Palmeira, 1987). It is not always, however, appropriate to employ the apparent friction coefficient f^* when comparisons are made between different types of sands since the friction angle ϕ of the soil is not explicitly reflected in equation (1.2). Considering the similarity between the pull-out test of a stiff - rough nail and the direct shear test of unreinforced sand, in which the horizontal directions are regarded nearly as a direction of zero - extension, as shown in section 3.2.1, it is suggested that a more convenient and appropriate parameter for generally describing the friction of a nail is a friction coefficient μ^*, defined as

$$\mu^* = \frac{f^*}{\tan\phi_{ds}} = \frac{F_p}{\pi D l \sigma_m \tan\phi_{ds}} \qquad \text{...(3.21)}$$

where ϕ_{ds} is the direct shear friction angle. In the case of pull-out tests of a stiff - smooth nail or a flexible nail, the critical state friction angle ϕ_{cv} or the mineral - to - mineral friction angle ϕ_u may be more appropriate in equation (3.21). For almost all cases, the friction coefficients μ^* are observed to be greater than 2 / 3 in sand (*e.g.* Gourc and Beech, 1989).

Fig.3.15(a) and (b) show the relationship between the friction coefficient μ^* and the diameter D and normalized diameter D / D_{50} of a nail respectively, estimated from the pull-out tests of stiff - rough nails, carried out in section 3.2.1. Here, D_{50} is the mean particle size of the sand. The figures also include a data point for stiff - rough nail with 14/25 dense sand conducted by Jewell (1980), showing a good agreement between those two tests. It is clearly observed from Fig.3.15 that the friction coefficient μ^* gradually decreases as the diameter D of a rough nail increases, although μ^* were observed almost constant irrespective of the diameter D for the smooth nails, as shown in Fig.3.12. The effect of D / D_{50} on the friction coefficient μ^* is significant for D / D_{50} in the range 1 ~ 35, but for higher values of D / D_{50} (which is more normal in the field), the effect would not appear to be particularly significant.

It is easy to imagine that the pull-out of a nail, especially of a rough nail, causes stress change in dense sand due to dilatancy of the soil, and hence increases the peak pull-out force F_p, as reported by Johnston and Romstad (1989) from large scale pull-out tests of reinforcement. Yazici and Kaiser (1992) reported that the larger borehole diameter leads to a reduced normal stress σ_m and bond strength τ for cable bolts embedded in rock because the dilatancy effect is decreased as the diameter of the borehole becomes larger. Houlsby (1991), using cavity expansion theory, clearly showed that a pile of larger diameter exhibits less friction resistance than that of a small pile due to soil dilatancy. Significant increases of normal stresses on steel piles were reported by Hettler (1982) and Lehane *et al.* (1993) from model tests and *in -situ* pile loading tests, respectively. Schlosser and Elias (1978) also demonstrated that the effect of the restricted dilatancy of the soil on the peak pull-out force F_p of a nail is significant, and surprisingly, values of apparent friction coefficient f^* of up to 7.0 or friction coefficient μ^* up to 6.3 were reported from their pull-out tests of ribbed strips.

Heymann *et al.* (1992) performed a number of *in - situ* pull-out tests of nails of diameters from D = 20 *mm* to 30 *mm* in various ground conditions. They showed that the majority of the values of friction coefficient lay within a range of μ^* = 2 ~ 4, which bounds quite well the test data in Fig.3.15. They emphasized the importance of soil dilatancy in predicting the maximum pull-out force F_p of a nail.

Fig. 3.16(a), (b) and (c) show the relationships between the mobilized friction coefficient μ^*_{mob} and the pull-out displacement ξ of the stiff - rough nails calculated from Fig.3.3, together with the mobilized angle of dilation ψ_{mob} of the soil from the unreinforced direct shear tests, where

$$\mu^*_{mob} = \frac{f^*_{mob}}{\tan(\phi_{ds})_{mob}} \qquad ...(3.22)$$

It can be seen from the figure that the mobilized friction coefficient μ^*_{mob} has a very similar trend to the mobilized angle of dilation ψ_{mob}, indicating the close relationship between dilation of soil and the friction on a nail. In other words, it is understood that the increase of pull-out force F of a nail is closely related to the dilation in the soil. It is interesting in Fig.3.16 that even from the early stages of pull-out displacement ξ, the mobilized friction coefficient μ^*_{mob} is observed to be always greater than 1, namely

$$f^*_{mob} \geq \tan(\phi_{ds})_{mob} \qquad ...(3.23)$$

This suggests that even for small shear strains of the soil, the soil dilates and the normal stress σ_m on the nail increases, in contrast with the boundary measurements of direct shear tests which often exhibit a contraction in the early stage of the test. Palmeira (1987) measured the shear strain and volumetric strain at the central plane in direct shear tests, and reported that 14/25 dense sand dilates from the beginning of shearing (from the shear strain γ_{yx} = 1

~ 2%), as presented in Fig.3.17. In Fig.1.3, for example, $\xi(x) = \eta(x) = 0.1$ *mm* of pull-out displacement of the stiff - rough nail causes the shear strain of sand $\gamma_{yx} \approx 2\%$ for 50/100 dense sand and $\gamma_{yx} \approx 1\%$ for 14/25 dense sand, assuming that the thickness of shear zone is $h = 5$ *mm* and 10 *mm* for 50/100 dense and 14/25 dense sand, respectively (see the results obtained by *X* - ray, section 3.2.1).

When it is assumed that:

(1) the normal stress on a nail is increased from σ_m to $\sigma_m + \Delta\sigma_m$ owing to the soil dilatancy during pull-out test of a nail, and

(2) for the non - dilatant soil ($\Delta\sigma_m = 0$), such as the loose sand or the sand in the critical state, the friction coefficient for the rough nail is $\mu^* = 1$ or $f^* = \tan\phi_{ds}$,

then equation (3.21) is written, as

$$\mu^* = 1 + \frac{\Delta\sigma_m}{\sigma_m} \qquad ...(3.24)$$

From elastic cavity expansion theory (Fig.3.18), the radial stress change results in a displacement of the soil mass (Boulton *et al.*, 1986 and McGown *et al.*, 1989), as

$$\begin{aligned} \Delta\sigma_m &= 2G\Delta\varepsilon \\ &= \frac{2G\Delta h}{D + h} \end{aligned} \qquad ...(3.25)$$

in which $\Delta\varepsilon$ is the increment of the circumferential strain of the soil, h is the thickness of the shear zone, Δh is the increment of shear zone thickness due to the dilatancy of soil, and G is the shear modulus of the soil. Combining equations (3.24) and (3.25) gives:

$$\mu^* = 1 + \frac{2G}{\sigma_m}\frac{\Delta h}{D + h}$$
$$= 1 + \frac{2G}{\sigma_m}\frac{\Delta h/D_{50}}{D/D_{50} + h/D_{50}} \qquad ...(3.26)$$

where D_{50} is the mean particle size of soil. Equation (3.26) conceptually shows the increase of the friction coefficient μ^* from the direct shear friction angle ϕ_{ds} due to the increased normal stress $\Delta\sigma_m$ in the pull-out tests. While the rotation of principal stress of the soil during pull-out of a nail is not considered in equation (3.26), Symes (1983) pointed out that for dense sand the sensitivity to the rotation of the principal stress on the friction of a pile is not significant. The important features of equation (3.26) are,

(1) as observed in the pull-out tests, the friction coefficient μ^* decreases as the diameter D of the nail increases; the additional normal stress $\Delta\sigma_m$ on a nail due to the dilatancy sharply decreases as D increases, particularly for the smaller diameter D,

(2) for a range of larger diameters $D \geq 20\ mm$ of a nail, the friction coefficient μ^* can be assumed nearly constant; in the case of nail diameter $20\ mm \leq D \leq 30\ mm$ (excluding a borehole diameter filled with grout), as generally used in practice, the friction coefficients for 14/25 dense and 50/100 dense sands are extrapolated to $2 \leq \mu^* \leq 3$ from the test data given in Fig.3.15,

(3) the friction coefficient μ^* is closely related to the dilation of the soil; when there is no dilation in the sand, so that $\psi = \Delta h = 0$, then this leads to $\mu^* = 1$ or $f^* = \tan\phi_{ds}$. When the peak angle of dilation ψ_{max} is mobilized in the sand, then friction coefficient μ^* reaches a maximum (see Fig.3.16),

(4) as the thickness h of the shear zone increases, the influence of diameter D of a nail on the friction coefficient $(\mu^* - 1)$ decreases, where

$$\mu^* - 1 = \frac{2G}{\sigma_m} \frac{\Delta h}{D + h} \qquad ...(3.27)$$

This is consistent with the results of pull-out tests in Fig.3.15; for example, the ratio of $(\mu^* - 1)$ between the diameter of the nail D = 6.0 *mm* and D = 3.0 *mm* for 14/25 dense sand is estimated to be 0.85, which is greater than 0.73 and 0.78 for 50/100 dense and medium dense sands, respectively. In section 3.2.1, the thickness h of the shear zone was observed to be 4 *mm* ~ 5 *mm* larger for 14/25 dense sand than for 50/100 dense sand. From equations (3.26) and (3.27), it is also assumed that for larger nail diameters D, $(\mu^* - 1)$ is inversely proportional to the normalized diameter D / D_{50}, as shown in Fig.3.15(b).

(5) the friction coefficient μ^* increases as the normalized shear modulus G / σ_m increases; this indicates that the friction coefficient μ^* is influenced by both the strength and shear modulus of the soil.

From equation (3.26), it is hypothesized that the friction coefficient μ^* is a function of:

$$\begin{aligned} \mu^* &= fn\left(\frac{G}{\sigma_m}, \frac{h}{D}, \frac{\Delta h}{D}\right) \\ &= fn\left(\frac{G}{\sigma_m}, \frac{D_{50}}{D}, \psi\right) \end{aligned} \qquad ...(3.28)$$

where it is also assumed in equation (3.28) that the thickness h of a shear zone and the radial increase Δh of the shear zone are a function of the mean particle size D_{50} and angle of dilation ψ of the soil, respectively. Thus, the friction of a nail is dominated by several factors and also complicated to formulate theoretically. It is hoped to establish a method which gives a reasonable prediction of the maximum pull-out force F_p of a nail, without carrying out an *in - situ* pull-out test.

Theoretically, it is imagined that shearing with constant volume $\Delta h = 0$ (such as in the constant volume direct shear test) in dense sand will produce the upper limit for the friction coefficient μ^* of a nail. San and Matsui (1992) formulated the following equation for restrained dilatancy with constant volume shearing for elasto - plastic material, as

$$\frac{d\sigma_m}{d\xi} = \frac{K_s K_n \tan\phi}{K_s + K_n \tan\phi} \qquad ...(3.29)$$

where K_s and K_n are the shear and normal stiffness of the soil. From equation (3.29), for example, for a typical case of $\phi = 45°$ and the isotropic condition $K_s = K_n = K = 100\ MPa / m$ gives,

$$\frac{d\sigma_m}{d\xi} = 0.5K = 50\ (MPa/m) \qquad ...(3.30)$$

In equation (3.30), pull-out displacement $\xi = 2\ mm$ approximately gives the additional normal stress $\Delta\sigma_m = 100\ kN/m^2$, and the $\Delta\sigma_m$ considerably increases the friction force on the nail. It is also understood that the increase in the friction on a nail is especially significant when the normal stress σ_m is relatively small.

Finally, it is suggested that special care is needed when extrapolating a maximum pull-out force F_p from small scale tests to full scale tests due to the effect of the diameter D of a nail, as observed in the tests.

3.5 Results of direct shear tests of nailed sand and interface tests

Direct shear tests of nailed sand and interface tests have been considered as other possible methods for investigating the interaction mechanism between a nail and soil. The detailed descriptions of the two tests in the current research programme were given in Chapter 2. By making an assumption that the intermediate principal stress is $\sigma_2 = 0.37(\sigma_1 + \sigma_3)$ (Stroud,

1971) on a nail in a direct shear test, Jewell (1987) was able to estimate successfully an angle of bond friction δ_b of a nail, as

$$\begin{aligned} f^* &= \tan\delta_b \\ &= \frac{P_R}{\sigma_{m\theta} A_r} \\ &= \frac{A_s}{A_r(\cos\theta\tan\phi_{ps} + \sin\theta)} \frac{\tau_{EXT}}{\sigma_v} \frac{\cos^2\phi_{ps}}{0.87 + 0.50\sin\phi_{ps}\sin(\phi_{ps} + 2\theta)} \end{aligned} \qquad ...(3.31)$$

where P_R is the limiting nail force, $\sigma_{m\theta} = (\sigma_1 + \sigma_2 + \sigma_3) / 3$ is the average normal stress on a nail at an angle θ, A_s is the plan area of sand, A_r is the total surface area of a nail, σ_v is the surcharge load, θ is the angle of the nail from the vertical, τ_{EXT} is the extra shearing resistance due to a nail, and ϕ_{ps} is the plane strain friction angle of the sand. Because of different stress condition around a nail between pull-out test of a nail and direct shear test of nailed sand, a slightly different definition of f^* is used in equations (3.31) and (3.12). In deriving equation (3.31), it was also assumed that:

(1) only the friction between the nail and soil contributes to the extra resistance τ_{EXT} in the direct shear test,

(2) the bond friction δ_b of the nail is fully mobilized at the peak shear force S_{max} in the sand, and

(3) the horizontal plane in the direct shear test is the plane of maximum stress obliquity in the direct shear test.

In the tests, parameters A_r, A_s, θ, ϕ_{ps}, σ_v and τ_{EXT} in equation (3.31) are all measured.

For the interface tests between the aluminium plate and sand, the angle of bond friction δ_b is deduced, as

$$f^* = \tan\delta_b = \left(\frac{\tau_{yx}}{\sigma_v}\right)_{\max} \qquad ...(3.32)$$

where τ_{yx} is the shear stress on the central plane and σ_v is the applied vertical stress. In the direct shear test of nailed sand and the interface tests, the constant surcharge stress σ_v = 20.3 kN/m^2 was maintained during the tests. Table 3.2 summarizes the specific details and results of the direct shear tests of nailed sand.

Fig.3.19 shows the apparent friction coefficient f^* with the diameter D of the nail, together with the experimental data reported by Jewell (1980) with θ = 25° (*Test 85Y, 75Y, 86Y, 88Y* and *89Y* in his thesis) using the medium size direct shear box, and by Pedley (1990) with θ = 25° (*Test O3* and *Test O6* in the thesis) and θ = 15° (*Test O2* and *Test O5* in the thesis) using a 1 *m* cubic large direct shear test apparatus. These data from Jewell and Pedley were independently analysed by the Author using equation (3.31). The extra shearing resistances τ_{EXT} are easily calculated by comparing the data of the maximum shear forces $(P_s)_{max}$ (Jewell, 1980) and $(\sigma_v / \tau)_{max}$ (Pedley, 1990) and those of the unreinforced direct shear tests. Since Pedley (1990) used two cement - grouted nails for each test in 14/25 White Leighton Buzzard Sand (ϕ_{ps} = 46°) with nail diameters of D = 15.88 *mm* and 25.40 *mm*, the surface area of a nail A_r is doubled in equation (3.31). Jewell used a spring steel bar containing a core of 0.78 *mm* radius steel to make an "ideally stiff" nail in 14/25 Yellow Leighton Buzzard Sand (ϕ_{ps} = 54.4°). The data from Pedley in Fig. 3.19 indicate that larger apparent friction coefficients f^* are obtained for the cement - grouted nail than from the rough nails with sand simply glued to the surface and the spring nails in the direct shear tests of nailed sand. The figure also includes the range of the apparent friction coefficients f^* deduced

from the gradient of the axial stress distribution of a nail in the direct shear tests on a nailed sand (*Test S9Y* in the thesis) carried out by Jewell (1980). An estimate of the apparent friction coefficient f^* from the measured axial stresses of the nail was made from equations (1.4) and (3.31). The important features of Fig.3.19 are as follows.

(1) Both the direct shear test and the interface test exhibited much smaller apparent friction coefficients, which were observed to be $0.50 \leq f^* \leq 1.15$, than do the pull-out tests of a nail.

(2) Similarly to the pull-out test of a nail, a decrease of the apparent friction coefficient f^* was clearly observed for all the test data as the diameter D of a nail increased. For larger values of the diameter D, the apparent friction coefficient f^* is found to be smaller than the direct shear resistance tan ϕ_{ds} and even smaller than the critical state shearing resistance tanϕ_{cv} of the sands. Okamoto *et al.* (1989) conducted drained direct dynamic shear tests reinforced with several stiff - rough bars, and reported very similar results; the bond friction δ_b between soil and the bar decreased as the diameter D of a bar increased.

(3) For a smaller diameter D of a nail, such as about $D \leq 1.5$ *mm* and 5.0 *mm* for 14/25 and 50/100 sands respectively, the apparent friction coefficients f^* exceeded the direct shear resistances tan ϕ_{ds} .

(4) While an abrupt increase in the apparent friction coefficient f^* was shown at D = 4.98 *mm* in the test carried out by Jewell (1980), an average of f^* deduced from the axial stress distribution of the nail exhibited a good agreement with other experimental data, giving confidence for interpretation of the test data using equation (3.31).

(5) For a relatively small diameter D of a nail, interface tests showed the smallest apparent friction coefficient f^* among the three types of the test, producing the apparent friction

coefficient f^* = 0.69, 0.57 and 0.27 for the sand - grout surface (Pedley, 1990), sand - rough steel surface and the sand - smooth steel surface, respectively. Thus, for a range of diameter $0 \leq D \leq 10$ *mm*,

$$f^*_{pull-out} \geq f^*_{direct\ shear} \geq f^*_{interface} \qquad ...(3.33)$$

On the other hand, for geogrid material, it is reported that the interface test generally provides the friction coefficients $\mu^* = 1.0 \sim 1.1$ (Cancelli *et al.*, 1992) for sand, which are much larger than those of the stiff - rough nails. However, their result contradicts several test results (*e.g.* Palmeira and Milligan, 1989) which indicate $\mu^* \leq 1$ in interface test.

It is not totally clear why the smaller apparent friction coefficients f^* were measured in the reinforced direct shear tests and the interface tests compared with those of the pull-out tests. A possible reason for this may be that for the former two tests, the soil was more deformed and free to move with respect to the nail than in the pull-out test, where the soil surrounding a nail was in an "at rest" condition and much more restrained. This leads to both a larger shear strength for the sand and also an increased normal stress σ_m on the nail, and hence, a larger apparent friction coefficient f^* for the pull-out test. While the "restrained dilatancy effect" (Schlosser, 1982, and Yoo, 1988) is considered to be zero for the interface test, this effect may be considerable for the pull-out test. Pedley (1990) carried out direct shear tests on nailed sand at different stages of nail installation, and pointed out that greater benefit from a nail was obtained whilst the soil was dilating.

The difference in the apparent friction coefficients f^* between these three types of test raises a practical implication for the design of soil nailing. Since the active zone (or deforming zone) in the nailed slope will mobilize a smaller apparent friction coefficient f^*

than in the resistance zone, as shown in Fig.3.20, it may be unsafe to directly apply the results of peak pull-out force F_p obtained from the pull-out tests to the nail in the active or already dilated zone. From this point of view, it is safer (or more conservative) for design of soil nailing for the "restrained dilatancy effect" not to be considered or at least overestimated in evaluating the peak pull-out force F_p of a nail until further research has been made into the interaction mechanism. Practically, under present conditions, it is a good idea to connect a rigid facing wall to the nail so that the failure of a slope due to the shortage of bond friction δ_b between a nail and soil in the active zone does not take place. In such a case, the majority of friction force between soil and nail in the active zone may be borne by the facing wall (Mc Gown *et al.*, 1989, Tatsuoka, 1992), and in turn by the nail in the resistant zone. Bastick *et al.* (1989) pointed out that the ratio between the tensile force T_0 at the facing wall and the maximum tensile force T_{max} increases as the rigidity of the facing wall increases, up to $T_0 / T_{max} = 0.85$, while T_0 is zero when the facing wall is not connected to the head of a nail.

Chapter 4

Centrifuge model tests of soil nailing

4.1 Introduction to centrifuge model testing

In earth structures including nailed slopes the principal body force which governs the movement and the failure is self weight of the soil. The centrifuge test, which is a useful tool for investigating the gravity effect in earth structures, has been independently developed both in the USSR and the USA (Craig, 1983); recently Schofield (1980) caused renewed interest in the world. The biggest advantage of using centrifuge model testing is that a centrifuge can artificially make a model material heavier, so that the stress distribution and magnitude are the same in the model as in the full scale prototype. Therefore, the centrifuge test can satisfy the influence of stress dependency of friction angle ϕ and shear modulus G of the model sand and of friction between soil and a nail (Garg, 1992). Another important advantage of the centrifuge is that loading on the upper ground surface is not necessarily required to cause collapse of a given nailed slope, where the shape and location of the failure surface are strongly dominated by the boundary condition of the loading.

In the centrifuge acceleration field the magnitude α and direction θ_α of the resultant acceleration are (Fig.4.1),

$$\begin{aligned} \alpha &= R\omega^2 \\ &= Ng, \\ \theta_\alpha &= \tan^{-1}\left(\frac{Ng}{R\omega^2}\right) \end{aligned} \qquad \ldots(4.1)$$

where R and ω are the radius and the angular velocity of the centrifuge, g = 9.806 m/sec^2 is the acceleration due to the earth's gravity, and N is the ratio of the centrifuge and gravity acceleration. The influence of Coriolis' force is ignored in equation (4.1) because Coriolis' force, which is proportional to the velocity of the soil movements and acts perpendicularly to both the axis of the rotation and direction of the movements, is very small and negligible in static problems (Schofield, 1980). The error due to ignoring Coriolis' force can be, however, significant in dynamic problems. Although the Base Friction Model (Egger, 1979) can also reproduce the self weight of soil in a model by increasing a frictional stress between the model and the base plate, a centrifuge test is a more convenient and reliable way to obtain a uniform and high acceleration field in the model.

The resultant vertical stress distribution in a centrifuge model deviates from that of a linear distribution under $N = 1g$ acceleration because the centrifuge acceleration is directly proportional to the distance from the centre of the arm. Taylor (1984) showed that the deviation of the vertical stress can be minimized by assuming a representative radius $R' = R_s + h / 3$, where R_s and h are the radius of the unstressed upper surface and depth of the model, respectively. When R_s / h is less than 1 / 10, the stress error in the centrifuge is about 2%, Schofield (1980). Another error in a centrifuge test comes from the inclination of the acceleration to the pseudo - vertical direction in the model, as shown in Fig.4.2. However, when the angle $\beta = \tan^{-1} (B / R_s)$ from the vertical is small, which means that the

representative radius R' is much longer than the distance B from the centre line, the error is negligible (Stewart, 1990).

In order to provide experimental evidence with respect to scale effect, the method of "*modelling of models*" (Ovesen, 1979) is usually applied in centrifuge tests; *i.e.* two models are tested of the same prototype with different scaling factors N_i and N_j. Theoretically both results with accelerations N_i and N_j should be identical.

4.2 Review of previous research work using a centrifuge

In recent years the use of centrifuge testing of soil reinforcement has increased, and the majority of this research work has been for reinforced soil walls. In general, studies using reduced scale models are useful because parameters in the models can be much more easily controlled than those of full scale models. The drawback of reduced model tests at $1g$ is that in most cases surcharge loading has to be used to collapse the models, where the unloading stress path induced by excavation is representative of real conditions (Delmas, 1989, and Arman, 1989).

Shen *et al.* (1982) may have been the first researchers to use centrifuge techniques to investigate soil nailing. Results of their experiments showed good agreement with their proposed design method using a limit equilibrium analysis, which assumed parabolic failure surfaces in the nailed slope. Unfortunately, their experiments did not simulate the process of slope excavation. Stewart (1990) investigated the effect of nails in heavily overconsolidated kaolin using a centrifuge, and found that the mobilization of the axial force in the nail is closely related to the dissipation of negative pore water pressure induced excavating the slope. Teramoto *et al.* (1992) performed centrifugal loading tests, and showed that locations of the observed failure surfaces changed as the length of the nails was changed. A series of dynamic

centrifuge tests was conducted by Tufenkjian and Vucetic (1992). They showed the excellent stability of nailed slopes against seismic loads, and observed a two part wedge failure mechanism in the slopes.

Bolton *et al.* (1978) and Bolton *et al.* (1982) performed a number of centrifuge tests in a reinforced soil wall and their main conclusions were:

(1) the assumption of simple anchor theory, as shown in Fig.4.3, is useful for interpreting the results of the tests,

(2) the peak tension in the zone behind the lower quarter of the facing wall is smaller than predicted by Rankine's active earth pressure,

(3) even if one reinforcement breaks due to tension, the reinforced soil wall still can sustain the earth pressure as stress re-distribution occurs in the soil, and

(4) As Santamarina (1984) pointed out, the conventional trapezoidal distribution of vertical earth pressure beneath the reinforced soil block is shown to be conservative for estimating the lateral earth pressures on the facing wall.

Jaber (1989) performed centrifuge tests and showed that the bending and longitidinal rigidity and the continuity of the facing affects the stability of a reinforced soil wall in a surprising way, and suggested the following simple design method against the breakage of reinforcement based on the results of the tests, as

$$F_s = \frac{n\,T_{ult}}{\frac{1}{2}K_a \gamma H^2 S_h} \qquad ...(4.2)$$

where F_s is the calculated safety factor, n is the number of reinforcements in the cross section, T_{ult} is the tensile strength of a reinforcement, K_a is Rankine's earth pressure coefficient, H is the wall height and S_h is the horizontal spacing of a reinforcement. However,

because equation (4.2) does not take into account the shape of the failure surface and failure by pull-out of the reinforcement, limitations in applying equation (4.2) still remain.

Yoo (1988) carried out a number of centrifuge tests on reinforced soil walls, and concluded that the existing design methods for reinforced soil walls appeared to be on the safe side. He also pointed out that Dovroba's method (1963), taking account of the distribution of the horizontal displacement of the facing wall, was useful for predicting the earth pressures on the wall.

4.3 Consideration of the similarity laws for centrifuge tests

When the physical scale of a prototype is reduced in a centrifuge model, some effort should be made to satisfy a similarity law between the prototype and the model. Table 4.1 (after Craig, 1983) summarizes the principal scaling relationships assuming that the same soil is used in the centrifuge model test and the prototype test. Jaber *et al.* (1990) investigated the scale effects between a centrifuge test and a prototype test, and suggested some typical *Buckingham's* Π numbers (non - dimensional) for the geometry and stress of the centrifuge model. For the reinforcement material, Gassler (1987) suggested the following similarity law, as

$$\frac{(E_a I)_m}{(E_a I)_p} = \frac{\gamma_m}{\gamma_p}\left(\frac{1}{N}\right)^5 \qquad ...(4.3)$$

where E_aI and γ are the bending stiffness of the reinforcement and the unit weight of the soil, respectively.

Bolton (1990) suggested two typical dimensionless parameters, Ω_t and Ω_r, for breakage and pull-out of a reinforcement, as

$$\Omega_t = \frac{A_r f_c}{C}$$

$$\Omega_r = \frac{C}{A_s \sigma_v} \qquad \ldots(4.4)$$

in which C is the maximum possible tension force in the reinforcement, A_r and A_s are the cross - sectional areas of reinforcement and soil respectively, σ_v is the local vertical effective stress, and f_c is the tensile strength of the reinforcement. Ovesen (1984), as shown in Fig.4.4, employed a model geotextile in a centrifuge test in which stress and strain relationships were similar to those of the prototype. Instead of using 1 / N thickness of a geotextile where N is the centrifuge acceleration, he employed a material which had 1 / N times the strength of the prototype by weakening a gauze with chlorine.

Now consider a similarity law for stress and strain of a nail and the friction along a nail between a prototype test and a centrifuge model test. In the nail model in Fig.1.3, the shear stress $\tau(x)$ on a nail and the relative displacement $\{\xi(x) - \eta(x)\}$ between the nail and the surrounding soil is related to the interaction parameter k_i from equation (1.3), as

$$\{\tau(x)\}_p = (k_i)_p \{\xi(x) - \eta(x)\}_p$$

$$\{\tau(x)\}_m = (k_i)_m \{\xi(x) - \eta(x)\}_m \qquad \ldots(4.5)$$

where the suffixes p and m denote the prototype and centrifuge model, respectively. From equations (1.3) and (1.4),

$$\left\{\frac{d^2\xi(x)}{dx^2}\right\}_m = \left\{\frac{d\varepsilon(x)}{dx}\right\}_m = \left(\frac{2k_i}{R_a E_a}\right)_m \{\xi(x) - \eta(x)\}_m \qquad \ldots(4.6a)$$

$$\left\{\frac{d^2\xi(x)}{dx^2}\right\}_p = \left\{\frac{d\varepsilon(x)}{dx}\right\}_p = \left(\frac{2k_i}{R_a E_a}\right)_p \{\xi(x) - \eta(x)\}_p \qquad ...(4.6b)$$

For the prototype test and the centrifuge model test, the stress $\tau(x)$ and the strain $\varepsilon(x)$ of the small elements of the nail are identical, as shown in Table 4.1, namely

$$\begin{aligned} \{\tau(x)\}_m &= \{\tau(x)\}_p \\ \left\{\frac{d\varepsilon(x)}{dx}\right\}_m &= N\left\{\frac{d\varepsilon(x)}{dx}\right\}_p \end{aligned} \qquad ...(4.7)$$

where N is the centrifuge acceleration. Combining equations (4.5), (4.6) and (4.7) gives,

$$\frac{(R_a E_a)_p}{(R_a E_a)_m} = N^2 \frac{(k_i)_p}{(k_i)_m} \qquad ...(4.8)$$

When the same sand is used in both the prototype test and the centrifuge model test, equations (4.5) and (4.7) lead to:

$$(k_i)_m = N\,(k_i)_p \qquad ...(4.9)$$

Combining equations (4.8) and (4.9), then

$$\frac{(R_a E_a)_p}{(R_a E_a)_m} = N \qquad ...(4.10)$$

Taniguchi *et al.* (1987) derived the same similarity law as equation (4.10) from a different assumption by considering the equilibrium of a plane strain model of soil reinforcement in a centrifuge test. Equation (4.3) is identical to equation (4.10) for reinforcement of circular cross - section with the second moment of area of the section $I = R^4_a / 64$. The model geotextile in Fig.4.4, which Ovesen employed (1984) in the centrifuge tests, also satisfies equation (4.10) under plane strain conditions.

In the same way, assuming a simple anchor theory (Bolton *et al.*, 1982), shown in Fig.4.3, the following similarity laws on the breakage at the connection between a nail and the facing wall, and on the pull-out of a nail are easily obtained, as

$$\frac{(T_{ult})_p}{(T_{ult})_m} = N^2 \left(\frac{D_m}{D_p}\right)^2$$

$$\frac{(f^*)_p}{(f^*)_m} = N^2 \frac{D_m l_m}{D_p l_p} \qquad \text{...(4.11)}$$

where T_{ult} is the tensile strength of a nail contained in a body of soil with dimensions S_v and S_h, D and l are the diameter and length of a nail respectively, and f^* is the apparent friction coefficient for the nail defined by equation (1.2).

Concerning the rupture zone of the soil around the nail, vertical and horizontal spacings between nails of at least 7 *mm* are necessary correctly to duplicate the interaction between a nail and dense 50/100 Leighton Buzzard Sand, as shown by the radiographs in Chapter 3. Jewell (1980) and Bolton (1990) pointed out that the interference of interaction between the adjoining rupture zone in the soil provides a smaller pull-out force for a nail, and hence produces different mechanical behaviour in the reinforced soil.

The application of these similarity laws, equations (4.10) and (4.11), on the current centrifuge tests are described briefly in the following chapter. It is, however, very difficult to totally satisfy the similarity laws in a centrifuge test because not only is there a problem with the grain size of the sand, including the thickness of the shear band at failure, and the size of the model (Ovesen, 1975) but also it is almost impossible to scale down the size of reinforcement when instrumenting the reinforcement with strain gauges at relatively large accelerations. Therefore, the results of centrifuge tests should be evaluated with care and

their limitations understood and appreciated. From this point of view, as suggested by Leshchinsky (1992), the centrifuge test can be used to verify and modify the analyses which are capable of dealing with the true problem of soil reinforcement, rather than trying to simulate directly the performance of a full - scale prototype test.

Chapter 5

Centrifuge apparatus and experimental procedure

In order to investigate the mechanical behaviour and a suitable design method for nailed slopes, a total of 24 centrifuge tests was performed at the London Geotechnical Centrifuge Centre at City University. The centrifuge there has a radius R = 1.8 m to the platform and a maximum capacity of 200 kg at 200 gravities. Table 5.1 gives the mechanical details of the centrifuge facility. The design of the model nailed slopes and the main features of the centrifuge facility are described below, along with a description of the centrifuge tests and details of the sample preparation, instrumentation and test procedure.

5.1 Design of the model nailed slopes

A brief description of the scaling factor N, which is the main basis for deciding the overall dimensions of centrifuge models from the dimensions of a particular prototype test, is given below. Details of the reinforcement materials, sand and layout of the nailed slope in the centrifuge tests are also described.

5.1.1 Scaling factor N

In a centrifuge experiment it is common and often useful to compare the behaviour of the

centrifuge model with that of a corresponding prototype test. Unfortunately, there have been few publications to date describing large scale tests whose boundary and initial conditions are described in detail, and whose results are well - known and fully reliable, except for the *in - situ* tests carried out by Gassler and Gudehus (1983) in Germany. In those tests, four types of *in - situ* nailed slopes were constructed to investigate the mechanical behaviour of soil nailing. Among those four tests, *Test B* was instrumented with several earth pressure cells, inclinometers and strain gauges on the nails. The nailed slope of *Test B* was of 6 *m* height inclined at 80° to the horizontal: 5 rows and 5 columns of nails of 3 *m* and 3.5 *m* in length were placed in a uniform fine sand, which had a relative density $I_d \approx 60\%$, as shown in Fig.5.1. In *Test B*, following excavation of the soil, a facing wall was constructed by shotcrete of thickness $t \approx 100$ *mm*. The steel nails of diameter $D = 22$ *mm* were grouted into pre - drilled holes of $D_h = 55$ *mm* at each construction stage. Finally, a strip load was applied at the top of the nailed slope until failure was observed. In the current research programme *Test B* was employed as a reference prototype test for deciding the overall dimensions of the centrifuge model slopes. The *Test B* seems, in addition, to be a typical case for soil nailing in practice. A geometric scaling factor $N = 30$ was chosen in the centrifuge tests so that the diameter D of the nail was not too small in comparison with that of the sand grains, of which the mean particle size was reported $D_{50} = 0.3$ *mm* for the prototype test.

5.1.2 Sand

In general, soil nailing and reinforced soil walls are built with sandy soils because of the need to ensure the sufficient pull-out resistance between reinforcements and soil, and through lack of knowledge of the influence of excess pore water pressures and creep in clay on the structures. The standard sand used throughout the centrifuge test programme was dry Yellow

Leighton Buzzard 50/100 Sand. This is a quartz laboratory sand passing the N°50 sieve (0.21 *mm*) but retained on the N°100 sieve (0.15 *mm*). Table 5.2 and Fig.5.2 show the properties of the sand in the prototype test, and comparison of the grading curves of the sands between the prototype test and the centrifuge tests (50/100 sand), respectively. From Fig.5.2, although the sand in the prototype test had a slightly larger grain size than the model sand, it can be seen that both sands have similar grain size distributions. For the prototype tests, it was reported that the unit weight of the soil was γ_t = 15.6 kN/m^3, the measured maximum and critical state friction angles were ϕ_p = 40.5° and ϕ_{cv} = 35°, and the angle of dilatancy from direct shear tests (Gassler, 1987) were estimated by the Author to be approximately ψ = 9° ~ 12°.

The relative density of Leighton Buzzard 50/100 Sand in the centrifuge tests was measured to be about I_d = 88% ~ 93%, which is almost the same as that of the sand (I_d = 92% ~ 94%) used in the pull-out tests presented in section 2.4. The measured direct shear friction angles ϕ_{ds}, the angles of dilatancy ψ and the unit weights γ of Leighton Buzzard 50/100 Sand were found to be almost identical in the pull-out tests (in section 2.4) and the centrifuge tests. For this reason, it was assumed in the current research programme that the properties of the sand and the pull-out characteristics were the same in the centrifuge tests and the pull-out tests of stiff nails reported in Chapter 3. However, because the sand used in the centrifuge tests is different from that of the prototype test, only qualitative comparisons can be made between the results of these tests.

5.1.3 Nails and facing walls

One of the following two types of nails of circular cross section was used for the centrifuge tests.

(1) A rough - surface nail made from a stainless steel bar with a nail diameter D = 1 *mm*, and

(2) A smooth - surface nail made of stainless steel bar with a nail diameter D = 3 *mm*.

The diameter D = 1 *mm* of the rough nail does not include the thickness of the sand layers glued on the smooth nail surface, which produced an additional thickness of about ΔD = 0.7 *mm*. This means that for the rough - surface nail, the real diameter of the nail becomes D = 1.7 *mm*. In the prototype test, a nail of diameter D = 22 *mm* made from deformed steel bar and a borehole of diameter D_h = 55 *mm* filled with cement grout were used for the nails. The scaling factor N = 30 on the nail nearly satisfies the similarity law in equation (4.10) for the stress - strain of a nail in the centrifuge test of D = 1 *mm* and D_h = 1.7 *mm*, namely

$$D_m = \frac{D_p}{N} = \frac{22mm}{30} = 0.73mm$$
$$(D_h)_m = \frac{(D_h)_p}{N} = \frac{55mm}{30} = 1.83mm \qquad ...(5.1)$$

where the elastic modulus E_a of nails was the same in the centrifuge tests and the prototype test. The similarity laws in equation (4.11) for the pull-out and breakage of a nail, derived by assuming the simple anchor theory (Bolton *et al.*, 1982) are also nearly satisfied when the apparent friction coefficient f^* and the earth pressure coefficient K_a are the same in the centrifuge tests and the prototype test. Considering the similar mechanical and physical properties of these two soils, the differences of the apparent friction coefficient f^* and the earth pressure coefficient K_a between the centrifuge tests and the prototype test may not be significant.

Every nail in the centrifuge tests was equipped with a circular head plate made of steel with a diameter of 12 *mm* and thickness of 0.05 *mm*, so that the outside of the facing wall

and the nail head were firmly connected to each other during the tests. By connecting the facing wall to individual nail heads, the earth pressure and the horizontal displacement on the facing wall can be transferred to the nail, and hence, increase the axial nail force (Bastick *et al.*, 1989). The peak pull-out force F_p or the apparent friction coefficient f^* and the load - displacement curves of the dense Leighton Buzzard 50/100 Sand for the rough - steel nails and the smooth - steel nails for the corresponding diameters D of the nail were shown in sections 3.2.1 and 3.2.2, respectively. The properties of the stainless steel nail are;
yield stress $\sigma_p = 393 \times 10^3\ kN/m^2$, yield strain $\varepsilon_y = 1920 \times 10^{-6}$ and elastic modulus $E_a = 206 \times 10^6\ kN/m^2$.

In order to investigate the influence of the stiffness of the facing wall on the stability of nailed slopes, the following two types of facing walls were used to cover the whole area of the nailed slope surface. The width and height of the facing walls were 192 *mm* and 200 *mm*, respectively.

(1) A flexible facing wall made of perspex with a thickness of $t = 0.6$ *mm*, and

(2) A stiff facing wall made of perspex with a thickness of $t = 5.2$ *mm*.

In this thesis, the terms "flexible facing wall" and "stiff facing wall" are used only to distinguish two types of bending stiffness of facing walls in the centrifuge tests, and do not indicate any practical meaning. This is due to the fact that the flexibility is related to the stress and dimensions of the facing wall.

Rowe (1951) and Milligan (1974) showed that the flexibility number ρ proved very helpful in comparing the results of full - scale tests with those of model tests on retaining walls of different sizes and bending stiffnesses, where

$$\rho = \frac{H^4}{EI} \qquad ...(5.2)$$

H is the wall height (m), E is the Young's modulus of the wall (N/m^2) and I is the second moment of area per unit length of the wall (mm^4/mm). It should be noted that ρ has dimensions of m^3/kN. Because equation (5.2) was derived from a consideration of the amount of bending deformation of structural members by the earth pressures at $1g$, it can easily be extended to the centrifuge acceleration field N to:

$$\rho = N\frac{H^4}{EI} \qquad ...(5.3)$$

Assuming that Young's modulus $E = 20 \times 10^6\ kN/m^2$ (Neville, 1973) and the thickness $t = 100\ mm$ for the prototype facing wall made of shotcrete, and that $E = 3.0\ kN/mm^2$ for the walls made of perspex in the centrifuge tests, the flexibility numbers ρ for each facing wall is estimated from equation (5.3), as

$\rho = 1.555 \times 10^{-6}$: for the shotcrete facing wall of the prototype test at $1g$,

$\rho = 2.540 \times 10^{-5} \cdot N$: for the flexible facing wall of the centrifuge tests at Ng, and

$\rho = 3.901 \times 10^{-8} \cdot N$: for the stiff facing wall of the centrifuge tests at Ng

Fig.5.3 compares the flexibility numbers ρ for a range of acceleration $N = 1g$ to $80g$. When the accelerations N are smaller than $40g$, the flexibity number ρ of the prototype test is observed to lie between the stiff facing wall and the flexible facing wall in the centrifuge tests. When the acceleration N is larger than $40g$, on the contrary, both types of facing wall in the centrifuge tests show a larger flexiblity number ρ than that of the prototype test. This indicates that care is needed when comparing the behaviour of the centrifuge tests with that of the prototype in cases when more than $40g$ of acceleration was applied in the centrifuge tests.

In addition to two types of stiffness of the facing walls, some of the facing walls in the tests were also made rough by glueing sand on the smooth surfaces of the perspex, to

investigate the influence of the roughness of the facing walls on the stability of the nailed slopes. Interface tests between dense 50/100 Leighton Buzzard Sand and the rough facing wall and the smooth facing wall were carried out using the medium size direct shear box (Chapter 2) to obtain the friction angles δ_w of the facing walls. The applied vertical stresses were σ_v = 22.7 kN/m^2 and 16.2 kN/m^2. From the interface tests, it was found that:

for the smooth perspex wall : $\delta_w = 15°$, and

for the rough perspex wall : $\delta_w = 30°$.

These friction angles δ_w of the facing walls were found to be very close to those of the rough steel plate - soil and the smooth steel plate - soil values obtained in Fig.3.19. It is also worthwhile to remember that the friction angles δ_w from the interface tests were always found to be less than the direct shear friction angle ϕ_{ds}, and even than the critical state friction angle ϕ_{cv}, as shown in Chapter 3.

5.1.4 Mechanical layout and geometry of the centrifuge tests

The centrifuge container used in the tests was the plane strain strong box whose front surface is partly made from thick perspex so that the model could be viewed and photographed during and after testing. The rest of the sides of the strong box were made from thick dural, the internal dimensions of the strong box were 375 *mm* × 550 *mm* × 200 *mm*. Because the maximum acceleration applied in the tests was decided to be relatively small, N_{max} = 80*g*, the out of plane movement of the perspex as well as the dural was very small and negligible, as shown by Powrie (1986). Bransby and Smith (1973) also pointed out that with smooth side walls and a relatively wide model compared to the height, side friction does not have a significant effect on either the active earth pressure P_a or the velocity field in the active state. It was reported that the estimated decrease in total earth pressure P_a was usually

less than 5%, as presented in Fig. 5.4. In the experiment the 4 *mm* thick glass plate was placed at the front and rear faces of strong box to reduce the side friction.

Fig.5.5 and Plate 5.1 show the mechanical layout of a centrifuge test, together with the total of 9 horizontal and vertical LVDTs on the facing wall and the upper ground surface. The dimensions of every structural member were chosen to ensure that the deformations were negligible and that sufficient safety factors were maintained against the maximum design acceleration $N = 100g$.

In order to simulate the excavation procedure in the centrifuge tests, two rubber bags filled with water and supporting nearly the whole area of the facing wall were placed in front of the facing on the sand surface which was 70 *mm* above the base of the strong box. The rubber bags were made of neoprene with a thickness of 1 *mm*. Rubber bags of two different shapes were prepared for the two cases of a vertical facing wall ($\beta = 90°$ from horizontal) and an inclined facing wall ($\beta = 80°$ from horizontal). The water in the two rubber bags was slowly drained from two holes of 8 *mm* diameter located under the bags to a reservoir, situated next to the strong box, by electrically opening a solenoid valve during flight. The rubber bags were underlain by a sand bed of depth 70 *mm* and length 70 *mm* so that a base failure of the nailed slope would be observed, and influence of the base friction of the strong box was eliminated. Similarly, the upper ground surface had a length of at least 330 *mm* to ensure that the critical state failure surface at $\phi_{cv} \approx 33°$ from the horizontal could form within the strong box.

Since the rubber bags were highly flexible, they could easily follow any movements of the facing wall, while being able to provide a hydrostatic pressure on the wall with depth. The water drained from the rubber bags was passed through two tubes of 5 *mm* diameter. These tubes were firmly connected to both the valve beneath and the rubber bags and the solenoid

valve on the swing.

A horizontal LVDT gantry was tightly bolted to the mounting box and side wall of the strong box. A vertical LVDT gantry was supported by three H - beams made of dural, so that the bending of the gantry should be kept very small during the flight.

Fig.5.6 shows an overview of the cross and plane sections of the nailed slope model for the case of the inclined nailed slope ($\beta = 80°$). The dimensions of the facing wall are 200 *mm* in vertical height and 192 *mm* in width, reinforced by a total of 25 nails (5 rows and 5 columns). The geometrical dimensions of the facing wall and layout of the nails were determined by exactly reducing the prototype test, as shown in Fig.5.1, with the scaling factor of $N = 30$.

5.2 Instrumentation

During testing, data readings of the earth pressures on the facing wall, horizontal displacements of the facing wall and the vertical displacements of the upper ground surface were taken using 9 LVDTs and 5 earth pressure cells, as shown in Fig.5.6. Data acquisition and analysis were accomplished by means of personal computers, and the data were recorded on hard disk every 1 second after starting the centrifuge tests. The data were converted into engineering units and also formatted for analysis using a spreadsheet.

The horizontal displacements of the facing wall and the vertical displacements of the upper ground surface were measured using LVDTs (±5 *mm* stroke) on the central plane. In order to reduce the subsidences of the vertical LVDTs due to the self weight as the centrifuge acceleration increased, circular plates were fitted to the points of the vertical LVDTs. The earth pressures on the facing wall were measured using PS-2KA pressure cells with a diameter of 5 *mm* and thickness of 0.2 *mm*, manufactured by Kyowa Co.,ltd. The maximum

range of the pressure cells was 200 kN/m^2, with a rated output of 0.856 mV/V, and the excitation was $3V$. As the measurements of earth pressure were very sensitive to the model conditions and displacements of the facing wall, and after trying several centrifuge tests, it appeared that some data for the rough facing walls and the inclined facing walls (ß = 80°) were not fully reliable and should be abandoned. The thin electric wires from the 5 earth pressure cells to a junction box were bundled at several points and were taped to the facing wall. The junction boxes were mounted on top of the strong box , and all the wires for the LVDTs, earth pressure cells and water pressure cells were connected to the junction boxes. The draining of water from the two rubber bags was monitored using two pore water pressure transducers, which were placed at the bottom of the rubber bags before starting the centrifuge. Fairly good agreement of water levels between the two rubber bags was observed during the draining of the water, indicating that nearly the same water levels were maintained in the two rubber bags using one solenoid valve on the swing.

In all cases, calibration was carried out at $1g$ in the centrifuge laboratory using various calibration instruments to obtain the correct calibration factors taking due regard of the mounting of the transducers and the specific system into which they were wired. The calibration procedure also confirmed the accuracy of the transducers.

Finally, during some of the tests, photographic measurements of the displacement of markers placed in the sand were taken through the perspex. The position of the markers related to reference points with known co - ordinates attached to the front perspex wall were digitised using a programme entitled BIT.PAD, written by Houlsby. From the data, relative displacements between the start and end of the test were calculated, and the critical failure surfaces were determined.

5.3 Sample preparation

The method of sample preparation is described below, and the main stages are summarised diagramatically in Fig.5.7. Before preparing the sample, the internal walls of the strong box were thoroughly cleaned to remove grease or dirt, and to ensure a repeatable surface condition. The horizontal LVDT gantry, mounting box and the valve were placed in the box before sample preparation.

The first stage of sample preparation involved pluviating the 50/100 Yellow Leighton Buzzard Sand in a standard fashion, through a tube in a funnel - shaped hopper the diameter of which is 9 *mm,* held at a constant height of 0.8 *m* above the current sand surface. To obtain dense and uniform sand, Cole (1967) suggested that at least 600 *mm* of height of fall should be maintained. The rate of fall of the soil being pluviated was about 75 cm^3/min ~ 95 cm^3/min, and very homogeneous and dense samples with an average relative density I_D = 90% ~ 93% at the mid height of the slope (10 *cm* beneath the upper ground surface) were obtained by this method. Care was required to make the current sand surface as flat as possible during pluviation of the sand.

After the sand layer of 70 *mm* thickness was pluviated in the lower part of the strong box, a facing wall with 25 nails and 5 earth pressure cells was placed in the specified position on the sand layer. The nails were inserted through holes of 5 *mm* diameter in the facing wall. The small gaps of 0.2 *mm* ~ 0.3 *mm* between the facing wall and the strong box sizes were sealed by filling with grease so that the facing wall could move freely, while the sand was prevented from pouring out through the gaps. The nail heads and the facing wall were securely connected to each other using tapes. In order to prevent the facing wall from moving during the sample preparation, two wooden blocks, of which the rear surfaces were supported by the front faces of the horizontal LVDT gantry, were temporarily placed on the sand bed

and connected to the outside of the facing wall. Sand was then pluviated again in the same manner until a nailed slope of 200 *mm* vertical height was formed; markers (2 *mm* diameter) and / or thin coloured sand layers were placed in the sand adjacent to the perspex face. Some care was required during the pluviation of the sand to prevent it directly striking the nails. The upper ground surface was flattened by removing surplus sand using vacuum and a knife.

The two wooden blocks supporting the facing wall were then removed carefully so as not to disturb the nailed slope, and the two rubber bags were placed in the positions in which the wooden blocks had been located. There are two rubber bags in the tests because of the LVDTs down the middle. The bases of each rubber bag had a small circular hole with a diameter of 4 *mm*. These rubber bags were connected to two drain pipes (1/8″) located under the bags by tightening the specially shaped screws into the valves. Finally, water was poured slowly into the rubber bags until the full area of the facing wall was supported by water.

The next stage involved the setting of the vertical LVDTs and their gantries on the model sample. Two small pore water pressure cells were placed in the bottoms of the rubber bags. Two wooden blocks, which were supported at the top by a part of the vertical LVDT gantry and H - beam, were sunk in the water in the void of the rubber bags and reduced the unnecessary water volume in the rubber bags. The hollow rods of horizontal LVDTs were then fixed to the facing wall by locating the rods onto thin needles which had been firmly fixed onto the nail heads on the centre of the cross section of the facing wall. Photographs were taken through the perspex front wall of the strong box. The camera was fitted with a colour 200 ASA print film and the aperture settings were adjusted according to the light conditions.

Finally, the strong box with sand sample was moved carefully from the sample preparation room to the swing of the centrifuge. The drain tubes from the two valves located

beneath the rubber bags were connected to a solenoid valve and a reservoir on the swing, followed by again filling the whole of the draining system with water. A counter weight located on the opposite side of the swing was shifted to a position as determined by calculation, so that any out - of - balance forces were minimised during the centrifuge tests. On the swing, all the electric wires from the instrumentation were connected to the junction boxes mounted on the vertical LVDT gantry, leaving the sample ready for testing. All the signals from the instrumentation were sent to computers in the control room located next to the centrifuge room.

5.4 Test procedure

Before starting a centrifuge test, the initial displacements and pressures measured by various transducers were recorded to provide a datum, or reset to zero using the data acquisition control system.

A typical history of centrifuge acceleration and the water pressures measured at the bottom of the two rubber bags are shown in Fig.5.8. At first the centrifuge acceleration was slowly increased from 1g. The acceleration N is calculated at the point of the representative radius $R' = R_s + h / 3$, as shown in Chapter 4. During this stage all the data from the instrumentation were monitored and evaluated to check whether they showed reasonable values. After $N = 30g$ (angular velocity $\omega \approx 127$ *rpm*) was achieved, about 2 minutes after starting the test, the water in the two rubber bags was simultaneously drained slowly by opening and closing the solenoid valve repeatedly, while the acceleration was kept constant at $N = 30g$. When a collapse of the nailed slope was observed using the video camera during draining of the water, the acceleration was decreased slowly and the test was finished. When no collapse was observed after draining all the water from the rubber bags, the acceleration

was again increased gradually until the nailed slope collapsed. An acceleration of up to N_{max} = 80g was applied in the tests as the maximum acceleration in cases where no collapse was observed in the nailed slope.

After finishing the test, due to the failure of the nailed slope or achieving the maximum acceleration N_{max} = 80g, the sample was moved to the preparation room and photographs were taken again so that the failure mechanism or displacements of the nailed slope were investigated and recorded in detail. At the same time, general locations of the failure surfaces were also determined by eye observation. The post - test deformations of the nails were then observed by removing the soil carefully from the strong box to check whether breaking or permanent bending due to shearing of the soil occurred in the nails. When the sand layer glued on the nail was found to have peeled off due to wearing, or any permanent deformation was detected in a nail, such a nail was not used any more in the test series. A similar check was also made on the facing wall after completion of each test.

Chapter 6

Results of centrifuge tests of nailed slopes

A detailed description of the centrifuge test apparatus and test procedure was presented in Chapter 5. In this chapter, results concerning the behaviour of the nailed slopes in the centrifuge tests are presented. Brief comments are also made with respect to the comparison of the results between the prototype test and the centrifuge model tests. Results of stability analyses for the failure accelerations N_f using limit equilibrium theory are presented in the following chapter.

6.1 Summary of observed failure mechanisms and failure accelerations N_f

A total of 24 tests on nailed slopes without instrumentation on the nail was performed in the centrifuge. The descriptions of the tests, together with the observed failure accelerations N_f for each test, when overall failure or excessively large displacements of the nailed slope were observed during the test, are summarized in Table 6.1. In test *V20-F-S* an overall failure of the nailed slope, accompanied by a permanent deflection of the facing wall occurred during preparation of the model slope at 1*g* (gravity) acceleration. This failure may have been due to the inadequency of the total pull-out force of the nails. While in tests *V23-F-S, V7.0-R-R, V'7.0-F-R, V7.0-F-R, A18.0-R-R* and *A6.5-F-R*, the nailed slopes collapsed during draining of

the water at 30g accelerations, 8 tests (except tests *Proto - F* and *Proto - R*) did not exhibit failure of the nailed slopes after achieving the maximum applied acceleration N_{max} = 80g. Most of the tests were carried out with all of the nails placed horizontally, except for the four tests *A'6.5-R-R, A'20.0-F-S, A'20.0-R-S* and *V'7.0-F-R* in which all of the nails were placed inclined 10° downward to the horizontal in order to investigate the effect of nail angle Γ on the stability of the nailed slope. In practice, it is very common to insert the nails inclined downward at Γ = 10°~20° to the horizontal for convenience of grouting the nails.

Regarding the failure profiles of the nailed slopes in the centrifuge tests, all of the nailed slopes were observed to have collapsed due to the inadequency of the total anchorage length $\Sigma\, l_i$, or of the total available force T_{ava} of the nails beyond the failure surfaces, to resist the earth pressures on the facing wall. This unique failure mechanism is attributed to the fact that in the current centrifuge tests the nails and facing walls had sufficient material strength to resist the earth pressures, such as against the breakage of nails and bending or shear failure of the facing walls, and the only possible failure mechanism in the tests was pull-out of the nails. Since all the nail heads and the facing wall are firmly connected to each other, as shown in Chapter 5, pull-out of the nails is always accompanied by a horizontal displacement (or deflection) of the facing wall. All the observed failure surfaces passed through the toe of the facing wall, and no base failure of the nailed slopes or failure of the "*nailed soil block*" occurred, as shown in Chapter 7. From this point of view, it is necessary to assess accurately the apparent friction coefficients f^* of each nail defined in equation (1.2), in order to evaluate and analyse the pull-out failures of the nailed slopes which were observed in the centrifuge tests. However, an overall failure of the nailed slope followed by a breakage of one of the circular nail head plates, which were connected to the facing wall, occurred in test *A20.0-F-R* at N = 80g acceleration. This breakage of the nail head may be attributed to the fact that the

connection between the circular head plate and the nail was structurally the weakest place in the manufacture of the model nail.

It was commonly observed during the tests that as the centrifuge acceleration N increased, several minor curved failure surfaces developed progressively, initially from near to the facing wall, then further inside the nailed slope, followed by the collapse of the entire nailed slope. This whole collapse was accompanied by both large horizontal and vertical displacements of the facing wall and a distinctive critical (or final) failure surface, as shown in Fig.6.1 and Plate 6.1. Similarly, this tendency to progressive failure was also frequently observed during the tests of the flexible facing walls, as draining of the water in the rubber bags proceeded at the constant acceleration $N = 30g$. These observed failure mechanisms indicate that a number of possible failure surfaces should be considered in the stability analysis of nailed slopes, instead of considering a unique (or single) failure surface as is commonly assumed in the conventional design of rigid retaining walls. In other words, while Coulomb's or Rankine's earth pressure theories can provide the maximum earth pressures on the facing wall and the corresponding failure surfaces, analysis of a nailed slope requires an iterative investigation of all of the possible failure surfaces in the nailed slope during and after construction. This progressive failure mechanism observed in the tests is also consistent with the results of *in - situ* measurements of nailed slopes reported by several research workers; for example, (Schlosser, 1982) during slope excavation, and Gassler (1987) during and after slope excavation. In Fig.6.1, it may be possible to regard the observed critical failure surfaces as the velocity characteritics (Chen and Liu, 1990).

Plate 6.1 also shows a typical failure surface observed at the upper ground surface. It may be noted that the failure surface was found to be nearly two dimensional on the plane section, indicating that the influence of the wall friction between the strong box and the model sand

seems to have a negligible effect on the shape of the failure of the nailed slopes in the centrifuge tests. It should be noted, however, that this observation does not prove that the wall friction is unimportant in the current centrifuge tests, as suggested by Bransby and Smith (1975).

In spite of the relatively large shear band of h = 1 ~ 2 *cm* thickness measured in the middle and upper parts of the nailed slopes along a critical (or final) failure surface, it is interesting to note that the post - test deformation of the nails which extended beyond the failure surfaces showed no distinguishable and visible bending deformation except in test *V7.0-R-R*. In this test, excessive horizontal displacements of the facing wall, δ_h = 32 *mm* and 8 *mm* at the top and bottom of the facing wall respectively, were accidentally allowed after causing the failure of the nailed slope. An S - shaped bending deformation was produced in all of the nails in the test. These horizontal displacements δ_h of the facing wall are extremely large (the displacement ratio δ_h / H = 16%) and would not usually be allowed in practice. This result suggests that sharp bending of a nail with significant plastic deformation, and therefore the dowel force P_s in equation (1.10), in which the direction of P_s is perpendicular to the direction of a nail, can be expected only after excessive horizontal displacements δ_h have been allowed in the nailed slope. Pedley (1990) concluded that for a typical soil and nail, the maximum available shear force $(P_s)_{max}$ of the nail was less than 5% ~ 10% of the axial capacity P_p of the nail. It was observed in the centrifuge test that there was a wide shear zone along a critical failure surface, accompanying a relatively small change of velocity inside the zone. Such relatively wide failure zones were also reported in the centrifuge tests of nailed slopes by Shen *et al.* (1982) and the *in - situ* test by Gassler (1992).

Fig.6.2(a) and (b) show the critical failure surfaces of the vertical (β = 90°) and inclined (β = 80°) facing walls observed in the centrifuge tests, together with the co - ordinates (x ,

y) of the failure surfaces tabulated in the figures (unit: *cm*) when the toe of the facing wall is taken as an origin of the co - ordinate system. Since these co - ordinates of the failure surfaces were determined simply by measuring the centre points of the observed shear zone, some tests slightly deviated from smooth curves. Some tests also exhibited nearly identical failure surfaces to each other. It is easily understood from Fig.6.2 that the failure surfaces will be quite well fitted by logarithmic spirals passing through the toe of the facing wall. Davis (1968) and Chen *et al.* (1990) pointed out, from plasticity theory, that for a cohesionless soil with a plane strain friction angle $\phi \neq 0$ and unit weight $\gamma = 0$, a logarithmic spiral is a kinematically admissible failure surface in the soil. It should also be noted that the shapes and locations of these failure surfaces are very similar to one another, regardless of the length and roughness of the nails and of the flexibility and roughness of the facing walls.

The ratios of the horizontal distance w of the failure surface at the upper ground surface from the facing wall to the height H of the facing wall are observed to be:

for the vertical walls ($\beta = 90°$) : $w / H = 0.43 \sim 0.49$, and

for the inclined walls ($\beta = 80°$) : $w / H = 0.42 \sim 0.47$

These observed ratios w / H in the tests are, however, much larger than $w / H = 0.3 \sim 0.35$, which was proposed for the design of vertical reinforced soil walls based on model tests by Schlosser *et al.* (1983) and *in - situ* tests of soil nailing by Plumelle *et al.* (1989). The results of the centrifuge tests indicate that simply fixing the ratio $w / H = 0.3 \sim 0.35$ is not appropriate and also unsafe for the analysis of nailed slopes.

With regard to an angle λ of the failure surface to the horizontal at the point where the failure surface and the upper ground surface intersect, the angle

$$70° \leq \lambda \leq 80°$$

was commonly measured in the centrifuge tests. It is also seen that the observed angles λ were steeper for the vertical facing wall than the inclined facing walls. This range of angle λ observed in the tests just lies between $\lambda = 90°$ suggested by Juran *et al.* (1990) and $\lambda = 45° + \phi_{ps} / 2 = 66.5°$ where a plane strain friction angle of soil $\phi_{ps} = 43°$ was assumed (see section 6.5), suggested by Leschinsky (1991) for the analysis of soil - nailed structures. Theoretically, the angle λ should be equal to $(45° + \phi_{ps} / 2)$ or $(45° + \psi / 2)$ when the upper ground surface is assumed to be one of the principal planes of stress or incremental strain, respectively.

From Table 6.1 it is also understood that the failure accelerations N_f increase as the pull-out capacity of nails increases due to an increase in the total nail length $\Sigma\ l_i$ and the roughness (bond) of the nails, and also the slope inclination ß decreases from vertical to 80°. While the roughness δ_w of the facing wall lead to an increase in the failure acceleration N_f of the nailed slopes, the flexibility of the facing wall did not have a well defined effect on their stability. Regarding the effect of the facing wall, it is suggested that a continuous facing wall with some amount of bending and longitudinal stiffness is superior to a segmented facing wall both for the stability of nailed slopes and the reduction of overall displacements of the facing wall. This discrepancy may be owing to the fact that even the flexible facing wall in the tests had some amount of the longitidinal stiffness, as shown in Fig.5.3.

6.2 Influence of simulated excavation

In the centrifuge tests, excavation of the soil was simulated by draining of the water from two rubber bags, which were placed next to the facing wall. A typical history of the

centrifuge speed and the water pressures measured at the bases of the two rubber bags was shown in Fig.5.8. The water in the rubber bags was drained slowly and intermittently using the solenoid oparated valve while the centrifuge acceleration was maintained constant at N = 30g.

Fig.6.3(a), (b) and (c) present the results of test *V8.0-F-S*, showing the relationships between draining of the water and the elapsed time T from the beginning of the test and (a) the horizontal displacements δ_h of the facing wall, (b) vertical displacements δ_v of the upper ground surface, and (c) the horizontal earth pressures P_h on the facing wall, respectively. A similar trend in the results were observed during almost all of the centrifuge tests, apart from the magnitude of these measurements, irrespective of the roughness of the facing wall and the roughness and length of the nails. The horizontal displacements δ_h of the facing wall during the increasing acceleration from N = 1g to N = 30g were found to be nearly zero, which is due to the external support provided by the rubber bags filled with the water. From Fig.6.3, it is clearly understood that both the horizontal dispalcements δ_h of the facing wall and the vertical displacements δ_v on the upper ground surface are closely linked with the process of draining of the water, and therefore, to the earth pressures P_h on the facing wall; for example, sudden increases of those displacements and decreases of earth pressures were observed as the water was drained step - by - step. Little vertical displacement δ_v was observed during draining of the water at point 4 of the vertical LVDTs which is located at a distance of about 210 *mm* from the facing wall. On the other hand, much larger vertical displacements occured at points 1 and 2.

The decreases in earth pressures P_h on the facing wall due to draining of the water were more significant at deeper locations of the pressure cells from the upper ground surface. Indeed, a decrease in initial earth pressure of more than 55% was observed in the lower part

of the facing wall after draining the water, while the magnitude of decrease of the earth pressure was about 35% ~ 50% in the upper part of the facing wall. The sum of the earth pressures ΣP_h after draining the water was 49 kN/m^2, which is about 50% of the initial value before draining the water. Although the influence on data interpretation was very small, the pressure cells used in the tests often suffered from instantaneous fluctuations of output, as shown at 5 sec and 22 sec after starting the test in Fig.6.3(c).

It is worthwhile considering whether the stress paths of the slope excavation may cause a different behaviour in the nailed slope, especially for the failure acceleration N_f. This is not only because the mechanical properties of soil exhibit stress path dependency, but also because the generation of nail force was found to be closely related to time of the installation of the deforming soil in the reinforced direct shear tests, as reported by Pedley (1990).

The test *A*18.0-F-R*, which had exactly the same layout of the facing wall and nails as test *A18.0-F-R*, was carried out simply by increasing the acceleration from $N = 1g$ to failure, without being supported by rubber bags at any stage of the test. This allowed the facing wall of test *A*18.0-F-R* to deform against the earth pressures in a range of acceleration $1g \leq N \leq 30g$. The failure accelerations were found to be $N_f = 33g$ for test *A18.0-F-R* just after complete draining of the water, and $N_f = 24g$ for test *A*18.0-F-R*. This result indicates that although test *A-18.0-F-R*, which is supported by the rubber bags with water, exhibited a slightly larger failure acceleration N_f than that of test *A*18.0-F-R*, the two tests were not significantly different. Both types of test were, however, different from the actual sequence of construction of nailed slopes. In practice, inserting the nails and placing the facing wall are usually carried out regularly after excavation of the slope, while the nails and facing wall had already been placed in both types of centrifuge test. The difference of the construction sequences requires a careful interpretation of the measurements, as presented in section 6.5.

6.3 Horizontal displacements of the facing wall

The additional horizontal displacements of the facing wall, produced by increasing the centrifuge acceleration N after completely draining the water from the rubber bags, are described below. Fig.6.4 compares typical examples of horizontal displacements δ_h of the four types of facing walls, (stiff - smooth, stiff - rough, flexible - smooth and flexible - rough) at the different accelerations N = 30g, 60g and 80g, depending on the failure acceleration N_f of the nailed slopes. It may be seen from the figure that additional horizontal displacements δ_h of the facing walls took place as a result of simply increasing the acceleration from N = 30g. These increases of the horizontal displacements are mainly attributed to decreases in both the friction angle ϕ and the shear modulus G of the soil, and also the decrease in the apparent friction coefficient f^* of the nails, as the vertical stress σ_v of the soil increases due to the increased centrifuge acceleration N. Details of the decrease in the friction angle ϕ of the soil and of the apparent friction coefficient f^* of the nails are shown in the following chapter. For all of the centrifuge tests shown, the largest horizontal displacements were observed at the top of the facing walls, irrespective of the stiffness and roughness of the facing wall, and length and roughness of the nails. This trend of the horizontal displacements δ_h of the facing wall for nailed slopes is commonly reported in practice, for example, by Jones (1990). The deflected shapes of the flexible facing walls were found to be very similar to those of cantilever flexible sheet pile walls in which the bending of the wall plays a major role in the wall displacement, as pointed out by Bransby and Milligan (1975). The magnitude of the horizontal displacements observed in the nailed slopes was, however, much smaller than that of the cantilever flexible wall at 1g for which horizontal displacements of 4 *mm* to 15 *mm* at the top of the cantilever wall were observed for a wall height of H = 300 *mm* with 14/25 dense Leighton Buzzard Sand, as reported by Milligan (1974). Milligan used walls of

flexiblity number $\rho = 0.61 \times 10^{-6} \sim 2.97 \times 10^{-6}$ m^4/Nmm (*units*: wall height H in metres, elastic modulus E in N/mm^2 and second moment of area I in mm^4/mm) which were about 2 to 3 times stiffer than the flexible facing wall in the current centrifuge tests (see section 5.1.3). However, the cantilever flexible walls produced more than 10 times the horizontal displacements of the nailed slopes in the centrifuge tests. It is, therefore, reasonable to suggest that:

(1) In a stable nailed slope, the nails can decrease the magnitude of the horizontal displacement δ_h of the facing wall in comparision with an unreinforced slope, and

(2) the measurement of horizontal displacement δ_h at the top of the facing wall is particularly important when evaluating the overall performance and stability of a nailed slope.

Another important feature of Fig.6.4 is that some horizontal displacement occurred at the bottom of the facing walls, and these horizontal displacements were not negligible especially for the flexible facing walls. This result indicates that a nailed slope cannot be seen as a cantilever wall nor a ground anchored wall in which there is usually a point of fixity in the wall embedded in the sand. For the walls with flexible facing the horizontal displacements of the facing wall exhibited more complicated profiles than those of the stiff facing walls; that is, the horizontal displacements of the flexible facing wall consists of rotation, sliding and bulging which is due to bending of the facing walls, while the stiff facing wall only suffered the rotation and sliding. For stiff facing walls horizontal displacements δ_h of up to about 0.65 *mm* and 0.20 *mm* were observed at the top and bottom of the facing walls respectively, and a rotation of the facing wall about its toe of $\theta = 3.5 \times 10^{-3}$ *rad* was measured. For the flexible facing walls horizontal displacements δ_h at the top of the facing wall of up to 1.3 *mm* were observed in test *V8.0-F-S*, which is 0.65% of the height H of the facing wall. This horizontal

displacement ratio δ_h / H for the test *V8.0-F-S* is two to three times larger than those of *in - situ* measurements of the stable nailed slopes, as shown in Fig.1.6. That the flexible facing wall produces larger horizontal displacement δ_h than those of the stiff facing wall indicates the important role of the stiffness of the facing wall in soil nailing for restricting the overall horizontal displacements. This observation is in good agreement with the results of 1-g tests reported by Jaber (1989) and Tatsuoka (1992) for reinforced soil walls. It is imagined that these complicated components of the horizontal displacements δ_h of the facing wall, especially rotation and bulging of the facing wall, will also change the earth pressure distribution on the facing wall in different ways. A simple hydrostatic distribution of earth pressure is conventionally assumed in the design of rigid retaining walls.

It is of interest to observe how the type of the facing wall and lengths l of the nails can affect the magnitude of the horizontal displacement of the facing wall. Fig.6.5 shows the relationships between the horizontal displacements δ_h of the facing wall at the highest horizontal LVDT (at point No.1) and 4 types of the facing wall with regard to the roughness and flexibility when the length l of a nail is same, after draining of the water at an acceleration of N = 30g. In the same way, Fig.6.6 compares the horizontal displacement δ_h of the facing wall at the highest LVDT (at point No.1) at 30g acceleration with the length l of a nail, taking account of the stiffness of the facing walls. The following trends are shown in both figures.

(1) Comparing the horizontal displacements between the tests *A18.0-F-R* and *A20.0-F-R*, and between *V8.0-R-S* and *V8.5-R-S* in Fig.6.4, there is a clear tendency of the longer the nail, the smaller the overall horizontal displacements of the facing wall. Since the maximum stress level of the soil in the current centrifuge tests is small compared to the tensile strength and axial stiffness of the nails, as shown in equation (7.4), most of the

horizontal displacements of the facing wall were not caused by the elongation of the nails, but by the pull-out (slip) of the nails due to the earth pressure. It was found in Fig.3.9 and Fig.3.12 that the displacements ξ_p of the stiff nail required to mobilize the peak pull-out force F_p was inversely proportional to the length l of a nail, which suggests that the interaction parameter k_i in equation (1.3) plays an important role in the analysis of the horizontal displacement of nailed slopes. Jewell and Milligan (1989) successfully predicted the horizontal and vertical displacements of reinforced soil walls using a concept of reinforcement material stiffness J, where J is in contrast to the interaction parameter k_i for ideally in - extensible reinforcement. As shown in Fig.3.3 and Fig.3.11, the interaction parameter k_i for the smooth nail is considerably smaller than that of the rough nail, leading to a much greater horizontal displacement ξ for a smooth nail than for a rough nail for a given pull-out force F of a nail.

(2) From Fig.6.5, roughness of the facing wall does not seem to decrease the magnitude of the horizontal displacements of the facing wall, although there is a clear distinction between the stiff and flexible facing walls. Theoretically, the change of roughness should alter the stress and strain of the soil near the facing wall (Chen *et al.*, 1990), and at the same time, should alter the displacement of the facing wall and the shape of the failure surface. The reason for the discrepancy between the theory and the current centrifuge tests may be that the difference in friction between the smooth facing wall ($\delta_w \approx 15°$) and the rough facing wall ($\delta_w \approx 30°$) is not large enough to change significantly the shape of failure surface for the dense sand, as shown by the tests in Fig. 7.15 and by theory in Fig.7.16.

(3) For nailed slopes with a stiff facing wall, unlike those with a flexible wall, the displacement ratios δ_h / H are observed to be mostly in a range of 0.1% ~ 0.3%, which

range is commonly reported in practice, as shown in Fig.1.6.

(4) Therefore, from the results of the centrifuge tests, in order to minimize the horizontal displacement δ_h of the facing wall, it is recommended to increase the length l of the nails, the bond friction between soil and the nail, and bending stiffness of the facing wall. It is important to recognize that not only does an increase in the length l of a nail decrease the deformation of nailed slope due to excavation of the soil (Schlosser *et al.*, 1992), but it also decreases the overall deformation in the post - excavation condition. Early installation of nails into the slope may also be an effective way of decreasing the displacement δ_h of a facing wall caused by excavation of the slope (Pedley, 1990).

Concerning the relationship between the length l of a nail and the horizontal displacement δ_h of the facing wall, which was described in (1) above, it is interesting to look at the influence of the interface stiffness k_i estimated from the pull-out tests of a stiff - rough nail in Chapter 3. From the simple anchor theory (Bolton, 1982) in a smooth - vertical facing wall, as shown in Fig.4.3, and equations (1.3) and (3.14), equilibrium of the axial force of an individual nail - facing wall model are described, as

$$\begin{aligned} K_a \sigma_v S_v S_h &= \pi D l \tau \\ &= \pi D l k_i \delta_h \\ &= \pi D l \frac{\delta_h}{a(\sigma_v) + b(\sigma_v)\delta_h} \end{aligned} \qquad \text{...(6.1)}$$

where S_v = 3.65 *cm* and S_h = 4.00 *cm* are the vertical and horizontal spacings of the nail in the tests respectively, D = 1.7 *mm* is the diameter of the nail, K_a is Rankine's earth pressure coefficient, and τ and σ_v are the shear and vertical stresses on the nail, respectively. It should be remembered that the horizontal displacement δ_h of the facing wall is equal to the

displacement ξ of the nail in the in - extensible nail, as presented in section 3.2. Because the interface stiffness k_i is nearly proportional to the vertical stress σ_v (*i.e.* parameters a and b reduce by nearly a half when the surcharge load σ_v doubles) as observed in the pull-out curves in Fig 3.3, horizontal displacements δ_h of the facing wall calculated from equation (6.1) are almost the same over the height of the facing wall. This indicates a lateral translation of the facing wall, provided that the length l of a nail and the profile of the soil with depth are the same.

Fig.6.7 shows the results of equation (6.1) where the vertical stress σ_v = 22.7 kN/m^2 and hyperbolic parameters a = 0.022 cm^3/N and b = 0.120 cm^2/N based on the pull-out tests with the corresponding surcharge load σ_v were used, as described in section 3.3. In the analysis, three possible friction angles in the tests, ϕ = 36°, 41° and 43° were assumed, as presented in detail in section 7.2. Fig.6.7 also includes the measured horizontal displacements δ_h of the vertical facing wall at the point of the highest horizontal LVDT (No.1) in the centrifuge tests. In the figure, it is understood that both the length l of a nail and the friction angle ϕ strongly influence the displacement δ_h of the facing wall. Although the influence of the longitudinal stiffness of the facing wall was not considered in equation (6.1), it appears that relatively reasonable estimates in the centrifuge tests were made by using equation (6.1). When the length l of a nail is small, it is predicted that the displacement taking place outside of the nailed soil block is not negligible in estimating the displacement of the facing wall. It is also noticed that the effect of lengthening a nail to decrease the horizontal displacement of facing wall has a greater effect for a short nail than for a long nail.

Finally, since the vertical and horizontal spacings of nails were unchanged in the centrifuge tests, further research is needed to study whether and how the spacing of nails affect the displacement δ_h of the facing wall.

6.4 Vertical displacements of the upper ground surface

Fig.6.8 shows the results of the increments of vertical displacements (subsidence) δ_v of the upper ground surface between before and after draining the water at $N = 30g$ acceleration. The stress characteristics and the velocity characteristics with a plane strain friction angle ϕ_{ps} = 43° and an angle of dilation ψ = 15° for the ideally smooth - vertical facing wall are together shown in Fig.6.8, where theoretically those characteristics are inclined at θ_{sc} and θ_{vc} to the horizontal, respectively, where

$$\textit{stress characteristics}: \quad \theta_{sc} = 45° + \frac{\phi_{ps}}{2} = 66.5° \qquad \textit{velocity characteristics}: \quad \theta_{vc} = 45° + \frac{\psi}{2} = 52.5° \qquad \text{...(6.2)}$$

The vertical displacements observed were always largest at the point 1 of the vertical LVDTs, located 20 *mm* or 24 *mm* from the facing wall, and gradually decreased at locations of the LVDTs further away from the facing wall. While the shape of the subsidence curve on the upper ground surface was found to vary depending on the conditions of the nailed slope, these curves of the subsidence may be approximately represented as triangles or hyperbolas. As pointed out in section 6.3, it is important that there was little or no vertical displacement δ_v observed at point 4, which is located outside the zone of the velocity characteristics. Considering the very limited rupture zone of the soil ($h \approx 5$ *mm* ~ 8 *mm* for 50/100 dense sand) when a nail is pulled out, as shown by radiographs in Fig.3.8(a), it may be reasonable to assume that the strains and displacements of the nailed slope were principally determined by the amount and distribution of the displacement of the facing wall, and nails did not influence the overall displacement of the nailed slope at all. The magnitudes of displacement of the facing wall were, however, strongly influenced by both the friction and length of the

nails, as shown in Fig.6.6. Since the strain increments and the deformation of the soil behind a facing wall were found to be dominated by the deflection of the facing wall in the velocity field (Bransby and Milligan, 1975), the amount of the vertical displacements δ_v at any location x of the upper ground surface with the smooth - vertical facing wall were estimated by integrating the vertical strain increment $\dot{\varepsilon}_{yy}$ of the soil throughout the region of the velocity field (Fig.6.9), as

$$\dot{\delta}_v = \int_{y_0}^{H} \dot{\varepsilon}_{yy} dy + \frac{(\dot{\delta}_h)_{base}}{\tan\left(\frac{\pi}{4} + \frac{\psi}{2}\right)}, \qquad \dot{\varepsilon}_{yy} = \frac{dV}{dH}\cos\left(\frac{\pi}{4} + \frac{\psi}{2}\right) \qquad \text{...(6.3)}$$

where $\dot{\varepsilon}_{yy}$ is the vertical strain increment of the soil, $(\delta_h)_{base}$ is the horizontal displacement at the toe of the facing wall, dV is the velocity of point C relative to point E at a rotation angle θ of the facing wall, y_o is the vertical distance of the ß - characteristic AB from the point of upper ground surface x, and dH is the vertical distance between two ß - characteristics, CD and EF. For small angles,

$$\theta \approx \tan\theta = \frac{dV}{dH}\sin\left(\frac{\pi}{4} + \frac{\psi}{2}\right) \qquad \text{...(6.4)}$$

In equation (6.4), the magnitude of velocity V and the increments of strain at points are constant along any β line (Wroth, 1972), and these increments of the strain were determined by the velocity of the facing wall at the point where the β line meets the facing wall. Combining equations (6.3) and (6.4) gives:

$$\dot{\delta}_v = \tan\left(\frac{\pi}{4} - \frac{\psi}{2}\right)\left\{\int_{y_0}^{H}\theta(y)\,dy + (\dot{\delta}_h)_{base}\right\} \qquad ...(6.5)$$

In the analysis using equation (6.5), the following assumptions were also made that:

(1) the direction of the principal strain increment $\dot{\varepsilon}_1$ was vertical; the α and ß velocity characteristics were therefore inclined at (45° - ψ / 2) to either side of the vertical direction,

(2) the angle of dilation ψ is constant throughout the velocity field,

(3) the soil outside the velocity field is rigid, and

(4) the velocity V at the characteristic AB is compatible with the increment of the horizontal displacements $(\delta_h)_{base}$ at the toe of the facing wall; the active zone moves as a rigid block with strains concentrated into a narrow zone at the boundary (Milligan, 1984).

Fig. 6.10 compares the increments of the vertical displacements δ_v measured in the centrifuge tests and those calculations from equation (6.5). The analysis was based on the observed deflections $\theta(y)$ of the facing wall and the displacements $(\delta_h)_{base}$ during the tests, at the point 1 of the vertical LVDT. Fig.6.9 included the results of both the vertical facing walls and inclined facing walls (ß = 80°) in the centrifuge tests. For the inclined facing wall, the velocity field was assumed the same as that of the vertical wall, in which the β - characteristics was inclined at θ_{vc} = 52.5° to the horizontal. After several trials of the analysis, it was found that the calculation of deflection $\theta(y)$ at 8 to 10 points along the facing wall was sufficient to obtain good accuracy in equation (6.5). The agreement between the measured and calculated vertical displacements δ_v were to be found to be better for the smaller vertical displacements, such as for a range of $0 \le \delta_v \le 0.5$ *mm*. Larger discrepancies between these results were found for a range of 0.5 *mm* $\le \delta_v$. The differences may result from the several assumptions made in equation (6.5). Although the analysis based on equation (6.5) generally

gives larger vertical displacements δ_v than the measurements, it is surprising that reasonably good predictions, especially for the small vertical displacements, were made for the inclined facing walls as well as the vertical facing walls using the simple analysis with hand calculations. These results are also consistent with the findings of Bransby and Milligan (1975) that good predictions could be made even for the cantilever walls with a rough surface, for which the velocity characteristics should be curved near the facing wall, as shown by Houlsby and Wroth (1981). It is expected that by considering a more sophisticated velocity field in the nailed slope which takes account of the roughness and inclination of the facing wall, a more accurate analysis for the displacements of the nailed slope could be made.

6.5 Earth pressures on the facing wall

Due to the magnitude of the roughness δ_w and the complicated deflection curves of the facing wall in the centrifuge tests, as shown in sections 6.1 and 6.2, it is easily predicted that the horizontal earth pressures on the facing wall will not simply exhibit an hydrostatic distribution. Fig.6.11(a) to (d) show typical examples of distributions of the normalized earth pressure at $N = 30g$ accelerations for the four types of facing wall reinforced with rough nails of length $l = 8.0\ cm$, where

$$\frac{p}{N\gamma} = K_a^* z \qquad \text{...(6.6)}$$

In equation (6.6), p is the measured horizontal earth pressure on the facing wall, γ is the unit weight of the soil, K^*_a is the apparent earth pressure coefficient, and z is the vertical distance from the upper ground surface. Because of the sensitivity of correctly measuring the earth pressures, especially for the rough facing walls and the inclined facing walls, much of the earth pressure data provided extremely unreasonable values, and only reasonably sensible data

are shown in Fig.6.11.

In the centrifuge tests, before draining of the water at 30*g* accelerations, slightly larger magnitudes of the earth pressures were observed on the facing wall than the at rest values p_o, estimated by Jaky's formula (1944) assuming the plane strain friction angle $\phi_{ps} = 43°$, where

$$\begin{aligned} \frac{p_0}{N\gamma} &= K_0 z \\ &= (1 - \sin\phi_{ps})\, z \\ &= 0.318\, z \end{aligned} \qquad \text{...(6.7)}$$

In equation (6.7), $K_0 = 1 - \sin\phi_{ps}$ is the earth pressure coefficient at rest. The increases of the earth pressures observed at rest may be due to the fact that the rubber bags, filled with the water, tended to push the facing wall into the slope because the pressure coefficient of the water equals 1, which is about three times larger than that of the soil estimated by equation (6.7). On the other hand, after draining the water, very large decreases in the earth pressures p were observed. It was found from Fig.6.11 that the centroid of the horizontal earth pressures are located at about $n_H \cdot H = 0.55 \cdot H \sim 0.6 \cdot H$ from the top of the facing wall, which is a little higher than $n_H = 2 \cdot H / 3$ for the hydrostatic distribution, where H is the height of the facing wall. These locations of the observed centroid of the horizontal earth pressure are also slightly lower than $n_H = 0.50 \sim 0.55$ suggested by Terzaghi and Peck (1948) for a strutted wall considering a parabolic earth pressure distrubution in sand. The active earth pressures calculated by Coulomb's theory assuming a hydrostatic earth pressure distribution are together shown in Fig.6.11, where the friction angle of the soil $\phi_{ps} = 43°$, the angle of wall friction $\delta_w = 15°$ for the smooth facing wall and $\delta_w = 30°$ for the rough facing walls were assumed. It is seen that while the Coulomb earth pressure is always conservative for the lower part of the facing wall, where the earth pressure is indeed 20% ~ 50% larger than those

measured, it is not usually the case for the upper and middle parts of the facing wall. The reason that the normalized earth pressures $p / (N\gamma)$ measured at the acceleration $N = 60g$ are larger than those at $N = 30g$ is attributed to the decreased plane strain friction angle ϕ_{ps} of the soil and the wall friction δ_v due to the increased vertical stress σ_v.

In the tests, no distinct features of the influence of stiffness of the facing wall were observed with regard to the horizontal earth pressures. Ho and Rowe (1992) pointed out that when the horizontal shear force transmitted to the soil below the base of the reinforced soil is included, total earth pressures on a reinforced soil wall will become nearly equal to those calculated by Coulomb's theory. The practical implication of the results for the earth pressure is that although Coulomb's theory was found to provide generally conservative total earth pressures on the nailed slopes, individual nails at the upper and middle parts of the facing wall may suffer larger earth pressures than those calculated using Coulomb's theory. At the same time, the lowest nail does not neccesarily provide the lowest factor of safety $(F_s)_{min}$ for the pull-out and breakage of an individual nail. This indicates that:

(1) assuming hydrostatic distribution for the earth horizontal pressures produces a conservative estimate for the overall quantity of the nails for the lower part of the facing wall, and

(2) all the possible failure surfaces passing through the middle and upper parts of the facing wall should be examined to check whether the quantity of nails can provide sufficient nail forces against the horizontal earth pressures on the facing wall.

6.5 Comparison of results between the centrifuge tests and the prototype tests

It is of interest to see whether centrifuge model tests can successfully reproduce the behaviour of prototype tests. The details of the prototype test performed by Gassler (1987)

in Germany, and of the properties of the *in - situ* soil were given in sections 5.1.1 and 5.1.2. Measurements were made of the horizontal displacements and earth pressures on the facing wall during and after the excavation of the slope using inclinometers and earth pressure cells, respectively.

Fig.6.12 compares the horizontal displacements δ_h of the facing walls between the prototype test and the centrifuge tests with the rigid - rough facing wall (test *Proto-R*) and the flexible - rough facing wall (test *Proto-F*) after completely draining the water at the acceleration $N = 30g$. In the centrifuge tests, only the rough facing walls were used because the shotcrete wall in the prototype test was assumed to be rough. For the comparison of these horizontal displacements δ_h, the displacements of the prototype test are exactly scaled down by the scaling factor $1 / N = 1 / 30$ in Fig.6.12. Excluding the middle and lower parts of the facing wall, in which the horizontal displacements δ_h for the prototype test were observed to be about twice as large as those for the centrifuge tests with the stiff - rough facing wall, the agreement between the prototype and centrifuge tests are generally good. The displacement ratio for the prototype test was $\delta_h / H = 0.23\%$, which is in good agreement with those of *in - situ* measurements in Fig.1.6.

It appeared that in comparing the shapes of the horizontal wall displacements δ_h, the shotcrete wall in the prototype test is more closely modelled by the rigid facing wall than by the flexible facing wall, although the magnitude of the horizontal displacements δ_h is closer to the flexible facing wall in the centrifuge tests; the flexible facing wall in the centrifuge test showed larger curvature or bending deformation than that of the prototype facing wall. From Fig.5.3, it is easily understood that at $30g$ accelerations the flexible facing wall has a flexibility number ρ more than 100 times larger than that of the prototype test. This result may also be due to the fact that the relative density I_D of soil in prototype test is less than

the model sand, giving larger deformation than those in the centrifuge tests. In the prototype test, it is found that the shotcrete wall exhibited bending deformation as well as nearly $(\delta_h)_{base}$ = 3 *mm* of horizontal displacement at the bottom and $\theta = 1.8 \times 10^{-3}$ *rad* of rotation about its toe. The larger magnitude of the horizontal displacement observed in the middle and upper parts of the shotcrete wall in the prototype test may partly be due to the different construction sequences between the prototype test and the centrifuge tests. In the prototype test, the nails and shotcrete wall were placed regularly after excavation of the slope, while all of the nails and the facing wall had already been placed in the slopes in the centrifuge tests. Early installation of nails contributed to an increase in the nail force, and hence smaller displacement of the nailed slope (Pedley, 1990). This result leads to the advantages of a new construction technique, in which the rigid facing wall was placed in the soil before excavating the soil in order to improve the stability of the nailed slope and decrease the overall displacement of the facing wall, as reported by Tatsuoka (1992).

Fig.6.13 compares the distributions of the normalized earth pressure $K_a \cdot z = p / (N\gamma)$ defined in equation (6.7), between the centrifuge tests and the prototype test, together with the Coulomb earth pressure distribution assuming the friction angles ϕ_{ps} = 40.5° for the prototype test (Gassler, 1987) and ϕ_{ps} = 43° for the centrifuge tests. It was observed that although the total magnitude of the normalized earth pressures $p / (N\gamma)$ were different between the prototype and the centrifuge tests, the trends of the distributions of the horizontal earth pressures were similar for both in that earth pressures were observed to be less than those calculated by Coulomb's theory assuming a hydrostatic distribution with wall height. The deviations of the measured total earth pressures from Coulomb's theory are not negligible, especially for the prototype test, in which only about 50% of the Coulomb earth pressure was observed. This result is consistent with the results of the horizontal

Chapter 7

Stability analysis of the centrifuge tests

In the previous chapter the results of the centrifuge tests were presented along with a comparison of behaviour between the centrifuge model tests and the prototype test. The data of the failure accelerations N_f of the nailed slopes are now compared with the results of a conventional limit equilibrium analysis based on the observed failure mechanisms in the tests, with the objective of investigating the appropriate design procedure for soil nailing. Some comments are also made with respect to the maximum horizontal earth pressure coefficients and the different failure mechanisms proposed by other researchers for the design of soil nailing and reinforced soil walls.

7.1 Limit equilibrium analysis of nailed slopes

Compared to the finite element analysis, which is probably the most sophisticated analytical method at present, there are some advantages in conventional limit equilibrium analyses, such as the simplicity and familiarity of the theory and calculations, simplicity of obtaining the input design parameters, and a great deal of accumulated data and experience, Leshchinsky (1992). At the same time, a common belief is that limit equilibrium analyses for soil nailing and reinforced soil walls tends to provide conservative designs, *e.g.* Pang (1990) and Schlosser and Juran (1983). In a limit equilibrium analysis, the stability of nailed slopes is commonly estimated from the following two kinds of factors of safety F_s ;

$$F_s = \frac{available\ stress}{required\ stress} \qquad ...(7.1)$$

$$F_s = \frac{total\ available\ force}{total\ required\ force} \qquad ...(7.2)$$

In general, the factor of safety F_s for pull-out and breakage of an individual nail are analysed using equation (7.1), while for the failure of the whole nailed slope or the overall stability, F_s is given by equation (7.2). Tatsuoka (1992) classified the analyses of reinforced soil walls into two categories:

(1) the simple anchor theory (Bolton *et al.*, 1982) and the Rankine theory (Lee *et al.*, 1973) based on equation (7.1) are called the "lower bound solution", and

(2) the overall stability analysis proposed by Jaber (1989) and Gassler (1988) based on equation (7.2) is called the "upper bound solution".

When the total available force is expected only from the nail forces, equation (7.2) becomes identical to the following definition of the factor of safety F_s introduced by Stocker *et al.* (1979), Jewell (1990) and Leschinsky (1992):

$$F_s = \frac{total\ available\ nail\ force}{total\ required\ nail\ force} = \frac{T_{ava}}{T_{req}} \qquad ...(7.3)$$

The contribution of the shear resistance of the soil is implicitly included in the total required nail force T_{req} in equation (7.3). In the centrifuge tests performed in the current research programme, limit equilibrium analysis using equation (7.2) or (7.3) is the only appropriate method because the facing walls had sufficient longitidinal and bending strength to prevent the failure of the nailed slopes, and neither pull-out nor breakage of individual nails was

observed. In other words, among several limit modes of failure of reinforced soil structures (Jones, 1993), pull-out of nails (mode 4) was dominant in the tests. These observations in the centrifuge tests were consistent with several previous research works which pointed out that the stiff facing walls improve the overall performance of nailed slopes, as shown in Chapter 1. As described in section 6.1, the development of several failure surfaces progressively from near the facing wall to the inside of the nailed slope during the centrifuge tests suggest that the most critical failure surface which should have the smallest factor of safety $(F_s)_{min}$ is found to be among many possible failure surfaces. This leads to the need for a number of calculations for the stability analysis of nailed slopes to investigate the minimum factor of safety $(F_s)_{min}$ of a given slope, instead of simply determining a unique (or a single) failure surface which produces the maximum total required force $(T_{req})_{max}$ as in the conventional analysis of rigid retaining walls.

It is important that the shapes of observed failure surfaces in the centrifuge tests were quite precisely represented by logarithmic spirals, passing through the toe of the nailed slope to the upper ground surface, as shown in Fig.6.2. The logarithmic spiral was also found to be a suitable failure mechanism for nailed slopes (Juran *et al.*, 1990) and reinforced soil walls (Leschinsky, 1992), assuming the failure zone as a quasi - rigid and incompressible block. When passing through the toe A of the nailed slope, the shape of a logarithmic spiral is fully determined by providing a combination of two variables of the failure surface; angles (θ_o , θ_f), radii (r_o , r_f) or location of pole O (X_c , Y_c), in Fig.7.1. The advantage of a logarithmic spiral in the analysis is that the direction of the reaction force R is known, acting through the pole O of the spiral.

7.2 Friction angles of soil and apparent friction coefficients for a nail

Any limit equilibrium analysis for soil nailing requires correct estimates of the friction angle ϕ of the soil and the peak pull-out resistance F_p of each nail. This is because in equation (7.2) or (7.3), the total required nail force T_{req} is directly related to the plane strain friction angle ϕ of the soil, and the total available nail force T_{ava} to the peak pull-out resistance F_p or the apparent friction coefficient f^* of each nail. It must be remembered that the amount of apparent friction coefficient f^* is also closely related to the direct shear friction angle ϕ_{ds}, and hence to the plane strain friction angle ϕ_{ps} of the soil, as shown in section 3.4.

Although the stress - strain relationship (or pull-out force F and pull-out displacement ξ) of a nail cannot be explicitly considered in a limit equilibrium analysis, it is worthwhile investigating the mobilization of both the friction angle of the soil and of the pull-out force of a nail in the current centrifuge tests. Fig.7.2 shows the relationships between the pull-out displacement ξ of the stiff - rough nails (or the shear displacement of soil in the direct shear test), and the mobilized friction coefficient $(\mu^*)_{mob}$ for dense 50/100 Leighton Buzzard Sand estimated from tests *R1-1, R1-10* and *R1-11* in Fig.3.3(a) and equation (3.12), where $(\mu^*)_{mob}$ has been defined in section 3.4, as

$$\mu^*_{mob} = \frac{f^*_{mob}}{\tan(\phi_{ds})_{mob}} \qquad ...(3.22)$$

The diameter of the nails was D = 1.7 *mm* including the thickness of sand layers glued onto the nail, surcharge loads are σ_v = 5.6 kN/m^2 and 22.7 kN/m^2, and the lengths of nail are l = 200 *mm* and 90 *mm*. Excluding the early stages of horizontal pull-out displacements of a nail, 0 *mm* $\leq \xi \leq$ 1.0 *mm*, the mobilizations of the friction coefficient $(\mu^*)_{mob}$ are fairly constant throughout the tests regardless of the surcharge loads σ_v and the lengths l of nail. Decreases

in $(\mu^*)_{mob}$ of less than 10% were observed for a range of the displacements of 1.0 *mm* $\leq \xi \leq$ 4.0 *mm*. This result indicates that compatibility of the mobilization of the friction between the stiff-rough nail and the friction angle of soil is nearly satisfied, including the peak conditions, except for the initial stages. This compatibility is due to the fact that, for a relatively low axial force in a stiff nail, the direction of the nail is nearly the direction of zero - extension, as shown in Chapter 3.

The compatibility of mobilization of an axial force of the nail and the friction angle of soil is also affected by the axial extension of a nail caused by the increased axial tensile force due to the increased centrifuge acceleration N. In section 3.3, it was clearly observed that the extensibility of a nail has a remarkable effect on the responses of both peak pull-out force F_p and the displacememt ξ_p of the nail required to mobilize the peak pull-out force F_p. The maximum extension Δl at the head of the lowest nail at the centrifuge acceleration $N = 80g$ for the test *V23.0-F-S* is, for example, estimated assuming the simple anchor theory in Fig.4.3 (Bolton *et al.*, 1982) and the constant shear stress τ along a nail, as

$$\begin{aligned} \Delta l &= \frac{p l}{2 E_a A} \\ &= \frac{2 K_a \gamma N H^2 l}{E_a \pi D^2} \\ &= 2.5 \cdot 10^{-4} \cdot l \quad (\textit{unit: mm}) \end{aligned} \qquad \ldots(7.4)$$

where p is Rankine's active earth pressure at the base of the facing wall with the friction angle $\phi_{ps} = 43°$, E_a and A are the elastic modulus and the area of cross section of the nail, and l is the total length of the nail. In equation (7.4), a nail length of $l = 23$ *cm* produces the extension of the nail $\Delta l = 0.05$ *mm*, which is only 2 ~ 3% of the shear displacement $\xi_p \simeq 2$ *mm* required to mobilize the peak pull-out force F_p and the direct shear friction angle ϕ_{ds} of

the soil, as shown in Fig.3.3(a). Therefore, it is reasonable to assume that the nails used in the current centrifuge tests are assumed in - extensible in the given range of horizontal earth pressures, and also nearly satisfy the compatibility of the peak forces between the nail and the soil.

As already described, the relative density of the 50/100 Leighton Buzzard Sand used in the centrifuge tests was found to be I_d = 88% ~ 93%, which is very close to that of the 50/100 dense sand ($I_d \approx 93\%$) in the pull-out tests of nails, as shown in Chapter 2. It is therefore reasonable in the following analysis of the centrifuge tests to adopt the same friction angle ϕ and the apparent friction coefficient f^* deduced from the direct shear tests of sand and the pull-out tests of nails in 50/100 dense sand in Fig.3.3(a). In the estimates of the friction angle ϕ and the apparent friction coefficient f^*, however, attention should be paid to the influence of vertical stress σ_v on the friction angle ϕ and the apparent friction coefficient f^* because in the case of centrifuge acceleration N, the change of the vertical stress $\Delta\sigma_v$ with depth in the soil is N times larger than that of the model at $N = 1g$ acceleration. While the range of the vertical stress σ_v at $N = 80g$ acceleration was $0\ kN/m^2 \le \sigma_v \le 270\ kN/m^2$ at the upper ground surface and at the bottom of the nailed slope respectively, the vertical stress σ_v was limited to a maximum of about $\sigma_v = 55\ kN/m^2$ in the medium size direct shear box. For this reason, the standard Casagrande shear box was used to apply up to $\sigma_v = 150\ kN/m^2$ on the sand, as shown in Fig.7.3. Fig.7.3 also includes the direct shear results of 14/25 Yellow and White dense sands reported by Pedley (1990) and the plane strain friction angle ϕ_{ps} of 50/100 dense sand estimated from a flow rule from the Mohr's circle using equation (2.4) and measured direct shear friction angle ϕ_{ds} and dilation angle ψ for the soil. It is noticeable that the vertical stress dependency of the direct shear friction angle ϕ_{ds} of the 50/100 dense sand comes between those of 14/25 Yellow and White dense sands, and the influence of the

vertical stress cannot be negligible in the limit equilibrium analysis. Therefore, rather than assuming a single value of the friction angle ϕ for the 50/100 sand in the analysis, a range of friction angle ϕ which bounds the upper and lower values of ϕ was determined. Since the observed failure surfaces in the tests correspond to the velocity characteristics, using the direct shear friction angle ϕ_{ds} is appropriate in the analysis. The average vertical stresses $(\sigma_v)_{ave}$ in the middle height of the nailed slope (z = 10 cm) is 50 $kN/m^2 \leq (\sigma_v)_{ave} \leq$ 140 kN/m^2 at N = 30g to 80g accelerations, which gave approximately the friction angle $36° \leq \phi_{ds} \leq 38°$ from Fig.7.3. In the direct shear tests performed in section 2.4, in the same way, the typical direction of principal stress σ_1 was reported $\chi = 30° \sim 40°$ from the horizontal bedding plane (Dyer, 1986), and hence the measured friction angle exhibited the smallest friction angle in the sand. Tatsuoka (1987) reported that a plane strain friction angle ϕ_{ps} more than 10% larger was obtained when the direction of principal stress σ_1 was vertical to the bedding plane ($\chi = 90°$) in Toyoura Sand, as shown in Fig.7.4. In the soil in which the bedding plane is horizontal, the direction χ of the principal stress σ_1 can be estimated approximately from Fig.7.5, as

$$\chi_i = \frac{\pi}{4} + \alpha_i - \frac{\phi_{\chi i}}{2} \qquad ...(7.5)$$

where $\phi_{\chi i}$ is the friction angle of the soil taking into account the direction χ_i of the principal stress σ_1, and α_i is the angle of the failure surface to the horizontal. From the observed failure surfaces in the tests, the mean direction of the principal stress σ_1 is estimated to be approximately $\chi = 75° \sim 80°$ from horizontal, assuming $\phi_{\chi i} = 43°$ for the soil. Fig.7.5 shows the relationship between $\phi_{\chi i}$ and χ reported from Meyerhof (1978) for several different kinds of sands. The figure indicates that for a range of direction $60° \leq \chi \leq 90°$, the friction angles $\phi_{\chi i}$ are almost constant, and for a range of $0° \leq \chi \leq 60°$, $\phi_{\chi i}$ gradually decrease to 86% of

those for $\chi = 90°$. This effect of anisotropy increases the friction angles to $41° \leq \phi_{ds} \leq 44°$ in the case of $\chi = 90°$.

On the other hand, a progressive failure mechanism, as presented in section 6.1, which produces non - uniform mobilization of the friction angle ϕ along the failure surfaces makes the determination of a unique ϕ very difficult. As McGown *et al.* (1989) suggested, it is highly unlikely that the peak strength condition will occur simultaneously in all of the soil along the failure surface. The horizontal displacements and the deflections of facing walls observed in the centrifuge tests, Fig.6.4, suggested that the shear strains of the soil near the toe of the flexible facing walls were different from those of the upper parts of the facing wall where the critical state friction angle $\phi_{cv} = 33° \sim 36°$ (Bolton, 1986) may be mobilized. Considering these influences of vertical stress dependency, strength anisotropy and the progressive failure on the friction angle ϕ of the soil, a range of friction angles $36° \leq \phi_{ds} \leq 41°$ was finally determined for the following limit equilibrium analysis of the centrifuge tests. On the other hand, the plane strain friction angle of 50/100 dense sand for the corresponding surcharge load σ_v is $38° \leq \phi_{ps} \leq 42°$, which is slightly larger than the range of direct shear friction angle ϕ_{ds}.

As with the direct shear tests, there is also an absence of pull-out test data for the stiff - rough nails over a range of the applied vertical stress $\sigma_v \geq 50\ kN/m^2$. The apparent friction coefficient f^* of a nail was, therefore, deduced by extrapolating the results of pull-out tests in Chapter 3 proportionally, up to the vertical stress $\sigma_v = 200\ kN/m^2$ from the results of the direct shear tests of the sand, as shown in Fig.7.3. The relationships between the apparent friction coefficient f^* and the vertical stress σ_v are determined from Fig.7.3, as

for 0 $kN/m^2 \le \sigma_v \le 75\ kN/m^2$,

$$\begin{aligned} \textit{Rough nails:}\ f^* &= 2.80 - 2.80 \cdot 10^{-3} \cdot \sigma_v \\ \textit{Smooth nails:}\ f^* &= 0.26 - 2.60 \cdot 10^{-4} \cdot \sigma_v \end{aligned} \qquad \text{...(7.6a)}$$

and for 75 $kN/m^2 \le \sigma_v \le 250\ kN/m^2$,

$$\begin{aligned} \textit{Rough nails:}\ f^* &= 2.59 - 1.77 \cdot 10^{-3} \cdot (\sigma_v - 75) \\ \textit{Smooth nails:}\ f^* &= 0.24 - 2.57 \cdot 10^{-4} \cdot (\sigma_v - 75) \end{aligned} \qquad \text{...(7.6b)}$$

The basis of these extrapolations for the apparent friction coefficient f^* from the direct shear test data is the very close similarity between the mobilizations of f^* for the stiff - rough nails and the direct shear friction angle ϕ_{ds} of the sand, as was shown in Fig.3.3(a). For the stiff - smooth nails, the apparent friction coefficients f^* were also found to agree well with the results of the interface tests as discussed in section 3.5. In the following limit equilibrium analysis, the apparent friction coefficient f^* of each nail at the different elevations is easily deduced from Fig.7.3 or equations (7.6a) and (7.6b), depending on the current vertical stress σ_v on the nail,

$$\sigma_v = N \gamma z \qquad \text{...(7.7)}$$

where z is the depth of a nail from the upper ground surface, N is the centrifuge acceleration and γ is the unit weight of the soil.

7.3 Required force T_{req} and available force T_{ava} for the stability analysis of nailed slopes

The methodology of calculation for the total required force T_{req} and the total available force T_{ava} in equation (7.2) or (7.3) will now be discussed. Results of the external stability

analysis against horizontal sliding and the rotation about the toe A of the "*nailed soil block*", where the length of the nail l = 6.5 *cm* for the inclined wall (β = 80°) and l = 7.0 *cm* for the vertical wall, the lower friction angle ϕ = 36° (see section 7.2) and a range of the friction angle of the facing wall $0° \leq \delta_w \leq 35°$ were assumed. These analytical procedures for the "*nailed soil block*" are exactly the same as those of conventional rigid retaining walls with Coulomb's earth pressure force acting at one third of the height H of the facing wall from the base of the facing wall. As shown in Fig.7.6, the smallest factors of safety are obtained as F_s = 1.40 and F_s = 1.99 against rotation and sliding of the block respectively, when the roughness of the facing wall is δ_w = 0° at the worst case. It is, therefore, suggested that the "*nailed soil block*" had sufficient factors of safety against rotation and sliding, and hence the external failure of the "*nailed soil block*" did not occur in the current centrifuge tests. This result for external stability of the "*nailed soil block*" is consistent with the observed failure mechanisms in the centrifuge tests.

7.3.1 Total required force T_{req}

As described in Chapter 6.1 the observed failure surfaces coincide very well with logarithmic spirals passing from the toe of the facing wall. The general equation of a logarithmic spiral is

$$r = r_0 \exp(\theta \tan\phi) \qquad ...(7.8)$$

where r is the radius, r_0 is the radius at θ = 0°, and θ is the angle between r_0 and r. The derivation of the equation of the logarithmic spiral from the observed failure surface in the centrifuge tests was carried out by at first finding the pole O by trial - and - error, as shown in Fig.7.7, where there is a convenient relationship,

$$\tan\phi = \frac{1}{\tan\omega} \qquad ...(7.9)$$

It was pointed out that the agreement between the observed failure surface and the theoretical one depends very much on the accuracy of locating the position of the pole O of the logarithmic spirals (Jumikis, 1964). After specifying the several locations of poles O, which automatically determined the radius r_f and angle θ_f in Fig.7.7, the most suitable logarithmic spiral was determined by comparing many constructed spirals and the observed failure surfaces in the centrifuge tests.

For the given slope geometry and the logarithmic spiral failure surface in Fig.7.7, the weight W of the soil mass of the failure zone per unit width (b = 1 cm) is calculated, as

$$\begin{aligned} W &= \gamma \int_{\theta_0}^{\theta_f} dA - W_{OABC} \\ &= \gamma \int_{\theta_0}^{\theta_f} \frac{r^2}{2} d\theta - W_{OABC} \\ &= \gamma \left\{ \frac{(r_1^2 - r_0^2)}{4\tan\phi} - \frac{r_0^2 \sin(\theta_f - \theta_0)\sin\theta_0 + H^2 \sin(\theta_f + \beta)}{2\sin\theta_f} \right\} \end{aligned} \qquad ...(7.10)$$

where dA is the area of a slice of the logarithmic spiral and W_{OABC} is the weight of the imaginary block $OABC$ assuming the same unit weight γ as the soil in the slope. The moment M_w of the soil mass in the failure zone about the pole O per unit width is calculated, as

$$\begin{aligned} M_w &= \gamma \int_{\theta_0}^{\theta_f} \rho\, dA - \kappa W_{OABC} \\ &= \frac{\gamma}{3} \int_{\theta_0}^{\theta_f} r^3 \cos\theta\, d\theta - \kappa W_{OABC} \end{aligned} \qquad ...(7.11)$$

where ρ and κ are the distances of the area of the centroid of dA and $OABC$, respectively.

Equation (7.11) leads to:

$$M_W = \gamma (M_{W1} + M_{W2} + M_{W3})$$

$$M_{W1} = \frac{1}{3(1 + 9\tan\phi)} \{r_f^3(\sin\theta_f + 3\tan\phi\cos\theta_f) - r_o^3(\sin\theta_0 + 3\tan\phi\cos\theta_0)\}$$

$$M_{W2} = -\frac{r_0^3}{6}\frac{\sin(\theta_f - \sin\theta_0)}{\sin\theta_f}\sin\theta_0\left(\frac{\sin\theta_0}{\tan\theta_f} + \cos\theta_0\right) \qquad ...(7.12)$$

$$M_{W3} = -\frac{H^2}{2}r_0\frac{\sin(\theta_0 + \beta)}{\sin\theta_f}\frac{\sin\theta_0}{\tan\theta_f} - \frac{H^3}{6}\frac{\sin(\theta_f + \beta)}{\sin\theta_f}\left\{\frac{2\sin(\theta_f + \beta)}{\sin\theta_f} - \frac{1}{\tan\beta}\right\}$$

where H is the height of the slope and ß is the angle of the slope from the horizontal. The centre of the centroid ρ_x from the pole O of the logarithmic spiral failure surface is then given by,

$$\rho_x = \frac{M_W}{W} \qquad ...(7.13)$$

As the directions of the total reaction force R on the failure surface and the location and amount of the weight W of the soil mass are already known, the total required force T_{req} which is necessary to stabilize the slope in the limit equilibrium state is calculated using the force polygon (Fig.7.8), as

$$T_{req} = -W\frac{\sin(\beta + \delta_w)\cos\Xi}{\cos(\Xi + \beta + \delta_w)} \qquad ...(7.14)$$

where Ξ is the angle of the total reaction force R from the horizontal in the force polygon, and given as,

$$\Xi = \tan^{-1}\left(\frac{A_1 A_2}{W}\right)$$

$$A_1 = r_0 \sin\theta_0 + n_H H \qquad \text{...(7.15)}$$

$$A_2 = W - \frac{r_0\left\{\cos\theta_0 - \dfrac{\sin(\theta_f - \theta_0)}{\sin\theta_f}\right\} - \dfrac{n_H H}{\tan\beta}}{\tan(\beta + \delta_w)}$$

in which $n_H \cdot H$ is the depth of the centroid of the total required force T_{req} from the upper ground surface ($0 < n_H < 1$) and δ_w is the friction angle between the facing wall and soil.

The comparisons of the maximum total required force T_{req} calculated by equation (7.14) and those calculated by other conventional earth pressure theories will be shown in the following section, where very good agreements for those forces are obtained.

It was observed from the results of the centrifuge tests that although the location $n_H H$ of the centroid of the total required force T_{req} from the top of the facing wall was not constant for each test, it seems generally to be located between $n_H H = 0.6H$ to $2H / 3$ from the top of the facing wall, which is slightly higher than for the hydrostatic distribution, $n_H = 2 / 3$. Fig.7.9 (a) and (b) show typical examples of the influence of the location of the centroid n_H on the total required force T_{req} with the roughness δ_w of the facing wall, for tests *A'6.5-R-R* at acceleration $N = 45g$ and *V'7.0-F-R* at $N = 30g$. The calculations of the total required force T_{req} are based on the observed failure surfaces in the centrifuge tests, which can be seen in Fig.6.2. The width of the slope was taken as the horizontal spacing of the nail $b = 4$ *cm*, and the plane strain friction angles of the soil were $\phi = 36°$ and $41°$. It is clear from Fig.7.9 that the difference in the total required force T_{req} between $n_H = 2 / 3$ and $n_H = 0.6$ is small, and is less than 5 per cent for a range of the facing wall friction $15° \leq \delta_w \leq 30°$.

These results conform well with those of the earth pressure coefficient for braced walls in sand with a logarithmic failure surface, Kim and Preber (1969). There is a clear tendency that as the friction angle ϕ decreases and the roughness δ_w of the facing wall increases, the difference in the total required forces T_{req} between n_H = 2 / 3 and n_H = 0.6 is increased. In the following analysis, therefore, it was decided to assume the location of the centroid n_H = 2 / 3, which is also compatible with the conventional design of retaining walls as well as reinforced soil walls and nailed slopes, by the considerations of similarity of the total required force T_{req} with depth, Jewell (1990).

Finally, although the roughnesses of the facing walls were determined to be δ_w = 15° and 30° for the smooth and rough facing walls respectively from the interface tests, uncertainty still remains as to whether these wall angles δ_w correspond to those of facing walls including several stiff - rough nails.

7.3.2 Total Available force T_{ava}

In equation (7.2) or (7.3), the total available force T_{ava} is determined from the total pull-out force of the nails beyond the failure surface (or in the resistance zone), as

$$\begin{aligned} T_{ava} &= \sum_i T_i l_i \\ &= \sum_i \pi D_i l_i (\sigma_m)_i f_i^* \end{aligned} \qquad \text{...(7.16)}$$

in which T_i is the maximum pull-out resistance per unit length of a nail, l_i is the length of a nail beyond the failure surface, D is the diameter of a nail including the additional thickness of the sand layers, and σ_m is the mean normal stress on a nail. The axial force in a nail generated by the interaction between soil and the nail located inside the failure surface (or in

the active zone) are usually ignored in the analysis because such nail forces are considered as an internal force in the equilibrium of the soil mass. Equation (7.16) is based on the conclusion of the pull-out tests from a nail in section 3.2.1 that, for a stiff nail, the peak pull-out force F_p is almost proportional to the length l of a nail. The apparent friction coefficient f^* is not, however, observed to be constant as the vertical stress σ_v increases. The mean normal stress σ_m on the nail is approximately estimated using Jaky's formula (1944) and equation (3.12) with the plane strain friction angle $\phi_{ps} = 43°$, as

$$\sigma_m = \frac{(1 + K_0)\,\sigma_v}{2} = 0.659\,\sigma_v \qquad ...(7.17)$$

where the vertical stress σ_v in a given acceleration N is estimated using equation (7.7). Since the constant of 0.659 in equation (7.17) is consistent with the estimates of the apparent friction coefficient f^* from the pull-out tests in Fig.7.3, in which a range of friction angle $36° \le \phi \le 41°$ was assumed, it is not necessary to take into account the cases of the lower and upper friction angles $\phi = 36°$ and $41°$ in the analysis using equation (7.17).

7.4 Prediction of failure accelerations N_f from the limit equilibrium analysis

Equations for the factor of safety F_s for the overall failure of the nailed slopes were given in (7.3), (7.6), (7.7), (7.14), (7.16) and (7.17). In the following limit equilibrium analyses, to summarize, the following assumptions were finally made.

(1) Friction angles of the soil are $\phi = 36°$ and $41°$, for the lower and upper bounds, respectively.

(2) Location of the centroid of total required force T_{req} is two thirds of the height H of the facing wall from the upper ground surface ($n_H = 2 / 3$).

(3) Angles of the roughness of facing walls are δ_w = 15° and 30° for the smooth and rough facing walls, respectively.

(4) Apparent friction coefficients f^* for the smooth and rough nails for the corresponding vertical stress σ_v are estimated from Fig.7.3, or equations (7.6a) and (7.6b).

(5) Orientation of the nail is horizontal.

Concerning the assumption (5) above, there was little influence of the orientation of nail observed in the centrifuge tests, as shown in section 6.1. Further, it is also seen from Fig.1.2(b) that the difference of the normalized strain increments $\dot{\varepsilon}_s$ / $(\dot{\gamma}/2)$ along a nail is negligible (less than 7%) between nail directions Γ = 0° and 10° from the horizontal when the angle of dilation ψ = 20° and the angle of failure surface θ = 50° ~ 60° from the horizontal were assumed. This result with regard to the inclination of the nail is also consistent with the results of model tests and finite element analyses reported by Leschinsky (1992), which indicated that the inclination of reinforcement has a negligible influence on the stability of steep cohesionless slopes.

The calculated factors of safety F_s are now compared with the failure accelerations N_f observed in the centrifuge tests. Fig.7.10(a) and (g) show the relationships between the centrifuge accelerations N from 30g to 80g and the total required forces T_{req} per width of the horizontal spacing of a nail (b = 4 cm) for friction angles ϕ = 36° and 41° (shown by two dotted lines, calculated from equation (7.14)), and the total available forces T_{ava} (shown by dotted lines with open square, calculated from equation (7.16)). These calculations of the required forces T_{req} and the available forces T_{ava} in Fig.7.10 were based on the failure surfaces observed in the centrifuge tests. It is important to recognize that these forces T_{req} and T_{ava}, and the calculated factor of safety F_s do not necessarily correspond to those of the minimum factor of safety $(F_s)_{min}$ in the given nailed slopes. On the other hand, the iterative

calculations for a total of 7 tests were required to obtain the minimum factors of safety $(F_s)_{min}$ and the corresponding forces T_{req} and T_{ava}, where in those tests failures of the nailed slopes did not occur even after achieving 80g acceleration. These iterations were carried out by changing the location of the pole O of the logarithmic spiral, by vertical and horizontal intervals of 1 cm in Fig.7.8, until the minimum factor of safety $(F_s)_{min}$ for each nailed slope was found. Table 7.1 shows the details of the failure surfaces (radius r_0, angle θ_0, and co - ordinate of pole O (X_c, Y_c)) observed or analyzed in the centrifuge tests. While the total required force T_{req} increased proportionally to the acceleration N in Fig.7.10, the total available force T_{ava} did not increase in the same manner because of the vertical stress dependency of the apparent friction coefficient f^*. Fig.7.10 also shows the three kinds of factors of safety F_s (shown by two lines for $(F_s)_{36}$ and $(F_s)_{41}$, as well as a heavy line for $(F_s)_{ave}$), and a point of observed failure acceleration N_f (shown by ★) where the horizontal line of F_s = 1.00 intersects. Here, three kinds of factors of safety F_s are calculated for each test of the centrifuge tests, as

$$(F_s)_{36} = \frac{T_{ava}}{T_{req}} \qquad : when\ \phi = 36^\circ$$

$$(F_s)_{41} = \frac{T_{ava}}{T_{req}} \qquad : when\ \phi = 41^\circ \qquad ...(7.18)$$

$$(F_s)_{ave} = \frac{(F_s)_{36} + (F_s)_{41}}{2}$$

In Fig.7.10, all of the failure accelerations N_f in the centrifuge tests are observed to remain within a range of the calculated factors of safety between $(F_s)_{36}$ = 1.00 and $(F_s)_{41}$ = 1.00. Since the differences of these factors of safety $(F_s)_{36}$ and $(F_s)_{41}$ are up to 0.35 in Fig.7.10, and mostly less than 0.20 ~ 0.30, the close agreements of the calculated and observed failure

accelerations N_f support the adequate estimate of the upper and lower limits of the friction angles ϕ = 36° and 41° for the soil. It is also noticed that a difference of only 5° in the friction angle ϕ produces a difference in the factor of safety of 0.2 ~ 0.3. The observed failure accelerations N_f are also generally very close to the points of average factor of safety $(F_s)_{ave}$ = 0.90 ~ 1.00, although there are minor discrepancies observed for the test *V8.0-F-R* at N = 80g and tests *A(A')6.5-R-R* at N = 40g in which the failure accelerations N_f are found at $(F_s)_{ave}$ = 1.04 ~1.01 ≥ 1.00.

Fig.7.11 compares the average factors of safety $(F_s)_{ave}$ with the presence of a failure of nailed slopes for each test during the centrifuge acceleration N = 30g to 80g. In the figure, the cross symbols indicate the failure of nailed slopes at less than the given acceleration N, while the empty squares indicate the stable nailed slopes at the given acceleration N. As with Fig.7.10, decreases in the average factors of safety $(F_s)_{ave}$ are induced simply by increasing the centrifuge accelerations N. Although there are some discrepancies in the data for the accelerations of N = 60g and 80g, in which a slight overestimate and underestimate of the failure accelerations N_f were obtained respectively, the agreement between the theory based on the limit equilibrium analysis and the centrifuge tests are excellent throughout the accelerations from N = 30g to 80g. The error between the predicted and observed failure accelerations N_f based on the average factors of safety $(F_s)_{ave}$ was, surprisingly, less than 10%. These close agreements of the failure accelerations N_f indicate that the limit equilibrium approach can be used accurately to evaluate the factor of safety F_s of nailed slopes when a suitable failure mechanism, reasonable friction angle ϕ of the soil and the correct peak pull-out force F_p of nails are used in the analysis. Further, the limit equilibrium analysis could successfully take into account the influences of the roughness of the facing wall, in the same way as in the limit equilibrium analysis of conventional retaining walls. In practice, these

results imply that the additional margin of safety against the unknown factors is ensured by using a conservative friction angle ϕ and the peak pull-out force F_p of the nail. For natural slopes, as accurate properties for the sand and the peak pull-out forces F_p of nails are very difficult to obtain and control, reasonable factor(s) of safety F_s are indispensable for the design of soil nailing. It was, therefore, proved that the factor of safety F_s calculated from equation (7.2) or (7.3) is applied in the analysis of soil nailing with great confidence. However, because the centrifuge tests were perfomed using continuous facing walls with some amount of rigidity, further research is needed when applying the above - mentioned limit equilibrium analysis for the case of other types of facing wall. For the case of a segmented or flexible facing wall, it is suggested that the analysis for the individual nail and facing wall by equation (7.1) with a number of possible failure surfaces should be examined as well as the analysis of the overall equilibrium of the nailed slope.

Fig.7.12 shows the comparison of the predicted and observed failure accelerations N_f in the centrifuge tests. When an average factor of safety was calculated $(F_s)_{ave}$ = 1.00 in the limit equilibrium analysis, as the acceleration N increases, the nailed slope was assumed to collapse. For a range of accelerations N = 30g to 80g, it is seen in the figure that the observed failure accelerations N_f were generally 0% ~ 40% larger than those of the predicted failure accelerations N_f, except for one test which only exhibited 80% of the predicted failure acceleration N_f. Comparing Fig.7.11 and Fig.7.12, it is also noticed that the accurate prediction of the failure acceleration N_f of the nailed slopes is much more difficult than the predictions of the possibility of the failure at a given acceleration N. This difficulty may be attributed to the fact that several minor factors will significantly affect the failure acceleration N_f of the nailed slopes in the analysis, such as a slight underestimate of the friction angle ϕ, effects of the bending of nails and the friction of the side walls of the strong box. In practical

design, on the other hand, ignoring the effect of bending of nails contributes to an easier and more conservative analysis.

7.5 Comparison of critical failure mechanisms and total required force T_{req}

In the design of conventional retaining walls in which the earth pressures are sustained by the external forces of structures, a critical (or unique) failure surface (often called an active failure surface) which produces the maximum earth pressure is a matter of primary concern. In soil nailing, however, such a unique failure surface does not always coincide with the observed failure surface (*e.g.* Gassler, 1987, and Juran *et al.*, 1990), nor gives the minimum factor of safety $(F_s)_{min}$ in the limit equilibrium analysis. This is due to the fact that the factor of safety F_s of a nailed slope is not only related to the total required force T_{req} but to the total available force T_{ava} of the nails beyond the failure surface, as shown in equation (7.3). The stability analysis of a nailed slope should, therefore, be carried out by calculating the factors of safety F_s for all of the possible failure surfaces (Jones, 1993), including the base failure and stability of the "*nailed soil block*". There are several failure mechanisms proposed for the design of soil nailing and the reinforced soil walls, such as assuming a single plane, two part wedges, logarithmic spiral and a circle. It is of interest whether these different failure mechanisms provide similar maximum total required forces $(T_{req})_{max}$ and similar critical failure surfaces, which would give a great deal of confidence in applying a particular method in design. On the other hand, an estimate of the maximum total required force $(T_{req})_{max}$ is necessary in practice when the breakage of a nail and the bending or shear failure of a facing wall are considered in design.

Fig.7.13 compares the calculated maximum horizontal earth pressure coefficients $(K_{req})_h$ with the friction angle ϕ between 20° and 50°, where

$$(K_{req})_h = (K_{req}) \sin(\delta_w + \beta)$$
$$= \frac{2(T_{req})_{\max} \sin(\delta_w + \beta)}{\gamma H^2} \qquad ...(7.19)$$

in which K_{req} is the earth pressure coefficient and β is the inclination of the facing wall from horizontal. Two types of facing wall, the vertical facing wall (ß = 90°) and the inclined facing wall (ß = 80°), and 4 types of roughness of facing wall, δ_w = 0°, 10°, 20° and 30°, were considered in the analysis. Three typical failure mechanisms of Coulomb's single wedge, logarithmic spiral and two part wedge were applied here, where a number of iterative analyses were required to obtain each of the maximum horizontal earth pressure coefficients $(K_{req})_h$ for the latter two failure surfaces. For the two part wedge analysis in Fig.7.14, the angle θ_1 and the location (X_c , Y_c) of the point *C* were changed in the following range of:

$$0 < \theta_1 < \beta$$
$$0 \le \frac{X_c}{H}, \frac{Y_c}{H} \le 1 \qquad ...(7.20)$$

In the two part wedge analysis, the intervals of the location of *C* (X_c, Y_c) and the angle θ_1 were chosen as 1 *cm* and 2°, respectively. Two Angles θ_2 = 90° = *constant* and θ_3 = 45° + ϕ / 2 were also assumed in the analysis, giving the largest $(K_{req})_h$ among those obtained by changing the angles θ_2 and θ_3 freely, as reported by Gassler (1988). In this case, the earth pressures between the two blocks is the same as Coulomb's active pressure. The friction angle between the *block 1* and *the block 2* was also considered to be δ = ϕ. The critical failure mechanism for the vertical facing wall with the roughness of the facing wall δ_w = 0° is identical for these three mechanisms (Jewell, 1989), being a single plane with an angle of θ_1 = θ_2 = 45° + ϕ / 2. From Fig.7.13, it is found that the differences of $(K_{req})_h$ among these three

failure mechanisms were less than 10%, while the two part wedge analysis always provides a slightly larger $(K_{req})_h$ than Coulomb's theory and the logarithmic spirals. The comparisons of $(K_{req})_h$ reported by limit analysis (Chen and Liu, 1990) and stress characteristics (Sokolovski, 1965) were also made at some points in Fig.7.13. The agreement of the horizontal earth pressure coefficients $(K_{req})_h$ among the limit analysis, stress characteristics and the logarithmic spiral are generally very good. Although it seems that the discrepancies of $(K_{req})_h$ between the logarithmic spiral and the two part wedges are not negligible, Jewell (1989) pointed out that by correctly changing the reinforcement forces crossing the interwedge boundary between the *block 1* and *block 2*, the two part wedge analysis gives almost the same (or slightly smaller) $(K_{req})_h$ as the logarithmic spiral and also the upper bound limit analysis. It is also noticed that as the friction angle ϕ increases, the differences of $(K_{req})_h$ among these failure mechanisms become very small. Chen and Liu (1990) pointed out that for an active case, limit analysis gives results equal or close to Sokolovski's solution. It may be concluded from Fig.7.13 that for steep slopes ($80° \leq \beta \leq 90°$) with cohesionless soil, the several failure mechanisms shown above produce nearly the same horizontal earth pressure coefficients $(K_{req})_h$, irrespective of the friction angle δ_w and the friction angle ϕ of the soil.

Fig.7.15(a) to (h) show the critical failure surfaces yielding maximum horizontal earth pressure coefficients $(K_{req})_h$ with Coulomb's theory, two part wedges and logarithmic spiral, together with the range of the observed failure surfaces in the centrifuge tests (filled circles). Four types of nailed slopes are shown in the figure, with regard to the roughness (δ_w = 15° for smooth and 30° for rough) and the inclination (β = 90° and 80° from the horizontal) of the facing wall. The angles θ of the single failure surface from the horizontal obtained by Coulomb's theory are given, as

$$\theta = \tan^{-1}\left\{\frac{\sin\phi\sqrt{\sin(\phi + \delta_w)\sin\beta} + \sin\beta\sqrt{\sin(\beta + \delta_w)\sin\phi}}{\cos\phi\sqrt{\sin(\phi + \delta_w)\sin\beta} + \cos\beta\sqrt{\sin(\beta + \delta_w)\sin\phi}}\right\} \quad ...(7.21)$$

It is observed from Fig.7.15 that

(1) while the observed failure surfaces were generally located between the failure surfaces assuming the friction angles $\phi = 36°$ and $\phi = 41°$, they seem to be closer to the former surfaces ($\phi = 36°$). It is commonly reported that location of failure surface is changed (often moved deeper into the slope) by increasing the nail length, *e.g.* Teramoto *et al.* (1992).

(2) the influence of the roughness δ_w of the facing wall on the predicted failure surfaces is not negligible, and as δ_w becomes larger, the failure surfaces develop deeper in the slope; the deviation $\Delta\theta$ of the direction of the calculated failure surface from the frictionless vertical facing wall ($\delta_w = 0°$) at the toe of the facing wall is approximately estimated from Rankine's theory (Berry and Reid, 1987), as

$$\Delta\theta = \frac{\sin^{-1}\left(\frac{\sin\delta_w}{\sin\phi}\right) - \delta_w}{2} \quad ...(7.22)$$

Fig.7.16 shows some results of equation (7.22) with a range of the friction angle $20° \le \phi \le 50°$ and a range of roughness of the facing wall $\phi / 3 \le \delta_w \le \phi$. The figure indicates that in theory, the roughness δ_w of the facing wall greatly influences the shape and location of the failure surface, especially for loose sands.

(3) the shapes of the logarithmic spiral and two part wedges have similarity in that those two failure surfaces generally give the smaller anchorage lengths l_i of nails beyond the failure surface in the lower part of the nailed slope than those of Coulomb's theory with a single failure surface, while the situation is exactly the opposite in the upper part of

the nailed slopes. In general, nails placed in the lower part of nailed slopes make a much greater contribution to the total available force T_{ava} in the limit equilibrium analysis because of the larger vertical stresses σ_v on the nails, and hence, larger pull-out forces of the nails, as shown in Equation (7.16). In other words, nails in the lower part of the nailed slope play a more important role in the stability analysis than those in the upper part of the nailed slope. Regarding the shapes of the failure surfaces of the nailed slope, it appears that the logarithmic spiral may be more realistic than the two part wedges when no local surcharge load or no widespread uniform surcharge is applied on the upper ground surface, as shown in the small model tests carried out by Gassler (1987). It should be realized that the shape of the failure surface of the slope is strongly influenced by the shape of the boundary conditions of surcharge loads, and the majority of failures are induced by the unloading (excavation of soil) in soil nailing. In decreasing the overall displacements of nailed slopes, on the contrary, it is reported that nails placed in the upper part of the slope play a more important role than those in the lower part of the slope. Considering that the horizontal displacement δ_h is largest at the top of the facing wall, as observed in section 6.3, longer nails near the top of the facing wall may be more effective in restraining the horizontal displacement δ_h.

(4) The observed failure surfaces do not generally coincide with the critical failure surfaces (or characteristics) which produce the maximum earth pressure coefficient K_{req}. This indicates that the overall stability analysis simply based on the critical (or unique) failure surfaces may overestimate the factor of safety F_s of nailed slopes, and may lead to unsafe design.

The analysis of the horizontal earth pressure coefficient $(K_{req})_h$ and the failure surface

leads the Author to suggest that for safety, the logarithmic spiral or two part wedges are more suitable than the single failure surface, because the former two methods tend to give the smaller total anchorage length $\Sigma\ l_i$ of nails and the slightly larger total required forces $T_{req,}$ and therefore, the smaller factors of safety F_s . Two part wedge analysis, on the other hand, has an advantage over the logarithmic spiral in simplicity and flexibility for the various boundary conditions of nailed slopes. At the same time, two part wedge analysis is much easier than the logarithmic spiral analysis in taking of account of the complex strata and varying shear strengths of natural slopes.

Finally, further investigation should be made as to how the roughness δ_w of the facing wall improves the stability of nailed slopes, since not only does it decrease the total required force T_{req} but also decreases the total available force T_{ava} due to that failure surface moving deeper into the nailed slope, as shown in equation (7.22). It is also important to clarify:

(1) the relationships between critical failure surfaces and the velocity characteristics and the stress characteristics, and

(2) the horizontal earth pressure coefficient $(K_{req})_h$ and the corresponding velocity and stress characteristics.

7.6 Case history - the prototype test in Germany

In the prototype test carried out in Germany, a uniform surcharge, p, was applied at the top of the nailed slope, and achieved a value of p = 110 kN/m^2 when the facing wall collapsed. The failure mechanism observed was very close to a rigid body slip along a curved surface. The properties of soil and layout of the nailed slope (*Test B* in the literature) were described in Chapter 5. From the observed failure surface, as shown in Fig.7.17, the appropriate equation of a logarithmic spiral was calculated in the same manner as section

7.3.1,

$$r = 4.97 \exp[(\theta - 0.881)\tan\phi \ ] \quad (unit:\ m) \qquad ...(7.23)$$

where the location of the pole O of the logarithmic spiral was found to be at $X_c = 1.0\ m$ and $Y_c = 9.8\ m$, and the friction angle $\phi = 40.5°$. The effect of shear forces P_s perpendicular to the direction of the nails was ignored in the following limit equilibrium analysis because the improvement in the soil shearing resistance due to the shear force P_s is seen to provide less than 2.5% of axial force at failure, Pedley (1990). It is assumed in the analysis that the distance of the centroid d for the collapsed soil mass from the pole O of the logarithmic spiral is the same as that of the total surcharge load p. The friction angle of the shotcrete facing wall and soil is assumed to be three quarters of the friction angle of the soil (Jumikis, 1964):

$$\delta_w = \frac{3\phi}{4} \approx 30° \qquad ...(7.24)$$

The orientation of nails is assumed horizontal in the analysis. By increasing the surcharge load p, as shown in Fig.7.18, it was found that the location of the centroid of horizontal earth pressure became close to that of the hydrostatic distribution from that of the bulging - shape distribution, at two thirds of the height H of the facing wall from the upper ground surface. Therefore, the location of the centroid was taken as $n_H = 2 / 3$ in the analysis (also see Fig.7.9). Regarding the mobilizations of axial force of the nail at failure, the horizontal displacements δ_h of the facing wall observed were 52 *mm* and 145 *mm* at the first and the fourth row of the nails, respectively. Those horizontal displacements δ_h well exceeded the pull-out displacement $\xi_p = 30\ mm$ which was required to mobilize the peak pull-out force F_p of a nail, obtained from the *in - situ* pull-out tests of nails.

The total (horizontal) required force T_{req} per horizontal nail spacing ($S_h = 1.2\ m$) is

calculated from equation (7.14), as

$$T_{req} = \frac{113.0\ kN}{(1.2\ m)} \qquad ...(7.25)$$

The maximum horizontal earth pressure coefficient $(K_{req})_h$ is calculated from equations (7.19) and (7.25), as

$$(K_{req})_h = \frac{0.149}{(1.2\ m)} \qquad ...(7.26)$$

This total required force in equation (7.25) is very close to T_{req} = 118.2 *kN* / (1.2 *m*) which Gassler (1987) estimated using the friction circle method with an additional capillary cohesion of c' = 1.0 kN/m^2 for a circular failure surface of a radius r = 7.9 *m*. The possible reasons for the slight difference of these two values of total required force T_{req} calculated are that:

(1) the circular failure analysis did not take into account the effect of the friction of the facing wall $\delta_w = 30°$,

(2) the capillary cohesion c' was not considered in the current analysis, and

(3) Gassler (1987) assumed that the total available force T_{ava} acts through the centroid G of the total nail length $\Sigma\ l_i$ beyond the failure surface, as shown in Fig.7.17.

The total horizontal earth pressures measured by means of Glotzl cells behind the shotcrete facing wall were, however, P_h = 80 ~ 90 *kN* / (1.2 *m*), which provided only 70 ~ 80% of the calculated required force T_{req}. Coulomb's theory, on the other hand, gives T_{req} = 120.8 *kN* / (1.2 *m*), which was very close to the values calculated by the logarithmic spiral and circular failure surface.

Table 7.2 shows details of the estimate of the total available force T_{ava} based on the lower and upper bounds of the ultimate mean shear force $(T_m)_i$ from *in - situ* pull-out tests reported by Gassler (1987) for the corresponding depth of the nails, where

$$(T_m)_i = \frac{N_i}{L_i}, \quad or$$
$$N_i = (T_m)_i L_i \qquad \text{...(7.27)}$$

in which i is the number of row of the elevation ($i = 1 \sim 5$), N_i is the ultimate pull-out force per unit length (1 m) and L_i is the length of the nail beyond the failure surface. From Table 7.2, the total available forces for the upper and lower bounds are calculated as,

$$\textit{for lower bound:} \quad (T_{ava})_{lower} = 91.5\,kN/(1.2\,m), \qquad \text{...(7.28)}$$
$$\textit{for upper bound:} \quad (T_{ava})_{upper} = 123.0\,kN/(1.2\,m)$$

Equations (7.3), (7.25) and (7.28) provide the following upper and lower bounds of factors of safety F_s.

For the lower bound:

$$(F_s)_{lower} = \frac{(T_{ava})_{lower}}{(T_{req})} = \frac{91.5\ kN}{113.0\ kN} = 0.81 \qquad \text{...(7.29a)}$$

For the upper bound:

$$(F_s)_{upper} = \frac{(T_{ava})_{upper}}{(T_{req})} = \frac{123.0\ kN}{113.0\ kN} = 1.09 \qquad \text{...(7.29b)}$$

The average factor of safety $(F_s)_{ave}$ for those of the upper and lower bounds is,

$$(F_s)_{ave} = \frac{(F_s)_{upper} + (F_s)_{lower}}{2}$$

$$= \frac{1.09 + 0.81}{2} \qquad \text{...(7.30)}$$

$$= 0.95$$

This calculated average factor of safety $(F_s)_{ave} = 0.95$ is very close to $F_s = 1.00$ in the state of limit equilibrium, and an excellent prediction could be made regarding the failure of the *in - situ* nailed slope. The good agreement between the prediction and *in - situ* test as well as the centrifuge tests in the previous section supports the applicability for the limit equilibrium analysis for soil nailing, when accurate parameters are used in the analysis.

It should be noted that because an accurate measurement of the maximum pull-out force $(T_m)_i$ in every row of nails is crucial in applying the limit equilibrium analysis, great care should be taken in determining reasonable values of $(T_m)_i$. Further research is needed to establish a simple and reliable method which is able to estimate the pull-out force $(T_m)_i$ of nails with reasonable accuracy in advance, without carrying out *in - situ* pull-out tests.

Chapter 8

Concluding remarks

A review of the previous research work and the current understandings of soil nailing was given in Chapter 1. A summary of the overall conclusions resulting from this experimental study, involving pull-out tests of a nail and centrifuge model tests of nailed slopes, is described below. This is followed by suggestions for future research into soil nailing.

8.1 Pull-out tests of a nail

Since the interaction mechanism between a nail and soil is essentially dominated by the friction (bond) between them, it is of great importance to understand the friction mechanism of a nail. Pull-out tests of a nail, direct shear tests of nailed sand and interface tests were conducted using the medium size direct shear box. In order to eliminate the influence of the front wall of the box, a small plastic tube was placed horizontally near the front wall. Major parameters for the pull-out tests were,

(1) type of sands: 14/25 dense Leighton Buzzard Sand and 50/100 dense and medium dense Leighton Buzzard Sands,

(2) type of nail surface: smooth surface and rough surface which was made by glueing sand layers on it,

(3) type of axial stiffness of a nail: stiff nail made of steel and flexible nail made of

rubber tube, and

(4) diameter D of a nail.

In practice, a nail can be approximately assumed as "stiff (or in - extensible) - rough".

From the tests, the following results were obtained.

(1) The shapes of the pull-out curves of the stiff - rough nails and the load - displacement curves for the unreinforced direct shear tests of the corresponding sand are very similar, including the horizontal displacements ξ_p required to mobilize the peak stress. These similarities are due to the fact that both the horizontal central plane for the direct shear tests and the direction of a nail are approximately assumed as the direction of zero - extension, namely, $\varepsilon_x \simeq 0$. In contrast, it was analytically inferred that for a flexible - rough nail, the direction of the nail is $\varepsilon_x \neq 0$, and totally different pull-out curves and peak pull-out forces F_p were observed compared to those of the stiff - rough nails.

(2) Results of the radiographs indicate that both the roughness of the reinforcement and the types of sand influence the thickness h of the rupture zone of the soil. For rough reinforcement, the thicknesses h were observed to be 10 to 40 times the mean particle size D_{50} of the sand. For the smooth reinforcement, the thickness h was observed to be considerably smaller than that of the rough surface, showing why smaller peak pull-out forces F_p were obtained in comparison with those of the rough surface nail.

(3) The diameter D of a nail affects the amount of peak pull-out force F_p. By considering a simple elastic cavity expansion due to the dilatancy of the soil, it is understood that as D increases the apparent friction coefficient f^* of a nail decreases. This result suggested that great care is needed when extrapolating the maximum pull-out force F_p from a small scale test to a full scale test.

(4) Comparisons were made for the apparent friction coefficients f^* estimated by the pull-out test of a nail, direct shear tests of nailed sand and interface tests. Although a quantitative assessment was not made as to how the dilatancy of the sand affects the apparent friction coefficient f^*, it was found that a larger nail diameter produces a smaller f^* in the direct shear tests of a nailed sand, as observed in the pull-out tests of a nail.

(5) For a relatively small diameter of a nail, the interface test provides the smallest apparent friction coefficients f^* among the three tests, namely

$$f^*_{pull-out} \geq f^*_{direct\ shear} \geq f^*_{interface}$$

This order corresponds well to the degree of the restrained dilatancy in the soil when relative displacement between the soil and a nail or a reinforcement occurred.

(6) For the pull-out tests of a smooth nail and the interface tests between a smooth reinforcement and soil, the apparent friction coefficients f^* were found to be the same between the tests. Measured apparent friction coefficients f^* were considerably smaller than those of the rough nail, and smaller even than the critical state friction angle ϕ_{cv}.

8.2 Centrifuge tests of nailed slope

A total of 24 of centrifuge tests of nailed slopes was carried out to investigate the failure mechanism and the overall behaviour of nailed slopes. The height H of the model slope was 200 *mm* and 50/100 dense Leighton Buzzard Sand was used for the models. After reaching the test acceleration N = 30g, excavation of the slope was simulated by draining the water from two rubber bags located in front of the facing wall. After draining of the water the maximum acceleration applied was N_{max} = 80g. Consideration was given to the similarity laws for the stress - strain of a nail, pull-out of a nail and breakage of a nail between a

prototype test and the centrifuge model tests. Parameters varied in the centrifuge tests were as follows:

(1) Nail surface: smooth nail (diameter D = 3 *mm*) and rough nail (D = 1 *mm*)

(2) Nail length l: l = 6.5 *cm* to l = 23.0 *cm*

(3) Inclination of the nails: horizontal and 10° downward from horizontal

(4) Stiffness of the facing wall: stiff wall and flexible wall

(5) Roughness of the facing wall: rough wall (δ_w = 30°) and smooth wall (δ_w = 15°)

(6) Inclination of the facing wall: vertical wall and inclined wall (ß = 80° from horizontal)

Centrifuge tests were found to provide much useful information on the mechanics of soil nailing. The results of the centrifuge tests are as follows.

(1) As the centrifuge acceleration N increases, or as the excavation of a slope proceeds towards the bottom of the facing wall, several failure surfaces progressively develop initially from the proximity of the facing wall to the inside of the nailed slope, followed by the complete collapse of the nailed slope. This indicates that all of the possible failure surfaces should be considered in design of soil nailing. On the other hand, there were few nails in which the visible bending of the nail was observed across the failure surfaces, indicating the small contribution of bending stiffness of the nail to the stability of nailed slopes.

(2) Observed failure surfaces were well described by logarithmic spirals passing through the toe of the facing walls. The logarithmic spiral is found to be a kinematically admissible failure surface for cohesionless soil without self weight, Davis (1968).

(3) The horizontal displacements δ_h of facing wall were decreased by

(a) increasing the length l of a nail and the friction between the soil and the nail , and

(b) increasing the bending stiffness of the facing wall.

Only small differences observed between the horizontally placed nails and the inclined nails in terms of the failure acceleration N_f. On the other hand, roughness of the facing wall does not decrease the horizontal displacements δ_h. Reasonably good predictions for the subsidences δ_v of the upper ground surface could be made from the data of the deflection of the facing wall, by considering a simple velocity field in the nailed slope, as proposed by Bransby and Milligan, (1975).

(4) Although there was some difficulty in measuring the earth pressure on the facing wall, it is observed that the earth pressures do not simply exhibit a hydrostatic distribution. Near the bottom of the facing wall, earth pressures were found to decrease considerably, while near the top of the facing wall, larger earth pressures than the hydrostatic distribution were observed. This suggests the need for a careful estimate of the nail length and spacings in design.

(5) Fairly good predictions for the failure acceleration N_f were made by stability analyses of the nailed slopes based on limit equilibrium analyses. In the analyses, the factor of safety F_s was estimated, as

$$F_s = \frac{available\ (nail)\ force}{required\ (nail)\ force}$$

$$= \frac{T_{ava}}{T_{req}}$$

The available (nail) force T_{ava} was calculated by totalling the pull-out force of nails beyond the failure surface, as

$$T_{ava} = \sum_i \pi D_i l_i f_i^* (\sigma_m)_i$$

where D and l are the diameter and length of a nail beyond failure surface, f^* is the apparent

friction coefficient of a nail, and σ_v is the vertical stress on a nail. The required (nail) force T_{req} was estimated from a force polygon based on the observed or assumed failure surface. In the analysis of the centrifuge tests, the lower bound factor of safety $(F_s)_{36}$ and the upper bound factor of safety $(F_s)_{41}$ were calculated with regard to the corresponding friction angles of the sand, $\phi = 36°$ and $\phi = 41°$, respectively. The majority of the nailed slopes, which had the average factors of safety $(F_s)_{ave} = \{(F_s)_{36} + (F_s)_{41}\} / 2 \leq 1.00$ in the given acceleration N, were found to collapse during the tests. This suggested that $(F_s)_{ave}$ is a good indicator of the failure of the nailed slopes. The same limit equilibrium analysis was also applied to the prototype test performed by Gassler (1987). The average factor of safety calculated was $(F_s)_{ave} = 0.95$ from the given surcharge stress $p = 110\ kN/m^2$, observed failure surface and the results of *in - situ* pull-out tests, when the nailed slope collapsed. These agreements between analysis and the centrifuge and *in - situ* tests gave great confidence in the application of the limit equilibrium analysis to soil nailing.

(6) Comparison of the failure surfaces and the horizontal earth pressure coefficients $(K_{req})_h$ were made between calculations by the logarithmic spiral, two part wedges and the single plane (Coulomb's theory). It was found that the horizontal earth pressure coefficients $(K_{req})_h$ were nearly identical among the three failure mechanisms, the limit analysis and the stress characteristics. However, a logarithmic spiral and two part wedge were suitable for the failure surface of the nailed slope because those two failure mechanisms provided a smaller available force T_{ava} than that of a single plane, leading to a more conservative design. The two part wedge has an advantage over a logarithmic spiral because the former is more adaptable to the boundary conditions and soil profile of nailed slopes.

8.3 Suggestions for future research

8.3.1 Interaction between soil and a nail

Interaction mechanisms, typically described by the apparent friction coefficient f^* and the interaction parameter k_i, are very complicated owing to the uncertainty about the increased normal stress σ_m on the nail due to dilatancy in dense sand. In particular further investigations should be made for:

(1) the mechanism of the "restrained dilatancy effect" of soil when a nail is pulled out,

(2) the difference of the apparent friction coefficient f^* mobilized in the active zone and resistant zone in the nailed slope,

(3) the change of thickness h of the rupture zone in the soil as the pull-out displacement increases; the thickness h affects the apparent friction coefficient f^* and the interaction parameter k_i.

(4) the interaction between an extensible nail and soil because a nail is assumed neither "ideally extensible" nor "ideally in - extensible" in practice,

(5) a relatively simple method by which the apparent friction coefficient f^* can be estimated from given properties of soil with reasonable accuracy, without carrying out *in - situ* pull-out tests in advance,

(6) installation effect differences between grouted nails and fired nails,

(7) a range of nail stiffness to cover geosynthetics nails, and

(8) the effect of D / D_{50} on the apparent friction coefficient f^* for full scale nail diameters,

In addition, it is also important to standardize the specification of a pull-out test of a nail, as a basis for comparing pull-out data of nails reported by different research workers.

8.3.2 Analysis and behaviour of soil nailing

The experimental findings reported in the dissertation have concluded that limit

equilibrium analysis is a powerful tool for the stability calculations of soil nailing in sand. More sophisticated analysis may be required (for example, finite element analysis) for taking account into more complex boundary and initial conditions of a nailed slope.

In this research programme, spacing of the nails was maintained constant throughout the tests. Investigations are needed of the influence of the spacing on the stability of the nailed slope and the earth pressures on facing walls.

Other research which should be made in the analysis and behaviour of soil nailing are:

(1) an application of soil nailing into clay; recent developments of soil nailing technique in practice require investigation of the possibility of soil nailing in a wide range of ground conditions. The influence of pore water pressure and cohesion on the behaviour of nailed slopes should be examined and considered in design.

(2) a method for predicting the horizontal displacements of the facing wall during and after the excavation of slope; unlike displacement of geosynthetic reinforced walls, in which the majority of the displacement will be caused by that of extension of the reinforcement, slip between the soil and nail is a dominant source of the displacement in soil nailing. The finite element methods will play an important role for this purpose since the method is able to take into account the construction sequence and the constitutive equations of the soil. A precise estimate of the interaction parameter k_i between the soil and a nail should be important in the modelling of a nailed slope.

(3) consideration of an appropriate factor of safety F_s in the analysis of soil nailing; there are two factors of safety proposed for soil nailing, the partial safety factor and the lumped (overall) safety factor. The several possible failure modes of a nailed slope make the establishment of the factor of safety F_s confusing.

(4) the behaviour of nailed slopes without facing wall.

REFERENCES

Adib,M.E. (1988). *Internal lateral earth pressure in earth walls.* PhD. Thesis, University of California at Berkeley.

Airey,D.W. (1987). *Some observations on the interpretation of shear box test results.* Internal report CUED/D - SOILS/TR 196, University of Cambridge.

Arman,A.R.A. (1989). *Reinforced soil slopes and walls, Soil-Reinforcement.* General Report, Proc. of 12th Int. Conf. of Soil Mech. and Found. Engi., Vol.4, Rio de Janeiro, pp2629-2636.

Assadi,A. (1975). *Rupture layers in granular materials.* PhD. Thesis, University of London.

Basset,R.H. and Last,N.C. (1978). *Reinforcing earth below footings and embankments.* Symposium on Earth Reinforcement, Pittsburgh, pp202-231.

Bastick,M., Schlosser,F., Amar,S. and Canepa,Y. (1989). *Strains and deformations in an experimental reinforced earth abutment.* Proc. 12th Int. Conf. Soil Mech. & Found. Eng., Rio de Janeiro, pp661-664.

Bergado,D.T., Chai,J.C. and Balasubramanian,A.S. (1992). *Interaction between grid reinforcement and cohesive-frictional soil.* Proc. of Int. Symp. on Earth Reinforcement Practice, Vol.1, Fukuoka, pp29-34.

De Bernardi,E., Chionna,V.N. and Peila,D. (1992). *Parametric analysis of soil nailing stabilized excavation walls.* Proc. of the International Symposium on Earth Reinforcement Practice, Vol.1, Fukuoka, pp463-468.

Berry,P. and Reid,D. (1987). *An introduction to soil mechanics.* Mc.Graw Hill, pp164-166.

Bolton,M,D. (1986). *The strength and dilatancy of sands.* Geotechnique, Vol.36, N°.1, pp219-226.

Bolton,M.D. (1990). *Reinforced soil: Laboratory testing and modelling.* Proceedings of the International Reinforced Soil Conference, Glasgow, pp287-298.

Bolton,M.D., Choudhury,S.P., Pang,P.R.L. (1978). *Reinforced earth walls: a centrifugal model study.* Proc. of Symp. on Earth Reinforcement, Pittsburg, pp252-281.

Bolton,M.D. and Pang,P.R.L. (1982). *Collapse limit states of reinforced earth retaining walls.* Geotechnique, Vol.32, N°.4, pp349-367.

Bonaparte,R. and Schmertmann,G.R. (1988). *Reinforcement extensibility in reinforced soil wall design*. Proc. NATO Adv. Research Workshop, Kingston, Kluwer Academic Publishers, pp409-57.

Boulton,M., Plytas,C. and Foray,P. (1986). *Comportement de interface et prevision du frottement lateral le long des pieux, et tirants de ancrage*. Revue Francaise de Geotechnics, Vol.2, Helsinki, pp473-476.

Bransby,P.L. and Smith,I.A.A. (1975). *Side friction in model retaining-wall experiments*. Journal of the geotechnical engineering division, Vol.101, N°.GT7, pp615-632.

Bransby,P.L. and Milligan,G.W.E. (1975). *Soil deformation near cantilever sheet pile walls*. Geotechnique, Vol.25, N°.2, pp175-195.

Bridle,R.J. and Barr,B.I.G. (1990). *The analysis and design of soil nailing*. Proceedings of the International Reinforced Soil Conference, Glasgow, pp249-254.

Bruce,D.A. and Jewell,R.A. (1986/7). *Soil Nailing: Application and Practice*. Ground Engineering (Part 1 - November 1986, pp10-15. Part 2 - January 1987, pp21-38).

Burd,H.J. (1986). *A large displacement finite element analysis of a reinforced unpaved road*. DPhil. Thesis, University of Oxford.

Cancelli,A., Rimoldi,P. and Togni,S. (1992). *Frictional characteristics of geogrids by means of direct shear and pull-out tests*. Proc. of Int. Symp. on Earth Reinforcement Practice, Vol.1, Fukuoka, pp51-56.

Cartier,G. and Gigan,J.P. (1983). *Experiments and observation on soil nailing structures*. Proc. 8th European Conf. Soil Mech. & Found. Eng. Helsinki, Vol.2, pp473-476.

Chang,J.C., Hannon,J.B. and Forsyth,R.A. (1977). *Pull resistance and interaction of earth work reinforcement and soil*. Transport Research Record N°.640, Washington, U.S.A.

Chen,W.F. and Liu,X.L. (1990). *Limit analysis in soil mechanics*. Developments in Geotechnical Engineering, 52, Elsevier.

Coates,D.F. and Yu,Y.S. (1970). *Three dimensional stress distributions around a cylindrical hole and anchor*. Proc. 2nd Int. Soc. Rock Mech., pp175-182.

Cole,E.R. (1967). *The behaviour of soils in the simple shear apparatus*. PhD. Thesis, University of Cambridge.

Craig,W.H. (1983). *Simulation of foundations for offshore structures using centrifuge modelling*. Developments in soil mechanics and foundation engineering-1, Applied Science Publishers, London and New York, pp1-27.

Davis,E.H. (1968). *Theories of plasticity and the failure of soil masses*. Soil Mechanics, Selected Topics. Butterworths, London, pp341-380.

Delmas,P.H. (1989). *Instrumentation and evaluation of reinforced earth structures.* Contribution to discussion, Proc. of 12th Int. Conf. of Soil Mech. and Found. Engi., Vol.4, Rio de Janeiro, pp3009-3010.

Desrues,J. (1984). *La Localisation de la deformation dans les milieux granulaires.* PhD. Thesis, University of Grenoble 1.

Dobrova,G.A. (1963). *Interaction of soil and structures.* Rehnoy Transport, Moscow.

Dunham,R.K. (1976). *Anchorage tests on strain gauged resin bonded bolts.* Tunnels and Tunnelling, Vol.8, N°.6, pp73-76.

Dyer,M.R. (1985). *Observation of the stress distribution in crushed glass with applications to soil reinforcement.* DPhil. Thesis. University of Oxford.

Farmer,I.W. (1975). *Stress distribution along a resin-grouted rock anchor.* Journal of Int. Rock Mech. Min. Sci. and Geomech., Vol.12, pp347-351.

Egger,P. (1979). *Physical geomechanical models.* Int. Symp. on Rock Mech., Bergamo, pp67-81.

Garg,K.G. (1992). *Evaluating soil-reinforcement friction.* Proc. of Int. Symp. on Earth Reinforcement Practice, Vol.1, Fukuoka, pp67-72.

Gassler,G. (1987). *Vernagelte Gelandesprunge-Tragverhalten und Standsichrheit.* PhD. Thesis, University of Karlsruhe.

Gassler,G. (1988). *Soil nailing - theoretical basis and practical design.* Proc. of Int. Symp. of Theory and Practice of Earth Reinforcement, Fukuoka, pp283-288.

Gassler,G. (1990). *In-situ techniques of reinforced soil.* Proc. International Reinforced Soil Conference, Glasgow, pp185-196.

Gassler,G. (1992). *Full scale test on a nailed wall in consolidated clay.* Proc. of Int. Symp. of Earth Reinforcement Practice, Fukuoka, pp475-480.

Gassler,G. and Gudehus,G. (1981). *Soil nailing - some aspects of a new technique.* Proc. of 10th Int. Conf. Soil Mech. & Found. Eng., Stockholm, Vol.3, pp665-670.

Gassler,G. and Gudehus,G. (1983). *Soil nailing - statistical design.* Proc. of 8th Euro. Conf. of Soil Mech. and Found. Eng., Vol.2, Helsinki, pp491-494.

Giroud,J.P. (1989). *Introduction to discussion on soil reinforcement.* Contribution to discussion, Proc. of 12th Int. Conf. of Soil Mech. and Found. Engi., Rio de Janeiro, Vol.4, pp3003-3004.

Gourc,J.P. and Beech,J.F. (1989). *Soil-reinforcement interaction.* Contribution to discussion, Proc. of Int. Conf. of Soil Mech. and Found. Engi., Vol.4, Rio de Janeiro, pp3007-3008.

Guilloux,A., Notte,G. and Gonnin,H. (1983). *Experiences of a retaining structure by nailing in moraine soils*. Proc. of 8th Euro. Conf. of Soil Mech. and Found. Engi., Helsinki, pp473-476.

Guilloux,A., Schlosser,F. and Long,N.T. (1979). *Etude du frottement sable-armature en laboratories*. Proc. of Int. Reinforcement des sols, Paris.

Gutierreg,V. and Tatsuoka,F. (1988). *Role of facing in reinforcing cohesionless soil slopes by means of metal strips*, Proceedings of International Symposium on Earth Reinforcement Practice, Vol.1, Fukuoka, pp289-294.

Herrmann,L.R. and Al-Yassin,Z. (1978). *Numerical analysis of reinforced soil systems*. Proceedings of ASCE Symposium, Earth Reinforcement, Pittsburgh, pp429-457.

Hettler,A. (1982). *Approximation formula for piles under tension*. Proceedings of IUTAM Conference on Deformation and Failure of Granular Material, Delft, pp603-608.

Heymann,G., Rohde,A., Schwarz,K. and Friedlaender,E. (1992). *Soil nail pull out resistance in residual soils*. Proceedings of the International Symposium on Earth Reinforcement Practice, Vol.1, Fukuoka, pp487-496.

Hmadi,E.K. and O'Rourke,M.J. (1988). *Soil Springs for Buried Pipeline Axial Motion*. Journal of Geotechnical Engineering, Vol.114, N°.11, pp1335-1339.

Ho,S.K. and Rowe,R.K. (1992). *Finite element analysis of geosynthetic reinforced soil walls*. To appear in Geosynthetic Conference, '93 Vancouver.

Houlsby,G.T. and Wroth,C.P. (1981). *Direct solution of plasticity problems in soils by the methods of characteristics*. Proc. of 4th Int. Conf. on Numerical Methods in Geomechanics, Vol.3, Edmonton, pp1059-1071.

Houlsby,G.T. (1991). *How the dilatancy of soils affects their behaviour*. Invited Lecture, 10th Euro. Conf. Soil Mech. and Found. Engi., Florence.

Ingold,T.S. and Templeman,J.E. (1979). *The comparative performance of polymer net reinforcement*. Proc. of Int. Conf. on the Reinforcement of soils, Vol.1, Paris, pp65-70.

Irsyam,M. and Hryciw,R.D. (1991). *Friction and passive resistance in soil reinforced by plane ribbed inclus*. Geotechnique, Vol.41, N°.4, pp485-498.

Jaber,M.B. (1989). *Behaviour of reinforced soil walls in centrifuge model tests*. PhD. Thesis, University of California at Berkeley.

Jaber,M., Mitchell,K., Christopher,R. and Kutter,L. (1990). *Large centrifuge modelling of full scale reinforced soil walls*. ASCE Conference Design and Performance of Earth Retaining Structures, ASCE Geotechnical Special Publication, N°.25, pp379-393.

Jaky,J. (1944). *The coefficient of earth pressure at rest*. Journal of the Society of Hungarian Architects and Engineers, pp355-358.

Jarrett,P.M. and McGown,A. (1988). *The application of polymeric reinforcement in soil retaining structures*. NATO ASI Series E: Applied Sciences, Vol.147, Kluwer Academic Publishers,

Jewell,R.A. (1980). *Some effects of reinforcement on the mechanical behaviour of soils*. PhD. Thesis, University of Cambridge.

Jewell,R.A. (1989). *Direct shear tests in sand*. Geotechnique, Vol.39, N°.2, pp309-322.

Jewell,R.A. (1990a). *Revised design charts for steep reinforced slopes*. Reinforced embankments: Theory and Practice in the British Isles, Thomas Telford, London.

Jewell,R.A. and Pedley,M.J. (1990). *Soil Nailing Design: The Role of Bending Stiffness*. OUEL Report, N°1813/90.

Jewell,R.A. (1990b). *Strength and deformation in reinforced soil design*. Keynote Paper, 4th Int. Conf. on Geotextiles, Geomembranes and Related Products.

Jewell,R.A. and Milligan, G.W.E. (1989). *Deformation calculations for reinforced soil walls*. Proc. 12th Int. Conf. of Soil Mech. and Found. Engi., Vol.2, Rio de Janeiro, pp1257-1262.

Jewell,R.A. and Wroth,C.P. (1987). *Direct shear tests on reinforced sands*. Geotechnique, Vol.37, N°.1, pp53-68.

Johnston,R.S. and Romstad,K.M. (1989). *Dilation and boundary effects in large scale pull-out tests*. Proc. of 12th Int. Conf. of Soil Mech. and Found. Engi., Rio de Janeiro, pp1263-1266.

Jones,C.P.D. (1990). *In-situ techniques for reinforced soil*. Proceedings of the International Reinforced Soil Conference, Glasgow, pp277-282.

Jones,C.J.P.F. (1993). *Limit Modes of Analysis*. Reinforced soil: Mechanics and design, University of Oxford, pp24.1-24.14.

Jumikis,A.R. (1964). *Mechanics of Soils*. D. Van Nostrand Company, Inc. pp196-215.

Juran,J.H. (1991). *Soil nailing design and application*. A collection of papers, Deep Foundation Institute, USA.

Juran,J.H., Baudrand,G., Farrag,K. and Elias,V. (1990). *Kinematical Limit Analysis for Design of Soil-Nailed Structures*. Journal of Geotechnical Engineering, Vol.116, N°.1, pp54-72.

Kim,J.S. and Preber,T. (1969). *Earth pressure against braced excavations*. Journal of Geotechnical Engineering Division, Vol.107, N°10, pp1424-1428.

Koga,Y., Okamoto,M, Ochi,K. and Taniguchi,E. (1988). *Cyclic torsional shear tests on the seismic resistance of reinforced sand*. Tsuchi-to-Kiso, Japanese Soc. of Soil Mech. and Found. Engi., Vol.36, N°.363, pp33-38 (in Japanese).

Lee,K.L., Adams,B.D. and Vagneron,M,J,M. (1973). *Reinforced earth retaining walls.* Journal of Soil Mech. and Found. Division, Vol.99, N°.SM10, pp745-764.

Lehane,B.M, Jardine,R.J., Bond,A.J. and Frank,R. (1993). *Mechanics of shaft friction in sand from instrumented pile tests.* Journal of Geotechnical Engineering, Vol.119, N°.1, pp19-34.

Leschinsky,D. (1991). *Discussion on Kinematical Limit Analysis for Design of Soil-Nailed Structures.* Journal of Geotechnical Engineering, Vol.117, N°.11.

Leschinsky,D. (1992). *Issues in Geosynthetic-Reinforced Soil.* Special & keynote Lectures, International Symposium on Earth Reinforcement Practice, Fukuoka, Vol.1, pp117-143.

Long,N.T., Guegan,Y. and Legeay,G. (1972). *Etude la Terre Armee a L'apparail Triaxial Rapp. de Rhecherche.* LCPC, N°.17.

Long,J.H., Sieczkowski,W.F., Chow,E. and Cording,E.J. (1989). *Stability analyses for soil nailed walls.* Design and Performance of earth retaining structures, ASCE Geotechnical Special Publication, pp676-691.

Matsui,T., San,K.C. and Hayashi,K. (1990). *Design and field test on a reinforced cut slope.* Proc. of Int. Reinforced Soil Conference, Glasgow, pp235-239.

McGown,A., Andrawes,K.Z. and Al-Hasani,M.M. (1978). *Effect of inclusion properties on the behaviour of sand.* Geotechnique, Vol.28, N°.3, pp327-346.

McGown,A., Andrawes,K.Z. and Kabir,M.H. (1982). *Load-extension of geogrids confined in soil.* Proc. 2nd International Conference on Geotextiles, Las Vegas, Vol.3, pp793-798.

McGown,A., Murray,R.T. and Jewell,R.A. (1989). *State-of-the-art report on reinforced soil.* Proc. of 12th Int. Conf. of Soil Mech. and Found. Engi., Vol.4, pp2637-2648.

Meyerhof,G.G. (1978). *Bearing Capacity of Anisotropic Cohesionless Soils.* Canadian Geotechnical Journal, Vol.15, pp592-595.

Milligan,G.W.E. (1974). *The behaviour of rigid and flexible retaining walls in sand.* PhD. Thesis, University of Cambridge.

Milligan,G.W.E. (1984). *Soil deformations behind retaining walls.* Proc. of 3rd Int. Conf. of Ground Movements and Structures, Cardiff, pp707-721.

Milligan,G.W.E. (1991). *Personal communication.*

Mitachi,T., Yamamoto,Y. and Murai,S. (1992). *Estimation of in-soil deformation behaviour of geogrid under pull-out loading.* Proc. of Int. Symp. on Earth Reinforcement Practice, Vol.1, Fukuoka, pp121-126.

Muhlhaus,H.B. and Vardoulakis,I. (1987). *The thickness of shear bands in granular materials.* Geotechnique, N°.3, pp271-283.

Murray,R.T., Carder,D.R. and Krawczyk,J.V. (1979). *Pull-out tests on reinforcements embedded in uniformly graded sand subjected to vibration.* Proc. of 7th Euro. Conf. Soil Mech. Found. Engi., Vol.3, pp115-120.

Murray,R.T., Jones,C.J.F.P. and Smith,R.J. (1989). *Reinforced soil in areas of mining subsidence.* Proc. of 12th Int. Conf. of Soil Mech. and Found. Engi., Rio de Janeiro,

Neville,A.M. (1973). *properties of Concrete.* 2nd Edition, Pitman Publishing.

Okamoto,M., Ochi,K. Endou,O. and Kuroda. E. (1989). *Study on a new seismic method.* (Part 5), Tokyu Construction Technical Report, N°14, pp61-66.

Ovesen,N.K. (1975). *Centrifugal testing applied to bearing capacity of footings on sand.* Geotechnique, Vol.25, N°.2, pp103-120.

Ovesen,N.K. (1979). *Design parameters in geotechnical engineering.* Proc. of 7th Euro. Conf. on Soil Mech., Brighton, Vol.4, pp319-323.

Ovesen,N.K. and Krarup,J. (1983). *Centrifuge tests of embankment reinforced with geotextiles on soft clay.* Proc. of 8th Euro. Conf. on Soil Mech. and Found. Eng., Helsinki, Vol.1, pp393-398.

Ovesen,N.K. (1984). *Centrifuge tesys of embankments reinforced with geotextiles on soft clay.* Proc. of Int. Symp. on Geotechnical Centrifuge Model Testing, pp14-21.

Palmeira,E.M. (1987). *The study of soil-reinforcement interaction by means of large scale laboratory tests.* DPhil. Thesis, University of Oxford.

Palmeira,E.M. and Milligan,G.W.E. (1989). *Scale and other factors influencing the results of grids buried in sand.* Geotechnique, Vol.39, N°.3, pp511-524.

Pang,P.R.L. (1990). *Design of reinforced fill structures in Hong Kong.* Proc. of Int. Conf. of Performance of reinforced soil structures, Glasgow, pp25-30.

Pedley,M.J. (1990). *The performance of Soil Reinforcement in Bending and Shear.* DPhil. Thesis, University of Oxford.

Plumelle,C. (1984). *Improvement of the bearing capacity of soil by inserts of group and reticulated micropiles.* Proc. of Int. Conf. of In Situ Soil and Rock Reinforcement, Paris, pp83-89.

Plumelle,C. (1987). *Renforcement des sols par Clouage.* Le Frottement lateral le long des barres, C.E.B.T.P., France, pp1-16.

Plumelle,C., Schlosser,F., Delage,P. and Knochenmus,G. (1989). *French national research project on soil nailing.* Design and Performance of earth retaining structures, ASCE Geotechnical Special Publication, pp660-pp675.

Powrie,W. (1986). *The behaviour of diaphragm walls in clay.* Ph.D. Thesis, University of Cambridge.

Randolph,M.F. and Wroth,C.P. (1978). *Analysis of Deformation of Vertically Loaded Piles.* Journal of the Geotechnical Engineering Division, Vol.12, pp1465-1488.

Romstad,K.M., Al-Yassin,A., Herrmann,L.R. and Shen,C.K. (1978). *Stability analysis of reinforced earth retaining structures.* Proceedings of Symposium on Earth Reinforcement, ASCE, Pittsburg, pp685-713.

Roscoe,K.H. (1970). *The influence of strains in soil mechanics.* Geotechnique, Vol.20, N°.2, pp129-170.

Rowe,P.W. (1951). *Cantilever sheet piling in cohesionless soil.* Engineering, pp316-319.

Rowe,P.W. (1962). *The stress dilatancy relation for static equilibrium of an assembly of particles in contact.* Geotechnique, Vol.19, N°.1, pp500-527.

Rowe,P.W. (1969). *The relation between shear strength of sands in triaxial compression,* Geotechnique, Vol.19, N°.1, pp75-86

Rowe,R.K. and Ho,S.K. (1992). *A review of the Behaviour of Reinforced Soil Wall.* Special & Keynote Lectures, International Symposium on Earth Reinforcement Practice, Fukuoka, pp47-76.

San,K.C. and Matsui,T. (1992). *Application of finite element system to reinforced soils.* Proceedings of International Symposium on Earth Reinforcement Practice, Vol.1, Fukuoka, pp403-408.

Santamarina,J.C. (1984). *Effect of adjacent soils on reinforced soil structures - Centrifuge model testing.* MSc. Thesis, University of Maryland.

Schlosser,F. (1977). *Experience on reinforced earth in France.* Proc. of Symp. on Reinforced earth and other composite soil techniques. Edinburgh, pp195-209.

Schlosser,F. (1982). *Behaviour and design of soil nailing.* Proc. Symposium Recent Developments in Ground Improvement Techniques, Bangkok, pp399-413.

Schlosser,F. (1990). *Mechanically stabilized earth retaining structures in Europe.* Design and Performance of earth retaining structures, ASCE Geotechnical Special Publication, pp347-377.

Schlosser,F. and Elias,V. (1978). *Friction in reinforced earth.* A.S.C.E. Convention, Pittsburgh, U.S.A.

Schlosser,F. and Guilloux,A. (1979). *Le frottement sol-armature dans les ouvrages en Terre Armee.* Proc. of Int. Conf. on Soil Reinforcement, Vol.1, Paris.

Schlosser,F. and Guilloux,A. (1981). *Le frottement dans le reinforcement des sols.* Revue Francaise de Geotechnique, N°.16, pp65-77.

Schlosser,F. and Juran,I. (1983). *Behaviour of reinforced earth retaining walls from model studies.* Developments in soil mechanics and foundation engineering-1, Applied Science Publishers, London and New York, pp197-229.

Schlosser,F., Plumelle,C., Unterreiner,P. and Benoit,J. (1992). *Failure of a full scale experimental soil nailed wall by reducing the nails lengths.* International Symposium on Earth Reinforcement Practice, Vol.1, Fukuoka, pp531-535.

Schmertmann,G.R., Chew,S.H. and Mitchell,J.K. (1989). *Finite element modeling of reinforced soil wall behaviour.* Geotechnical Engineering Research Report N°89-01, University of California, Berkeley.

Schofield,A.N. (1980). *Cambridge geotechnical centrifuge operations. Geotechnique, Vol.30, N°.3, pp225-268.*

Shen,C.K., Mitchell,J.F., Denatale,J.S. and Romstad,K.M. (1979). *Laboratory testing and model studies of friction in reinforced earth.* C. R. Coll. Int. of Reinforcement des Sols, Paris, pp169-174.

Shen,C.K., Bang,S. and Herrman,L.R. (1981). *Ground Movement Analysis of Earth Support System.* Journal of the Geotechnical Engineering Division, Vol.107, N°.12, pp1609-1642.

Shen,C.K., Kim,Y.S., Bang,S. and Mitchell,J.F. (1982). *Centrifuge Modelling of Lateral Earth Support.* Journal of the Geotechnical Engineering Division, Vol.108, N°.9, pp1150-1164.

Smith,A.K.C. (1977). *Experimental and computational investigations of model reinforced earth retaining walls.* PhD. Thesis, University of Cambridge.

Snyder,V.W. (1979). *Factors governing the effectiveness of rock bolts.* Proc. of 20th U.S. Symposium of Rock Mechanics, pp342-358.

Sokolovski,V.V. (1965). *Statics of Granular Media.* Pergamon Press, Oxford.

Stewart,D.I. (1990). *Groundwater effects on in-situ walls in stiff clay.* PhD. Thesis, University of Cambridge.

Stocker,M.F., Korber,G.W., Gassler,G. and Gudehus,G. (1979). *Soil nailing.* Proc. of Int. Symp. of Reinforcement des Soils, Paris, pp469-474.

Stocker,M.F. and Reidinger,G. (1990). *The bearing behaviour of nailed retaining structures.* Proc. ASCE Conference Design and Performance of Earth Retaining Structures, ASCE Geotechnical Special Publication N°.25, pp676-691.

Stroud,M.A. (1971). *The behaviour of sand at low stress levels in the simple shear apparatus.* PhD thesis, University of Cambridge.

Symes,M.J. (1983). *Rotation of principal stresses in sand.* PhD. Thesis, Imperial College, University of London.

Tan,F.S.C. (1990). *Centrifuge and theoretical modelling of conial footings on sand.* PhD. Thesis, University of Cambridge.

Taniguchi,E., Koga, Y. and Yasuda,S. (1987). *Centrifugal Model Tests on Geotextile Reinforced Embankments.* Proc. of 8th Asian Regional Conf. of Soil Mech. and Found. Engi., pp499-502.

Tatsuoka,F. (1987). *Discussion on strength and dilatancy of sand.* Geotechnique, Vol.38, N°.1, pp219-225.

Tatsuoka,F., Tateyama,M. and Murata,O. (1989). *Earth retaining wall with a short geotextile and a rigid facing.* Proc. of 12th Int. Conf. of Soil Mech. and Found. Engi., Rio de Janeiro, pp1311-1314.

Tatsuoka,F. (1992). *Roles of Facing Rigidity in Soil Reinforcement.* Special & Keynote Lectures, Internatonal Symposium on Earth Reinforcement Practice, Fukuoka, pp77-115.

Taylor,D.W. (1948). *Foundations of Soil Mechanics.* Wiley, New York.

Taylor,R.N. (1984). *Ground movements associated with tunnels and trenches.* PhD. Thesis, University of Cambridge.

Teramoto,K., Taga,N., Naruse,T. and Tayama, S. (1992). *Model loading tests of reinforced slope with steel bars.* International Conference on Earth Reinforcement Practice, Fukuoka, Vol.1, pp561-566.

Tateyama,M., Tamura,Y., Tarumi,H. and Tatsuoka,F. (1992). *Permanent cut of an embankment slope by soil nailing allowing very small deformation.* International Conference on Earth Reinforcement Practice, Fukuoka, Vol.1, pp555-560.

Terzaghi,K. (1955). *Evaluation of coefficient of subgrade reaction.* Geotechnique, Vol.5., pp297-326.

Terzaghi,K. and Peck,R.B. (1948). *Soil Mechanics in Engineering Practice.* J.W. & Sons, New York.

Tubouchi,T., Tei,K. and Ochi,K. (1990). *An experimental study on a method which employs short steel bars and large-sized bearing plates to reinforce a cut slope.* Proc. of Int. Reinforced Soil Conference, Glasgow, pp225-229.

Tufenkjian,M.R. and Vucetic,M. (1992). *Seismic stability of soil nailed excavations.* Proceedings of International Symposium on Earth Reinforcement Practice, Fukuoka, Vol.1, pp573-578.

Vidal,H. (1969). *La Terre Armee.* Annales de l'Institute Technique du Batiment et des Travaux Publics, Paris, pp888-939.

Wernick,E. (1977). *Stresses and strains on the surface of anchors.* Special Session, Proc. of the 9th Int. Conf. of Soil Mech. and Found. Engi., Tokyo, N°.4,

Whittle,A.J., Germaine,J.T., Larson,D.G. and Abramento,M. (1992). *Measurement and interpretation of reinforcement stiffness in the APSR cell.* Proc. of Int. Symp. on Earth reinforcement Practice, Vol.1, Fukuoka, pp179-184.

Wroth,C.P. (1972). *General theories of earth pressure and deformation.* General Report, 5th Euro. Conf. of Soil Mech. and Found. Engi., Vol.2, pp33-52.

Yazici,S. and Kaiser,P.K. (1992). *Bond Strength of Grouted Cable Bolts.* Int. Journal of Rock Mech. Min. Sci. and Geomech., Vol.29, N°.3, pp279-292.

Yoo,N.J. (1988). *Centrifugal model experiments of reinforced earth retaining walls.* PhD. Thesis, University of Colorado, Boulder.

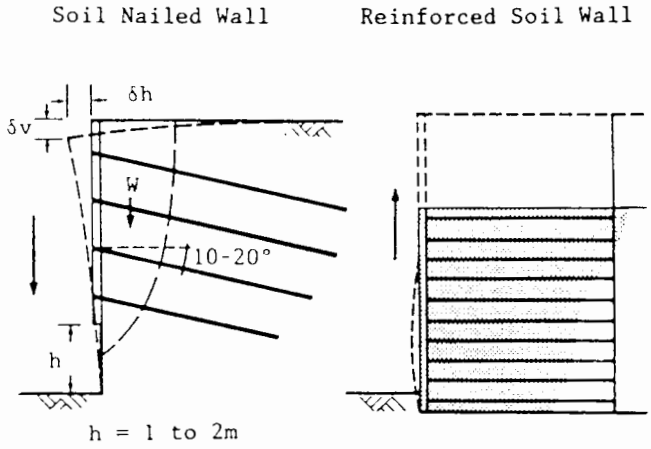

Fig.1.1 - Comparison of soil nailing and reinforced soil wall (after Jones, 1990).

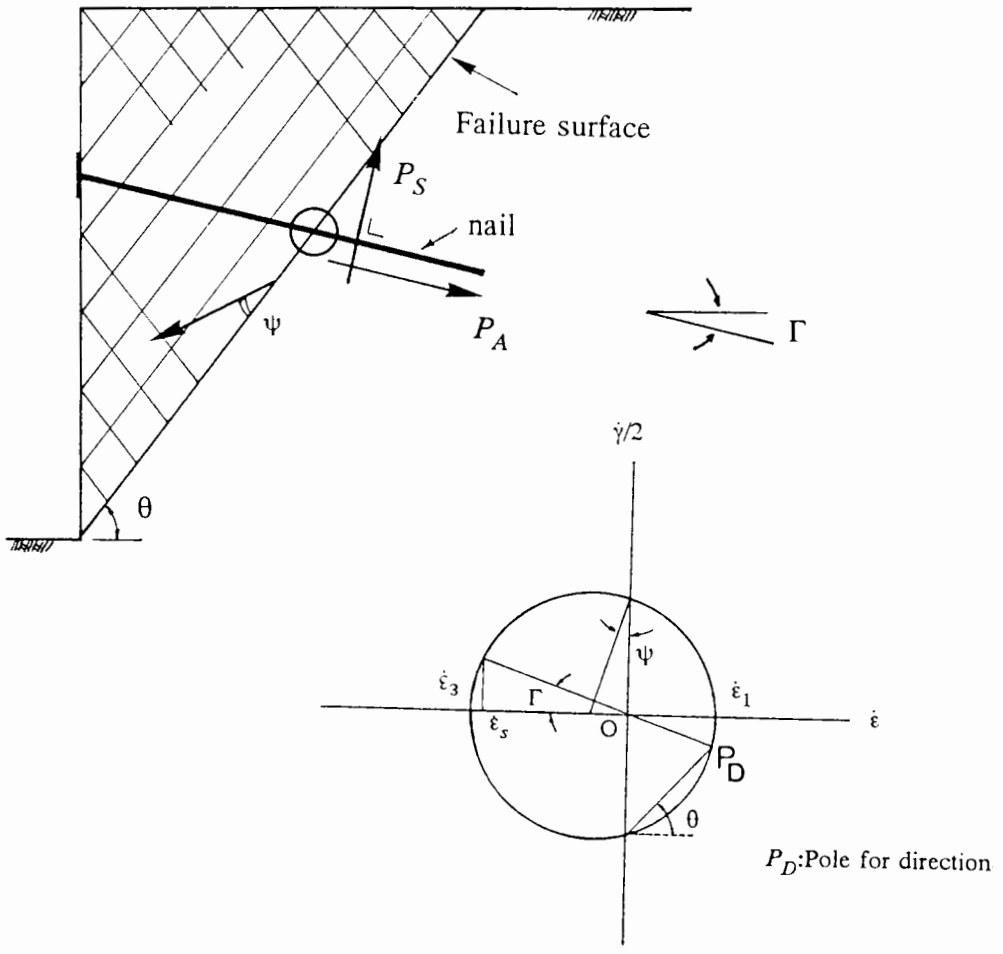

Fig.1.2 (a) - Strains of soil and nail forces

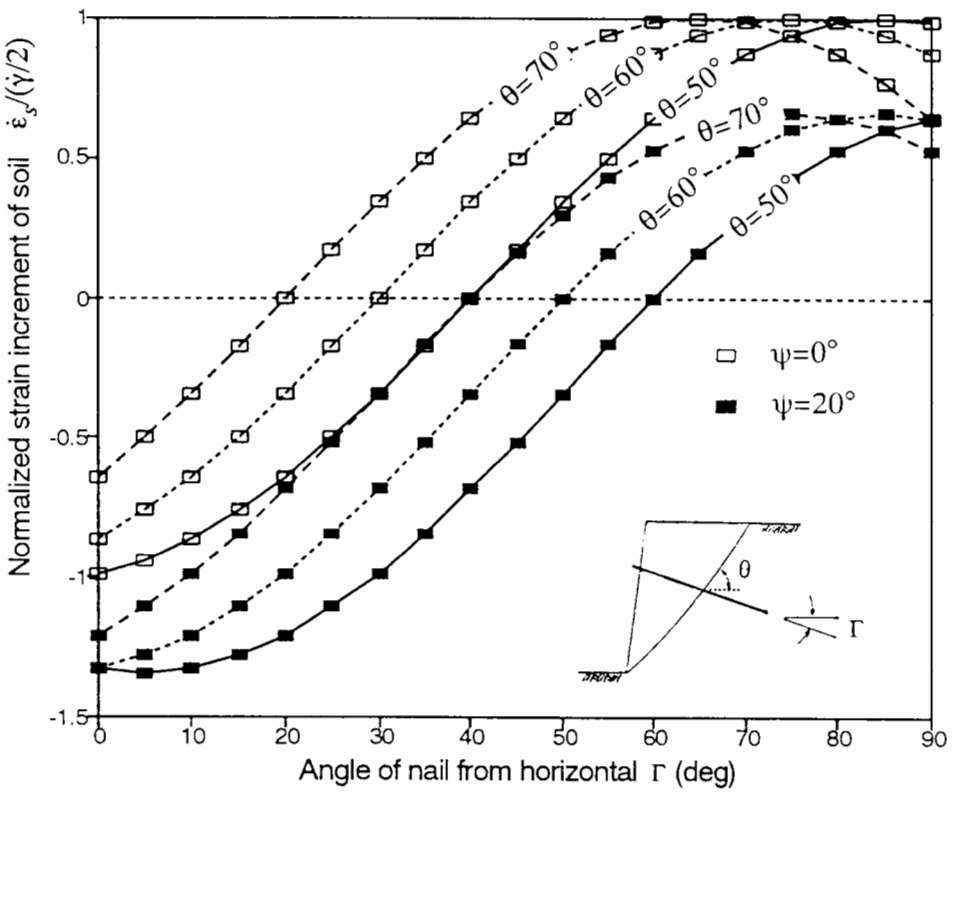

Fig.1.2 (b) - Normalized normal strain of soil and direction of nail

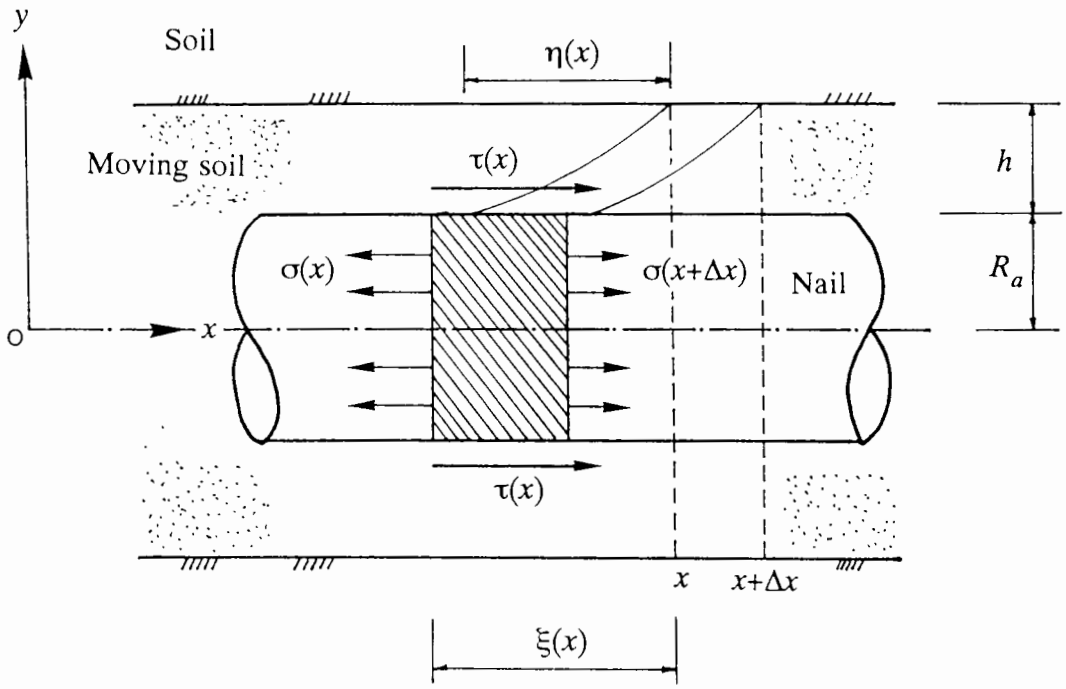

Fig.1.3 - Nail-Soil model in equilibrium

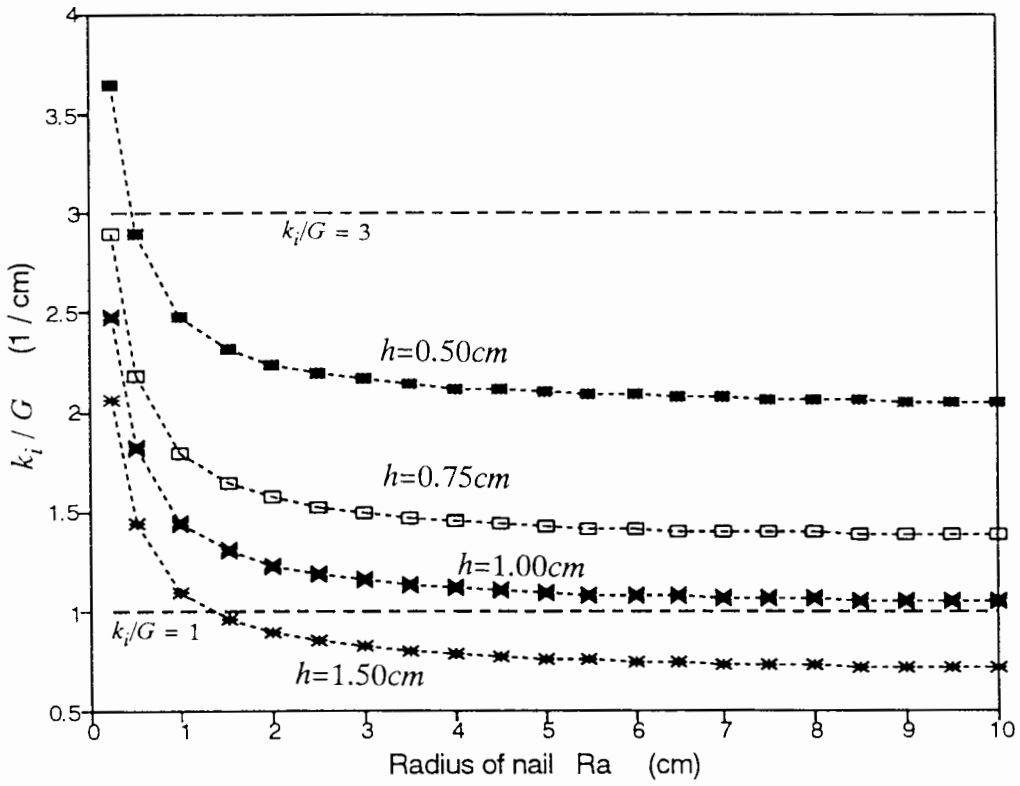

Fig.1.4 - Relationship between interaction parameter and radius of nail

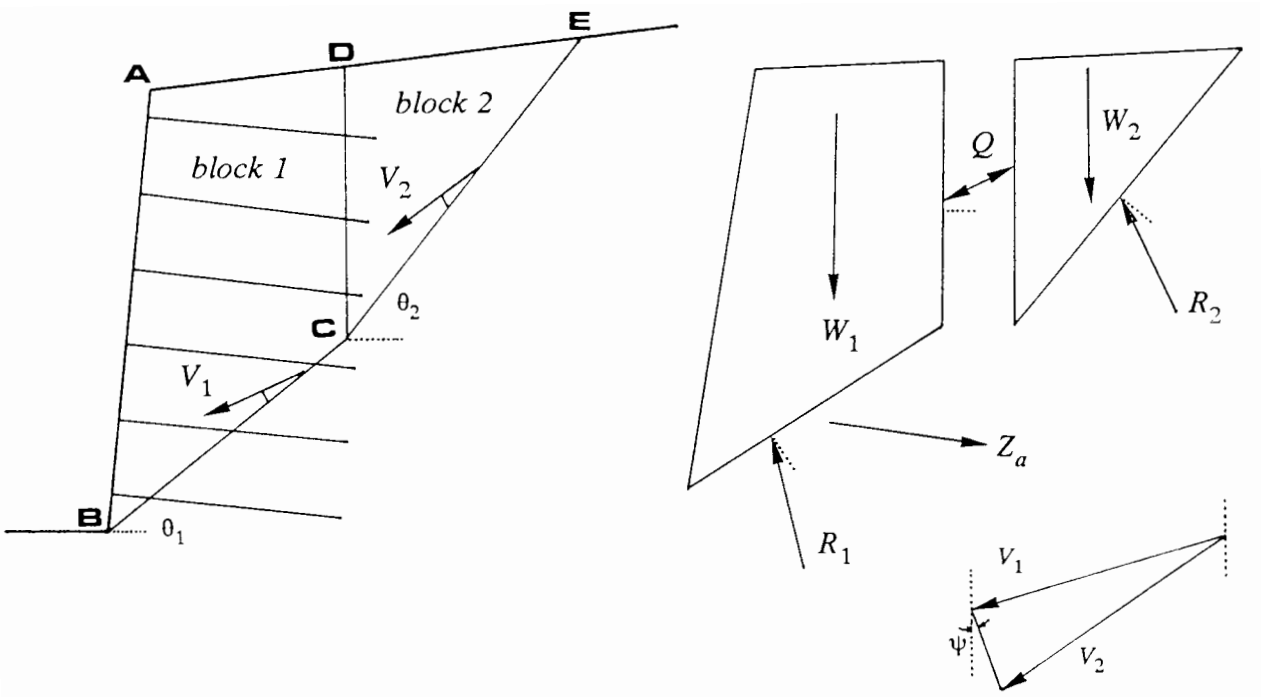

Fig.1.5 - Two wedge mechanism for limit equilibrium analysis

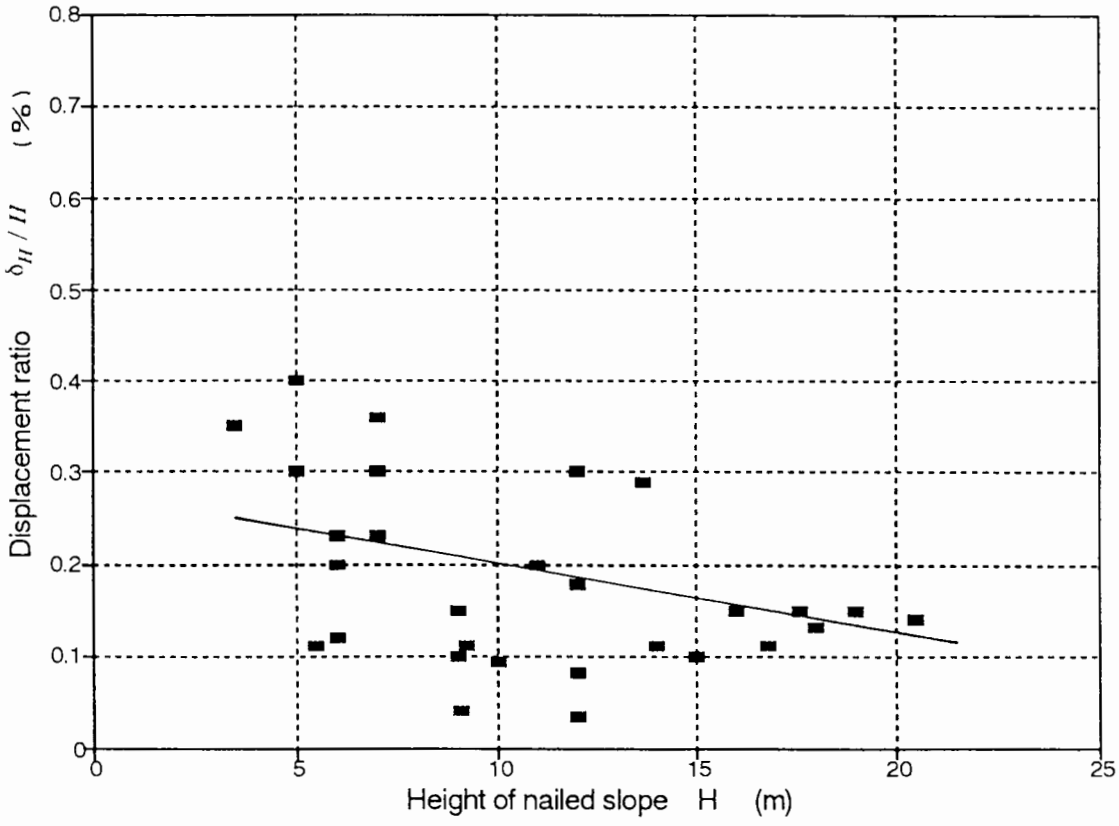

Fig.1.6 - Relationship between displacement ratio and slope height from *in - situ* data

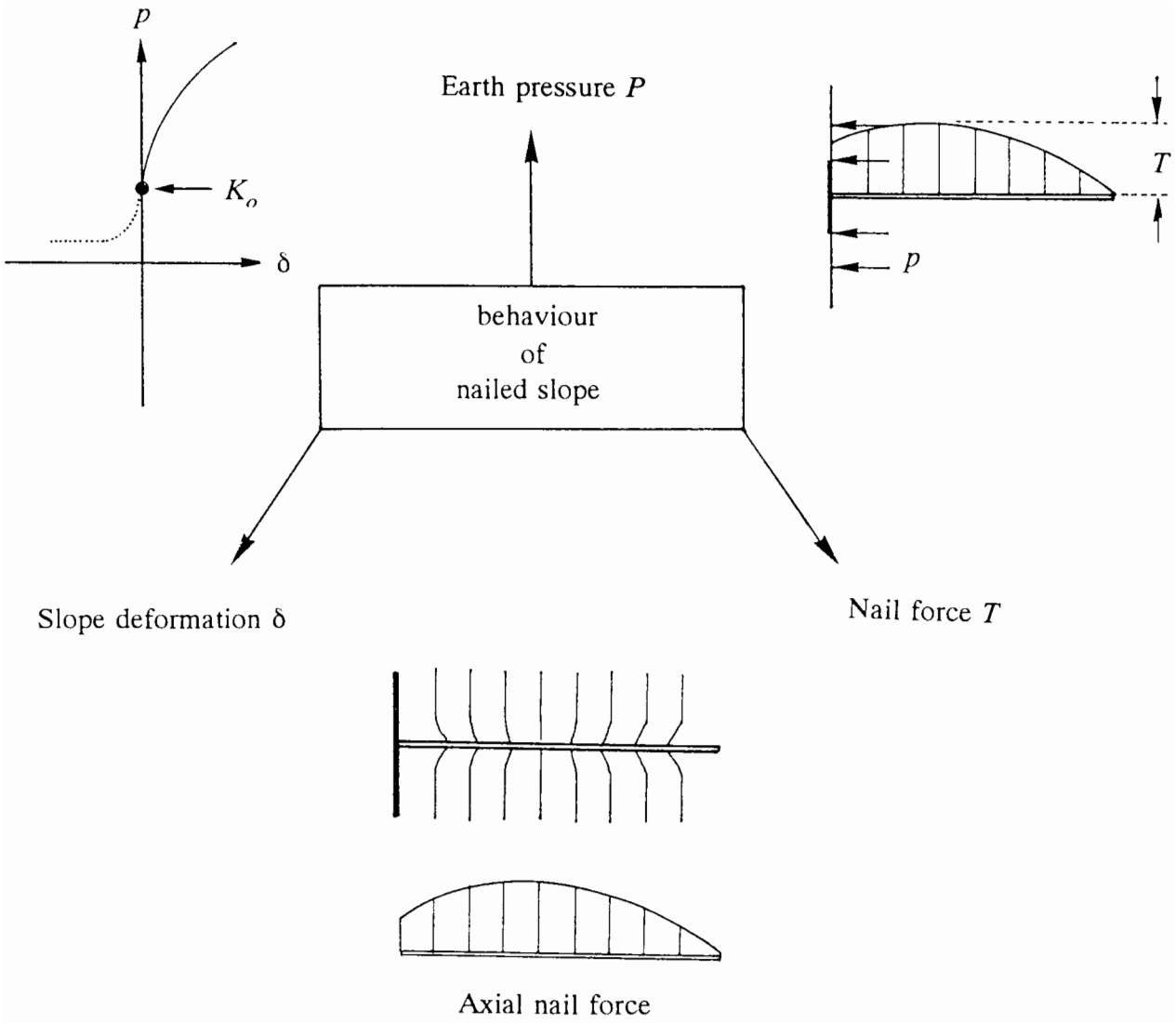

Fig.1.7 - Factors governing the mechanical behaviour of nailed slope

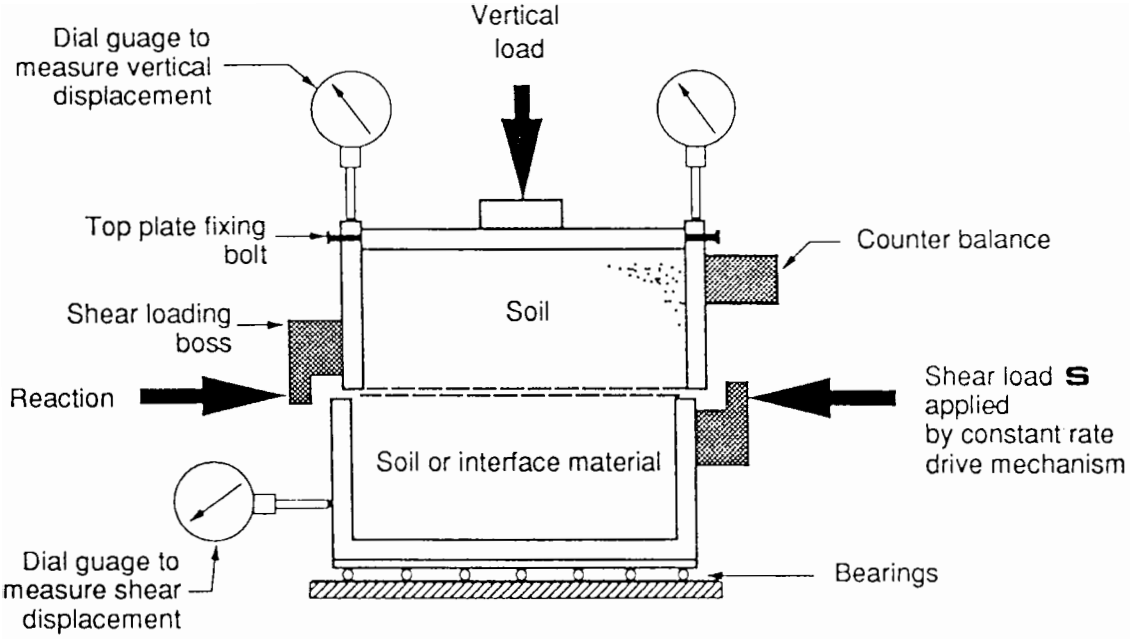

Fig.2.1 - Elevation of the Medium shearbox apparatus (after Pedley, 1990).

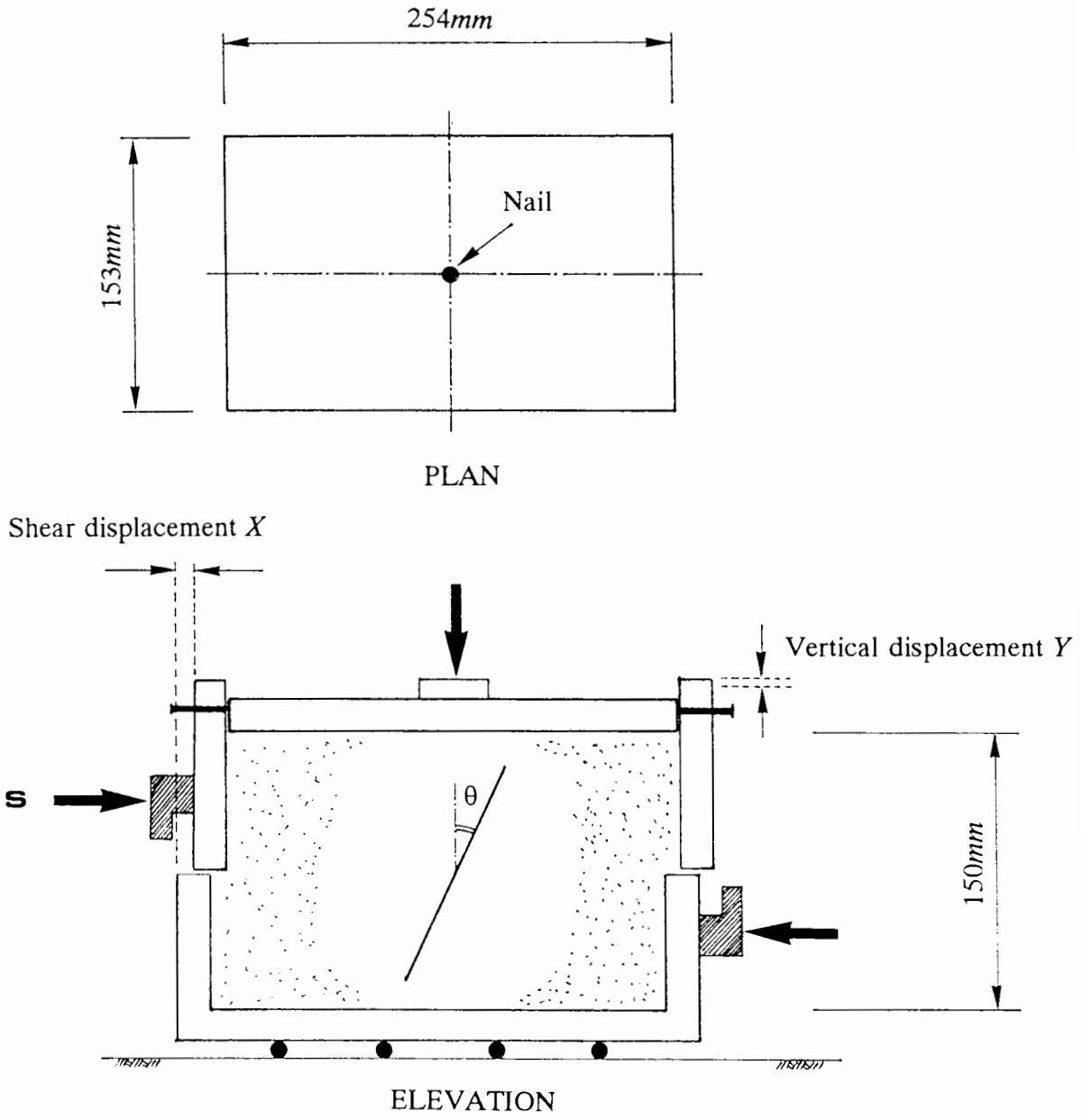

Fig.2.2 - Overview of the direct shear test of nailed sand

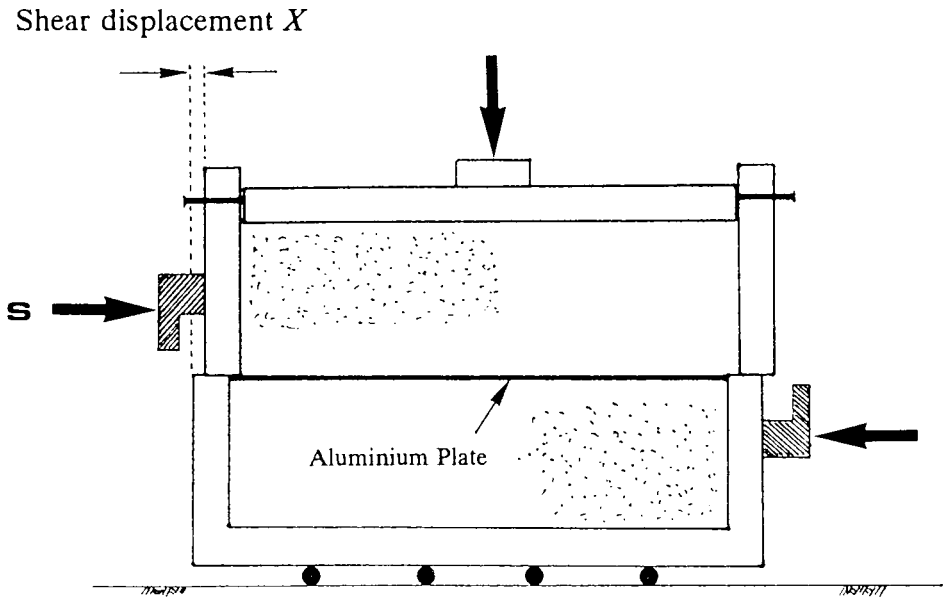

Fig.2.3 - Elevation of the interface test

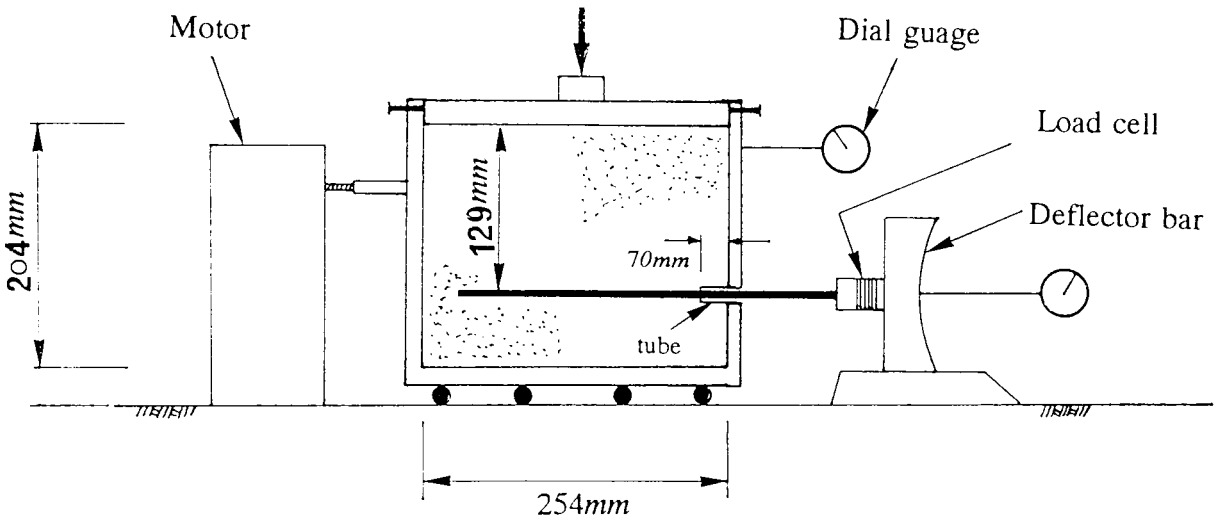

Fig. 2.4 - Elevation of the pull-out test of a nail

sand	G_s	e_{max}	e_{min}	$(\gamma_d)_{max}$ (kN/m^3)	D_{50} (mm)	Particle size (mm)
50/100	2.65	0.89	0.57	16.65	≈ 0.18	0.15 ~ 0.2
14/25	2.65	0.79	0.49	17.50	≈ 0.8	0.6 ~ 1.18

Table 2.1 - Summary of the properties of the Yellow Leighton Buzzard Sands

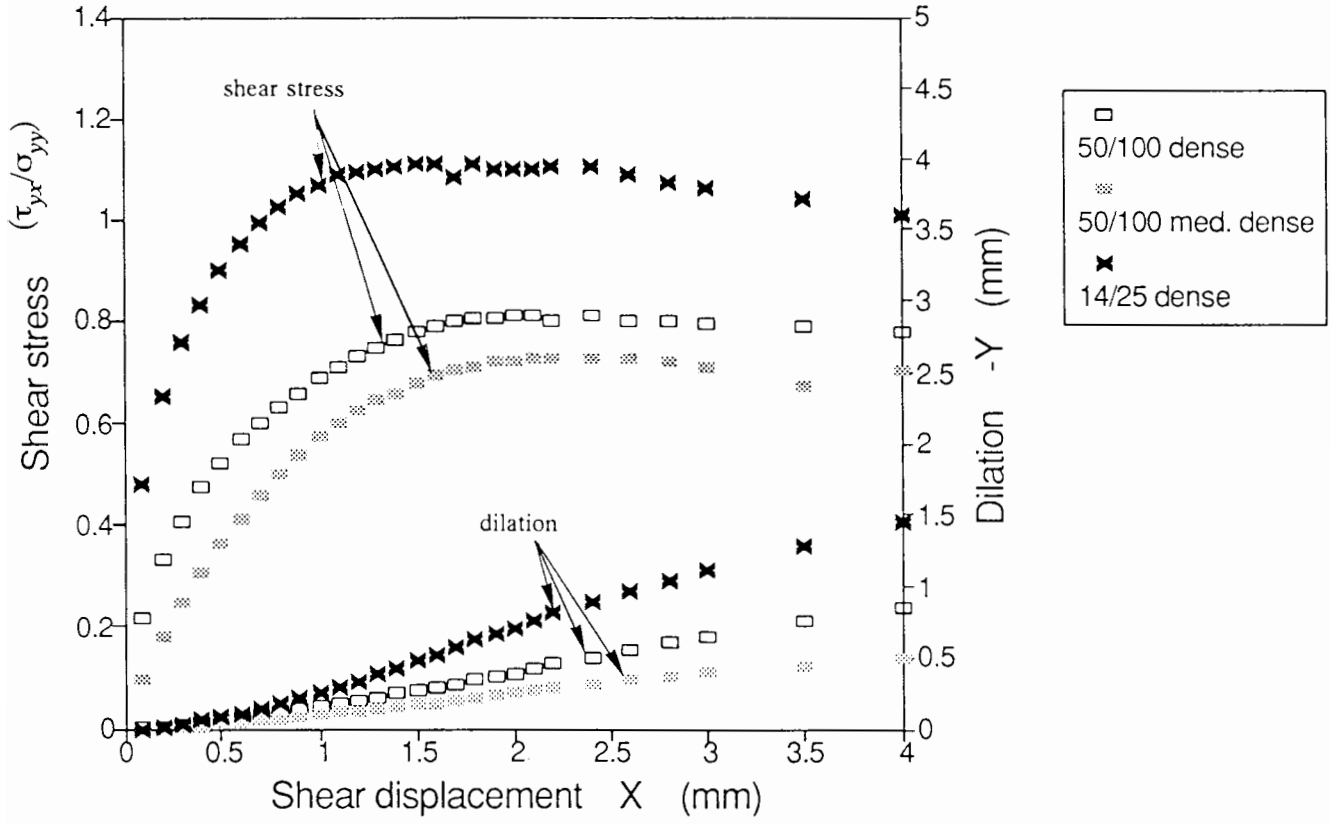

Fig.2.5 - Direct shear test data for sands

	50/100 dense	50/100 med. dense	14/25 dense
Friction angle ϕ_{ds}	39°	36°	48°
Dilation angle ψ	15°	10°	26°

Table 2.2 - Summary of the properties of the test sands

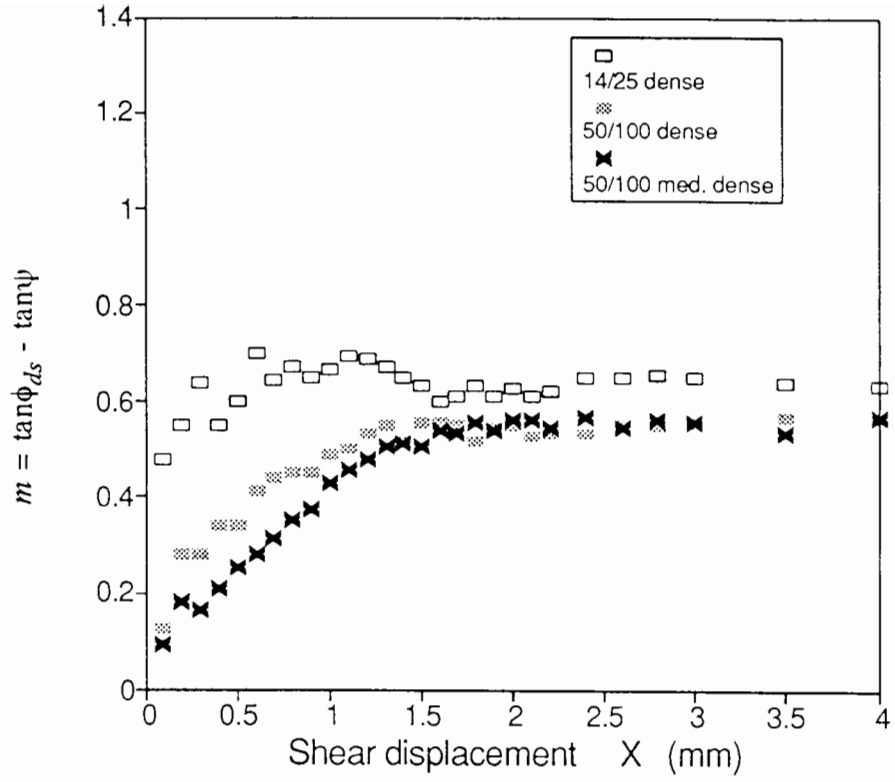

Fig.2.6 - Taylor's energy correction on sands

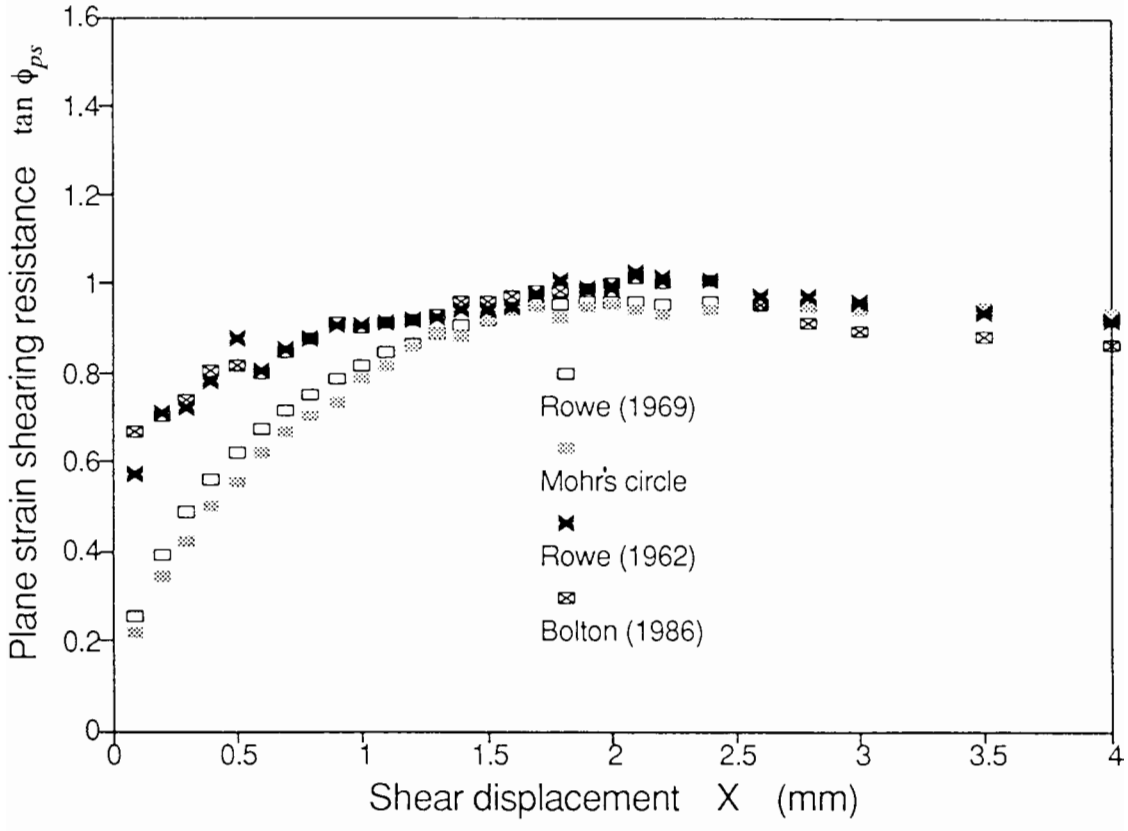

Fig.2.7 - Comparison between the mobilised plane strain friction angle deduced from different methods of analysis.

Test	Nail length l (mm)	Diameter D (mm)	Surcharge σ_v (kN/m^2)	Peak force F_p (N)	f^*	μ^*
R1-1	200	1.7	22.7	44.9	2.81	3.47
R1-2	200	2.1	22.7	54.3	2.75	3.40
R1-3	200	2.7	22.7	63.8	2.51	3.10
R1-4	200	3.3	22.7	76.1	2.45	3.02
R1-5	200	3.9	22.7	86.2	2.35	2.90
R1-6	200	4.7	22.7	96.8	2.19	2.70
R1-7	200	5.9	22.7	111.6	2.01	2.48
R1-8	180	1.7	22.7	39.0	2.71	3.35
R1-9	150	1.7	22.7	33.2	2.77	3.42
R1-10	90	1.7	22.7	19.1	2.66	3.28
R1-11	200	1.7	5.6	11.9	3.00	3.70
R1-12	200	1.7	11.0	22.7	2.93	3.62
R1-13	200	1.7	16.2	32.5	2.85	3.52

Table 3.1 (a) - Pull-out tests of stiff - rough nail (50/100 dense sand)

Test	Nail length l (mm)	Diameter D (mm)	Surcharge σ_v (kN/m^2)	Peak force F_p (N)	f^*	μ^*
R2-1	200	1.7	22.0	32.4	2.03	2.80
R2-2	200	2.1	22.0	36.9	1.87	2.58
R2-3	200	2.7	22.0	46.2	1.82	2.50
R2-4	200	3.3	22.0	54.3	1.75	2.41
R2-5	200	3.9	22.0	61.2	1.67	2.30
R2-6	200	4.7	22.0	72.0	1.63	2.24
R2-7	200	5.9	22.0	85.9	1.55	2.14
R2-8	180	1.7	22.0	28.5	1.98	2.73
R2-9	150	1.7	22.0	24.9	2.08	2.86
R2-10	90	1.7	22.0	14.2	1.98	2.72
R2-11	200	1.7	6.7	9.8	2.01	2.76
R2-12	200	1.7	10.3	15.3	2.04	2.81
R2-13	200	1.7	15.5	22.7	2.02	2.78

Table 3.1 (b) - Pull-out tests of stiff - rough nail (50/100 medium dense sand)

Test	Nail length l (mm)	Diameter D (mm)	Surcharge σ_v (kN/m^2)	Peak force F_p (N)	f^*	μ^*
R3-1	200	3.0	23.2	107.5	4.10	3.69
R3-2	200	3.5	23.2	111.9	3.92	3.53
R3-3	200	3.9	23.2	131.6	3.86	3.48
R3-4	200	4.4	23.2	146.6	3.81	3.43
R3-5	200	5.0	23.2	160.4	3.67	3.30
R3-6	200	5.8	23.2	184.6	3.64	3.28
R3-7	180	3.0	23.2	96.8	4.10	3.69
R3-8	150	3.0	23.2	82.6	4.20	3.78
R3-9	90	3.0	23.2	47.9	4.06	3.66
R3-10	200	3.0	16.7	77.2	4.09	3.68
R3-11	200	3.0	11.5	54.3	4.18	3.76
R3-12	200	3.0	6.1	27.9	4.04	3.64

Table 3.1 (c) - Pull-out tests of stiff - rough nail (14/25 dense sand)

Test	Nail length l (mm)	Diameter D (mm)	Surcharge σ_v (kN/m^2)	Peak force F_p (N)	f^*	μ^*
S1-1	200	2.0	22.7	4.9	0.26	0.32
S1-2	200	2.6	22.7	6.6	0.27	0.33
S1-3	200	3.2	22.7	7.7	0.26	0.32
S1-4	200	4.0	22.7	9.9	0.26	0.32
S1-5	200	5.2	22.7	12.7	0.26	0.32

Table 3.1 (d) - Pull-out tests of stiff - smooth nail (50/100 dense sand)

Test	Nail length l (mm)	Diameter D (mm)	Surcharge σ_v (kN/m^2)	Peak force F_p (N)	f^*	μ^*
S3-1	200	2.0	23.2	5.7	0.33	0.30
S3-2	200	2.6	23.2	7.0	0.31	0.28
S3-3	200	3.2	23.2	9.0	0.32	0.29
S3-4	200	4.0	23.2	11.1	0.32	0.29
S3-5	200	5.2	23.2	14.6	0.32	0.29

Table 3.1 (e) - Pull-out tests of stiff - smooth nail (14/25 dense sand)

Test	Nail length l (mm)	Diameter D (mm)	Surcharge σ_v (kN/m^2)	Peak force F_p (N)	f^*	μ^*
F1-1	200	3.7	22.7	65.4	1.88	2.32
F2-1	200	3.7	22.7	73.1	2.10	2.89
F3-1	200	5.0	23.2	107.9	2.47	2.22

Table 3.1 (f) - Pull-out tests of flexible - rough nail (50/100 dense and medium dense sands and 14/25 dense sand)

Test	Diameter D (mm)	Length l_b (mm)	Angle θ (deg)	Surcharge σ_v (kN/m^2)	τ_{EXT} (kN/m^2)	$f^* =$ tan δ
D1-1	2.7	63.5	25	20.3	0.72	0.88
D1-2	3.9	63.5	25	20.3	0.91	0.78
D1-3	5.9	63.5	25	20.3	1.24	0.70
D1-4	7.8	63.5	25	20.3	1.50	0.64
D1-5	10.5	63.5	25	20.3	1.90	0.59

Table 3.2 (a) - Detail of reinforced direct shear tests (50/100 dense sand)

Test	Diameter D (mm)	Length l_b (mm)	Angle θ (deg)	Surcharge σ_v (kN/m^2)	τ_{EXT} (kN/m^2)	$f^* =$ tan δ
D2-1	2.7	63.5	25	20.3	0.55	0.81
D2-2	3.9	63.5	25	20.3	0.72	0.73
D2-3	5.9	63.5	25	20.3	0.95	0.64
D2-4	7.8	63.5	25	20.3	1.16	0.59
D2-5	10.5	63.5	25	20.3	1.35	0.51

Table 3.2 (b) - Detail of reinforced direct shear tests (50/100 medium dense sand)

Test	Diameter D (mm)	Length l_b (mm)	Angle θ (deg)	Surcharge σ_v (kN/m^2)	τ_{EXT} (kN/m^2)	$f^* =$ tan δ
D3-1	3.0	63.5	25	20.3	1.12	0.90
D3-2	3.9	63.5	25	20.3	1.34	0.83
D3-3	5.0	63.5	25	20.3	1.57	0.76
D3-4	8.4	63.5	25	20.3	2.16	0.62
D3-5	11.6	63.5	25	20.3	2.64	0.55

Table 3.2 (c) - Detail of reinforced direct shear tests (14/25 dense sand)

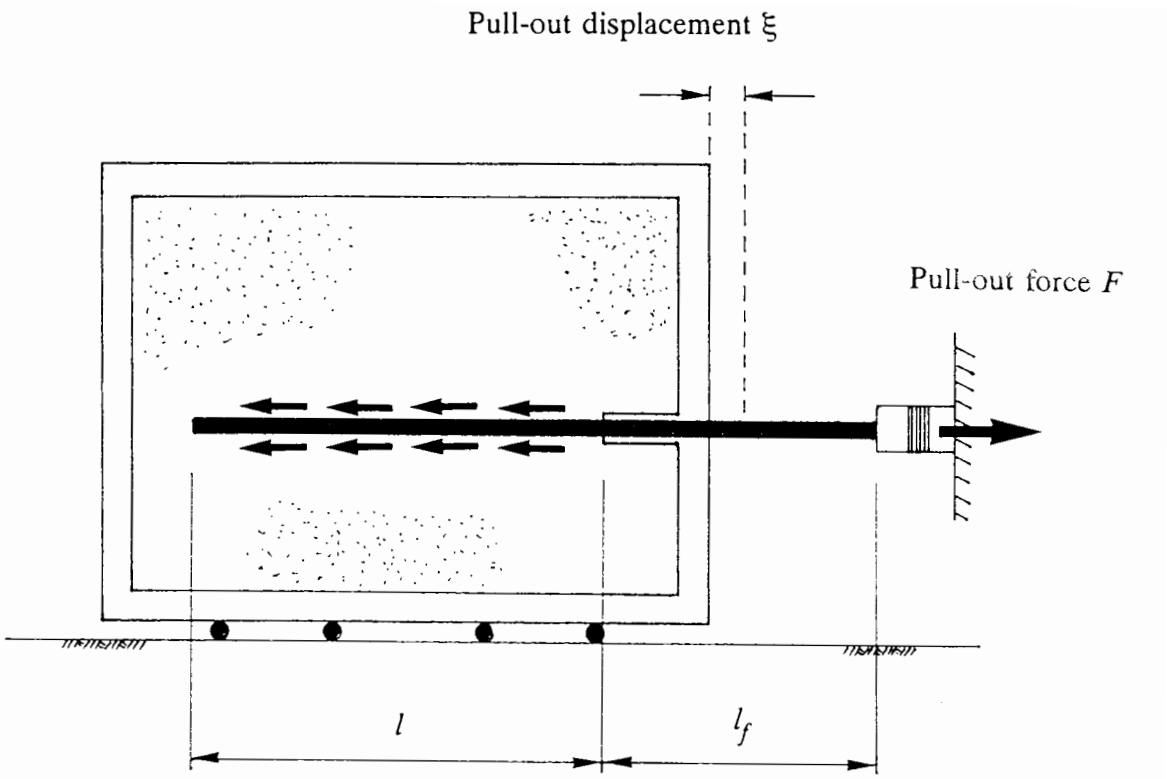

Fig.3.1 - Correlation of current nail length *l* during a pull-out test

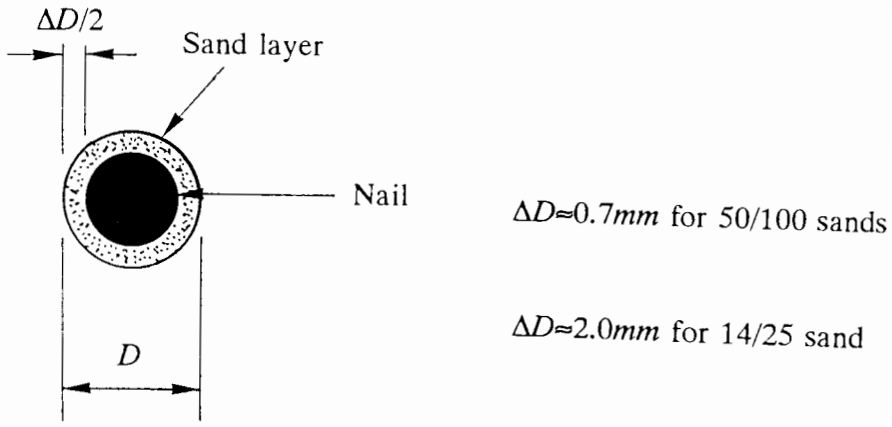

Fig.3.2 - Additional diameter ΔD due to sand layer

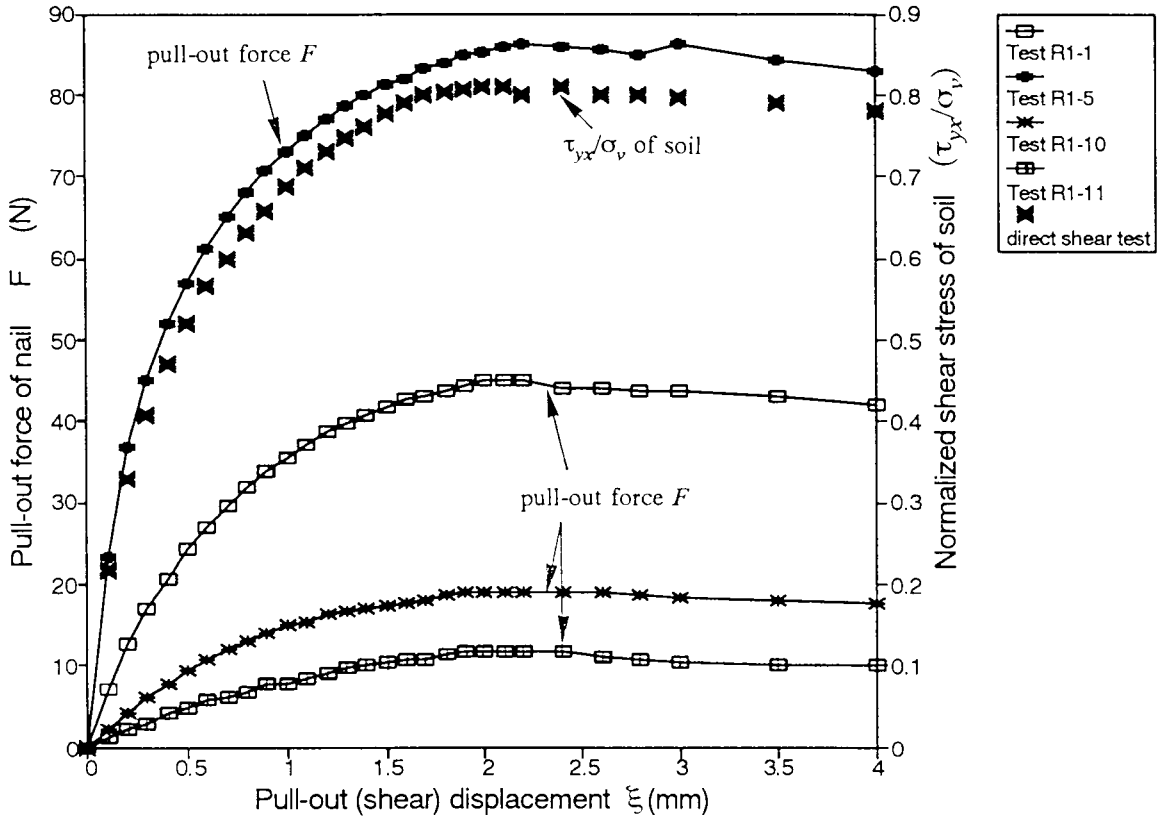

Fig.3.3 (a) - Pull-out curves of the stiff-rough nail on 50/100 dense sand

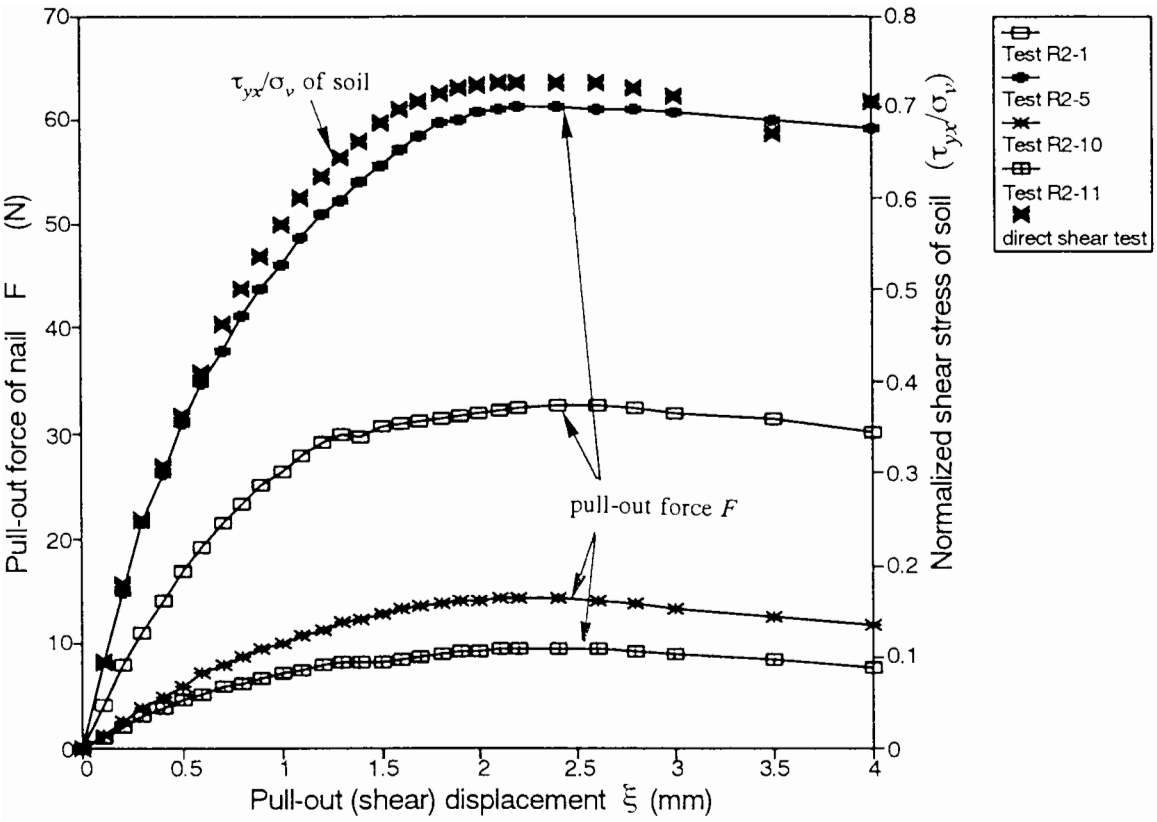

Fig.3.3 (b) - Pull-out curves of the stiff-rough nail on 50/100 medium dense sand

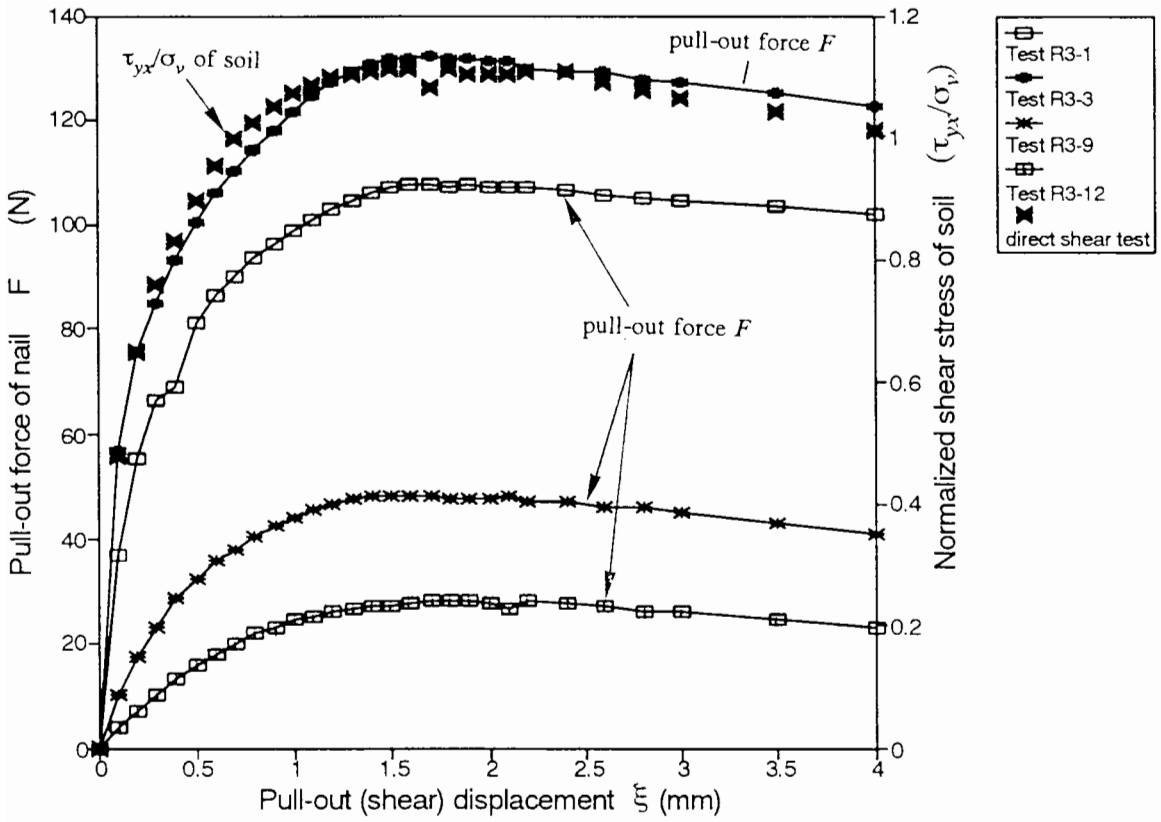

Fig.3.3 (c) - Pull-out curves of the stiff-rough nail on 14/25 dense sand

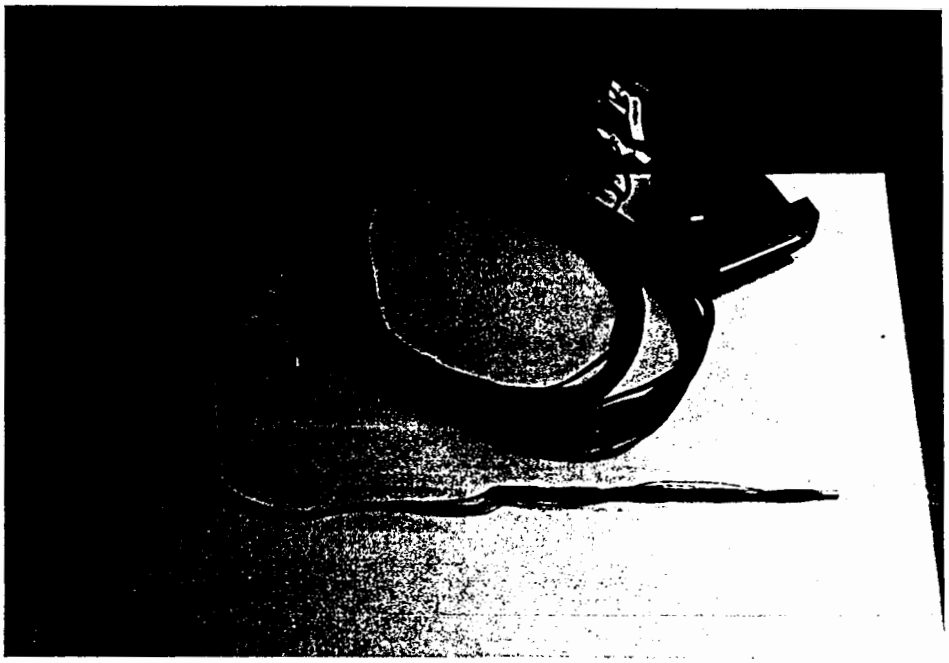

Plate 3.1 - Instrumented nail (before glueing sand on the surface)

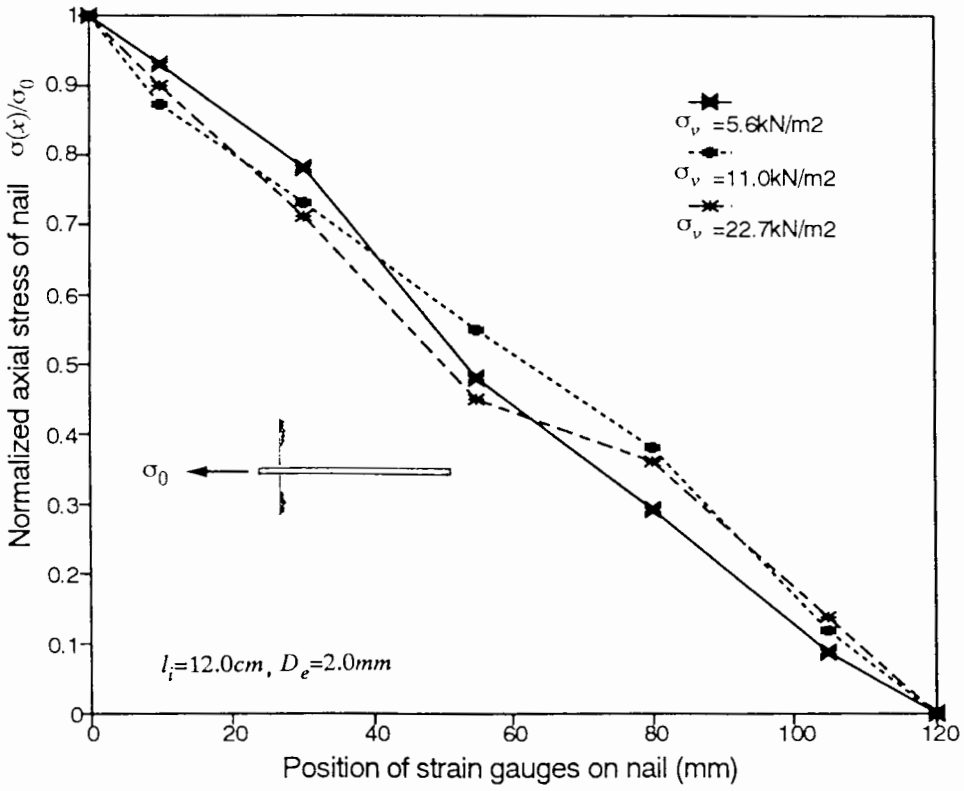

Fig.3.4 - Axial stress distributions of the stiff-rough nail as a function of surcharge in 50/100 dense sand (at peak pull-out force F_p)

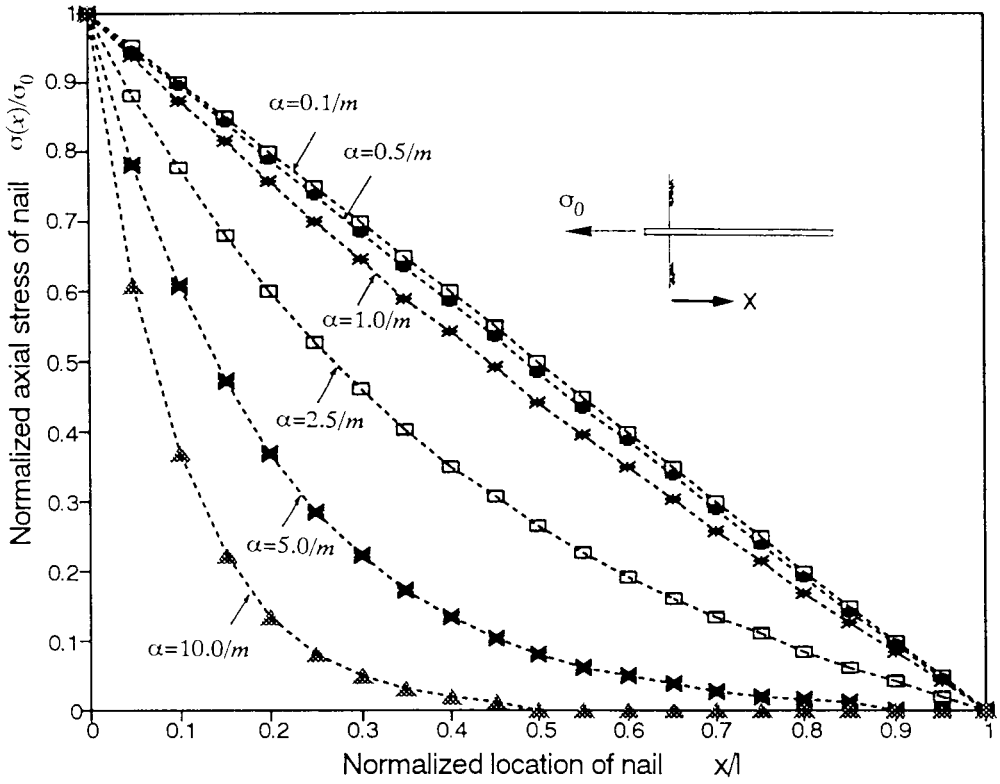

Fig.3.5 - Axial stress distributions of nail as a function of the parameter α

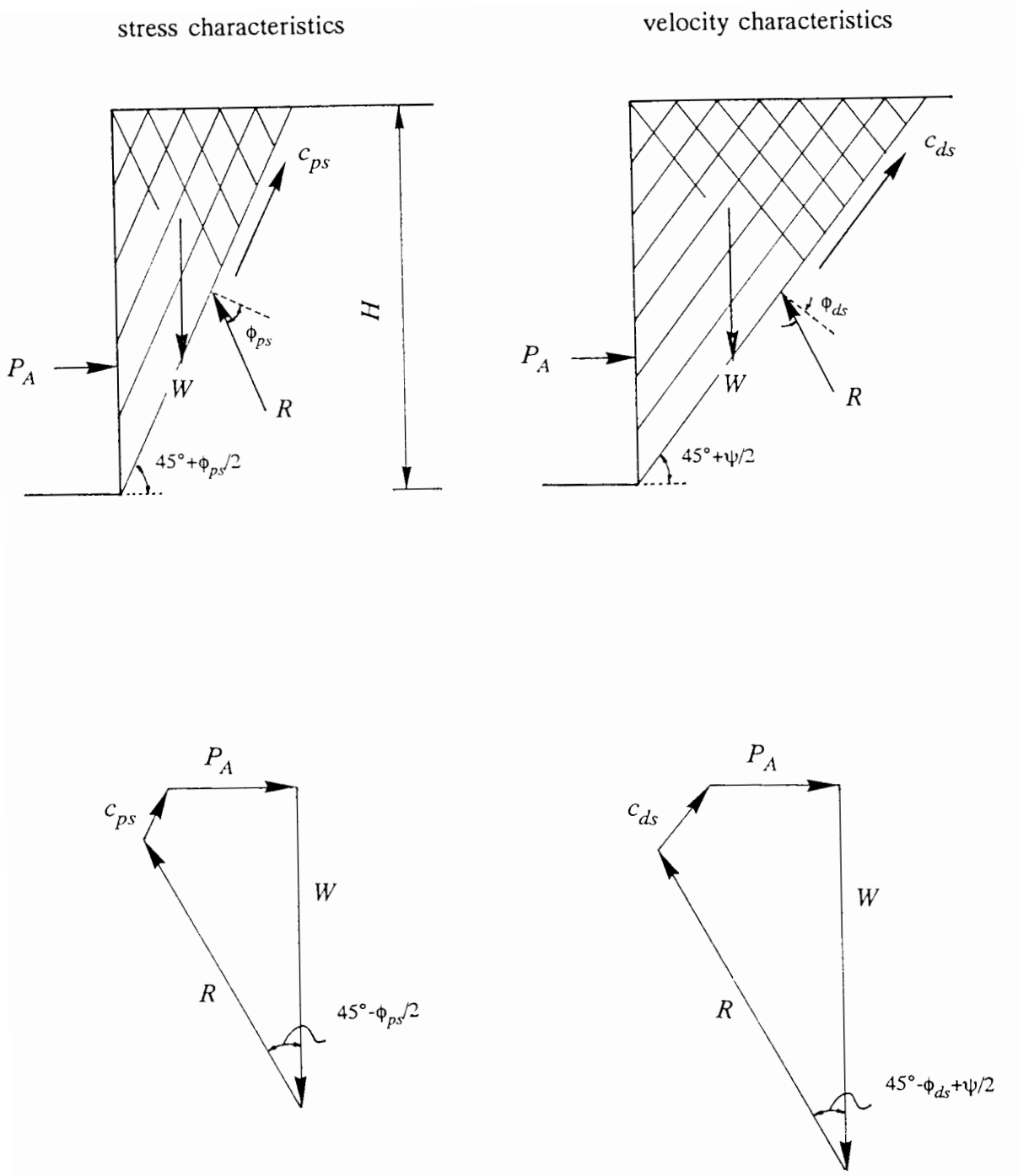

Fig.3.6 - Earth pressures obtained assuming the stress and velocity characteristics

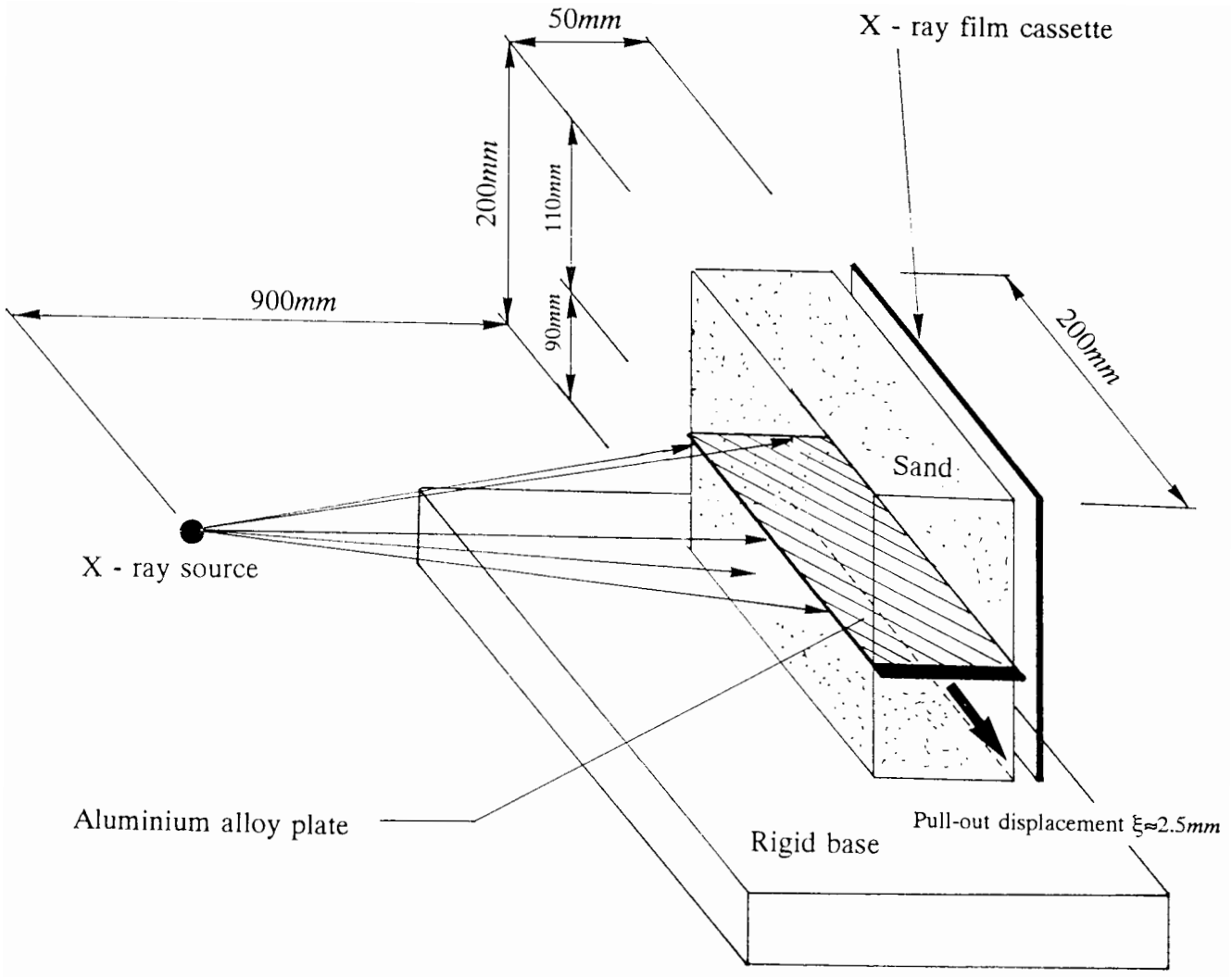

Fig.3.7 - Schematic view of the arrangement for the radiograph in pull-out test

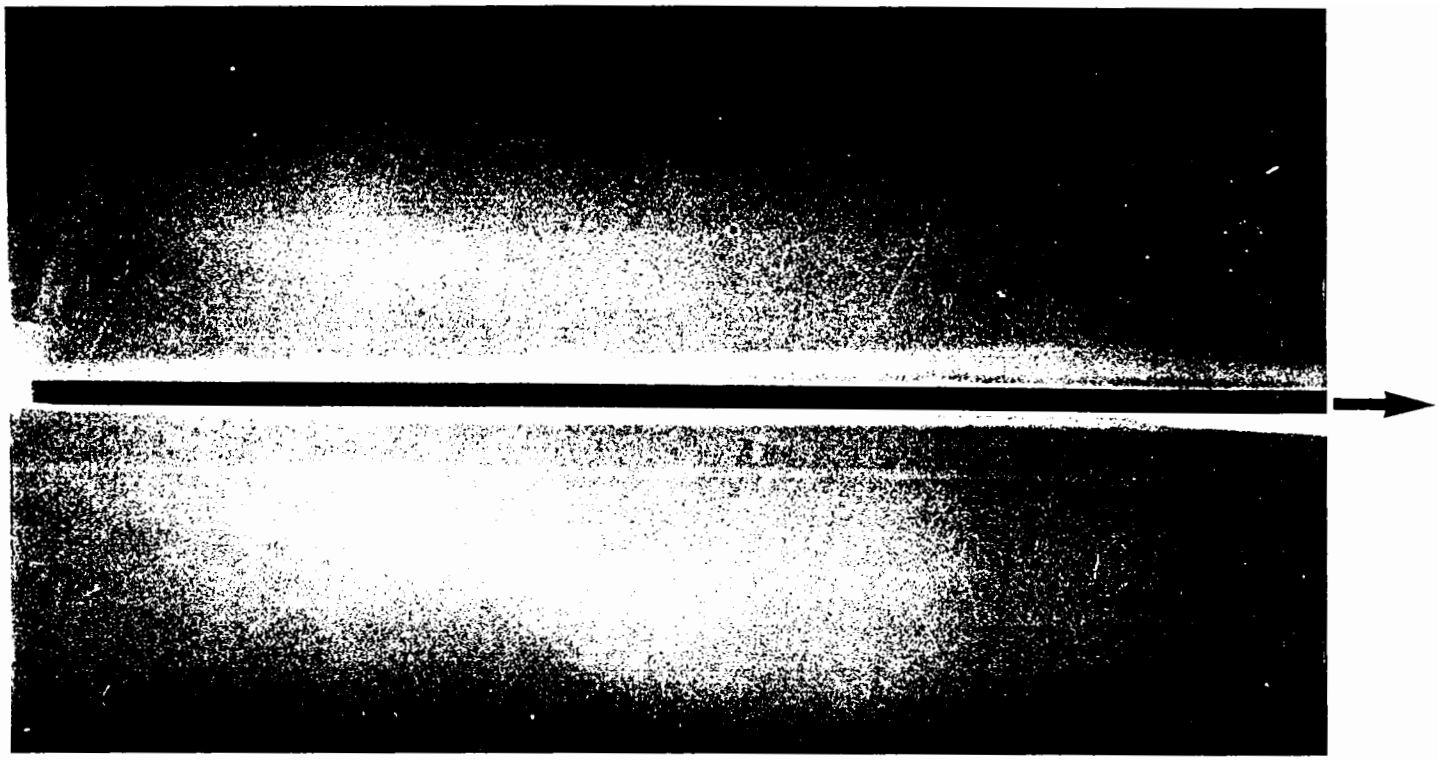

Fig.3.8 (a) - Rupture pattern around the rough reinforcement in 50/100 dense sand

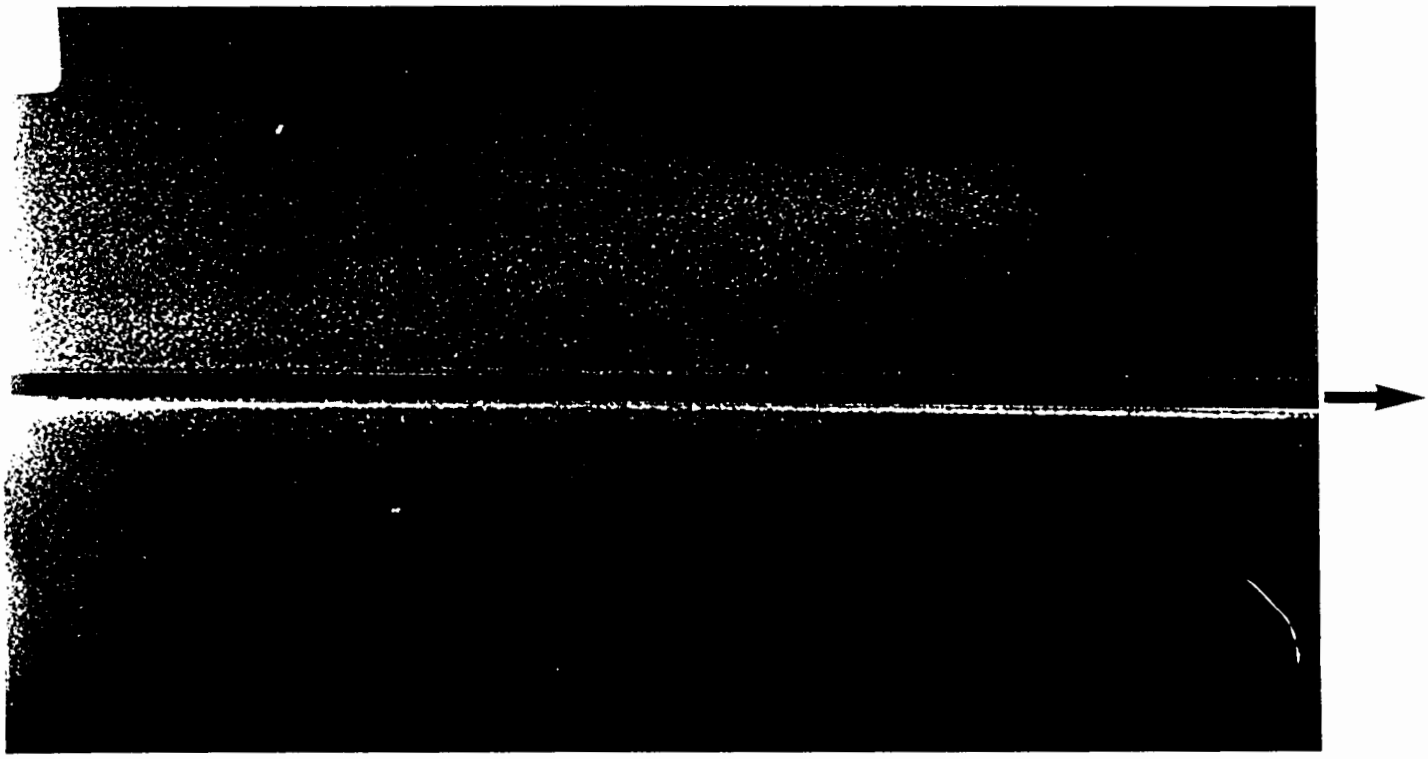

Fig.3.8 (b) - Rupture pattern around the smooth reinforcement in 50/100 dense sand

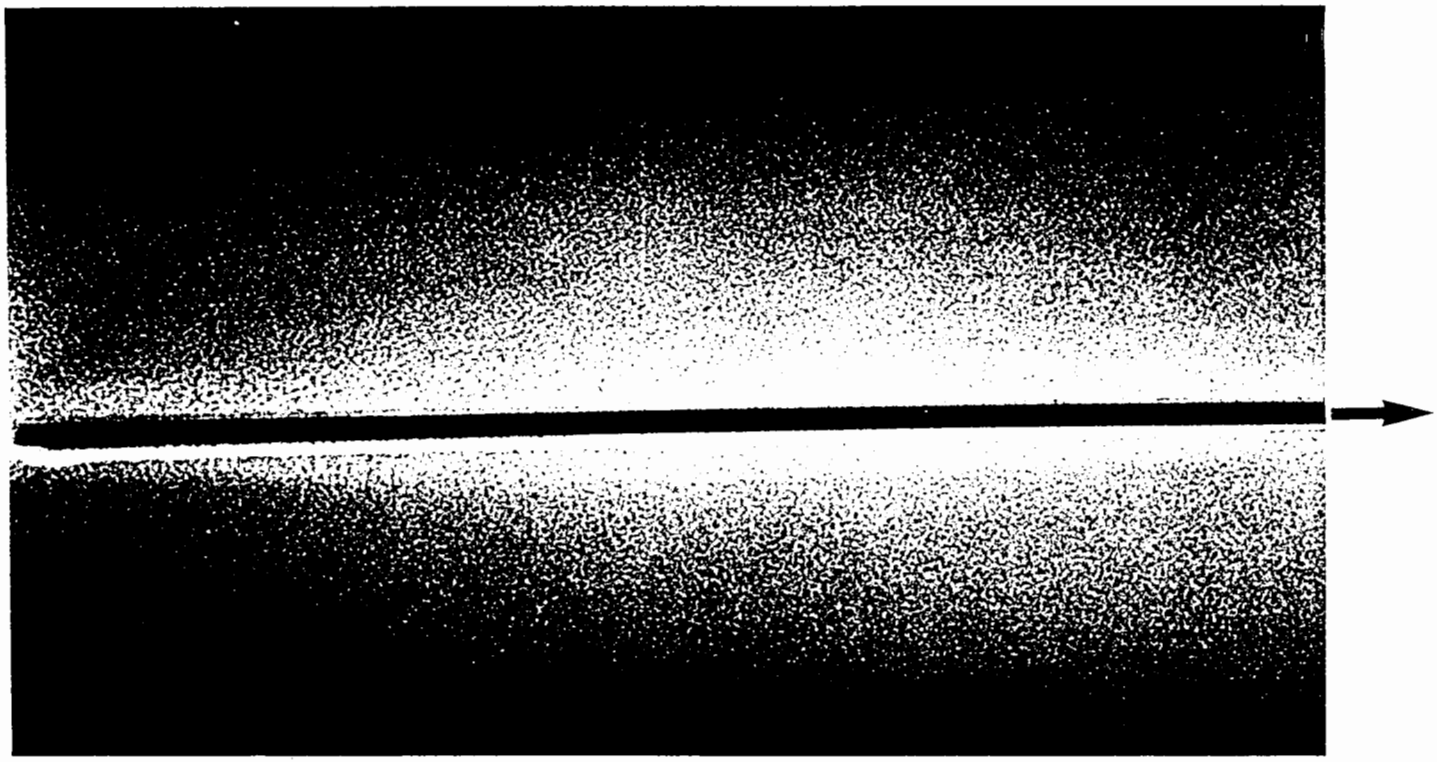

Fig.3.8 (c) - Rupture pattern around the rough reinforcement in 14/25 dense sand

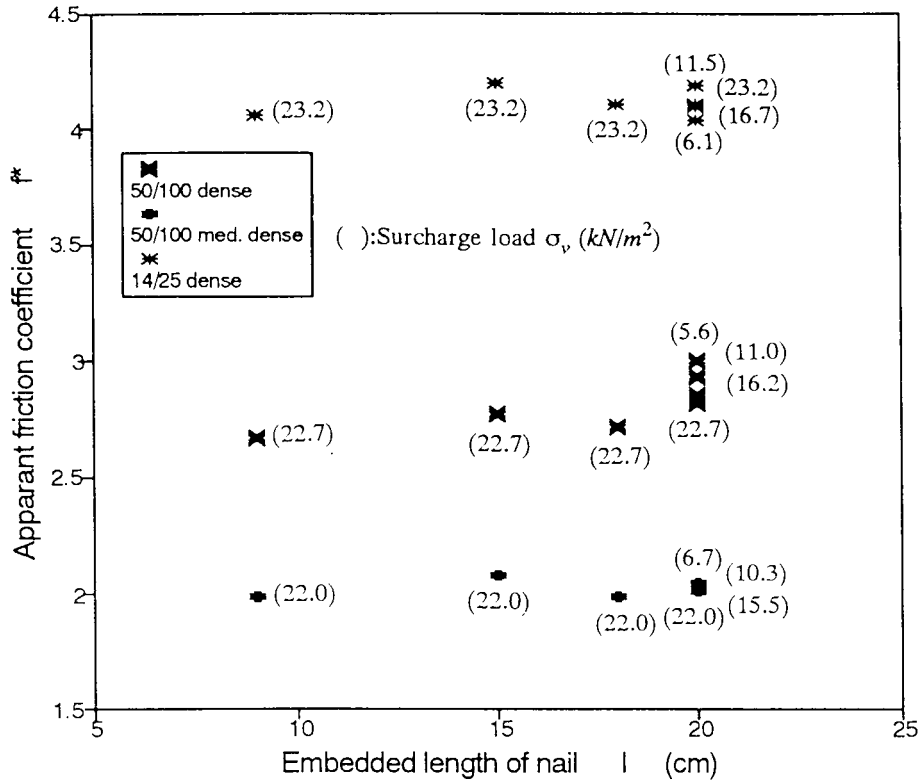

Fig. 3.9 - Influence of nail length l and surcharge load σ_v on the apparent friction coefficient

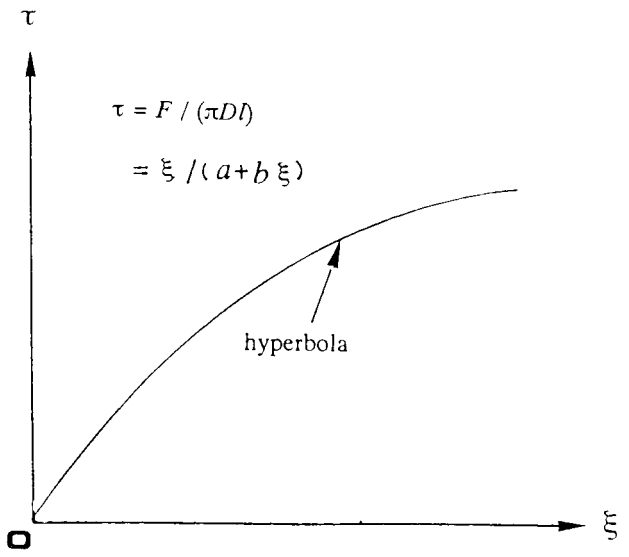

Fig.3.10 - Hyperbola for pull-out curve of the stiff-rough nail

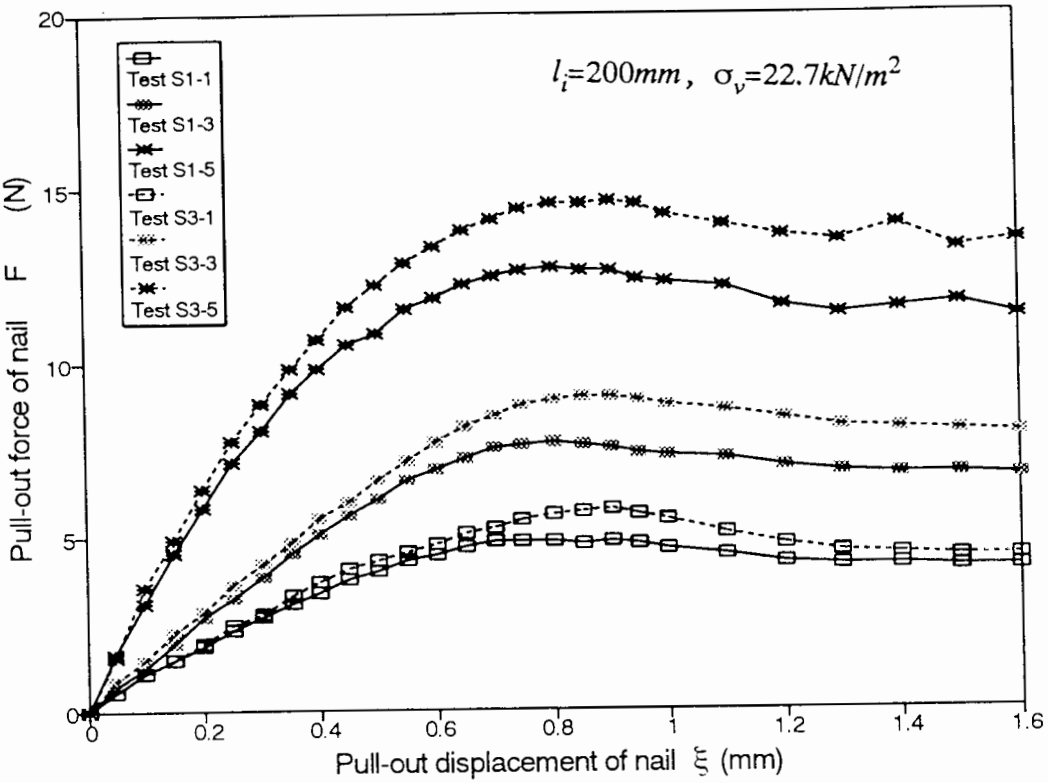

Fig.3.11 - Pull-out curves of the stiff-smooth nail on 50/100 and 14/25 dense sands

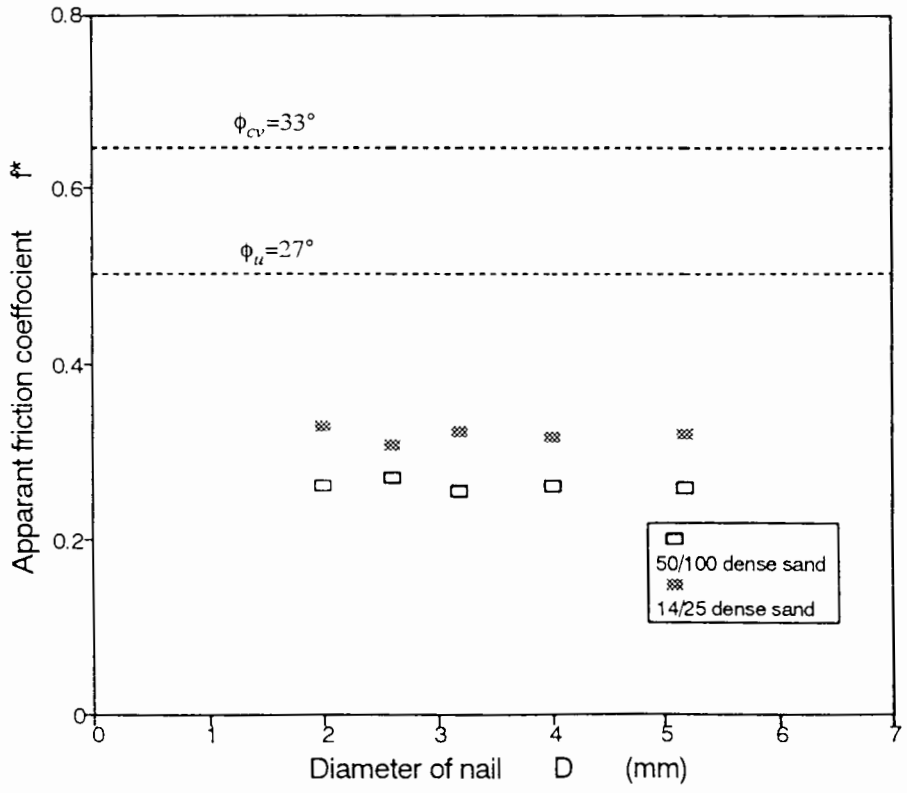

Fig.3.12 - Apparent friction coefficient of the stiff-smooth nail and diameter of nail

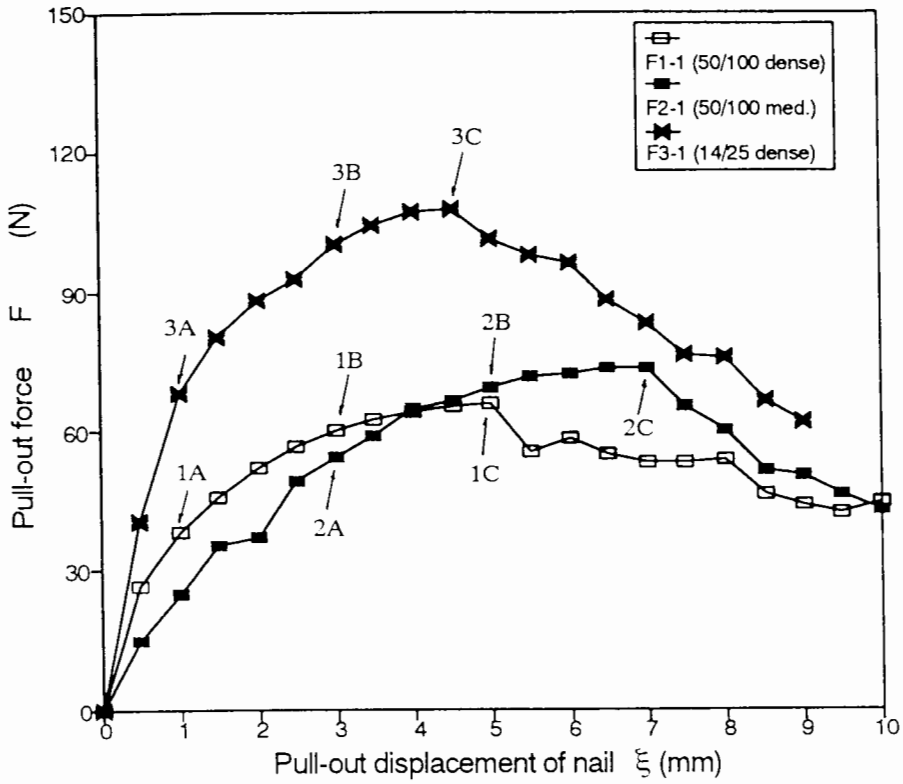

Fig.3.13 - Pull-out curves of the flexible rough nail

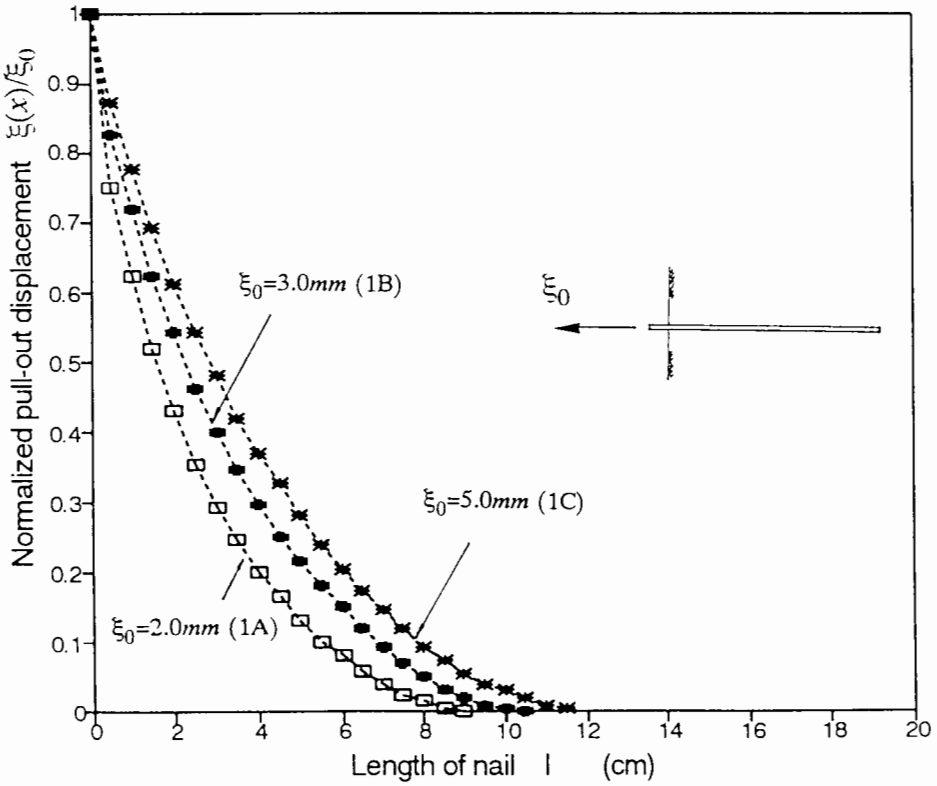

Fig.3.14 (a) - Results of the normalised pull-out displacement of the flexible-rough nail in 50/100 dense sand

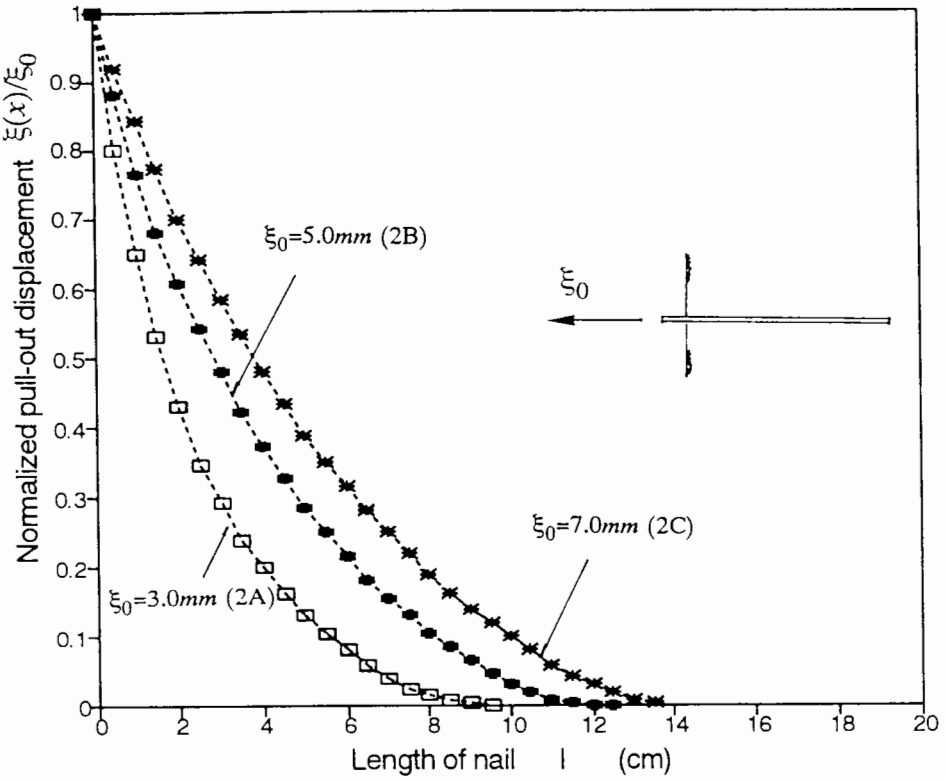

Fig.3.14 (b) - Results of the normalised pull-out diplacement of the flexible-rough nail in 50/100 medium dense sand

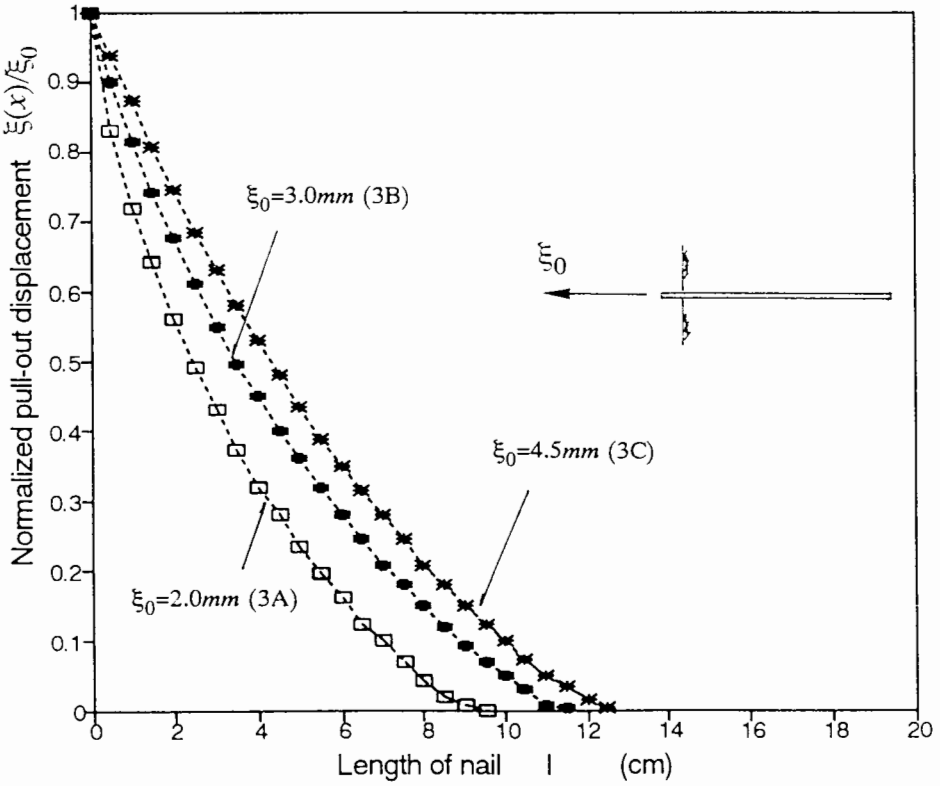

Fig.3.14 (c) - Results of the normalised pull-out displacement of the flexible-rough nail in 14/25 dense sand

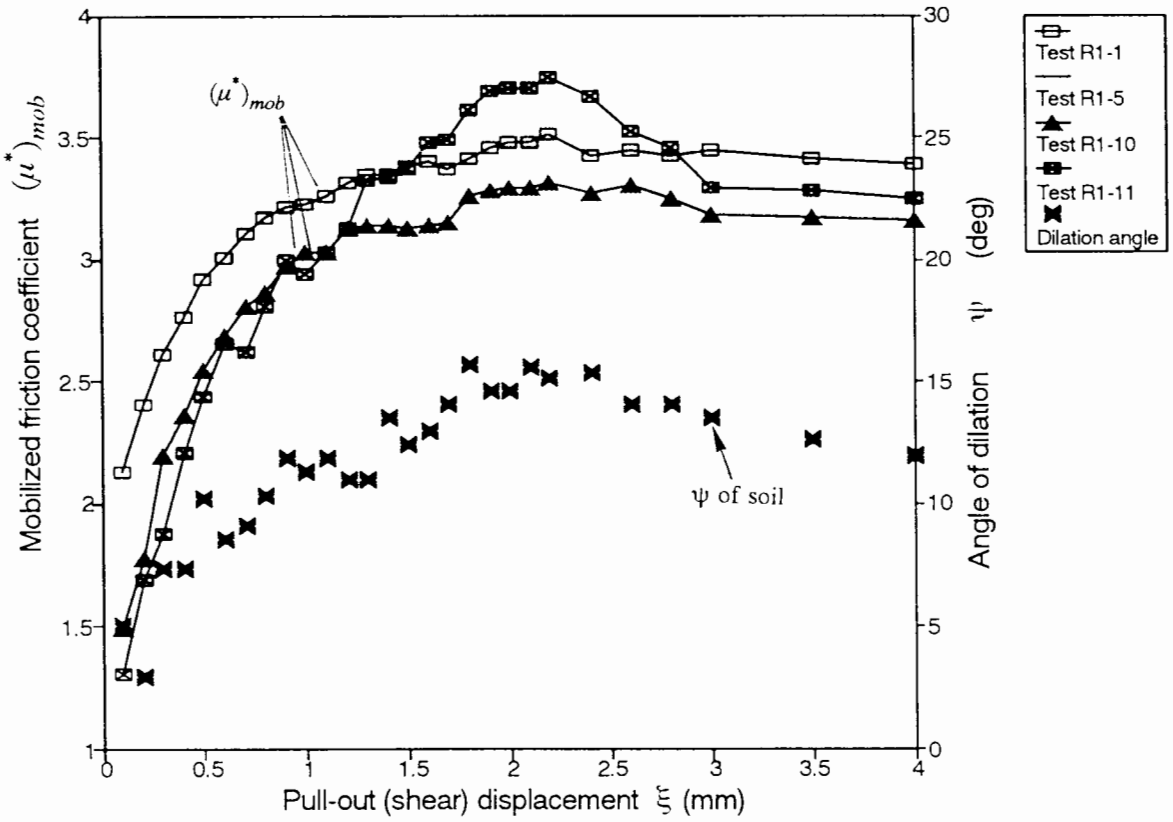

Fig.3.16 (a) - Relationship between the mobilised friction coefficients and the pull-out displacement of the stiff-rough nail in 50/100 dense sand

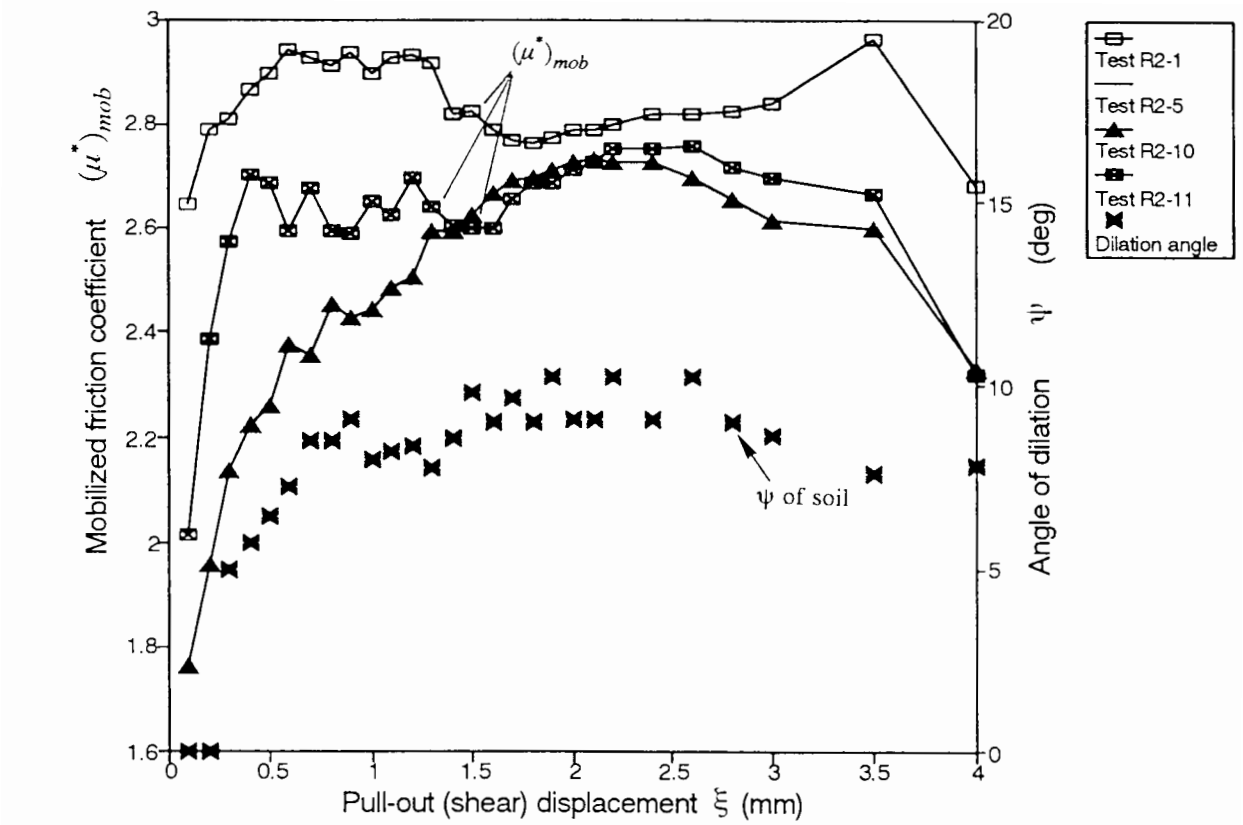

Fig.3.16 (b) - Relationship between the mobilised friction coefficients and the pull-out displacement of the stiff-rough nail in 50/100 medium dense sand

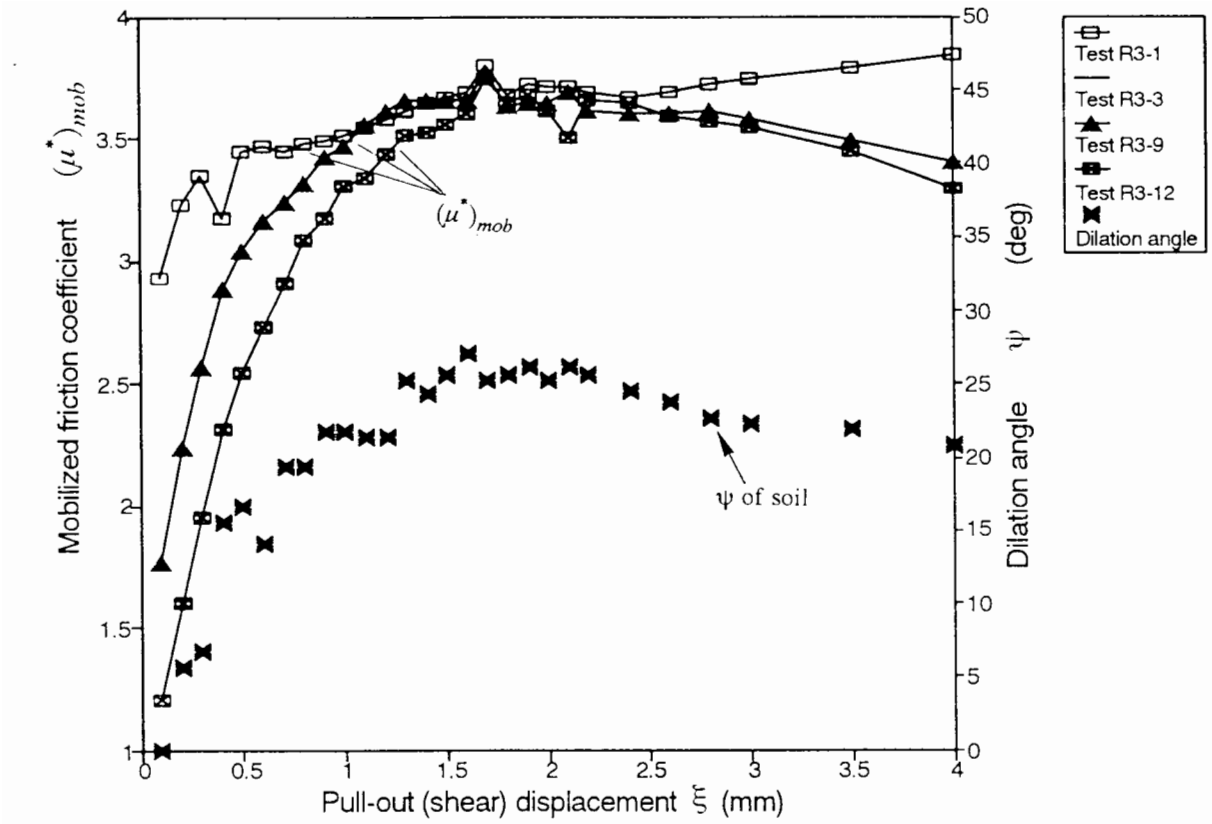

Fig.3.16 (c) - Relationship between the mobilised friction coefficients and the pull-out displacement of the stiff-rough nail in 14/25 dense sand

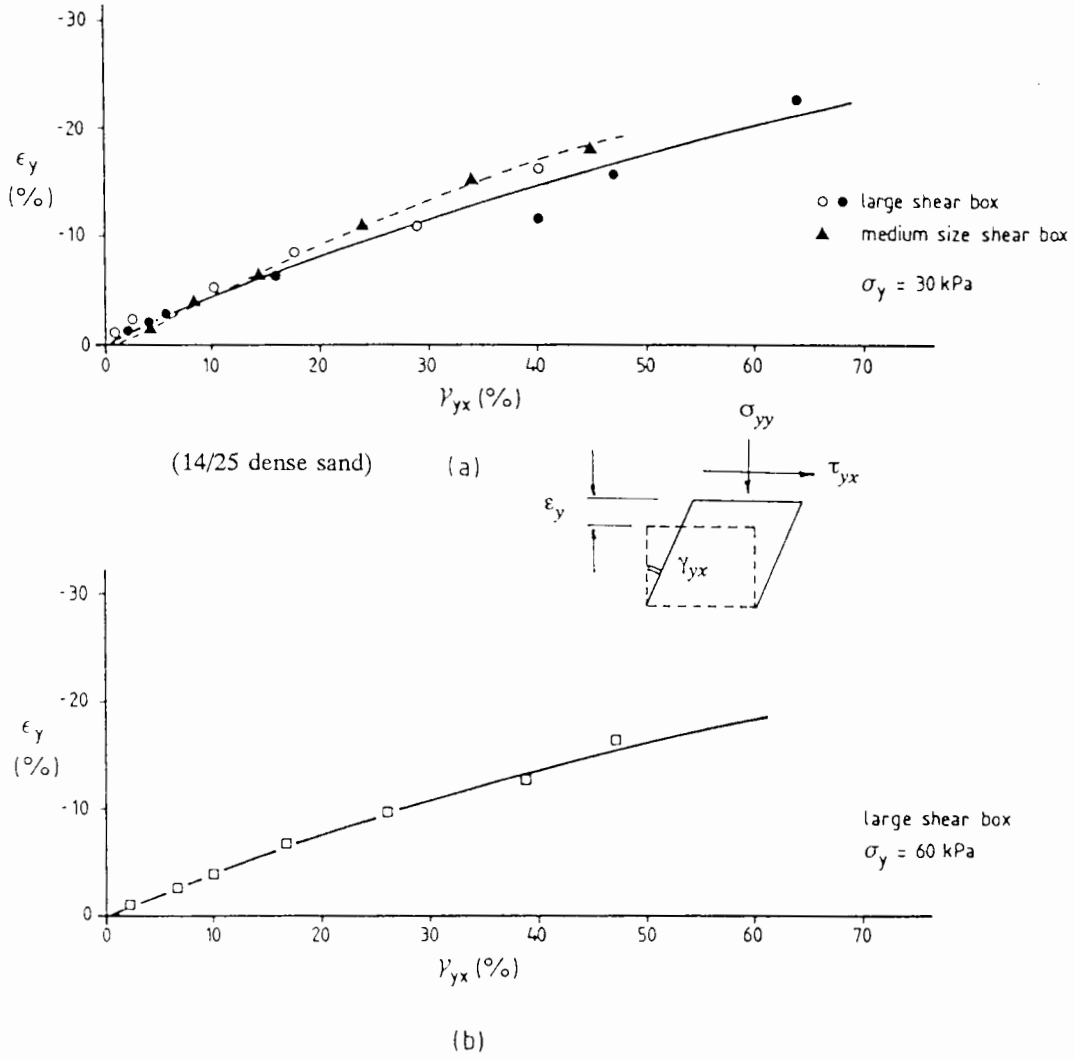

Fig.3.17 - Mean vertical strain versus shear strain in unreinforced direct shear tests (after Palmeira, 1987)

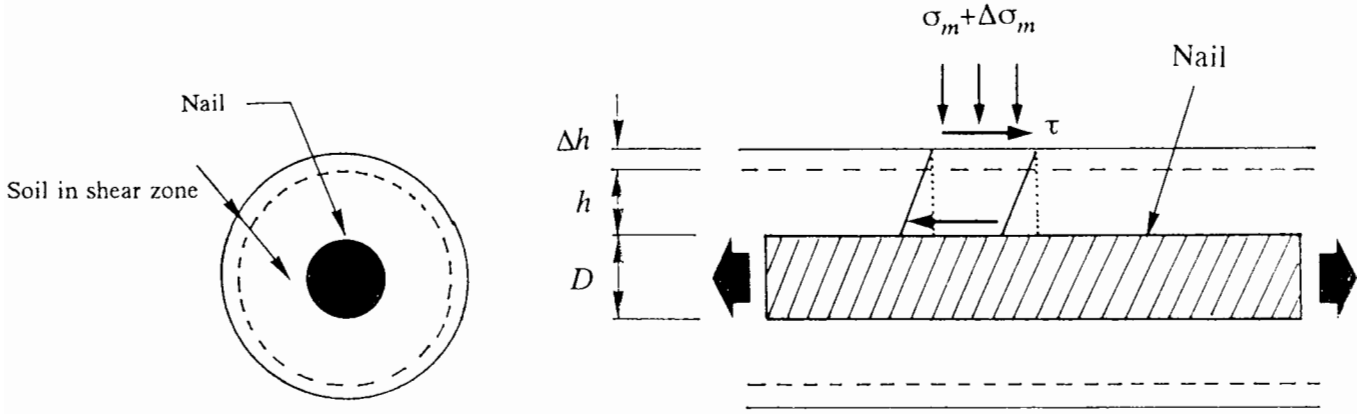

Fig.3.18 - Increase of normal stress on nail due to dilatancy of sand

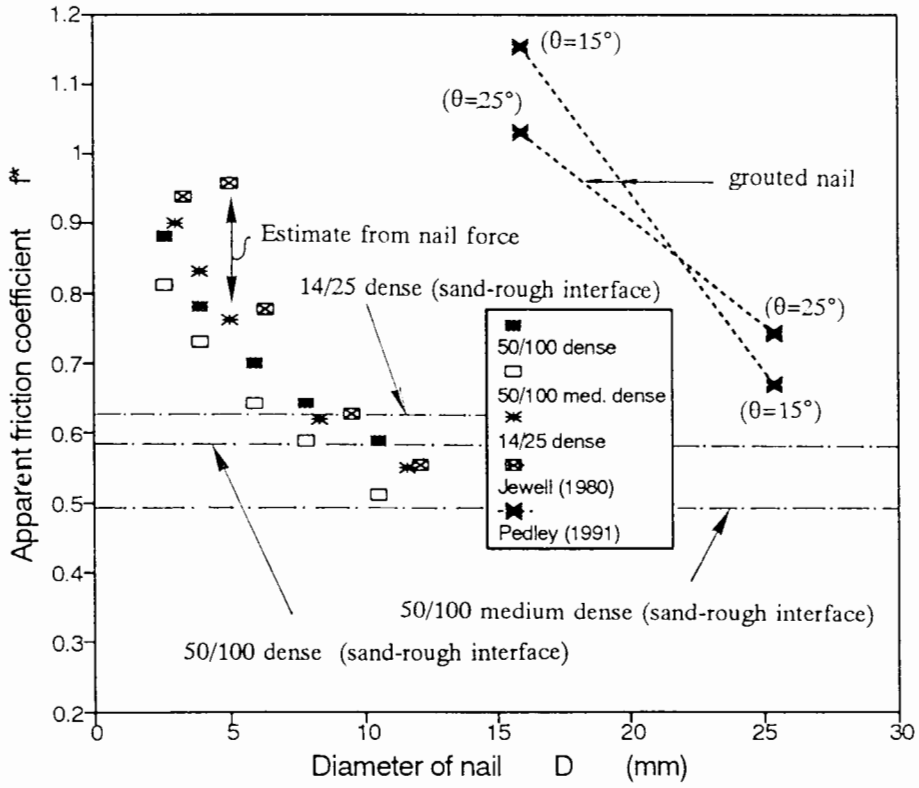

Fig.3.19 - Results of the direct shear tests of nailed sand and interface tests

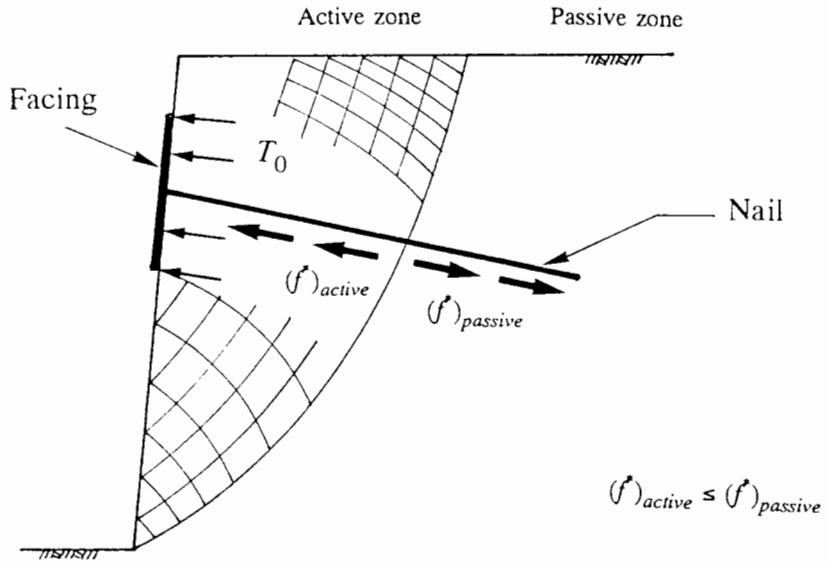

Fig.3.20 - Possible decrease of friction between soil and nail in active zone

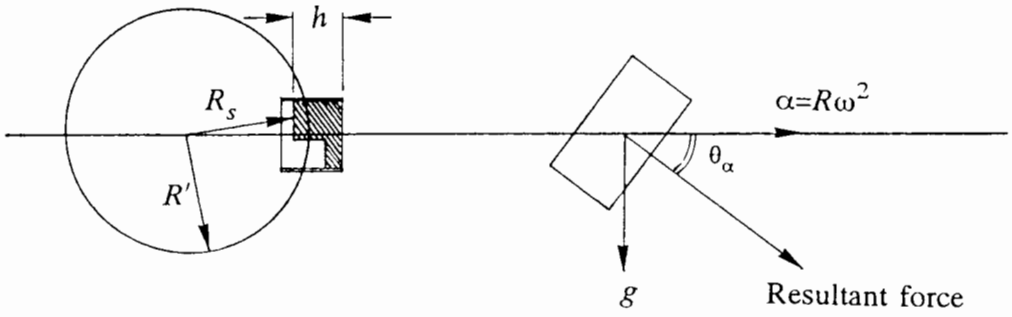

$R'=R_s+h/3$, $\tan\theta_\alpha=g/(R\omega^2)$

Fig.4.1 - Overview of centrifuge acceleration field

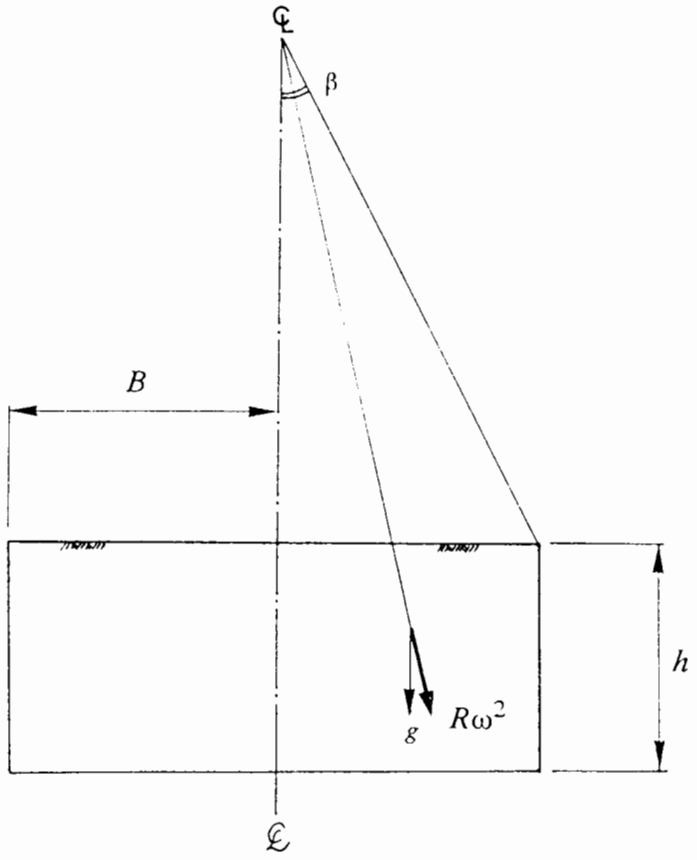

Fig.4.2 - Error due to pseudo-vertical direction in centrifuge model

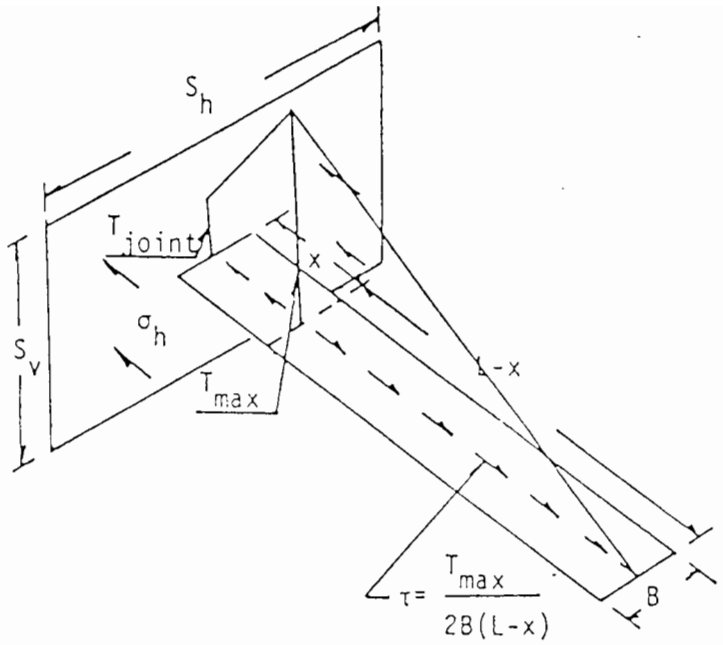

Fig.4.3 - Simple anchor theory proposed by Bolton *et al.* (1978)

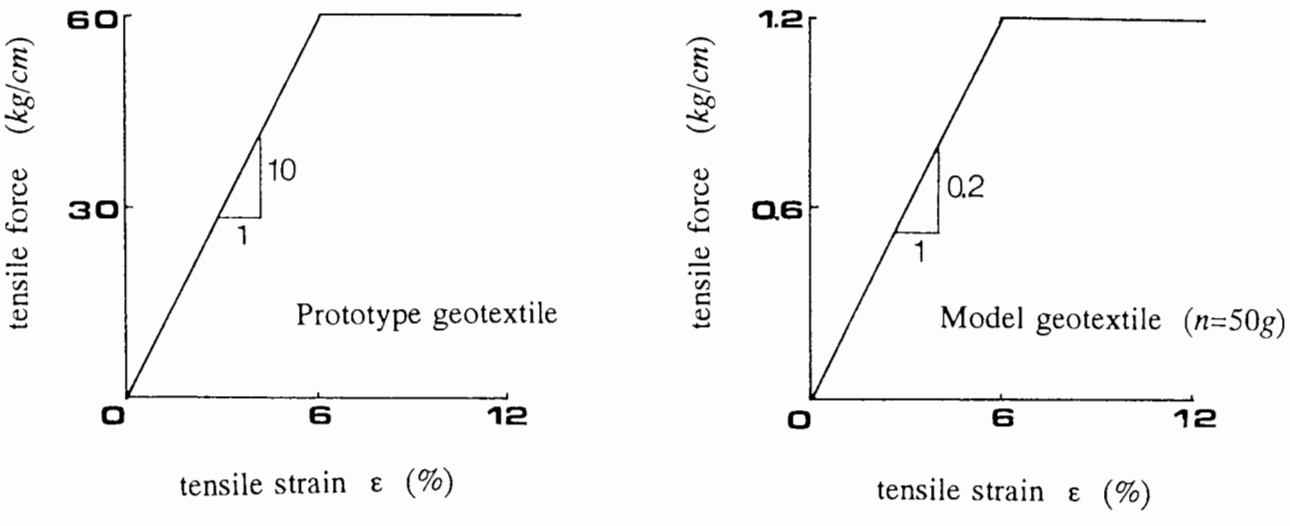

Fig.4.4 - Stress - strain characteristics of the prototype and model geotextiles in the centrifuge test (after Ovesen, 1984)

Quantity	Full scale : model at Ng
Length	$1 : 1/N$
Acceleration	$1 : N$
Area	$1 : 1/N^2$
Volume	$1 : 1/N^3$
Mass	$1 : 1/N^3$
Force	$1 : 1/N^2$
Stress	1 : 1
Strain	1 : 1
Displacement	$1 : 1/N$
Frequency of loading	$1 : N$
Density	1 : 1
Time of creep	1 : 1
Time of inertial effect	$1 : 1/N$
Time of fluid flow	$1 : 1/N^2$

Table 4.1 - Scaling factors between prototype and model (modified from Craig, 1983)

Acutronic 661 Geotechnical Centrifuge

Specification

Radius	1.8m to swing (typical working radius to model centroid 1.6m)
Capacity	200kg @ 200 gravities (340 rpm) 400kg @ 100 gravities
Package volume	500 x 700 x 500mm high
Maximum operating unbalance	20kN (ie 10kg @ 200g)
Slip rings	80 @ 1A (instrumentation signals) 20 @ 10A (power/control)
Hydraulic joint	4 @ 15bars (air/water) 1 @ 200bars (oil, liquid CO_2)

Table 5.1 - Mechanical detail of the geotechnical centrifuge at City University

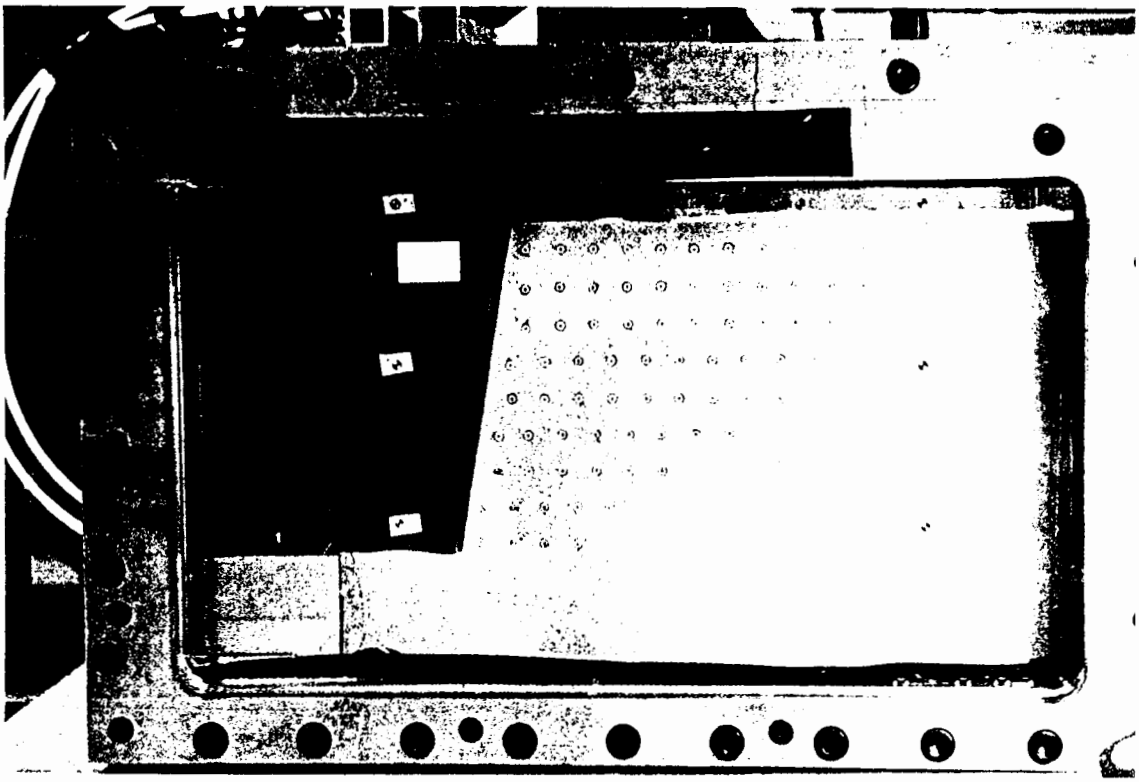

Markers buried in the sand

Plate 5.1 - Overview of the centrifuge test

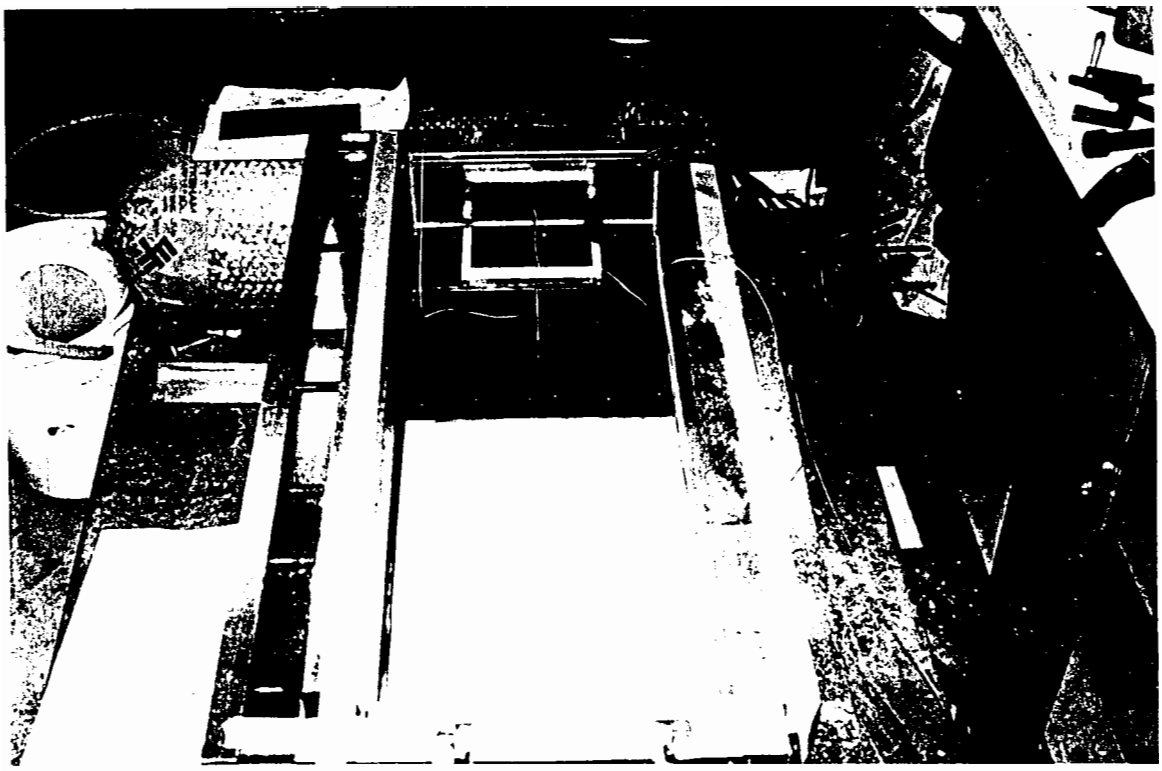

Two rubber bags and horizontal LVDT gantry

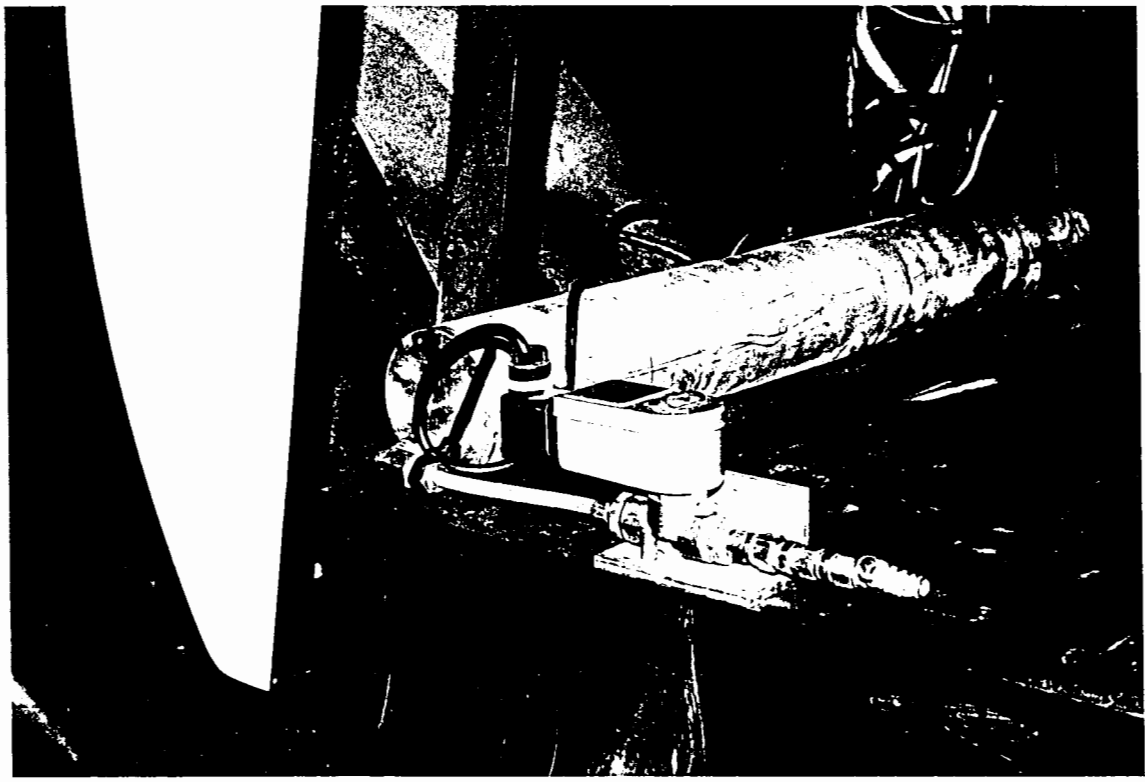

Reservoir and solenoid valve on the swing

Plate 5.1 - Overview of the centrifuge test

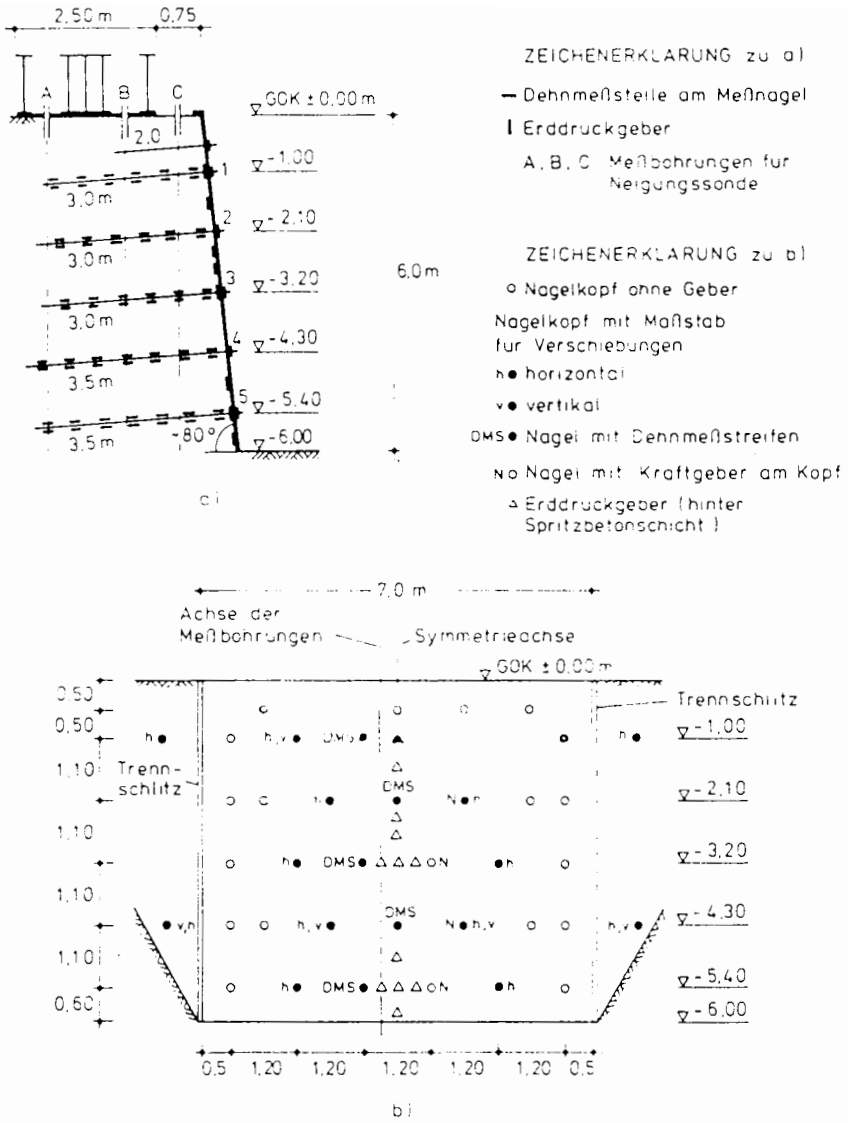

(Test B)

Fig.5.1 - Prototype test carried out in Germany (after Gassler, 1987)

γ_t (kN/m^3)	γ_d (kN/m^3)	e	I_D $(\%)$	D_{50} (mm)	ϕ' (deg)	ϕ'_{cv} (deg)
15.6	14.8	0.83	62	0.3	40.5	35

Table 5.2 - Properties of sand in the prototype test (after Gassler, 1987)

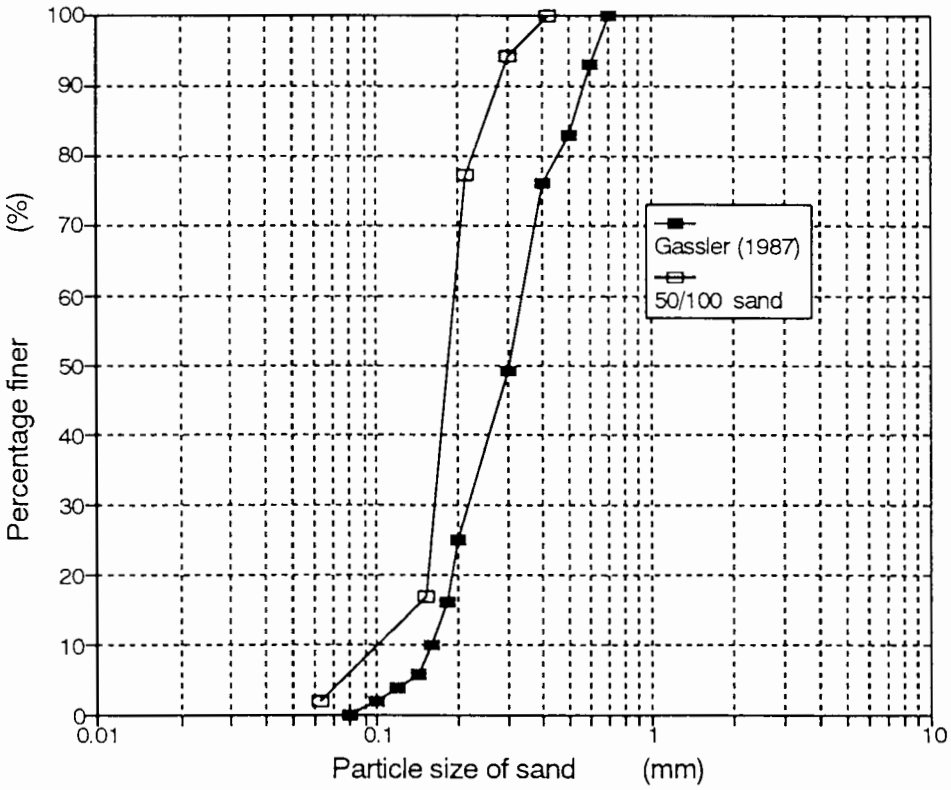

Fig.5.2 - Comparison of grading curves between the prototype and the centrifuge tests

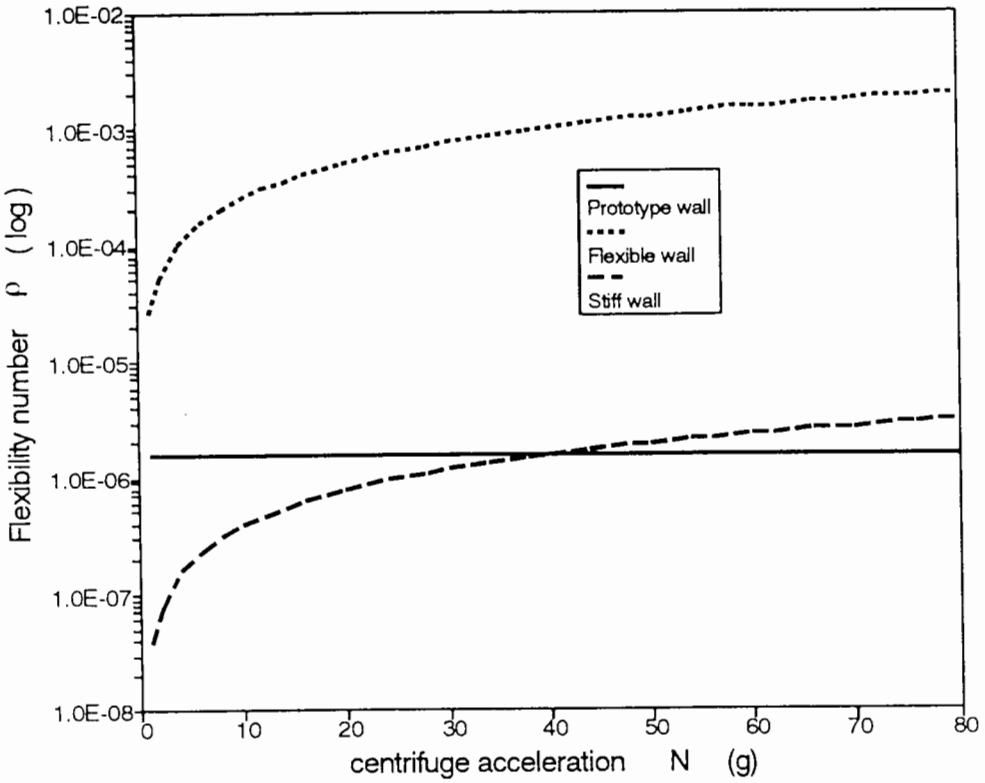

Fig.5.3 - Comparison of the flexible number ρ between the prototype and the centrifuge tests

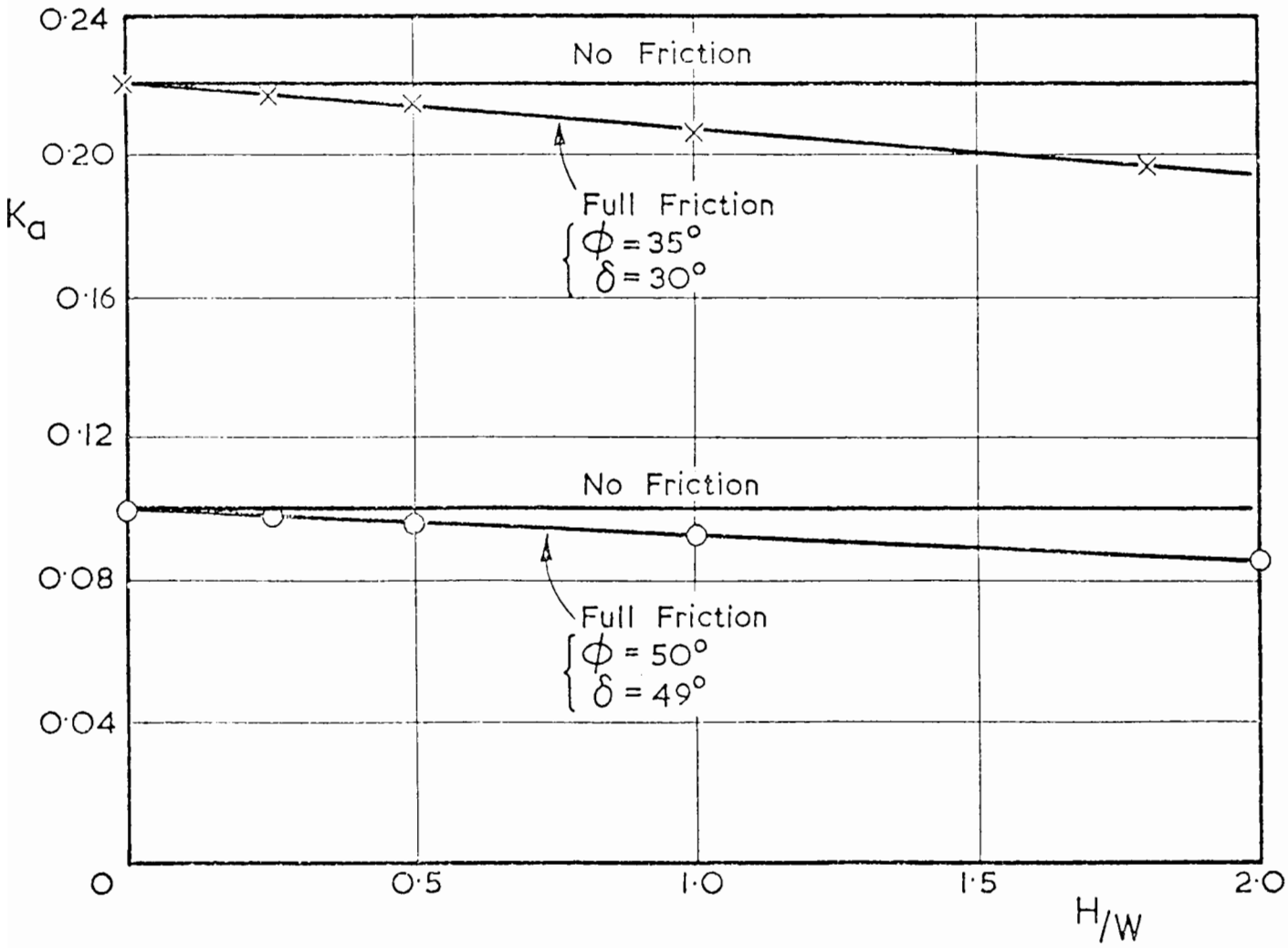

Fig.5.4 - Effect of side friction on the active earth pressure coefficient K_a (after Bransby and Smith, 1975)

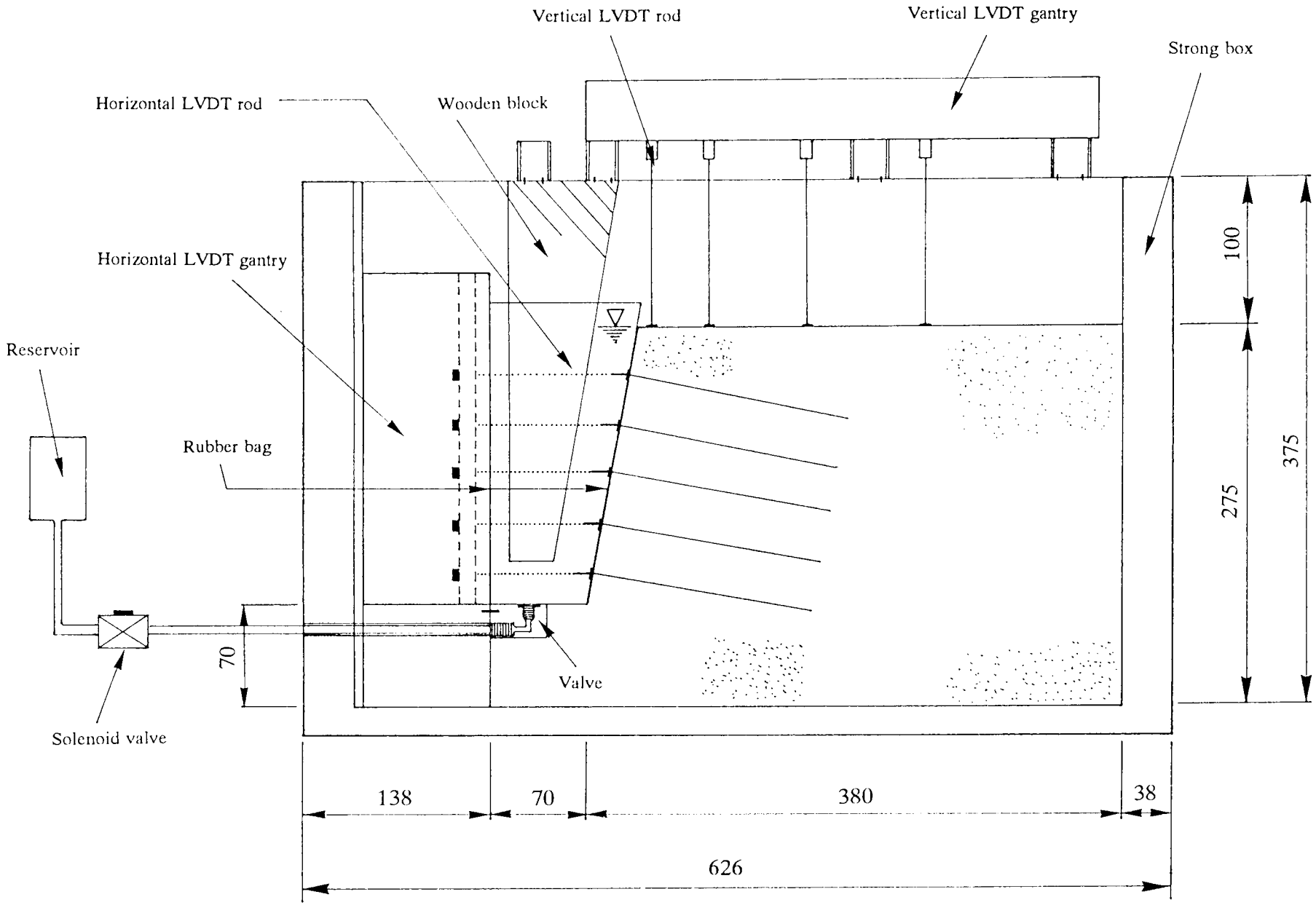

Fig.5.5 - Mechanical layout of the centrifuge test

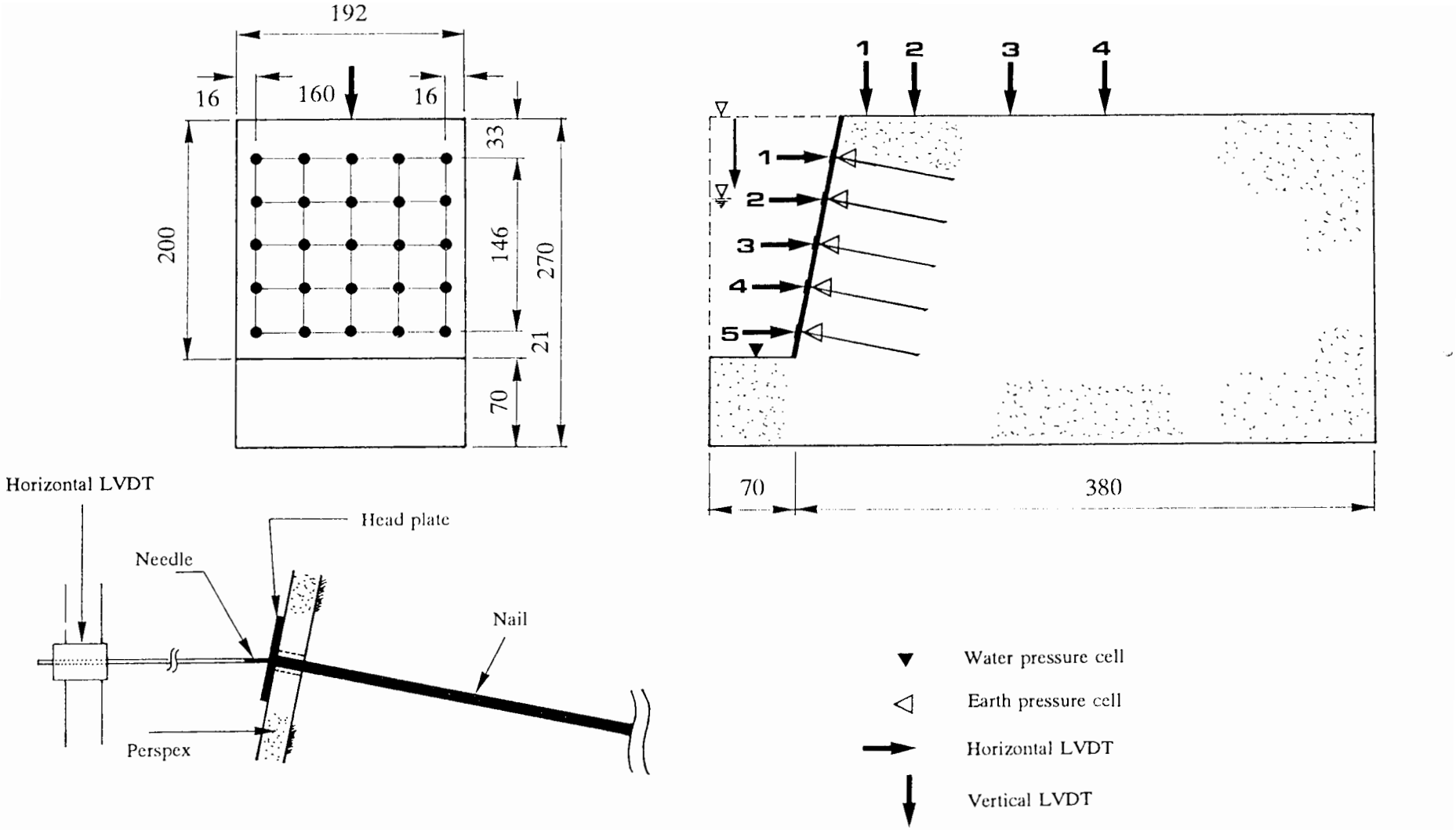

Fig.5.6 - Layout of instrumentation in the centrifuge test

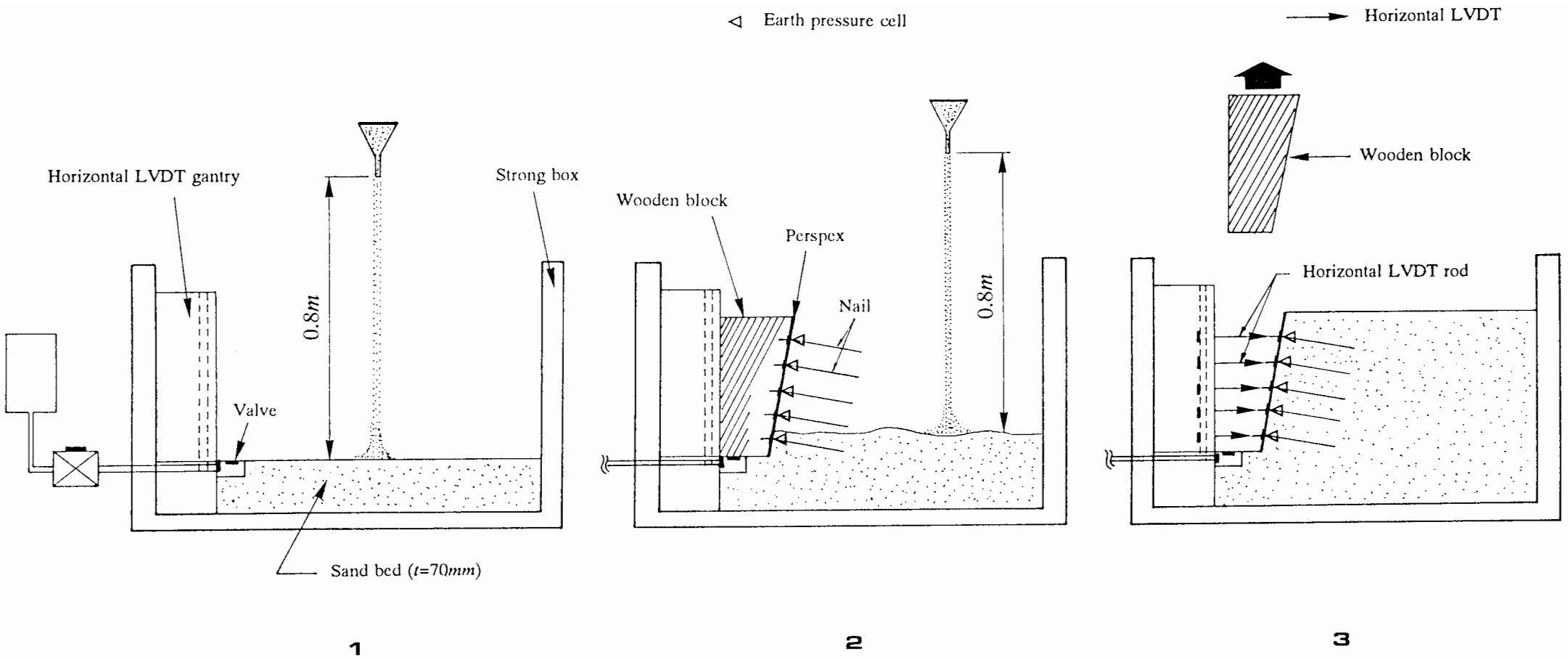

Fig.5.7 - Main stages of the sample preparation

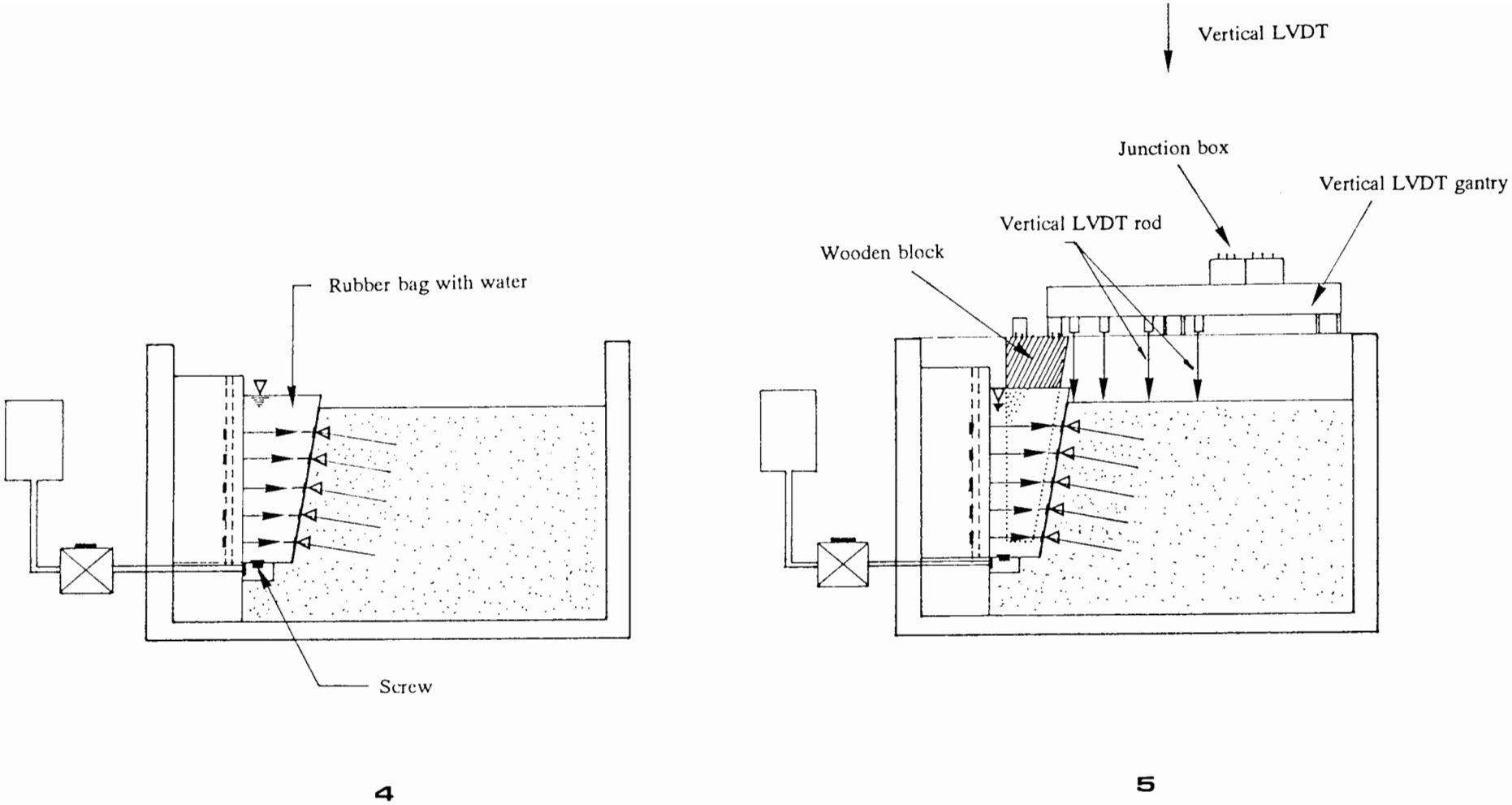

Fig.5.7 - Main stages of the sample preparation

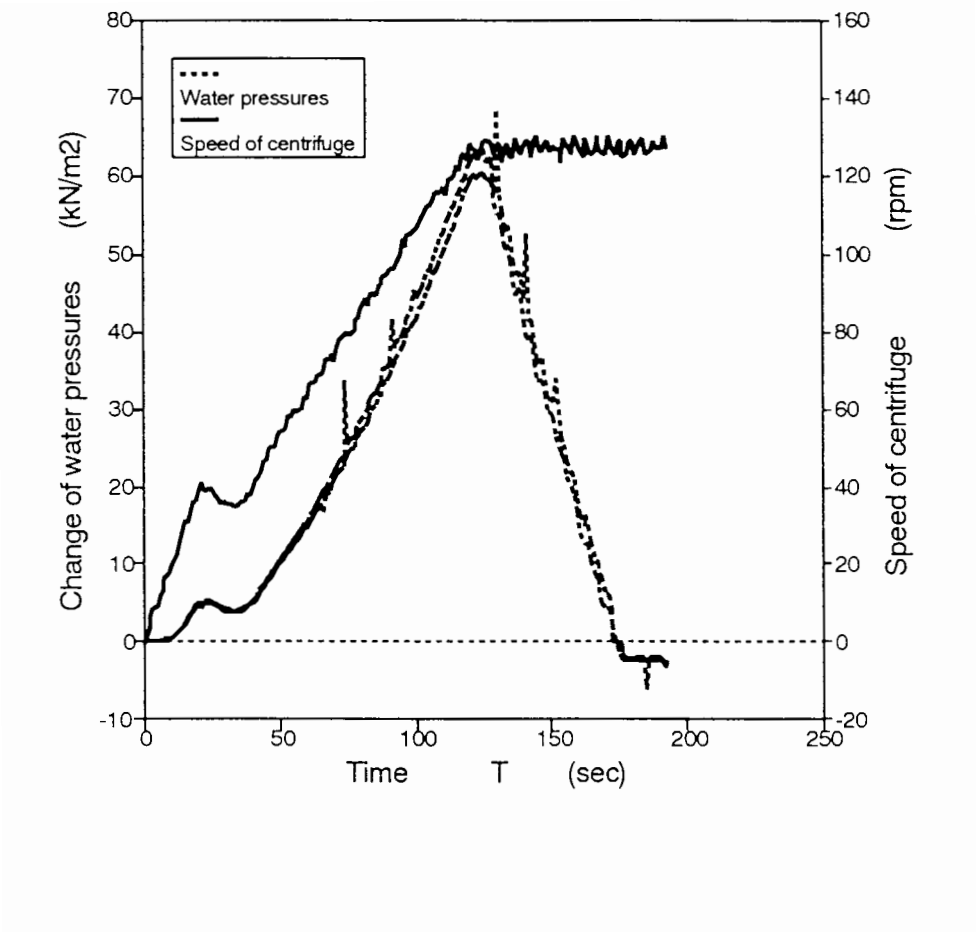

Fig.5.8 - Typical history of the centrifuge acceleration at $N_{max} \leq 30g$

Test	ß (°)	Nail l (cm)	Nail Rough-ness	Nail Γ (°)	wall stiff-ness	Wall Rough-ness	N_f (g)
A6.5-F-R	80	6.5	Rough	0	Flexible	Rough	30
A6.5-R-R	80	6.5	Rough	0	Rigid	Rough	36
A'6.5-R-R	80	6.5	Rough	10	Rigid	Rough	45
A7.0-R-S	80	7.0	Rough	0	Rigid	Smooth	No
A18-F-R	80	18.0	Smooth	0	Flexible	Rough	33
A18-R-R	80	18.0	Smooth	0	Rigid	Rough	30
A20-F-S	80	20.0	Smooth	0	Flexible	Smooth	72
A'20-F-S	80	20.0	Smooth	10	Flexible	Smooth	56
A20-R-S	80	20.0	Smooth	0	Rigid	Smooth	No
A'20-R-S	80	20.0	Smooth	10	Rigid	Smooth	64
A20-R-R	80	20.0	Smooth	0	Rigid	Rough	No
A20-F-R	80	20.0	Smooth	0	Flexible	Rough	No
A*18-F-R	80	18.0	Smooth	0	Rigid	Rough	24
Proto-F	80	10.0 11.6	Rough	0	Flexible	Rough	No
Proto-R	80	10.0 11.6	Rough	0	Rigid	Rough	No
V7.0-F-R	90	7.0	Rough	0	Flexible	Rough	30
V'7.0-F-R	90	7.0	Rough	10	Flexible	Rough	30
V7.0-R-R	90	7.0	Rough	0	Rigid	Rough	30
V8.0-F-S	90	8.0	Rough	0	Flexible	Smooth	No
V8.0-R-S	90	8.0	Rough	0	Rigid	Smooth	No
V8.0-F-R	90	8.0	Rough	0	Flexible	Rough	73
V8.0-R-R	90	8.0	Rough	0	Rigid	Rough	No
V8.5-R-S	90	8.5	Rough	0	Rigid	Smooth	No
V20-F-S	90	20.0	Smooth	0	Flexible	Smooth	1
V23-F-S	90	23.0	Smooth	0	Flexible	Smooth	30

Table 6.1 - Summary of centrifuge tests of nailed slopes and the observed failure acceleration N_f

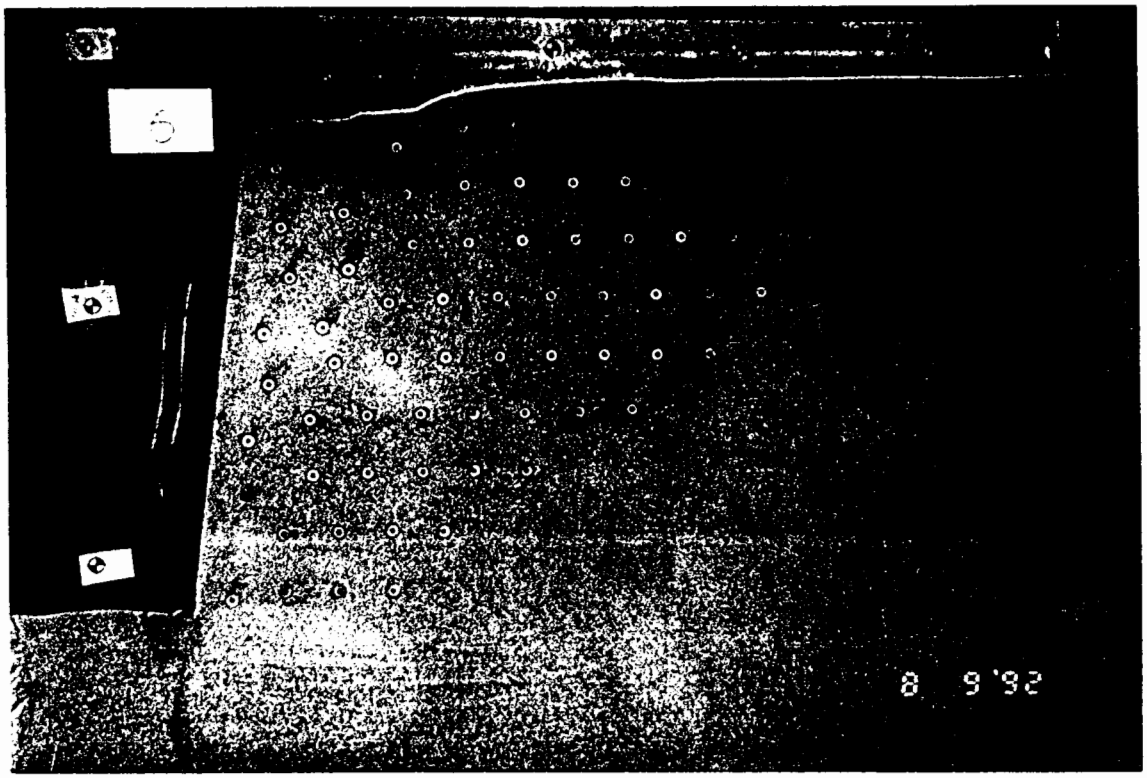

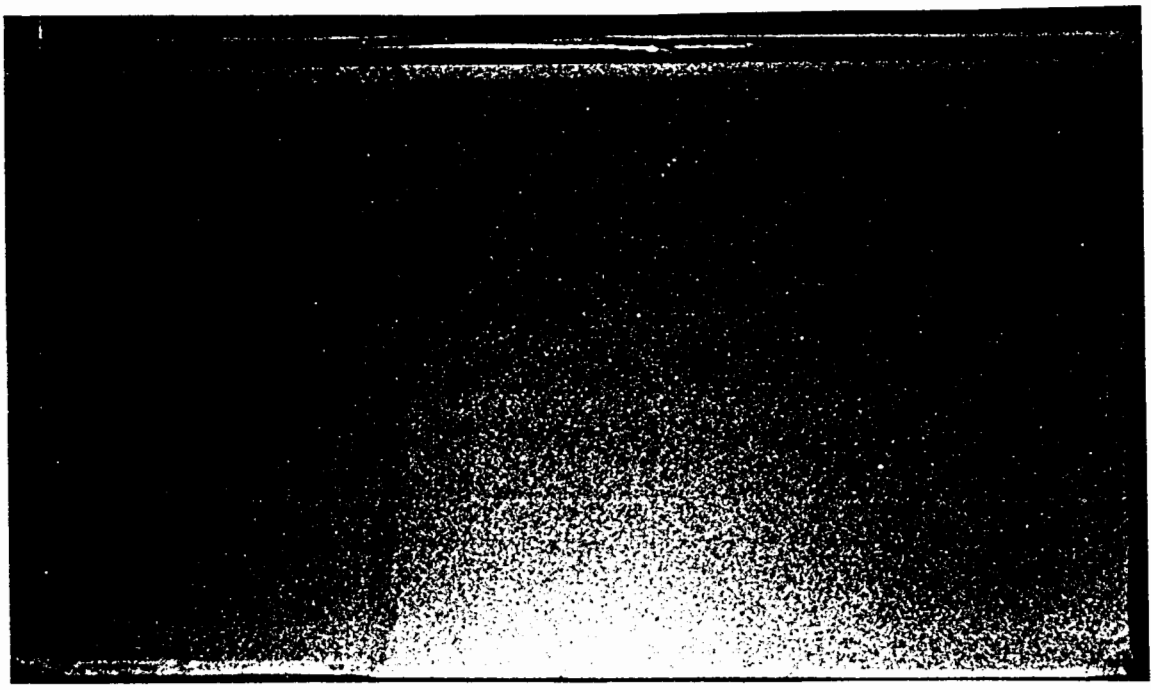

(Plan)

Plate 6.1 Development of failure surfaces observed in the centrifuge tests

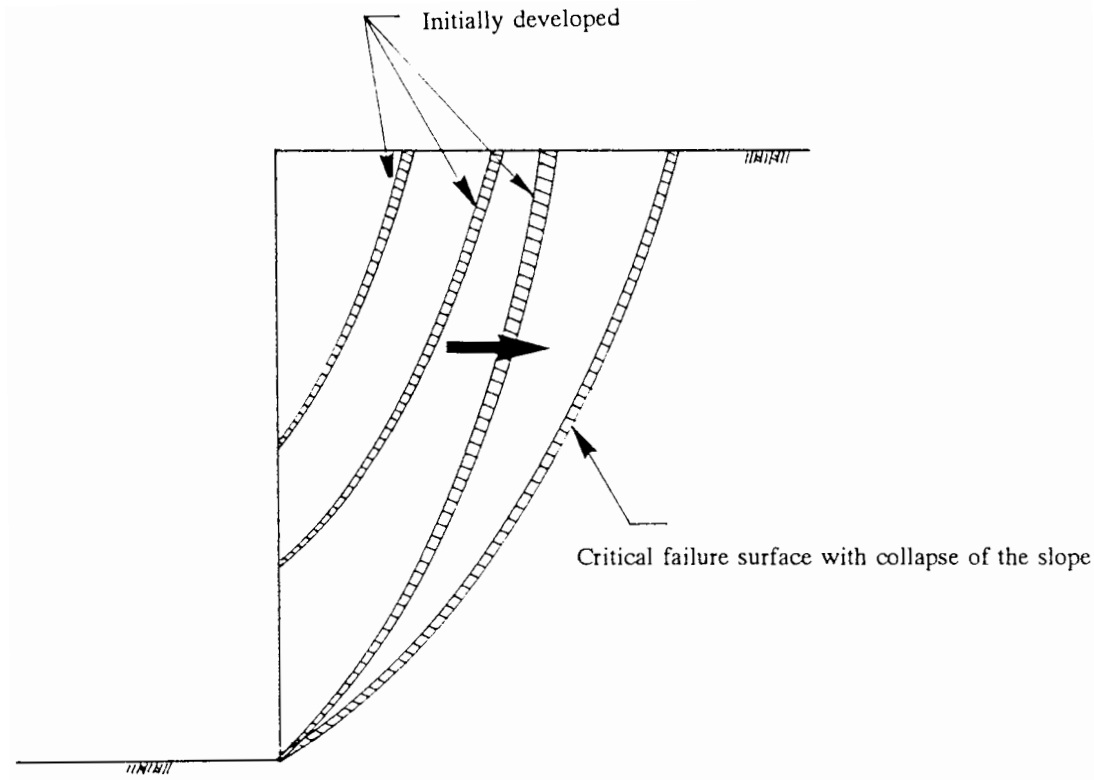

Fig.6.1 - Development of failure surfaces in the nailed slope

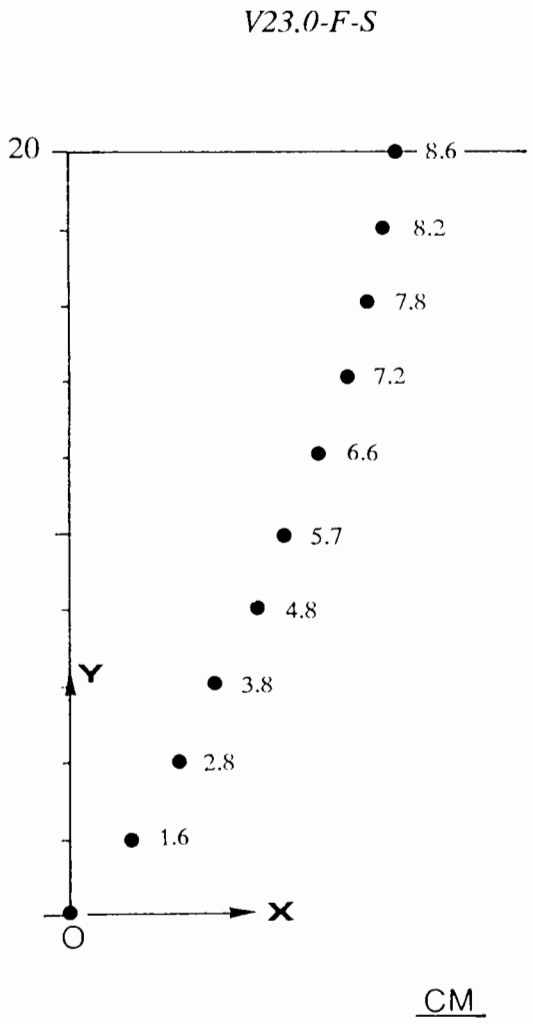

Fig.6.2 - (a) Critical failure surfaces observed in the centrifuge tests (β=90°)

( ): predicted failure surface with the minimum factor of safety $(F_s)_{min}$ for uncollapsed nailed slope

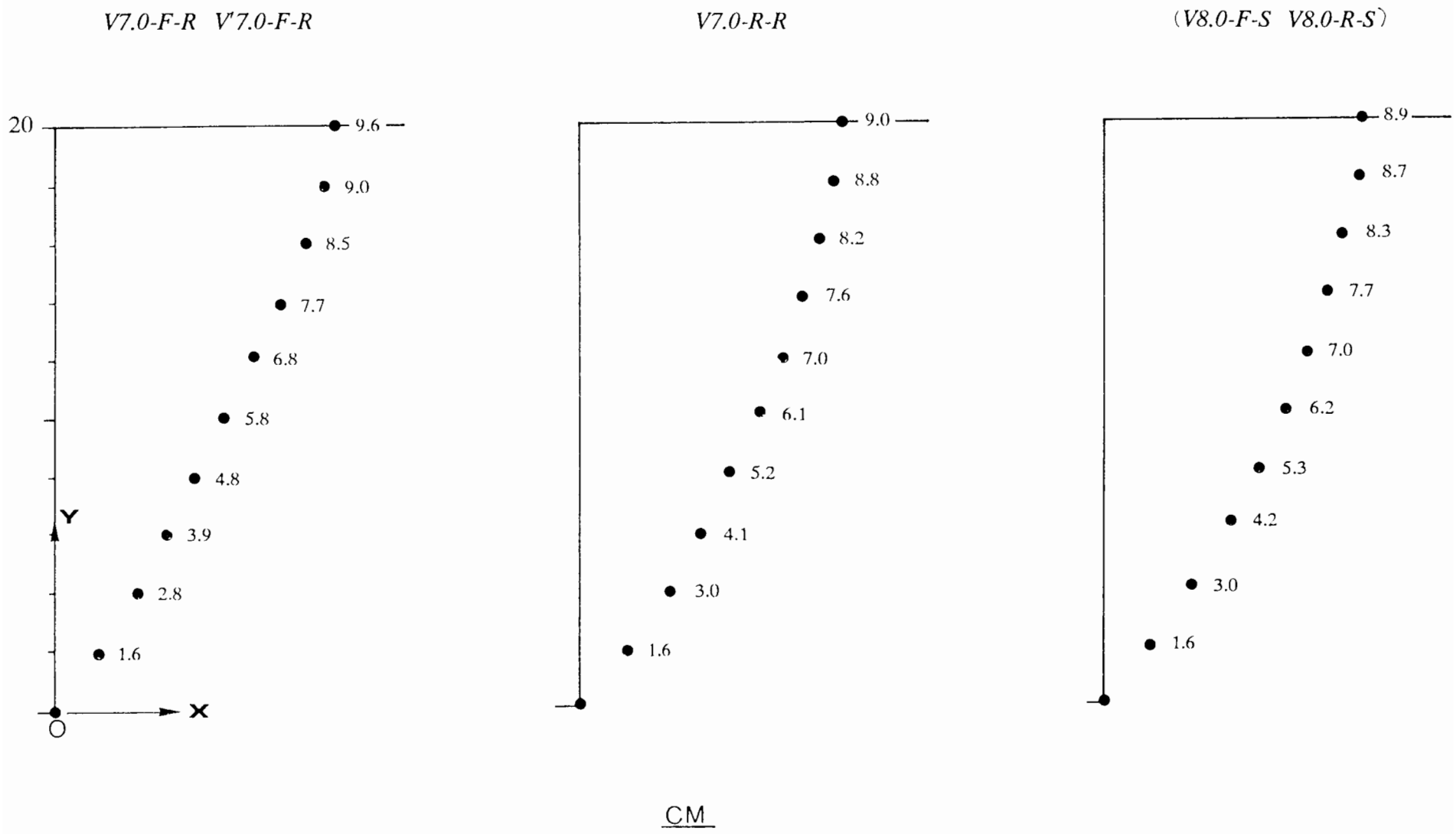

Fig.6.2 (a) - Critical failure surfaces observed in the centrifuge tests (β=90°)

( ): predicted failure surface with the minimum factor of safety $(F_s)_{min}$
for uncollapsed nailed slope

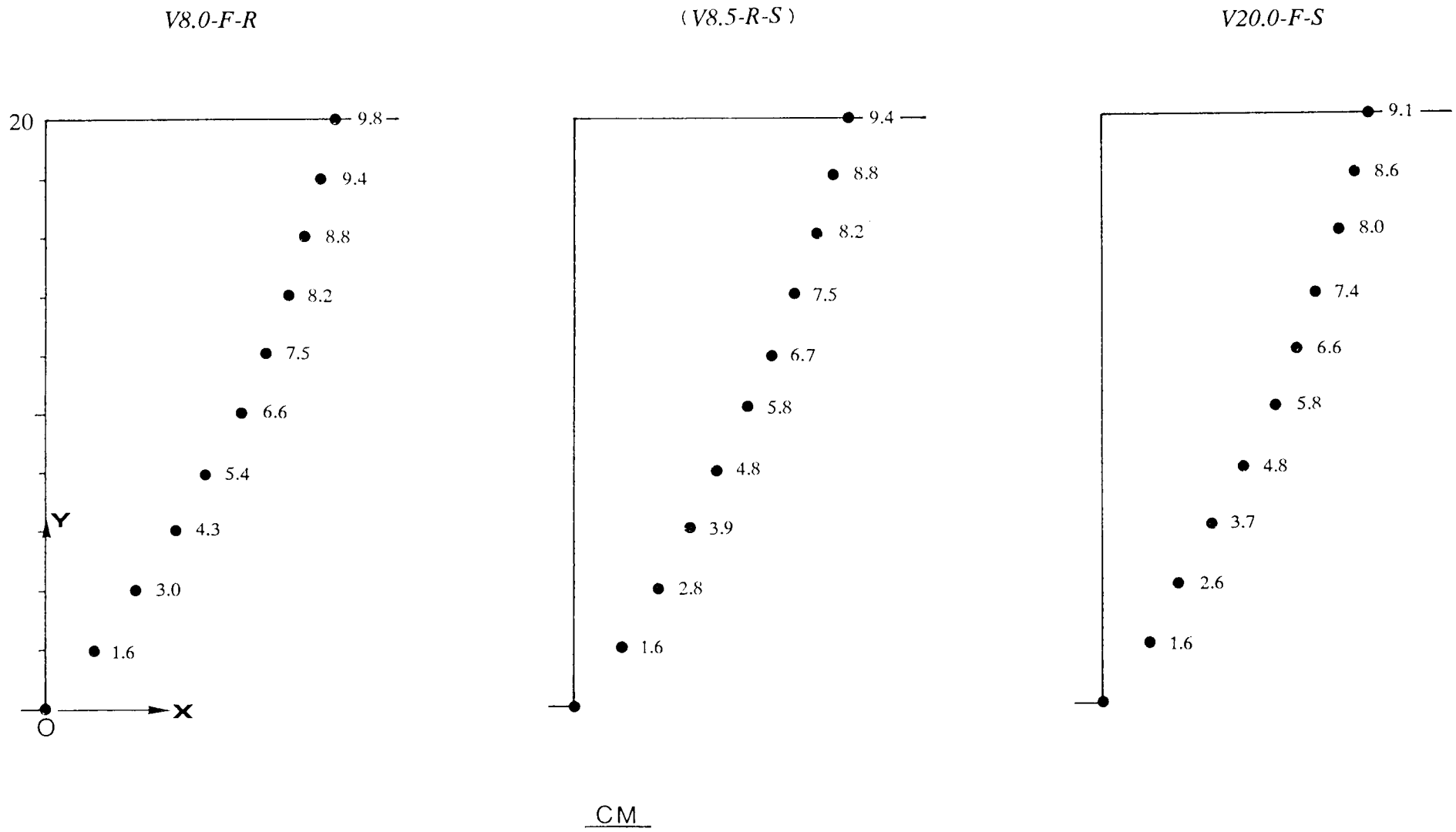

Fig.6.2 (a) - Critical failure surfaces observed in the centrifuge tests (β=90°)

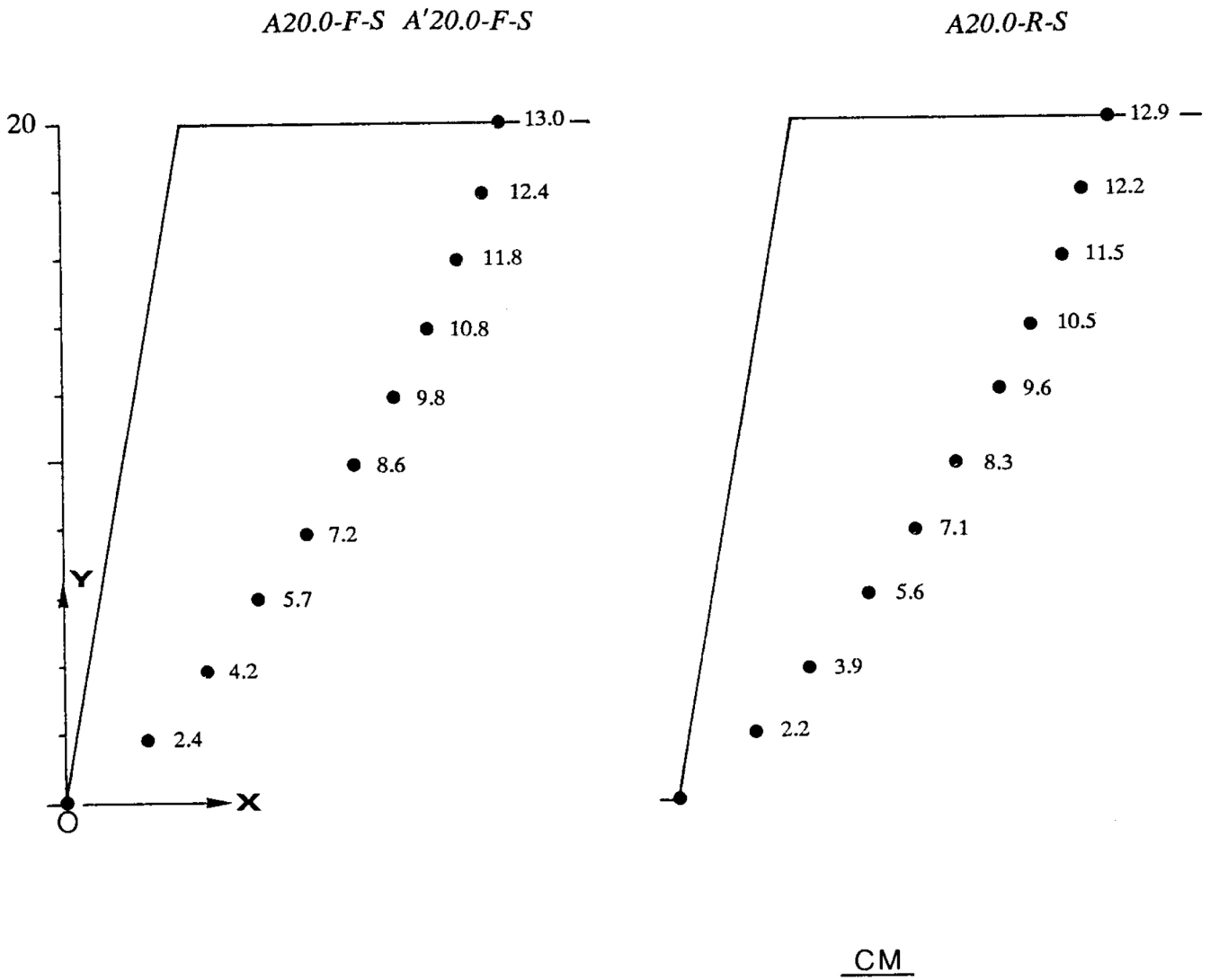

Fig.6.2 (b) - Critical failure surfaces observed in the centrifuge tests (β=80°)

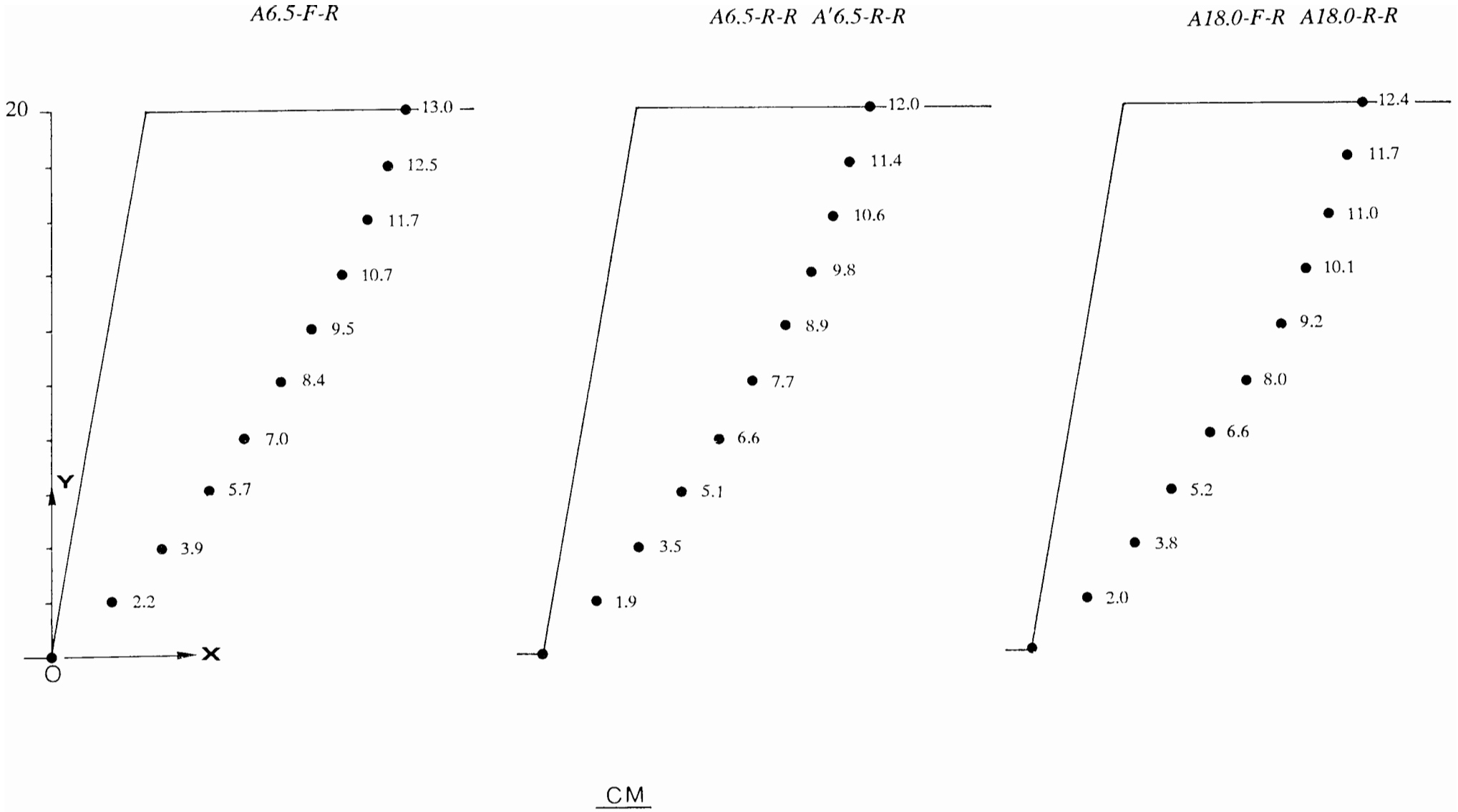

Fig.6.2 (b) - Critical failure surfaces observed in the centrifuge tests (β=80°)

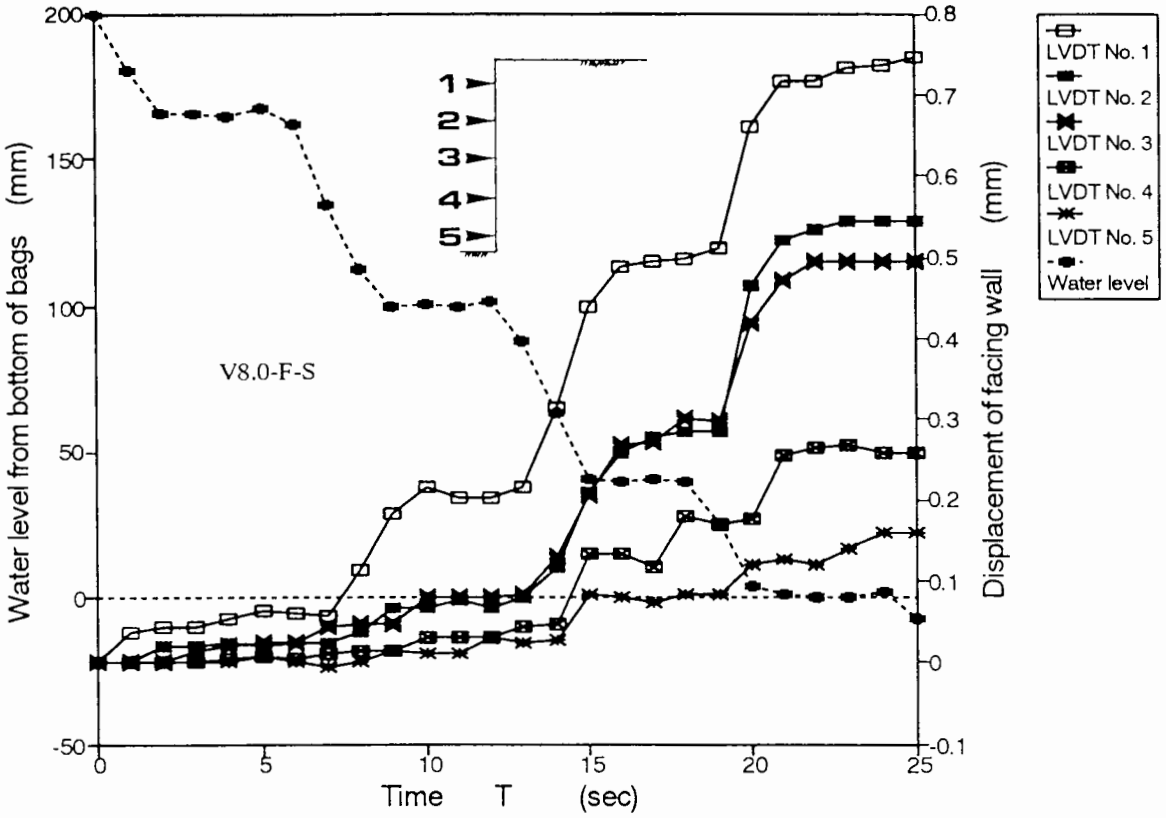

Fig.6.3 (a) - Influence of draining of water on the displacements of the facing wall

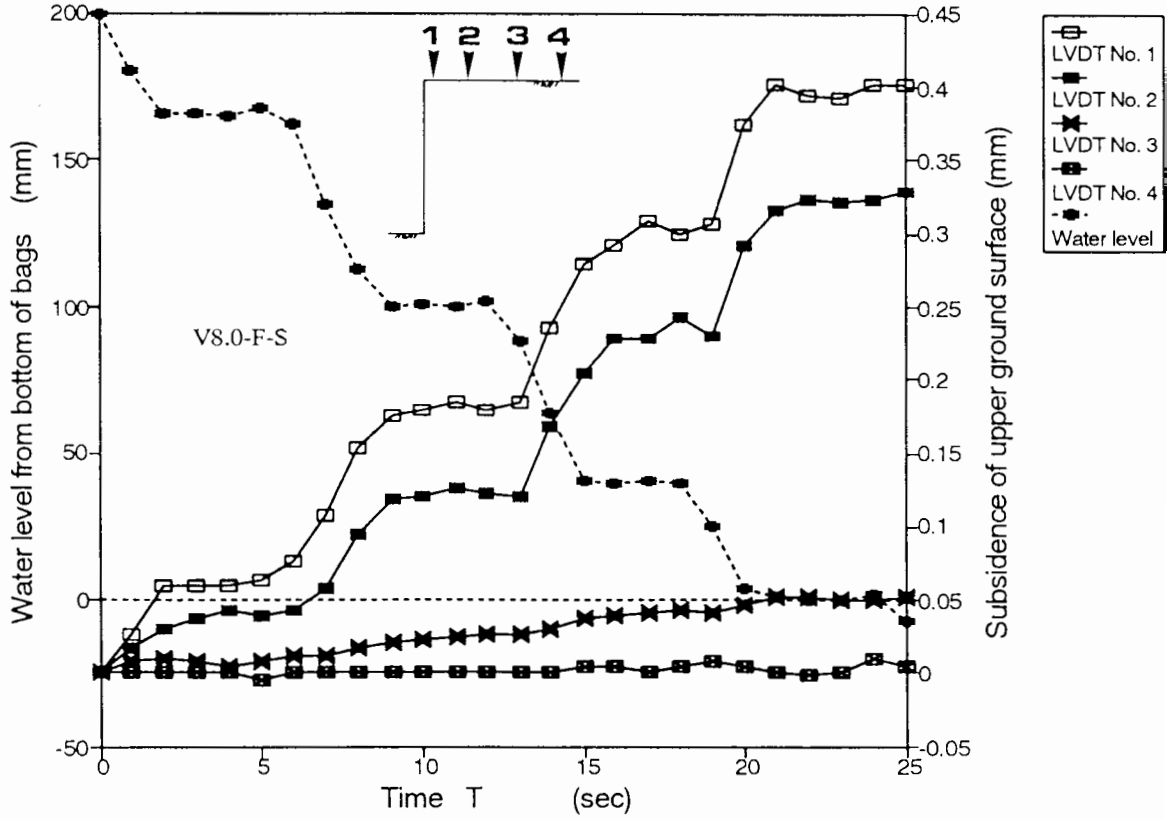

Fig.6.3 (b) - Influence of draining of water on the vertical displacements of the upper ground surface

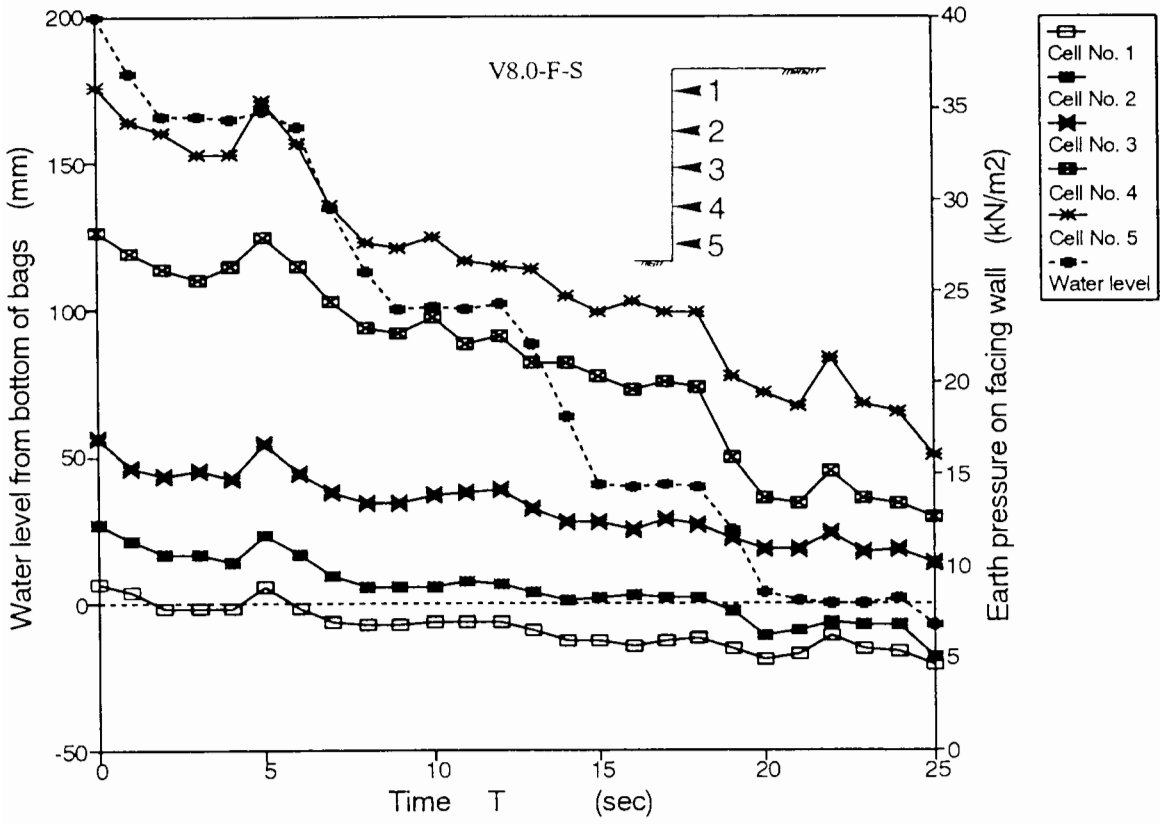

Fig.6.3 (c) - Influence of draining water on the earth pressures

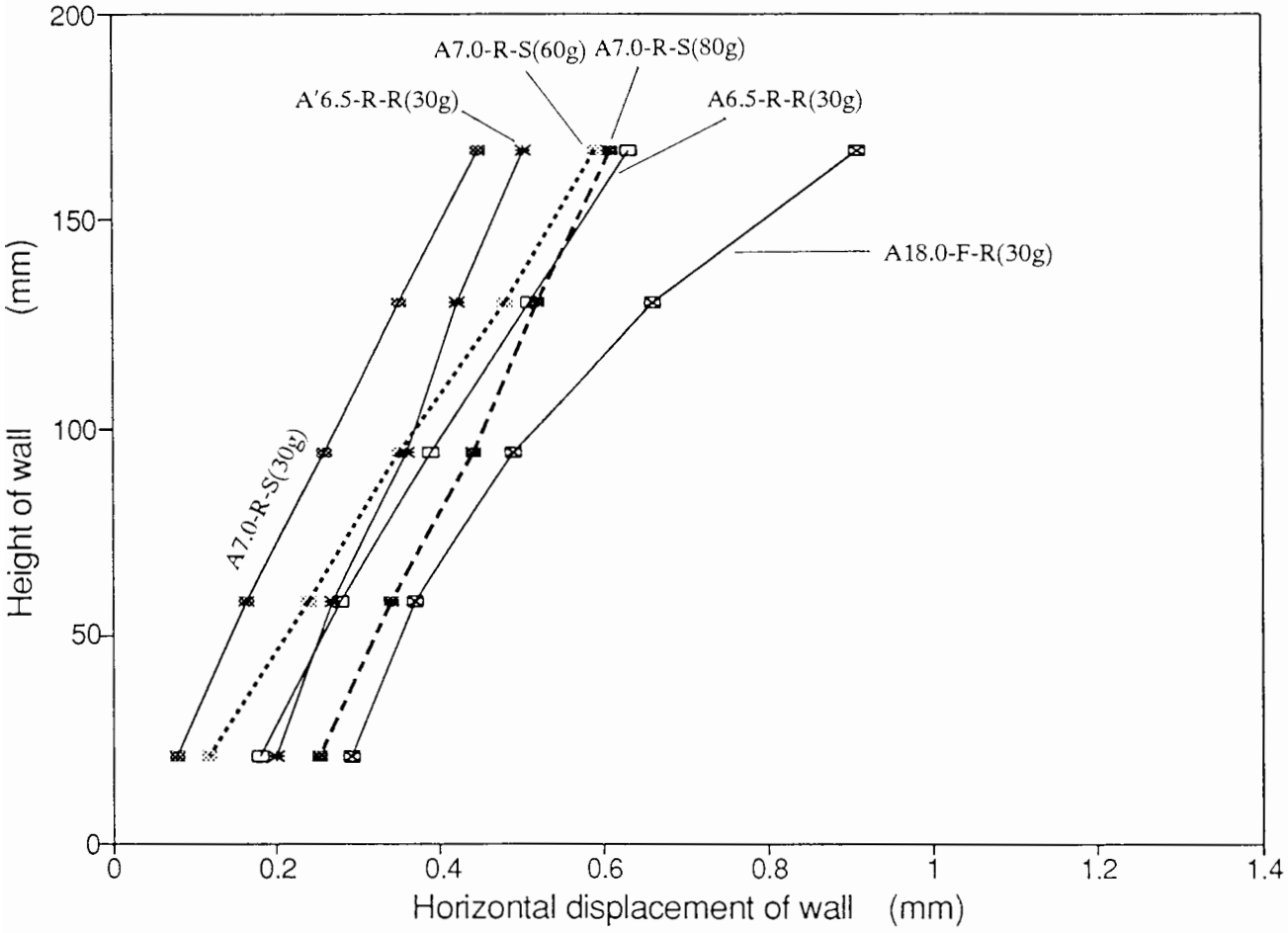

a

Fig.6.4 - Horizontal displacements δ_h of the facing wall after draining of the water

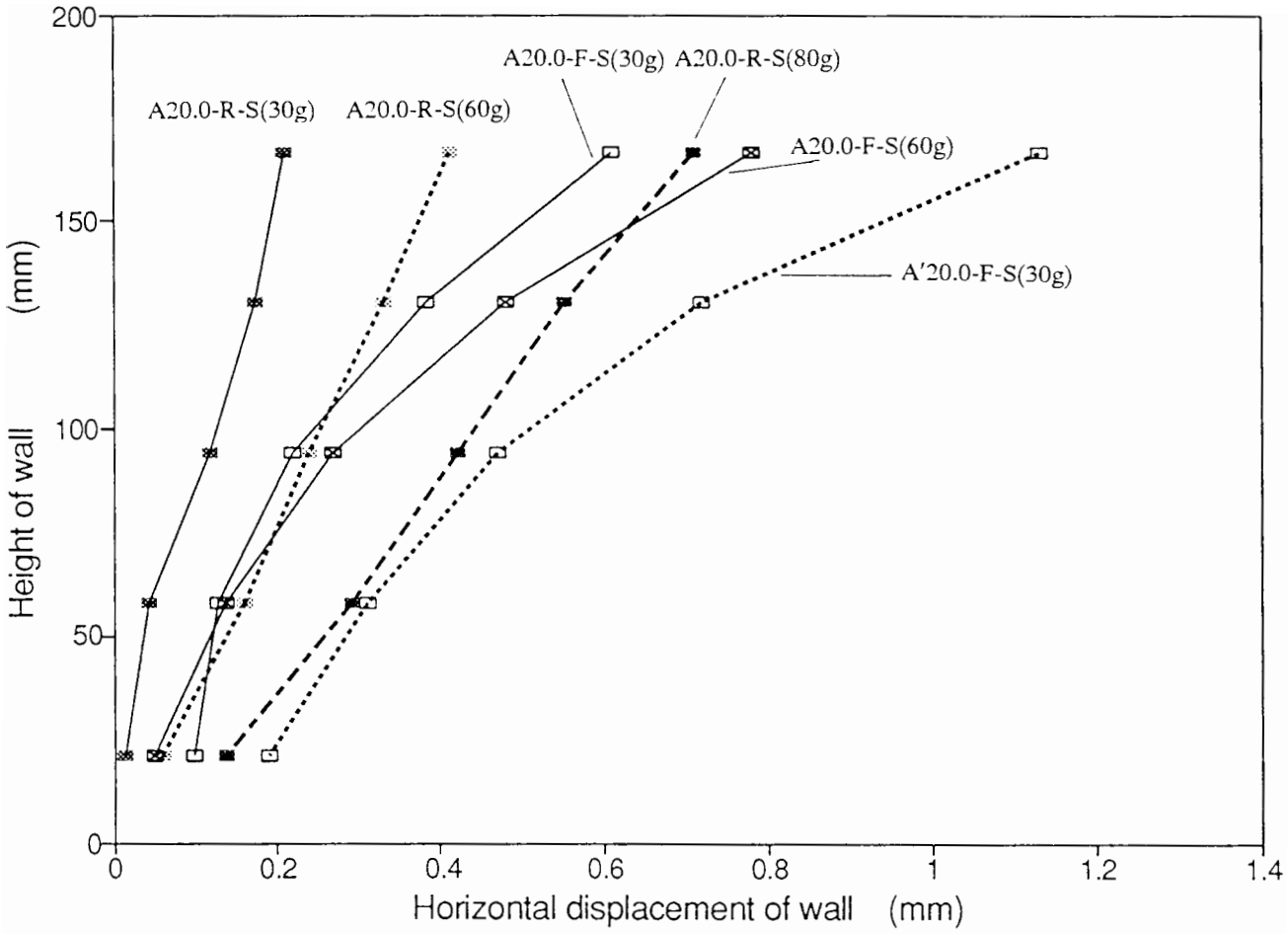

b

Fig.6.4 - Horizontal displacements δ_h of the facing wall after draining of the water

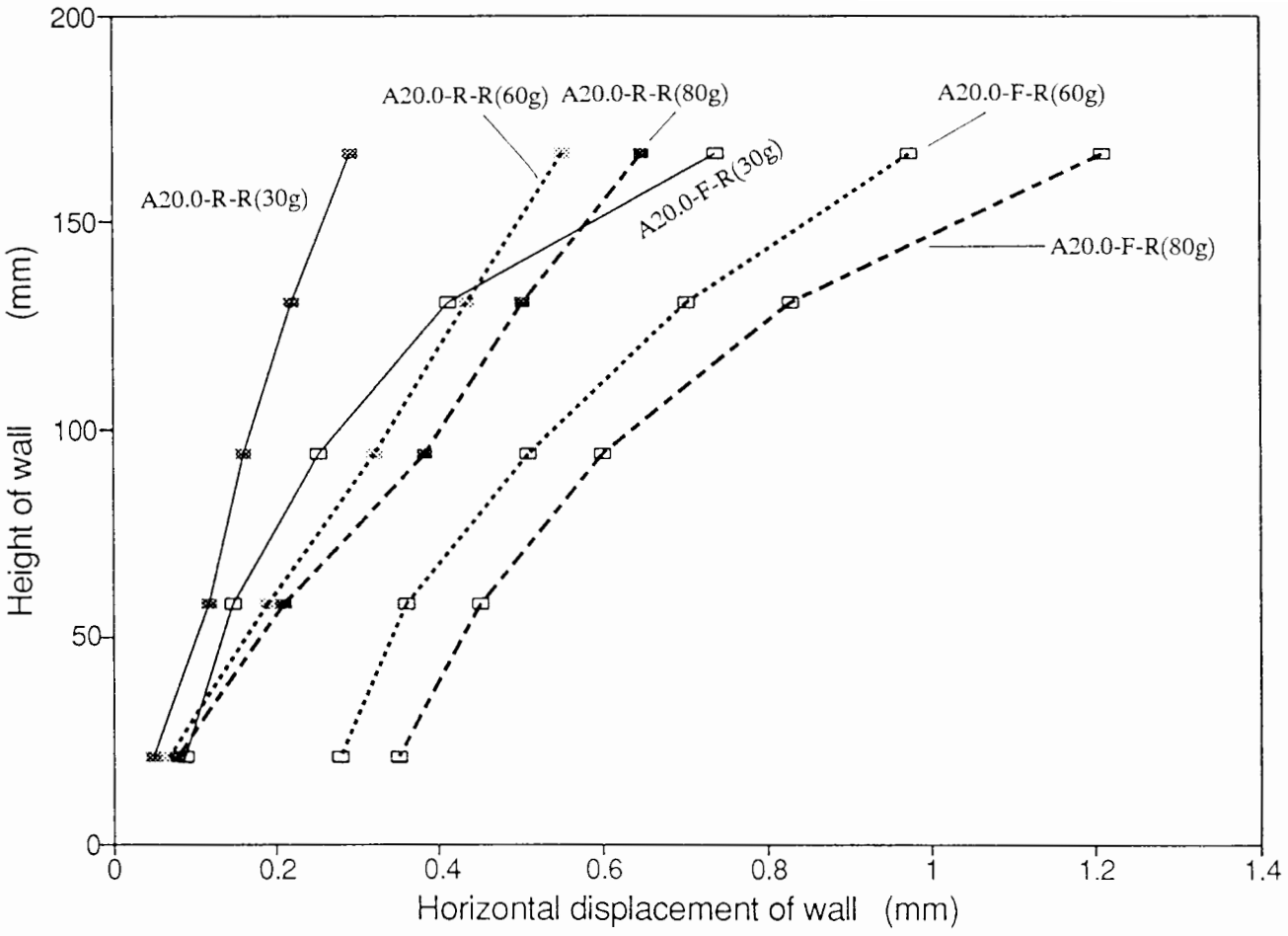

c

Fig.6.4 - Horizontal displacements δ_h of the facing wall after draining of the water

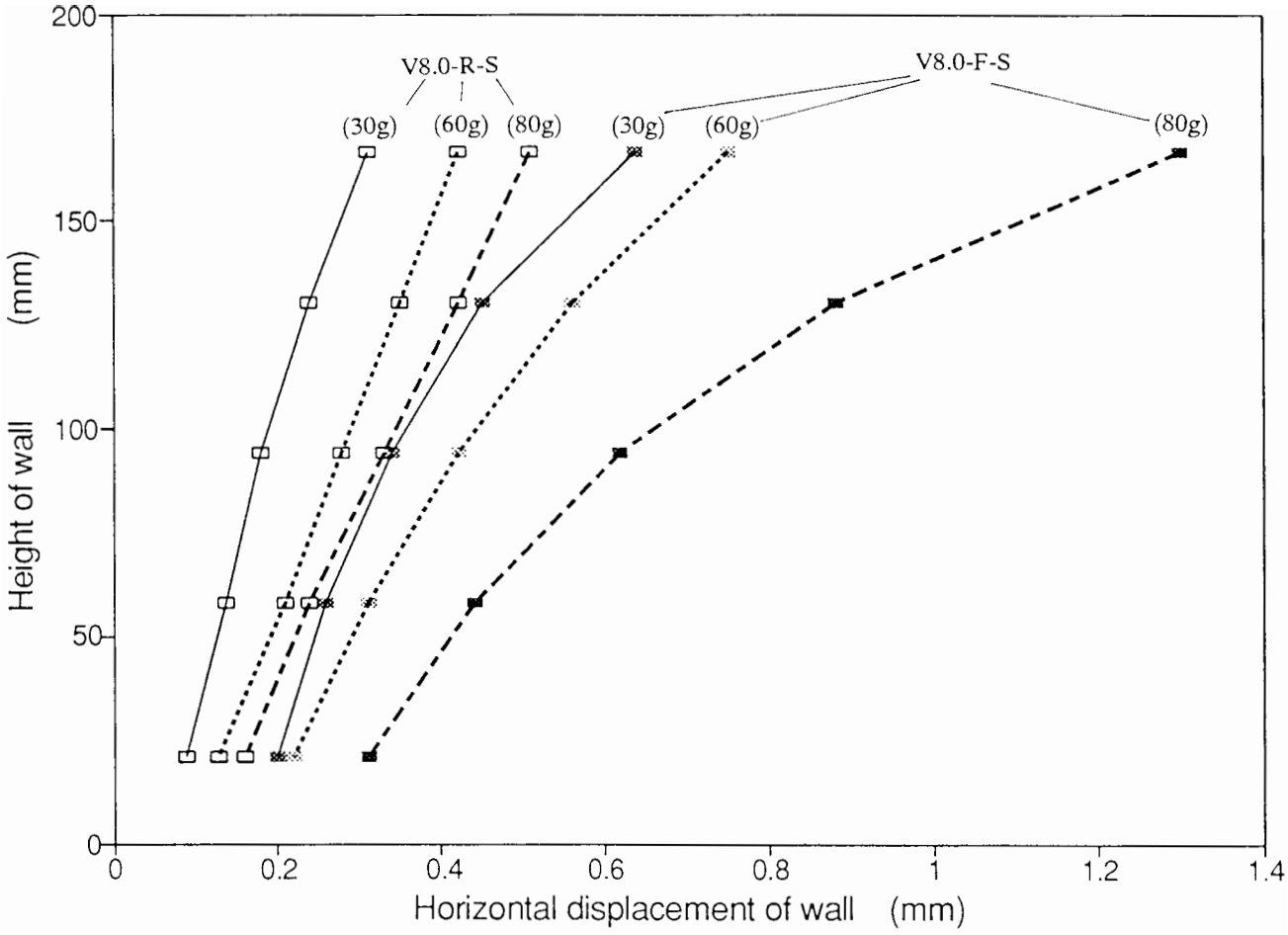

d

Fig.6.4 - Horizontal displacements δ_h of the facing wall after draining of the water

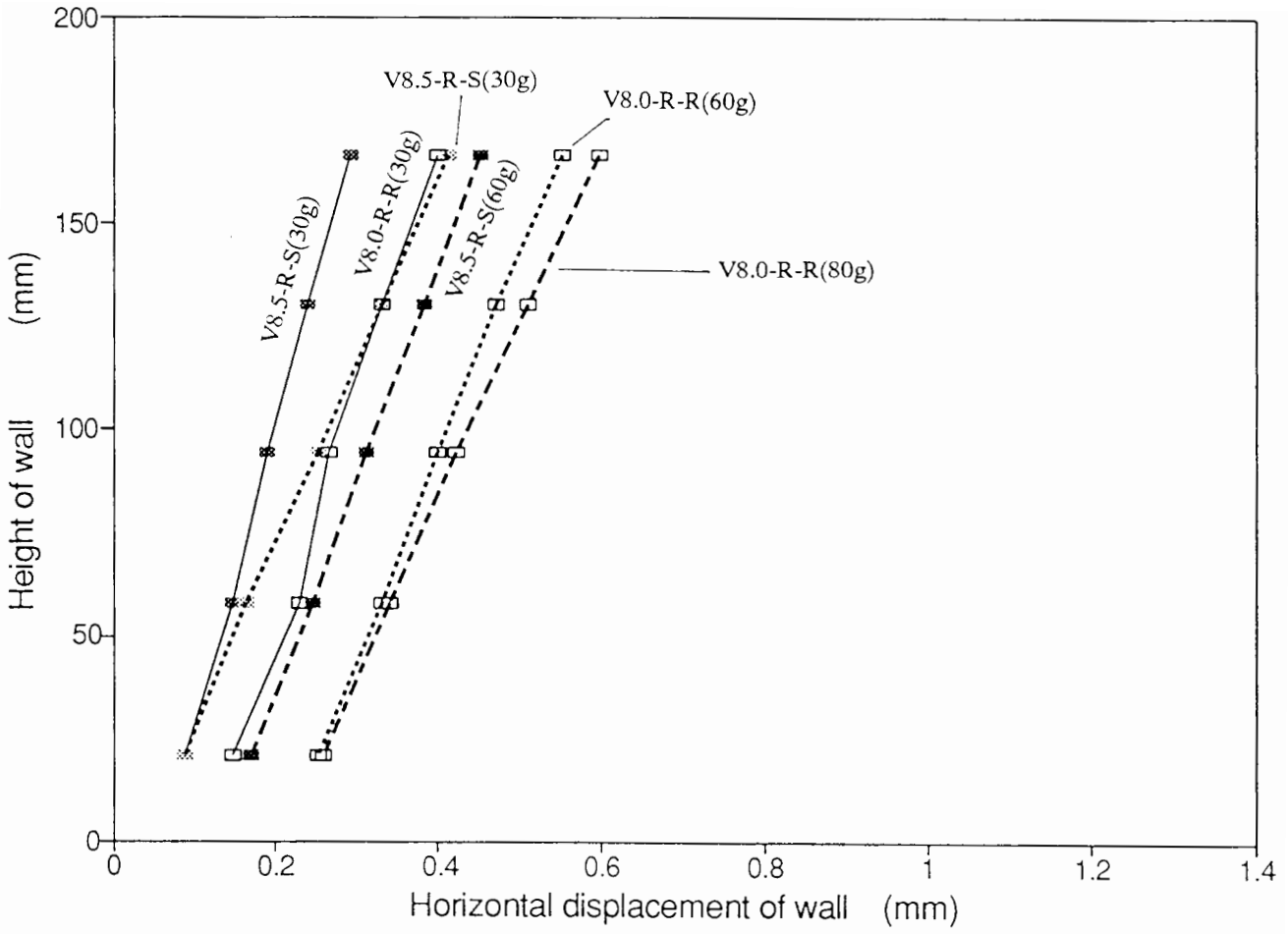

e

Fig.6.4 - Horizontal displacements δ_h of the facing wall after draining of the water

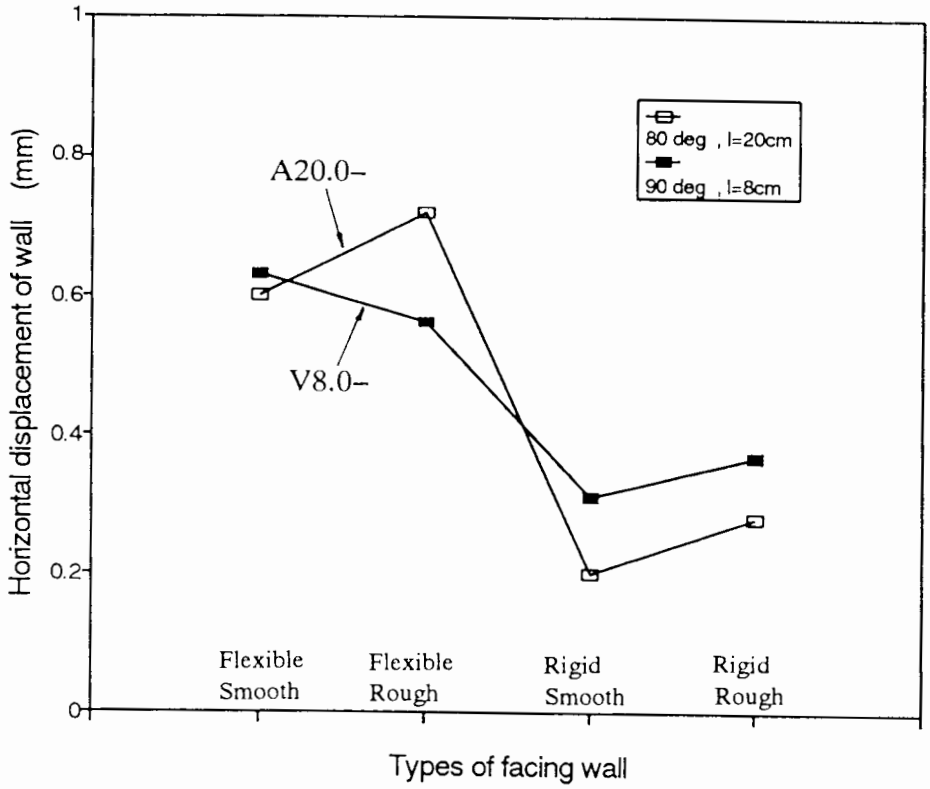

Fig.6.5 - Relationship between type of the facing wall and the horizontal displacement δ_h of the facing wall

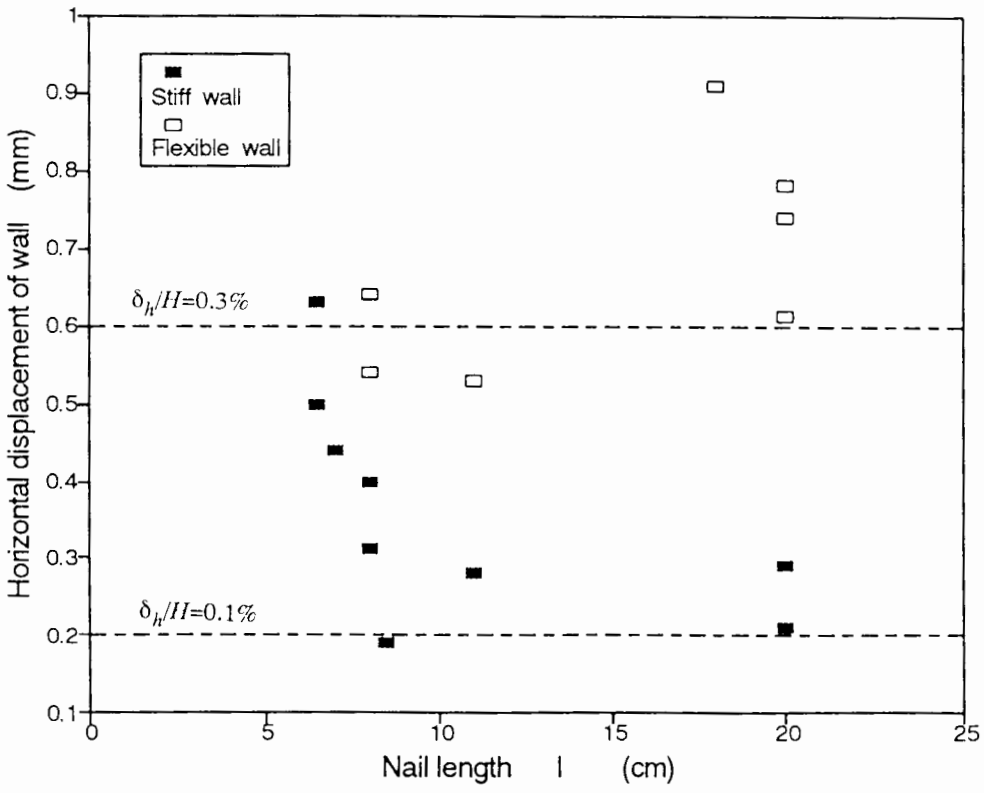

Fig.6.6 - Comparison between the nail length l and the horizontal displacement δ_h of the facing wall

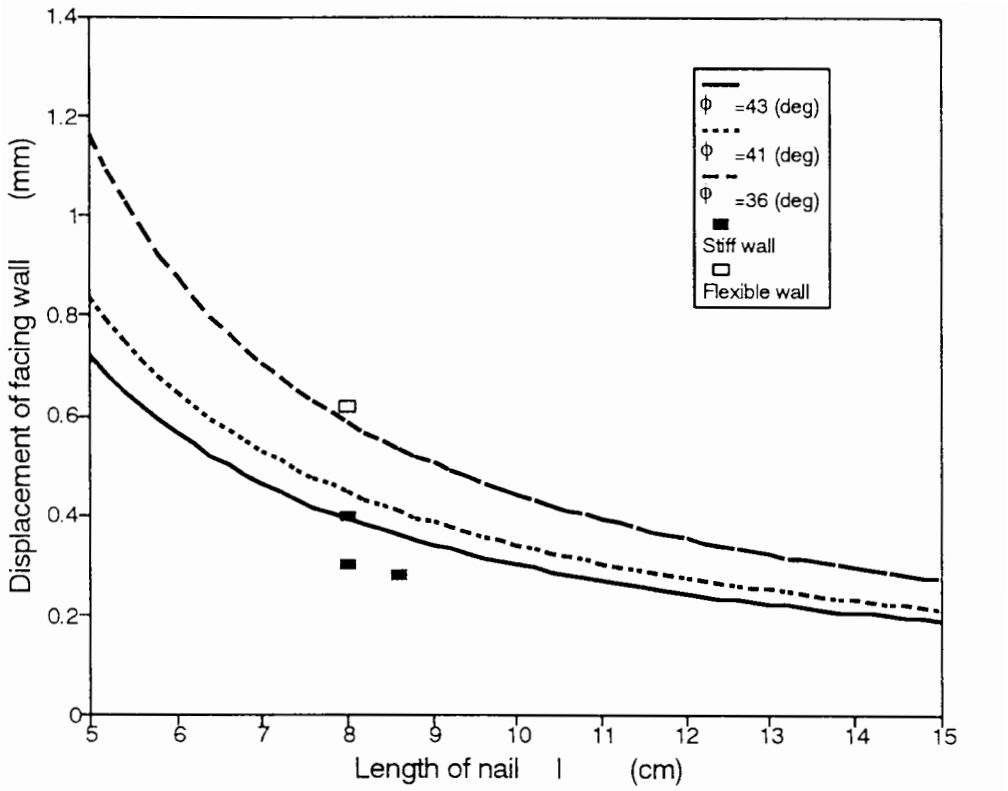

Fig.6.7 - Analysis of the horizontal displacement δ_h of the facing wall by the measured interface stiffness k_i

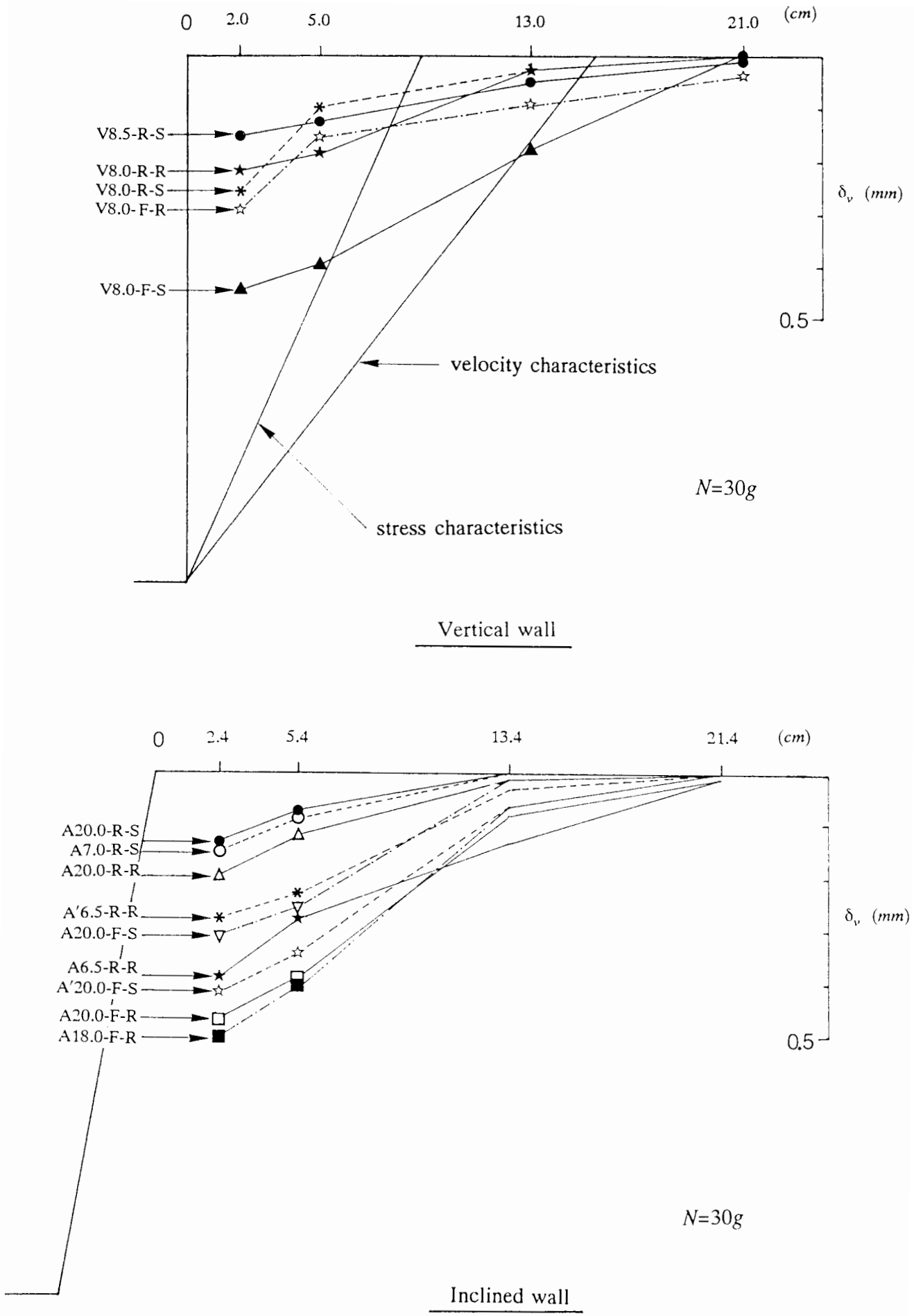

Fig.6.8 - Vertical displacements of the upper ground surface δ_v due to draining of the water

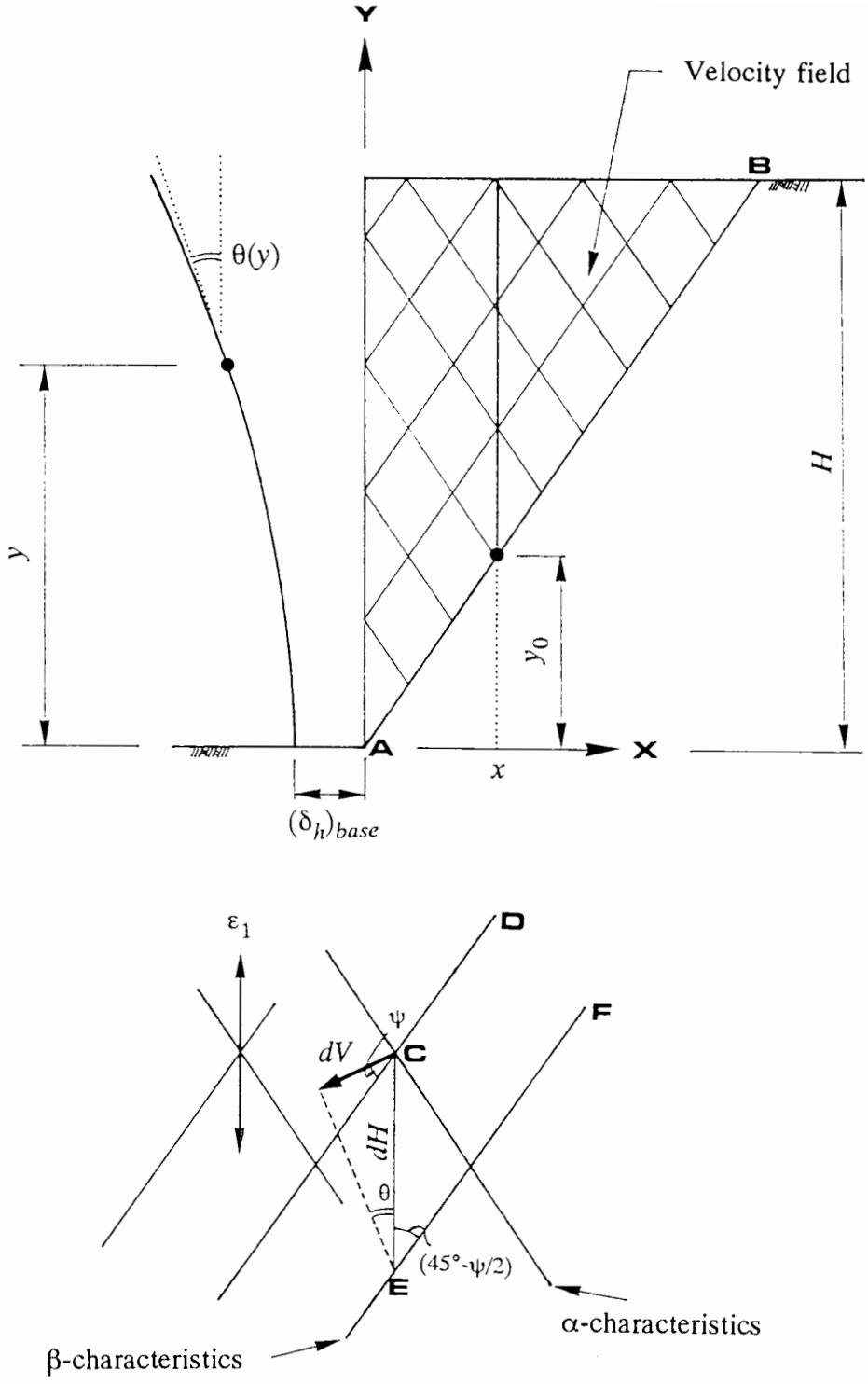

Fig.6.9 - Analysis of vertical displacement δ_v of the upper ground surface

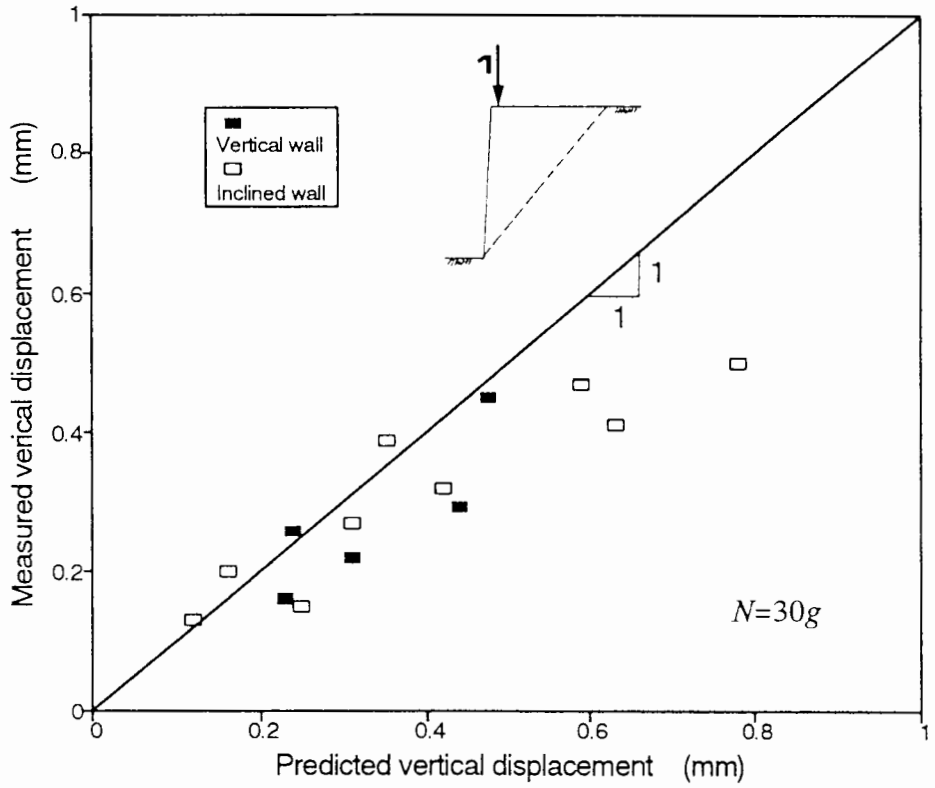

Fig.6.10 - Comparison of the vertical displacements δ_v of the upper ground surface

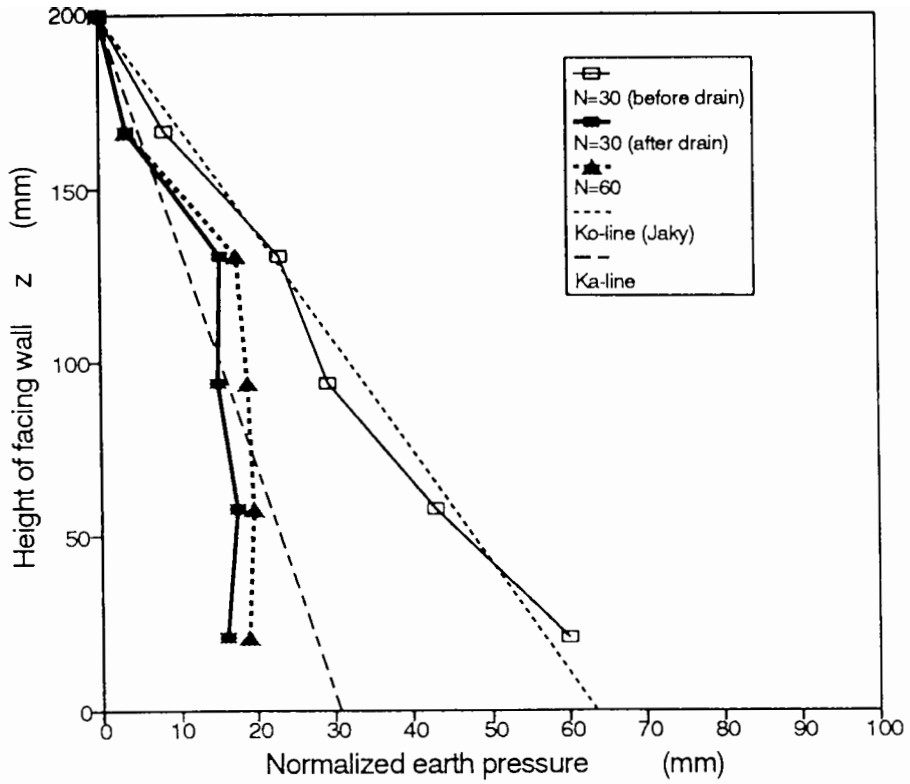

V8.0-R-R

Fig.6.11 (a) - Distributions of the normalised earth pressure $p/(N\gamma)=K_a^* z$

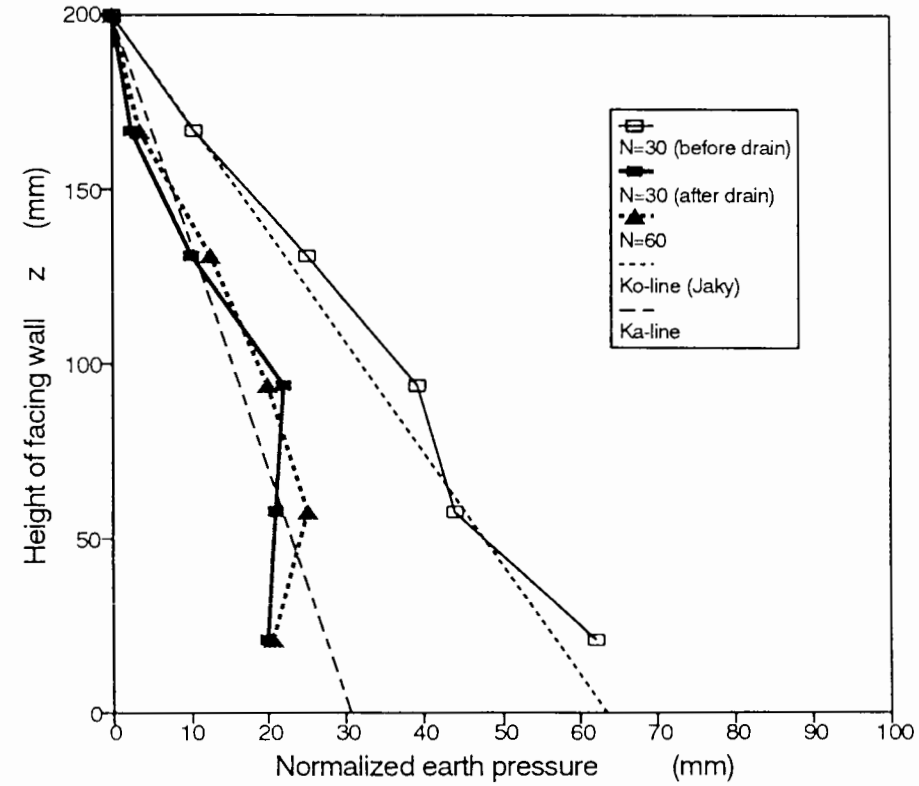

V8.0-F-R

Fig.6.11 (b) - Distributions of the normalised earth pressure $p/(N\gamma)=K_a^* z$

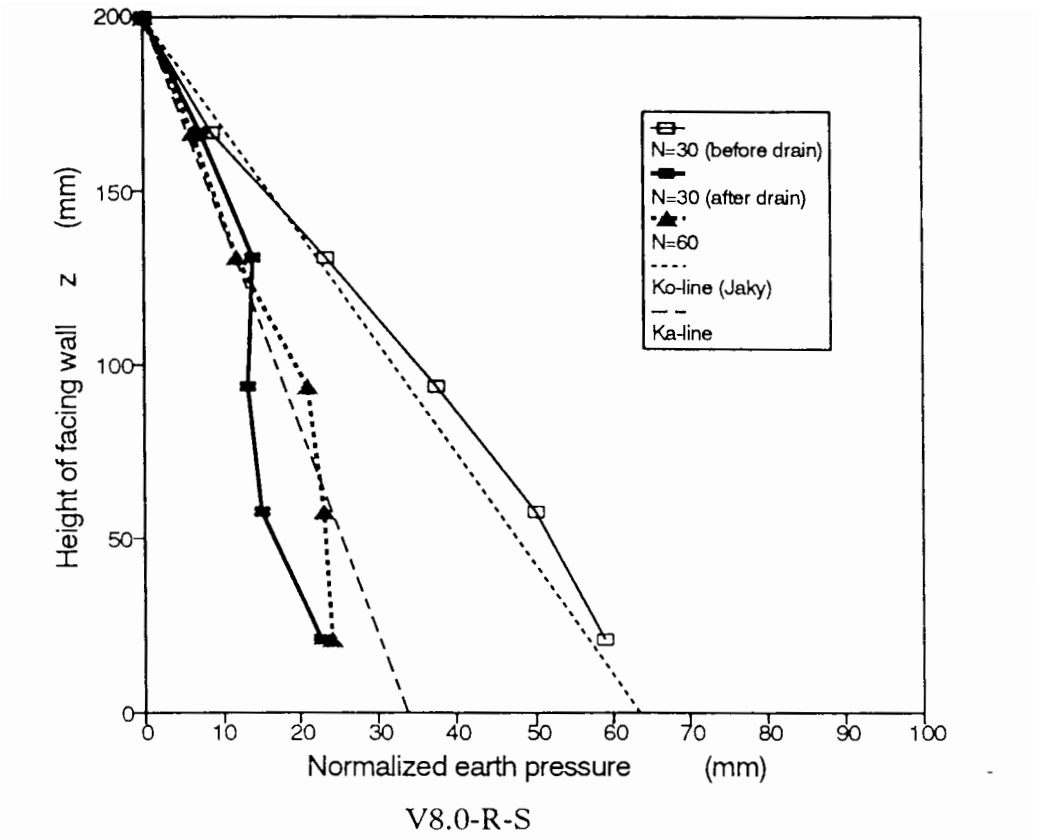

V8.0-R-S

Fig.6.11 (c) - Distributions of the normalised earth pressure $p/(N\gamma)=K_a^*z$

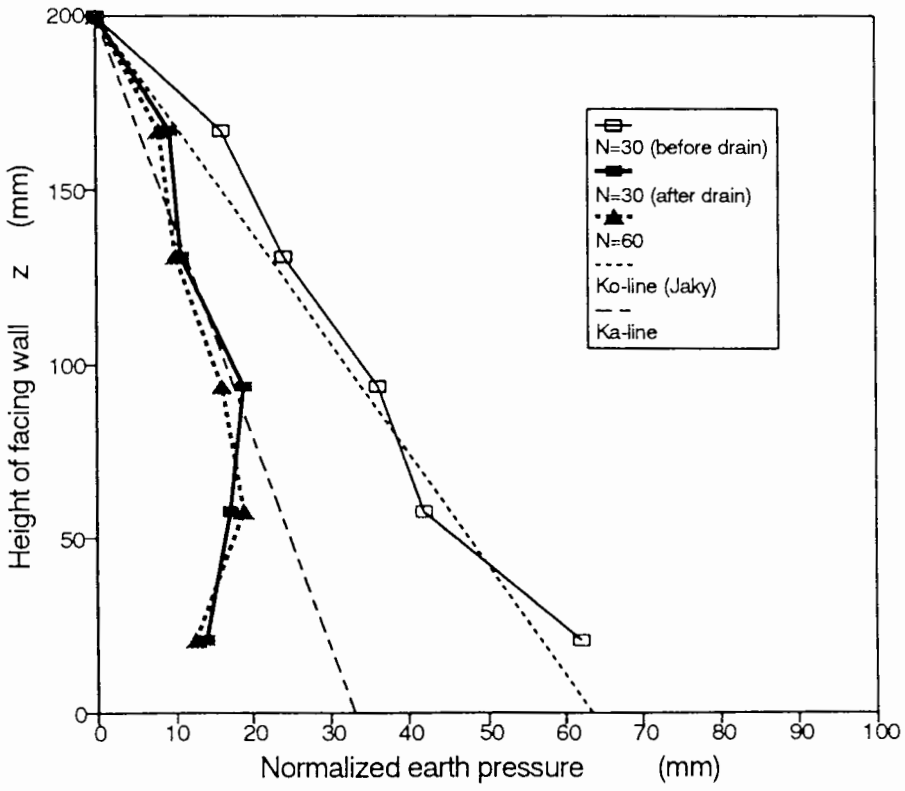

V8.0-F-S

Fig.6.11 (d) - Distributions of the normalised earth pressure $p/(N\gamma)=K_a^*z$

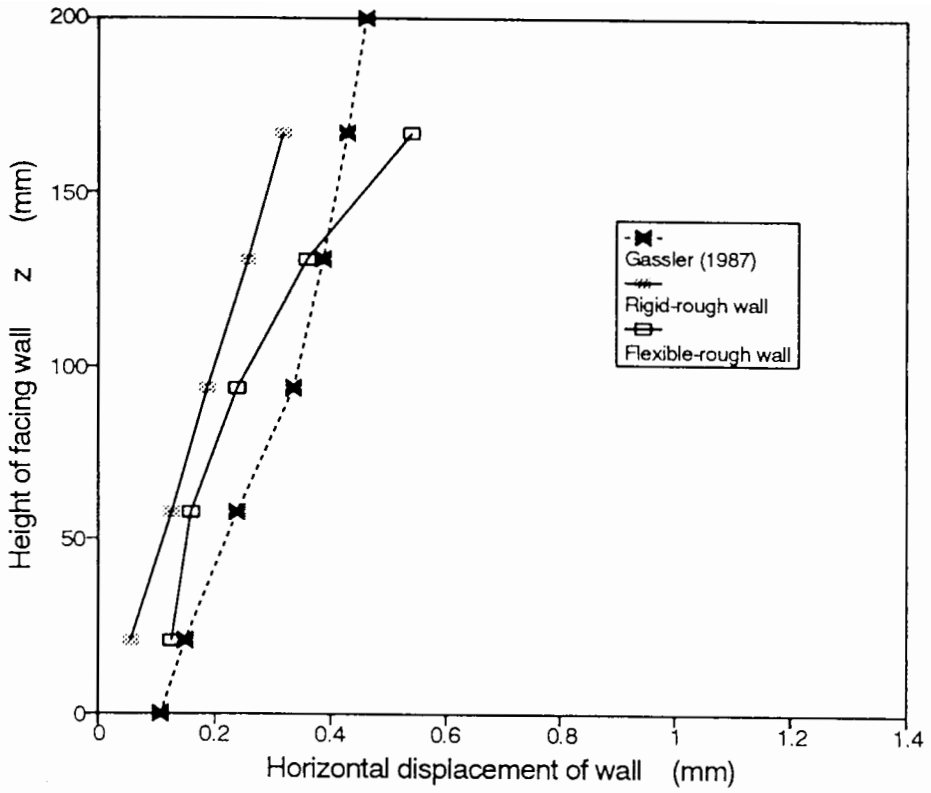

Fig.6.12 - Comparison of the horizontal displacements δ_h of the facing wall

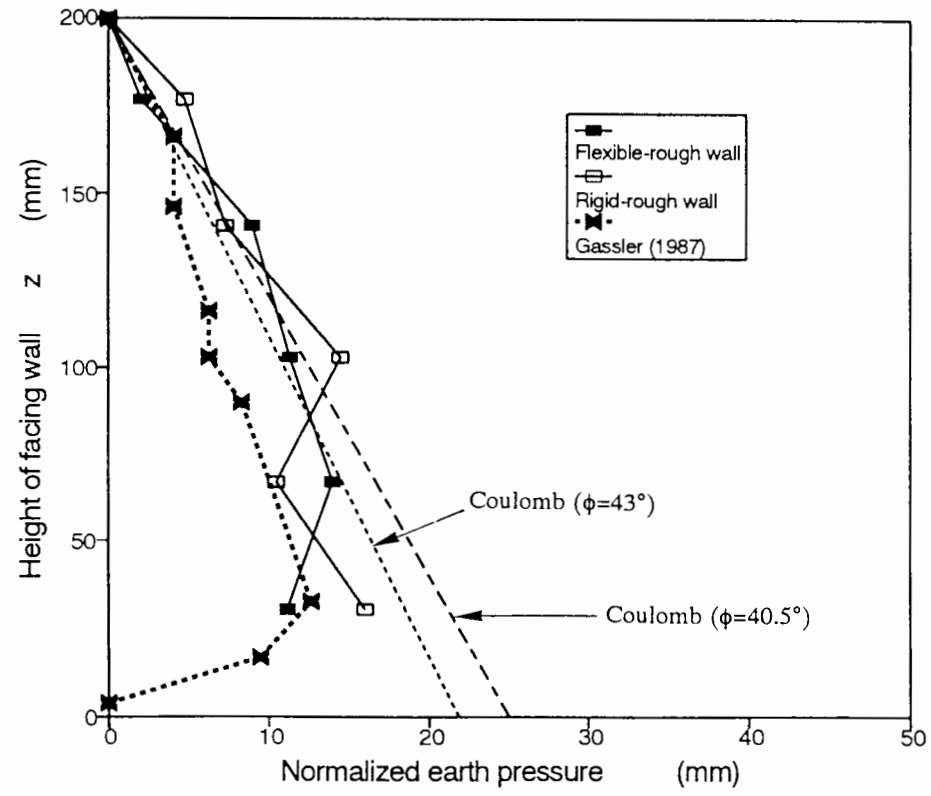

Fig.6.13 - Comparison of the normalised earth pressure $p/(N\gamma)$ of the facing wall

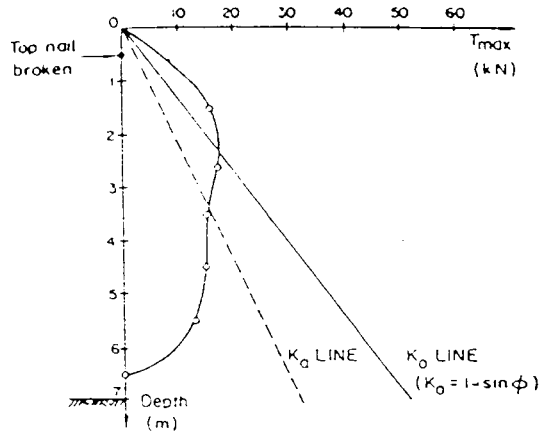

Fig.6.14 - Observed earth pressure distribution of facing wall in nailed slope (Plumelle *et al.*, 1989)

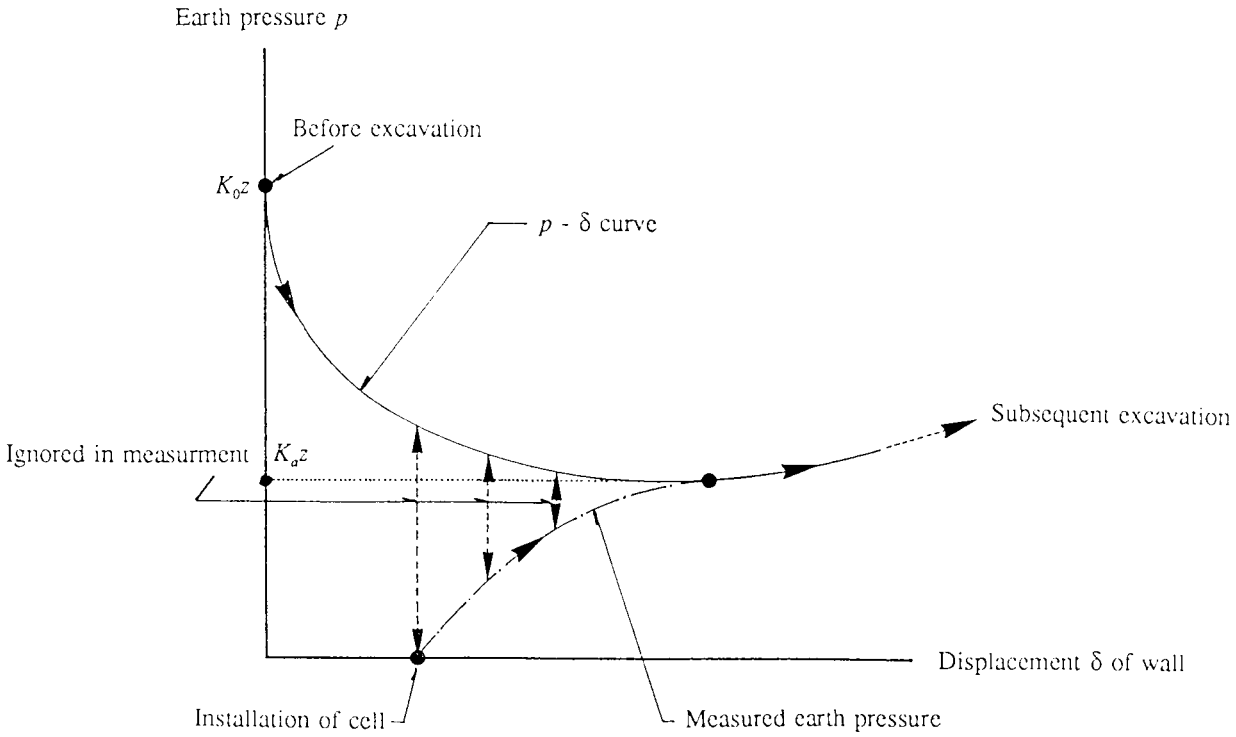

Fig.6.15 - Measured and ignored earth pressures on facing wall in practice

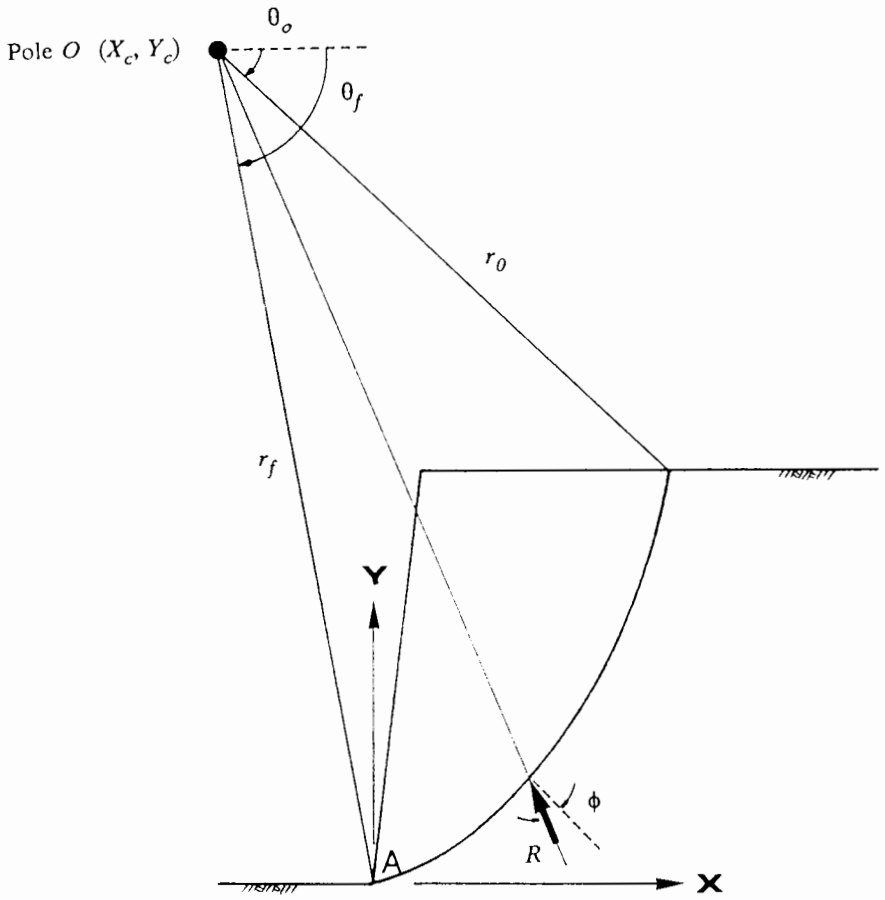

Fig.7.1 - Description of logarithmic spiral

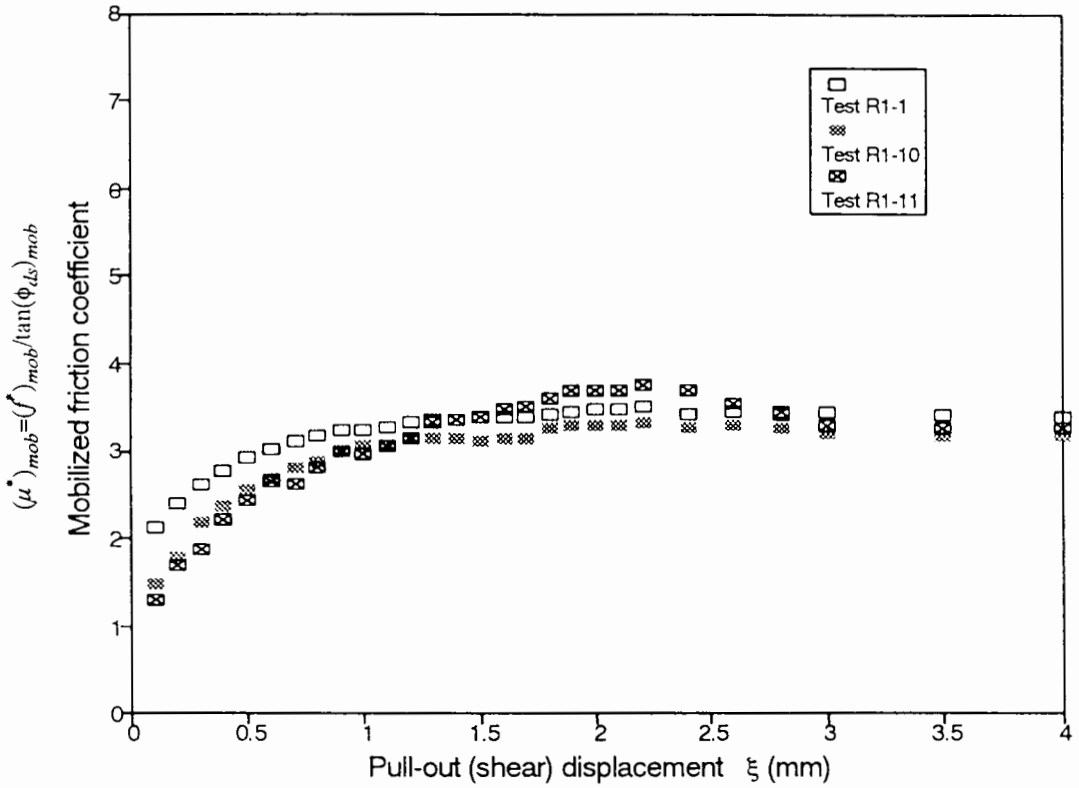

Fig.7.2 - Compatibility curves of the stiff-rough nails from pull-out tests

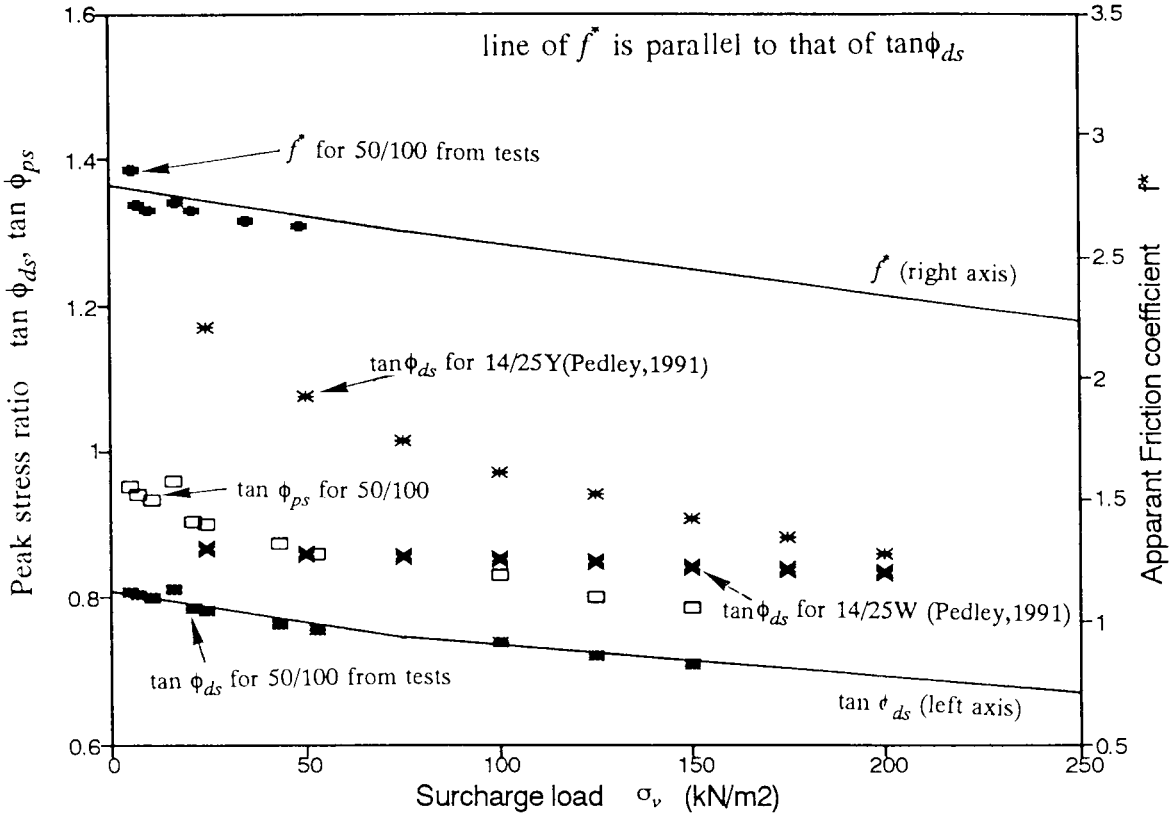

Fig.7.3 - Influence of surcharge load σ_v on the internal friction angle of soil and the apparent friction coefficient

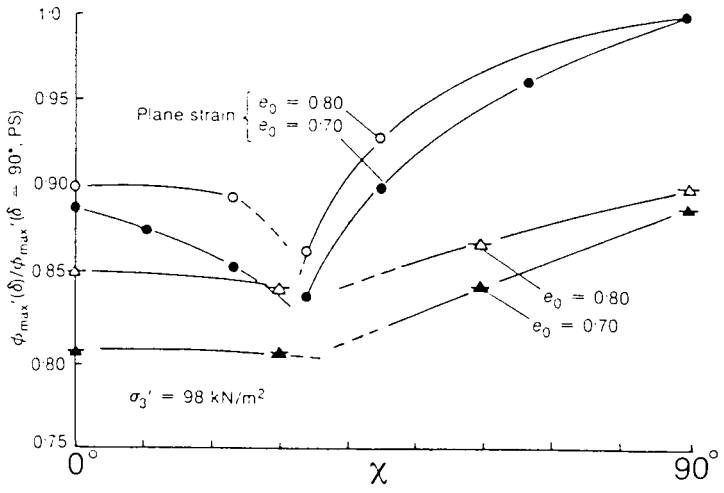

Fig.7.4 - Strength anisotropy in Toyoura sand (Tatsuoka *et al.*, 1987)

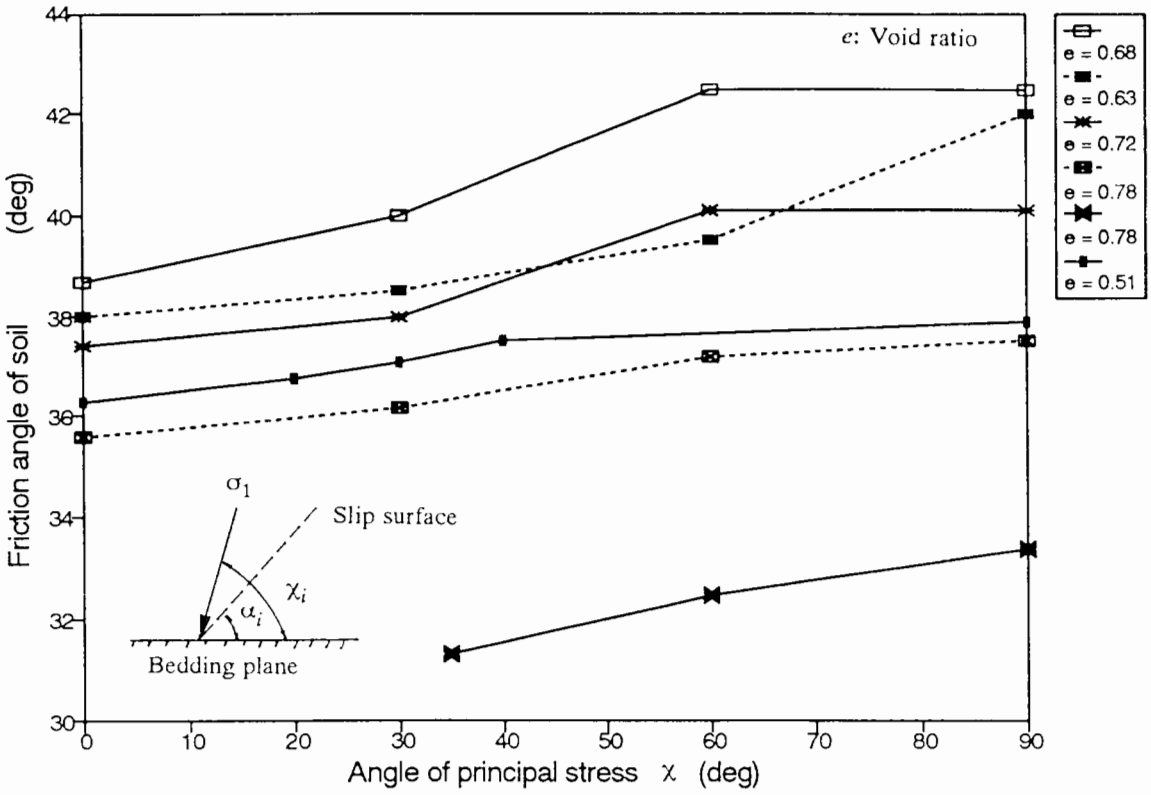

Fig.7.5 - Strength anisotropy in several types of sand (after Meyerhof, 1978)

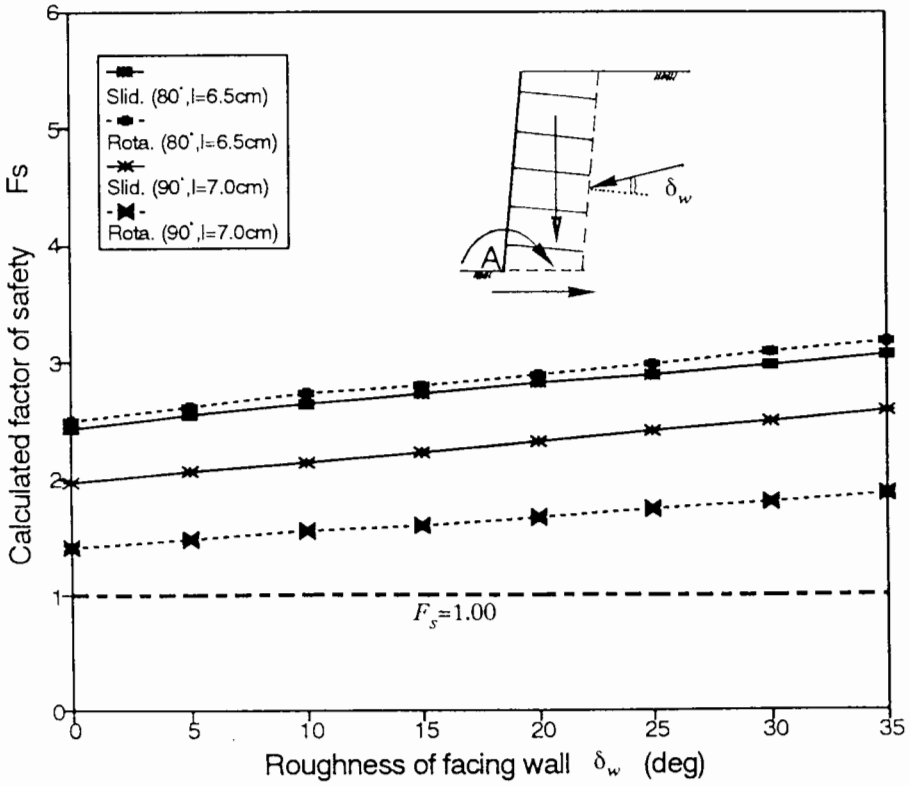

Fig.7.6 - External stability of the nailed soil block

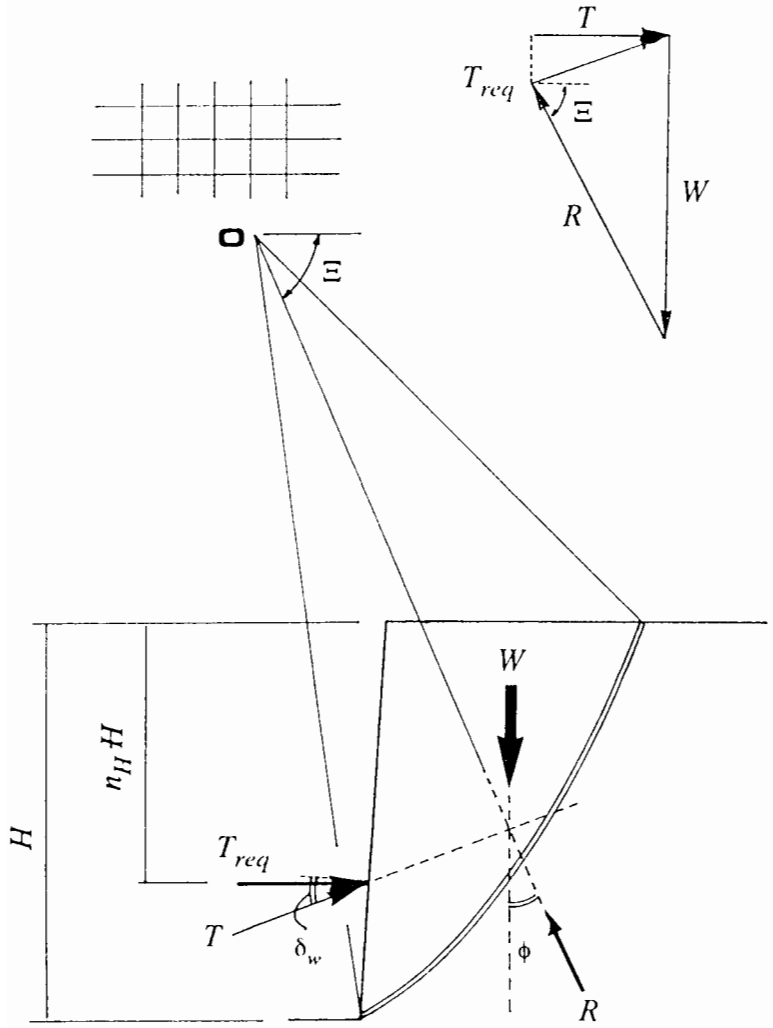

Fig.7.8 - Force polygon of the soil block

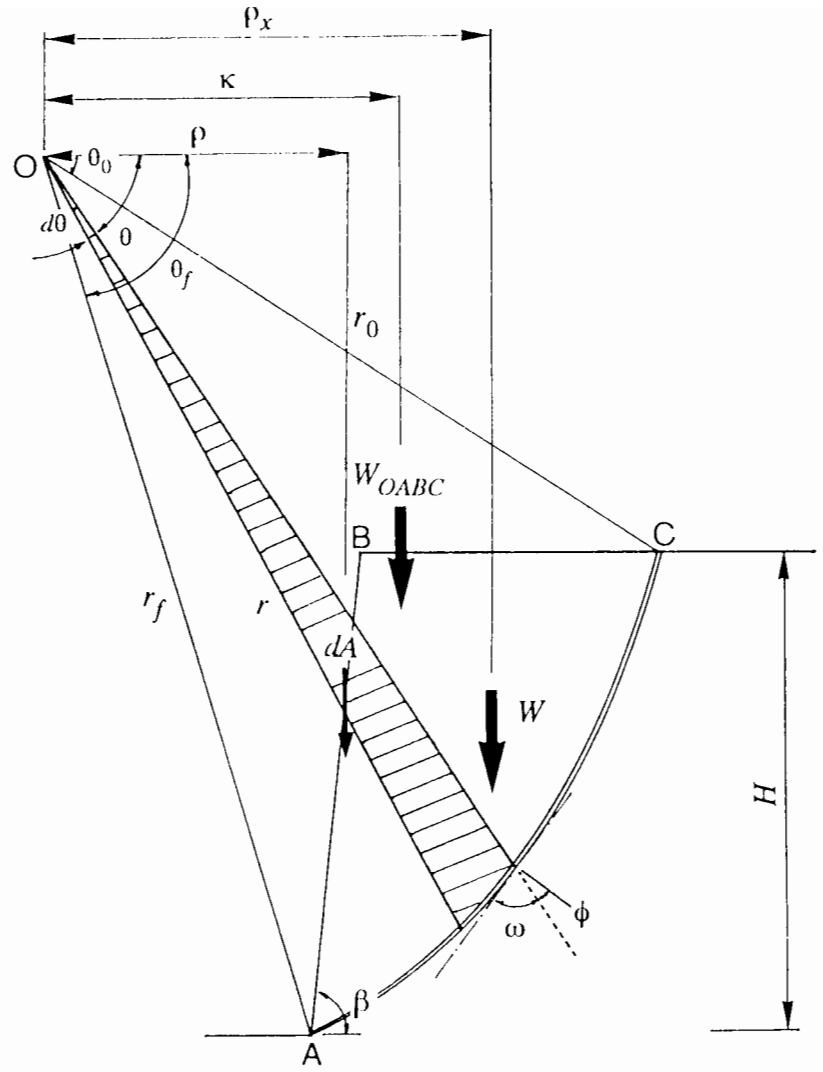

Fig.7.7 - Calculation of required force T_{ava} on the observed failure surface

Test	ϕ = 41°				ϕ = 36°			
	r_0 (cm)	θ_0	X_c (cm)	Y_c (cm)	r_0 (cm)	θ_0	X_c (cm)	Y_c (cm)
A6.5-F-R	29.78	1.029	-2.2	45.4	32.72	0.942	-6.2	46.2
A6.5-R-R	27.12	0.977	-3.0	42.3	29.70	0.890	-6.8	43.0
A'6.5-R-R	27.12	0.977	-3.0	42.3	29.7	0.89	-6.8	43.0
A18-F-R	26.10	0.977	-2.2	41.5	28.82	0.890	-5.8	42.2
A18-R-R	26.10	0.977	-2.2	41.5	28.82	0.890	-5.8	42.2
A20-F-S	28.31	1.012	-1.9	43.9	30.94	0.925	-5.6	44.6
A'20-F-S	28.31	1.012	-1.9	43.9	30.94	0.925	-5.6	44.6
A'20-R-S	24.70	0.977	-0.8	40.4	27.25	0.890	-4.2	41.0
V7-F-R	50.42	1.012	-16.9	62.7	55.17	0.925	-23.5	64.0
V'7-F-R	50.42	1.012	-16.9	62.7	55.17	0.925	-23.5	64.0
V7-R-R	31.63	0.907	-10.2	44.8	34.67	0.820	-14.4	45.2
V8-F-R	25.47	0.89	-6.2	39.6	28.38	0.802	-9.8	40.2
V20-F-S	36.84	0.942	-12.5	49.6	40.40	0.855	-17.2	50.4
V23-F-S	26.52	0.855	-8.6	40.0	29.37	0.768	-12.4	40.2

Table 7.1 (a) - Shapes of failure surface of logarithmic spiral observed in the centrifuge tests

Test	ϕ = 41°				ϕ = 36°			
	r_0 (cm)	θ_0	X_c (cm)	Y_c (cm)	r_0 (cm)	θ_0	X_c (cm)	Y_c (cm)
A7-R-S	27.12	0.977	-3.0	42.3	29.70	0.890	-6.8	43.0
A20-R-S	24.70	0.977	-0.8	40.4	27.25	0.890	-4.2	41.0
A20-R-R	24.70	0.977	-0.8	40.4	27.25	0.890	-4.2	41.0
A20-F-R	24.70	0.977	-0.8	40.4	27.25	0.890	-4.2	41.0
V8-F-S	20.82	0.802	-5.4	35.0	23.07	0.715	-8.4	35.1
V8-R-S	20.82	0.802	-5.4	35.0	23.07	0.715	-8.4	35.1
V8-R-R	25.47	0.890	-6.2	39.6	28.38	0.802	-9.8	40.2
V8.5-R-S	43.47	0.977	-14.8	55.8	46.28	0.890	-19.6	55.6

Table 7.1 (b) - Shapes of analyzed failure surface of logarithmic spiral which has the minimum factor of safety $(F_s)_{min}$ in the centrifuge tests (in case of uncollapsed nailed slopes)

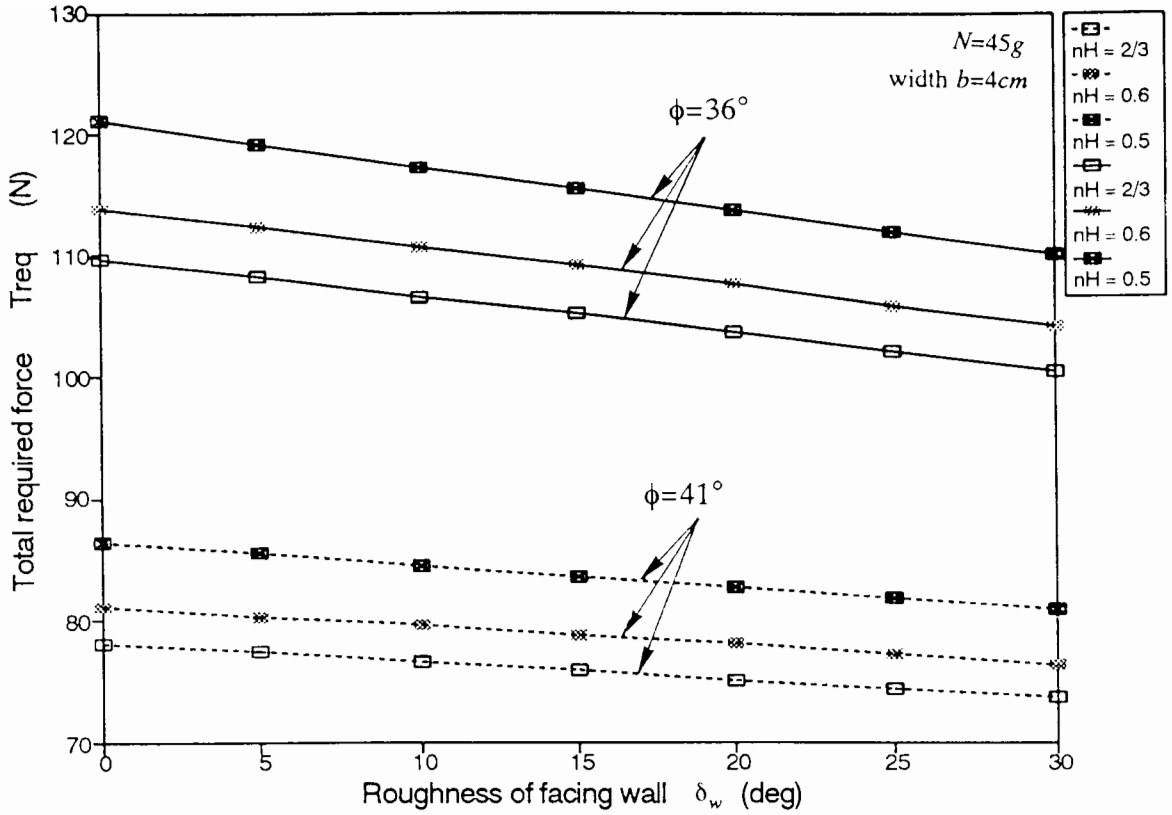

Fig.7.9 (a) - Influence of the location of centroid n_H
(Test *A'6.5-R-R)*

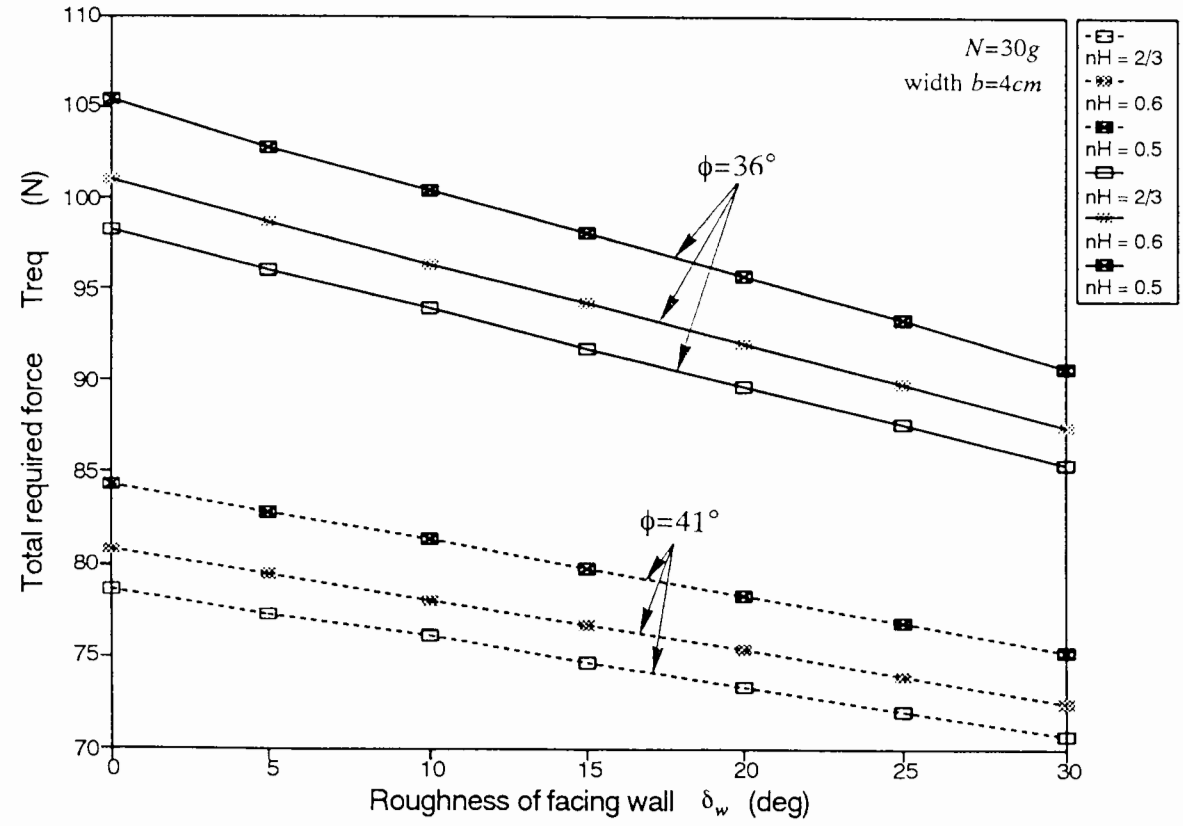

Fig.7.9 (b) - Influence of the location of centroid n_H
(Test *V'7.0-F-R)*

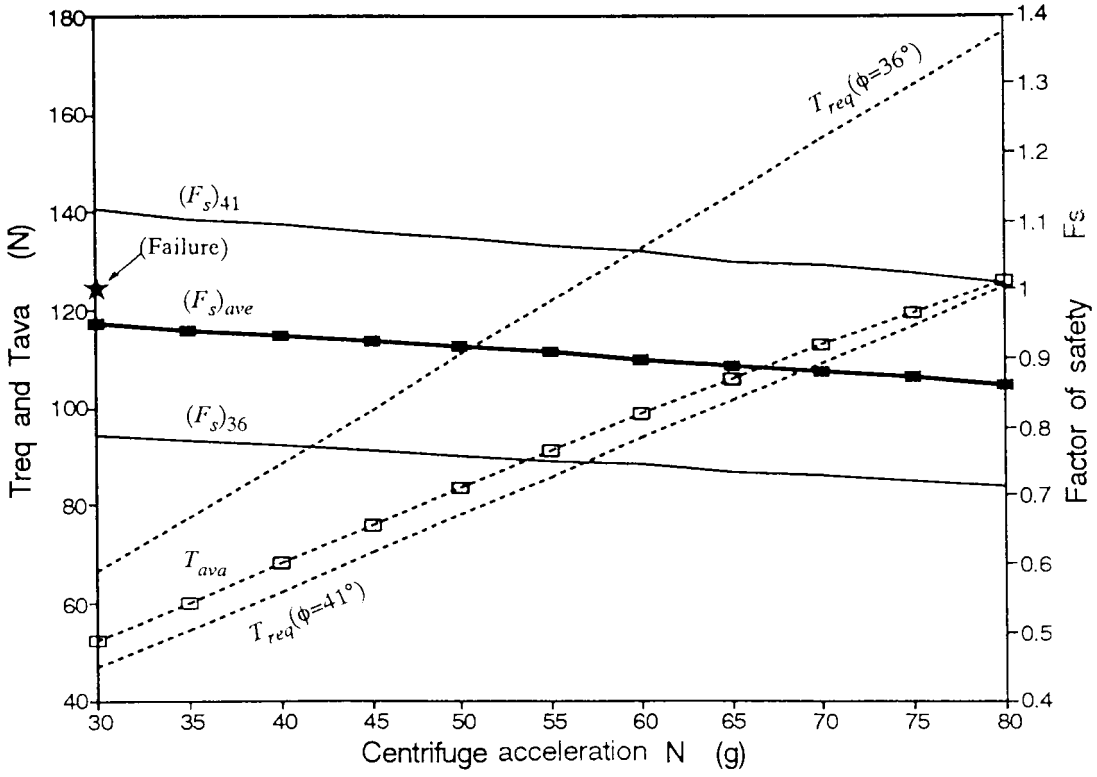

(a) Test A6.5-F-R

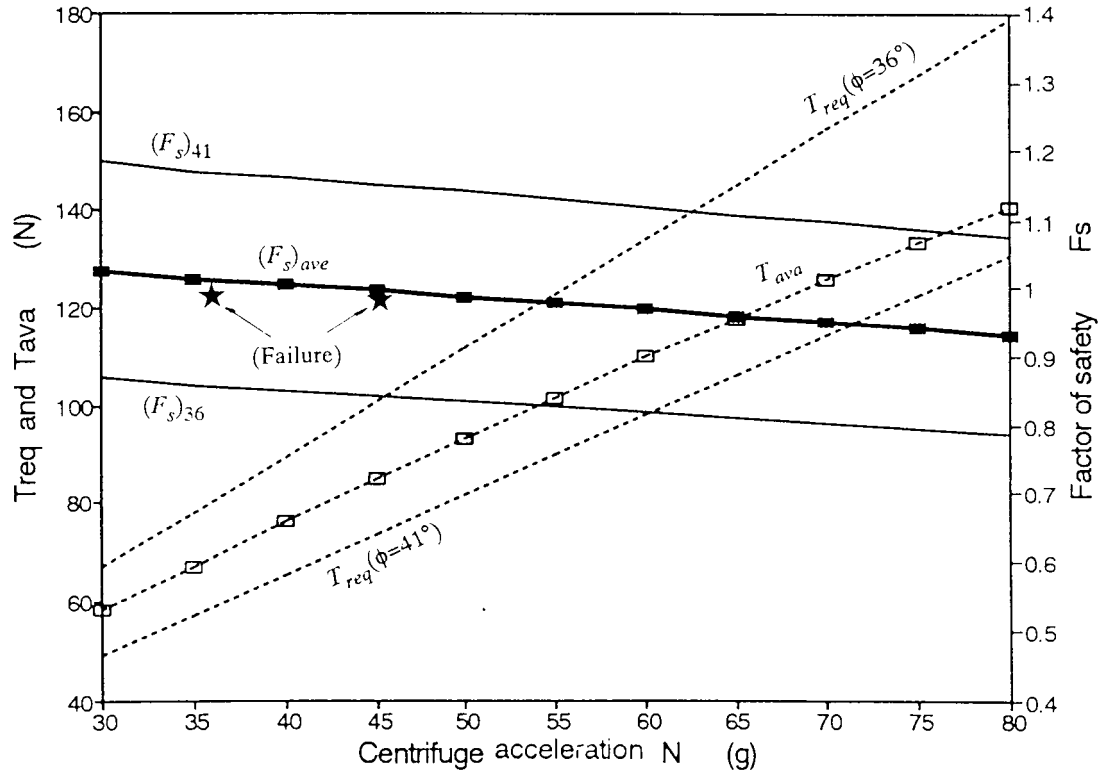

(b) Test A(A')6.5-R-R

Fig.7.10 (a) - Comparison of the total required force T_{req}, total available force T_{ava} and factor of safety F_s

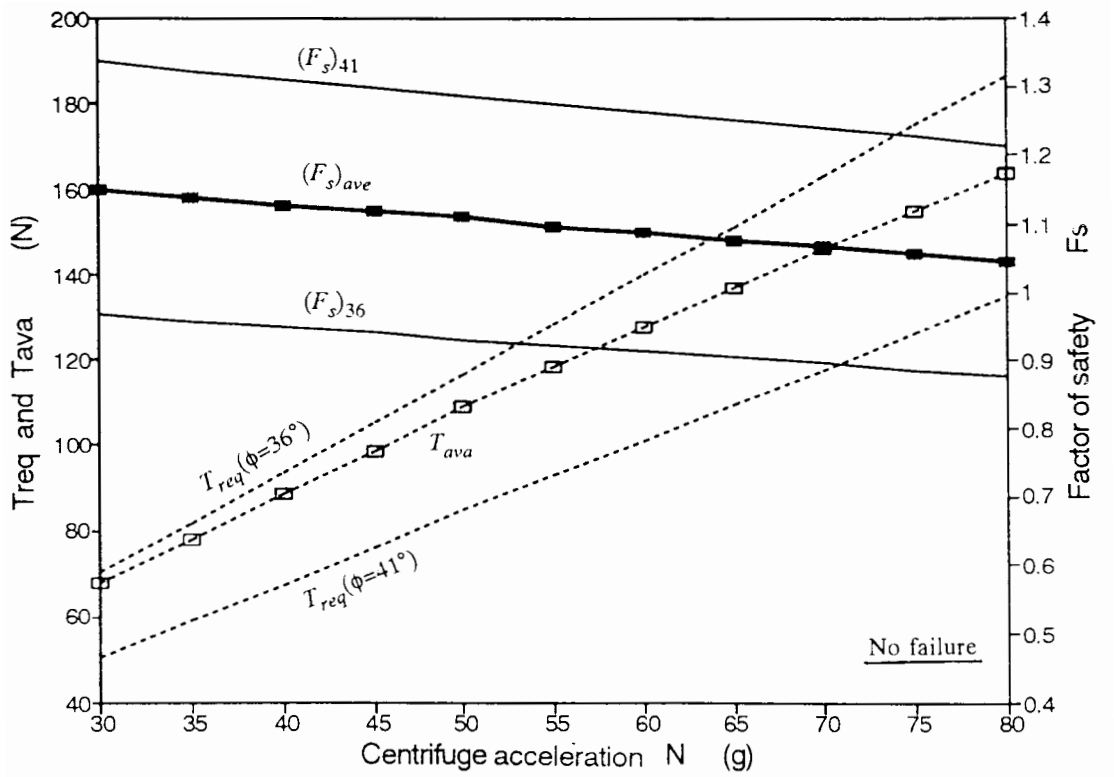

(c) Test A7.0-R-S

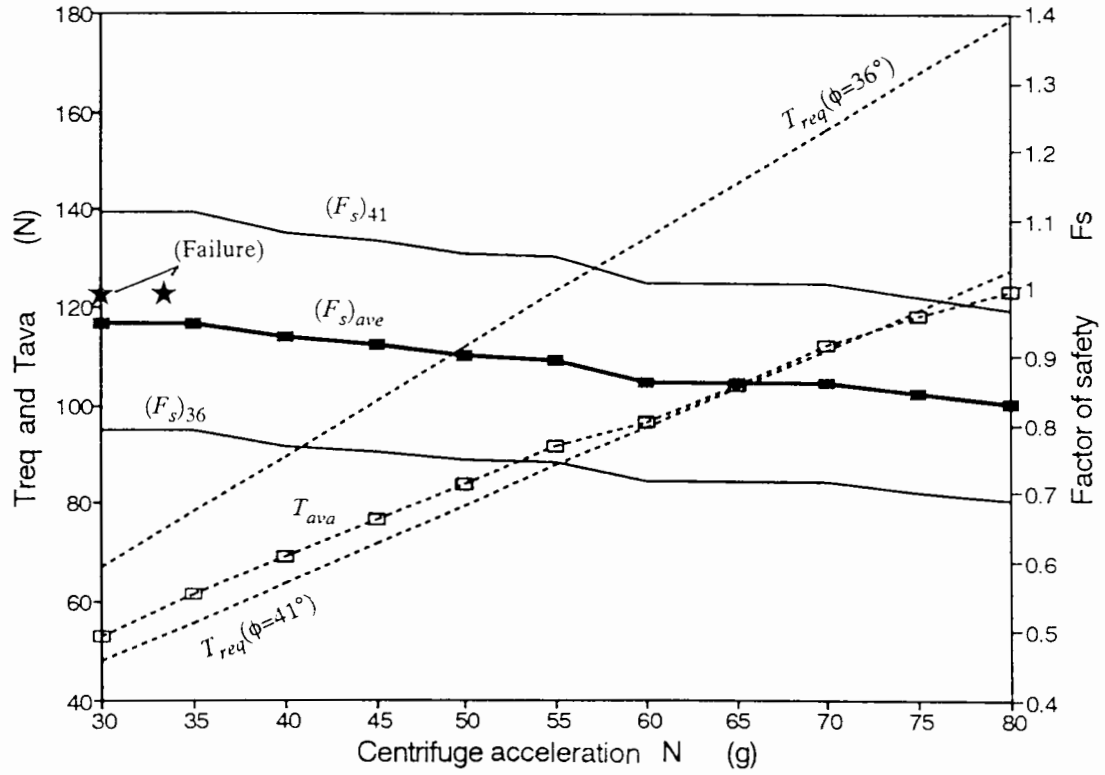

(d) Test A18.0-F(R)-R

Fig.7.10 (b) - Comparison of the total required force T_{req}, total available force T_{ava} and factor of safety F_s

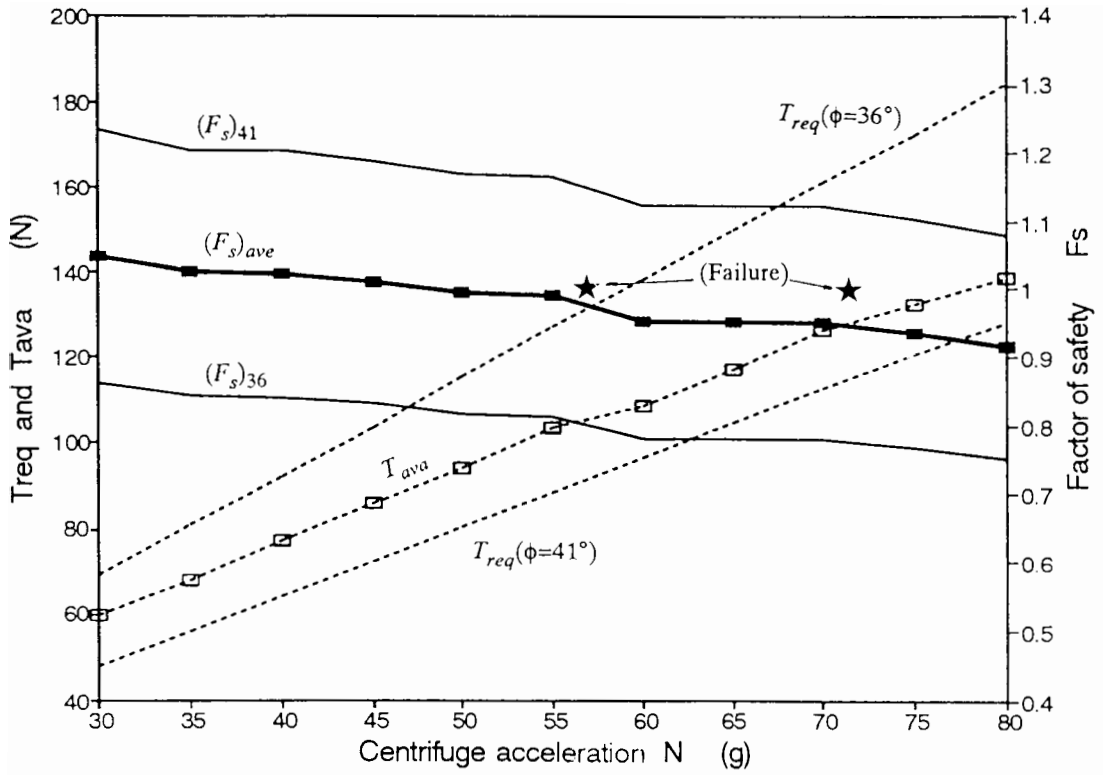

(e) Test A(A')20.0-F-S

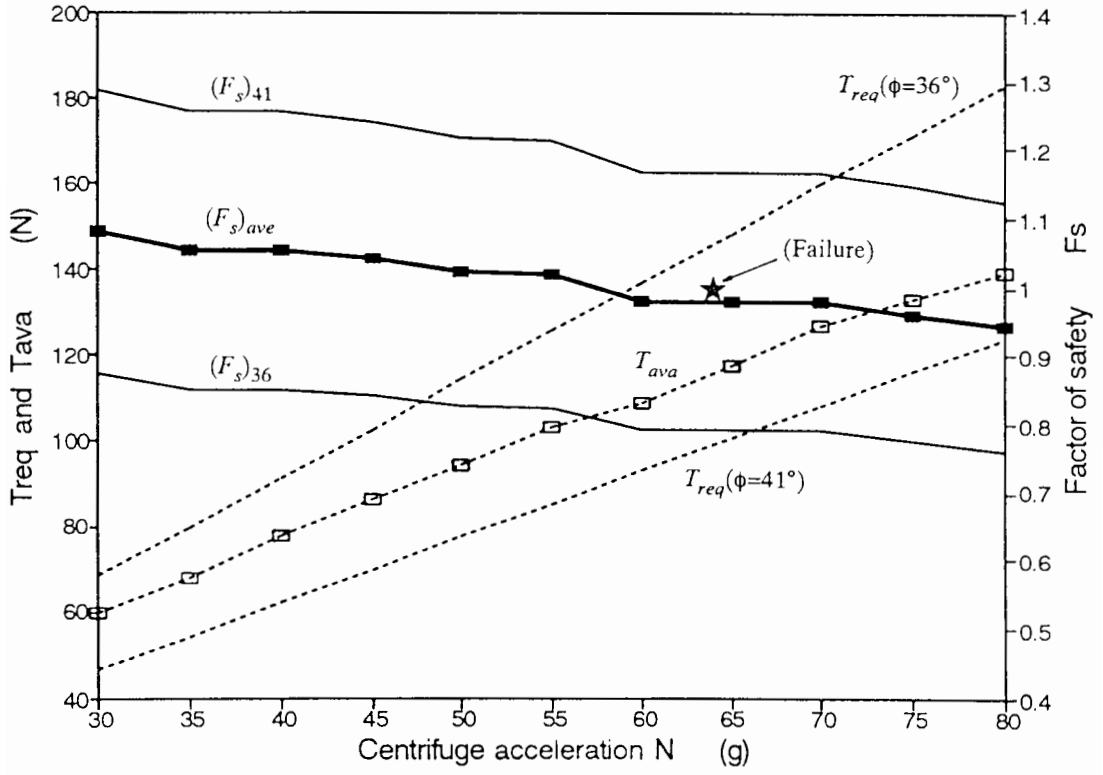

(f) Test A(A')20.0-R-S

Fig.7.10 (c) - Comparison of the total required force T_{req}, total available force T_{ava} and factor of safety F_s

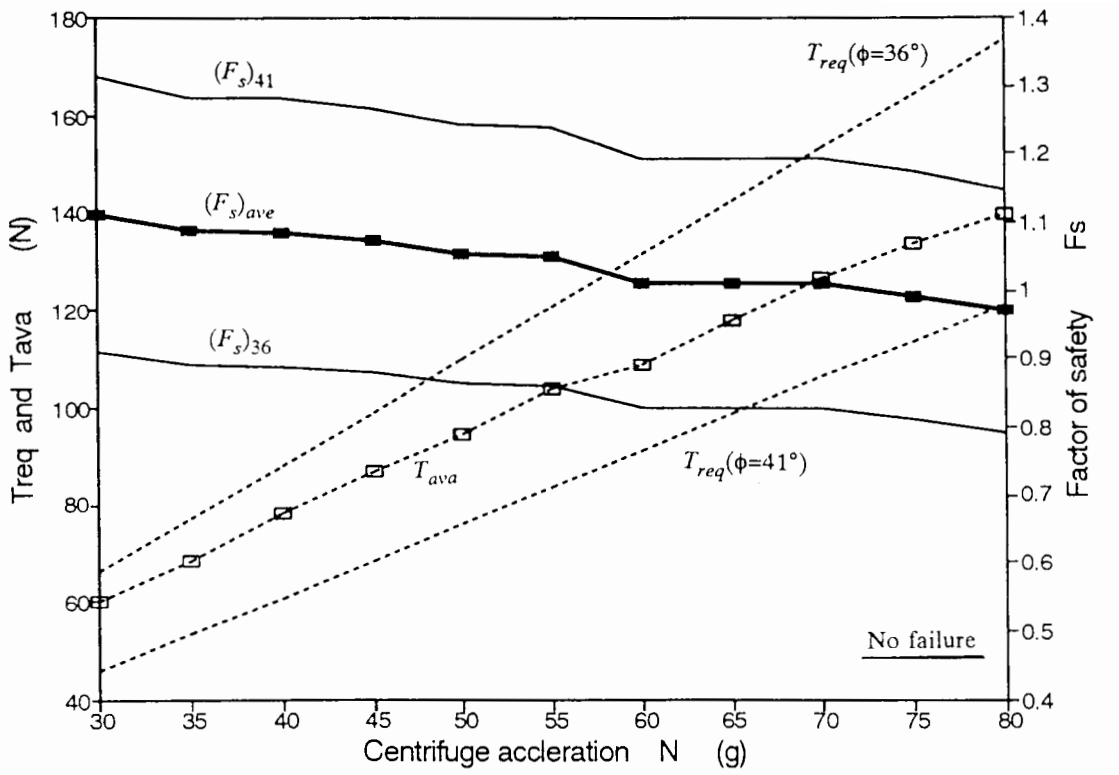

(g) Test A20.0-R(F)-R

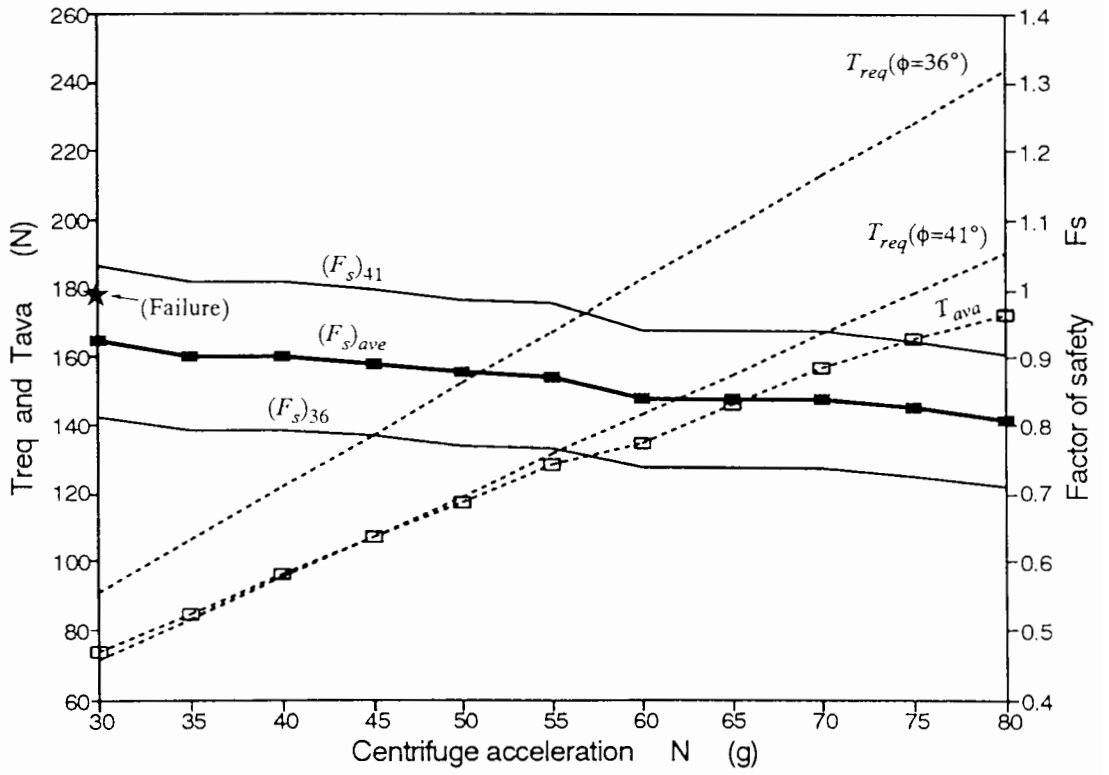

(h) Test V23.0-F-S

Fig.7.10 (d) - Comparison of the total required force T_{req}, total available force T_{ava} and factor of safety F_s

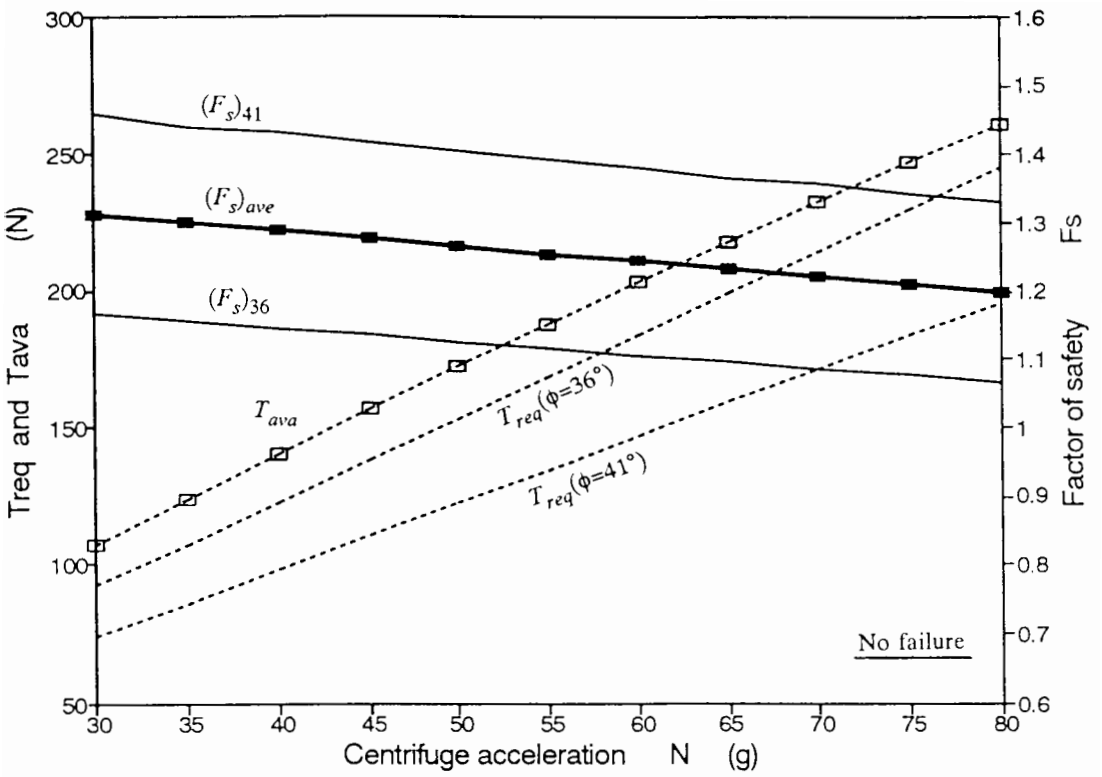

(i) Test V8.5-R-S

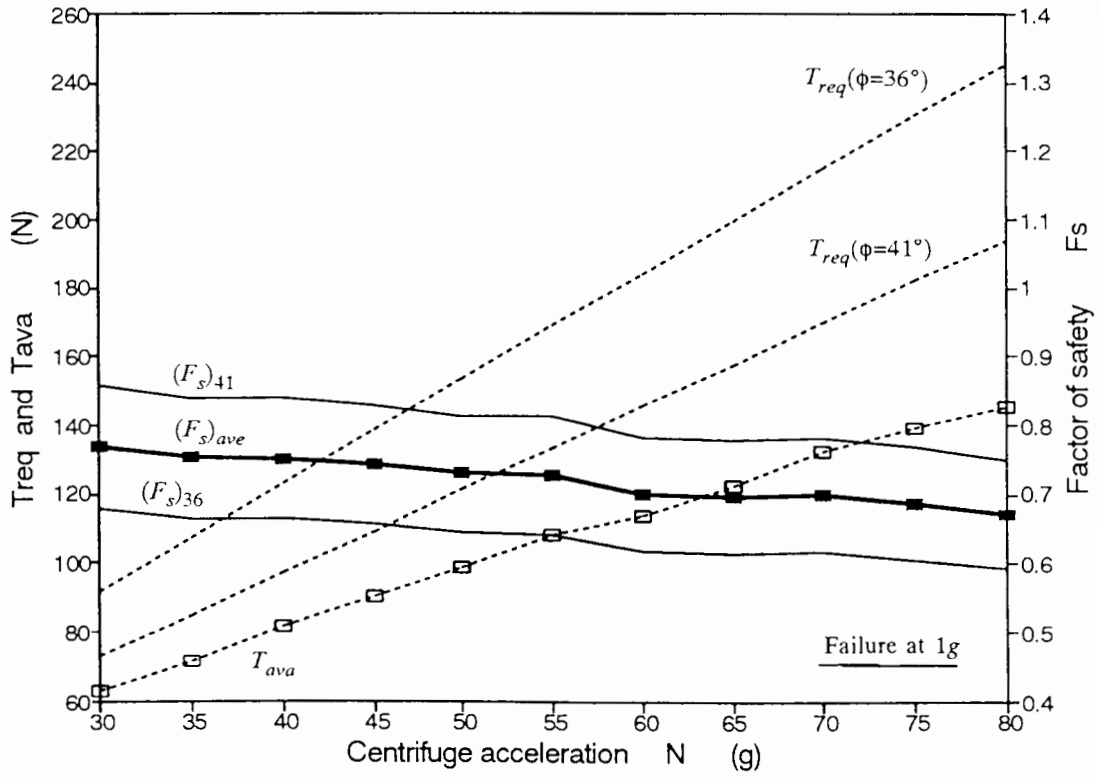

(j) Test V20.0-F-S

Fig.7.10 (e) - Comparison of the total required force T_{req}, total available force T_{ava} and factor of safety F_s

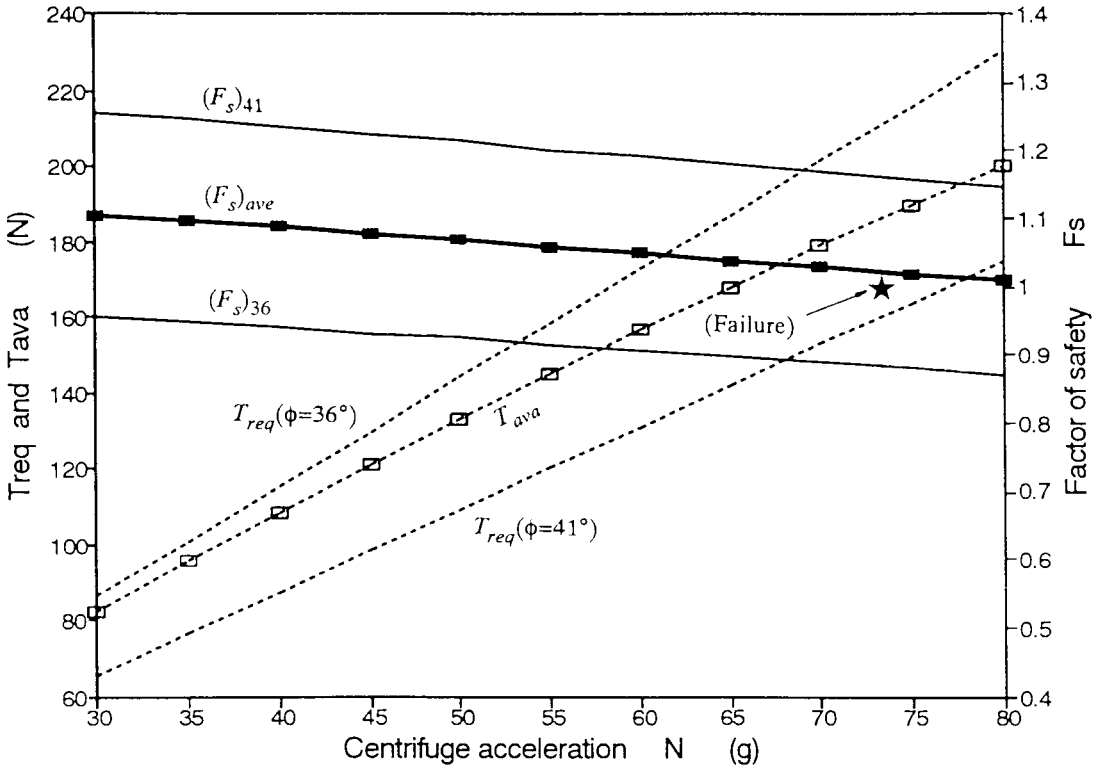

(k) Test V8.0-R(F)-R

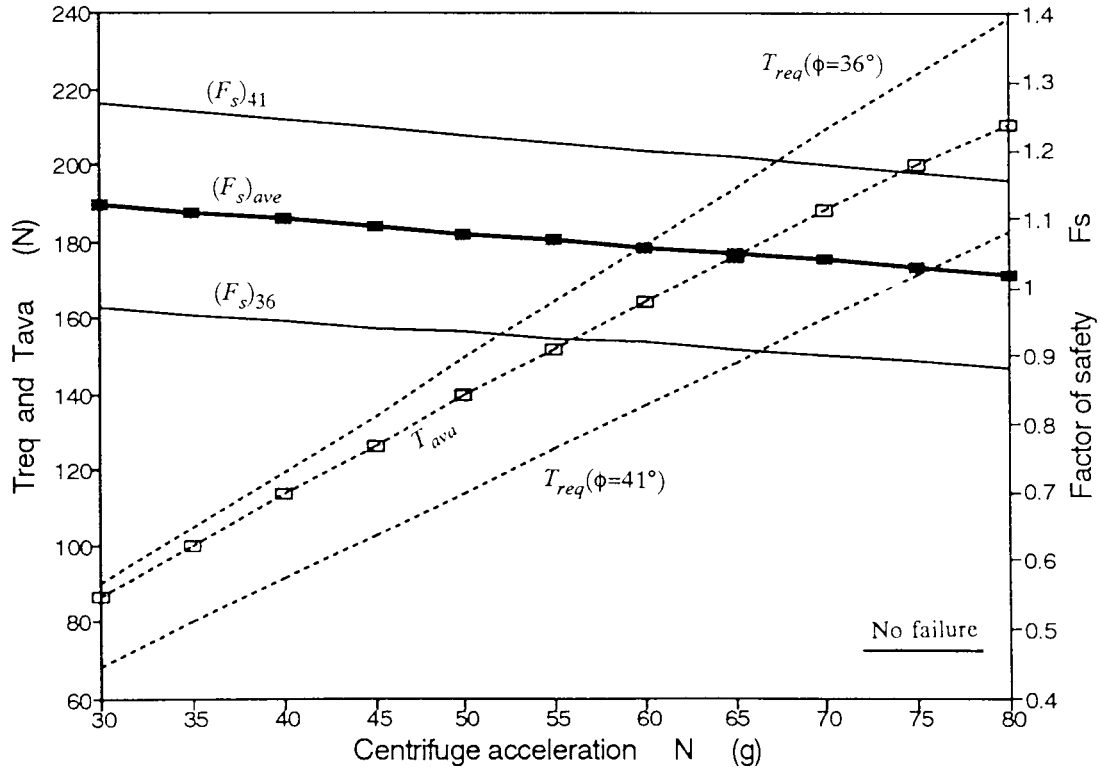

(l) V8.0-R(F)-S

Fig.7.10 (f) - Comparison of the total required force T_{req}, total available force T_{ava} and factor of safety F_s

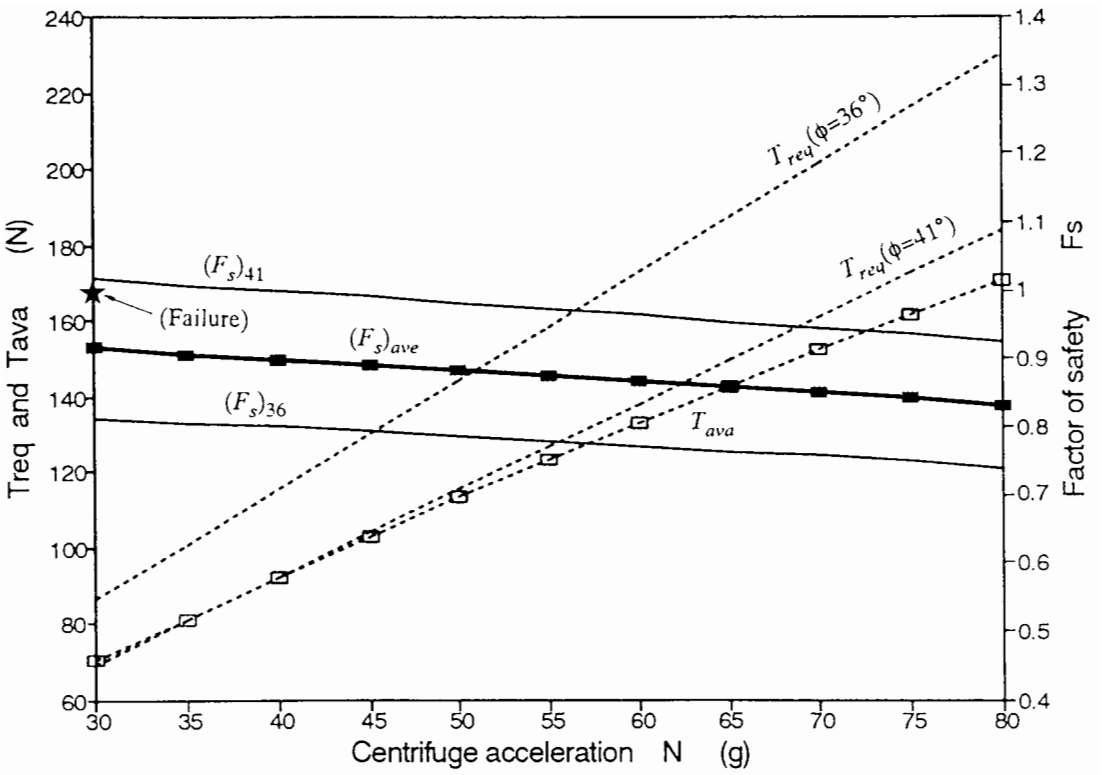

(m) Test V7.0-R-R

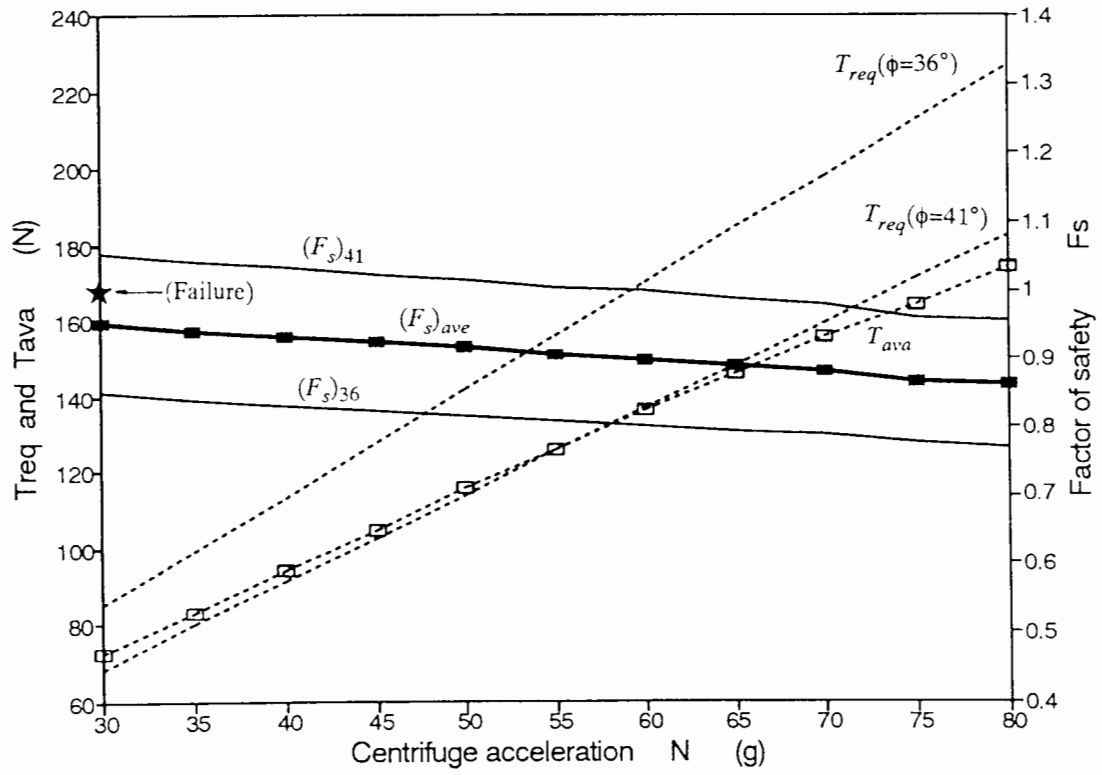

(n) Test V(V')7.0-F-R

Fig.7.10 (g) - Comparison of the total required force T_{req}, total available force T_{ava} and factor of safety F_s

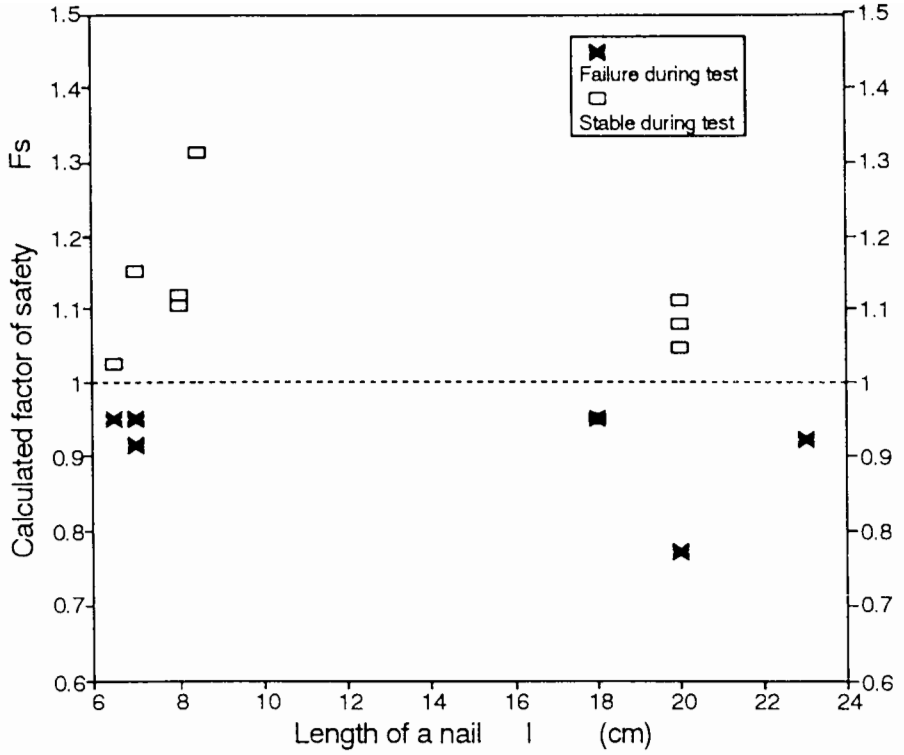

(a) N=30g acceleration

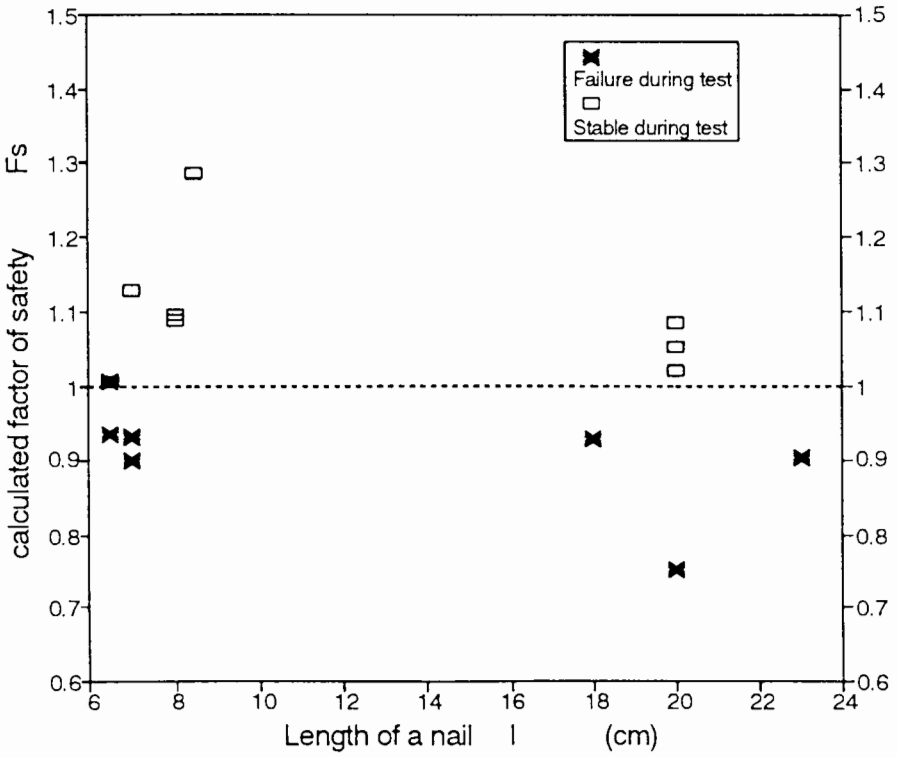

(b) N=40g acceleration

Fig.7.11 - Average factor of safety $(F_s)_{ave}$ and results of the centrifuge tests

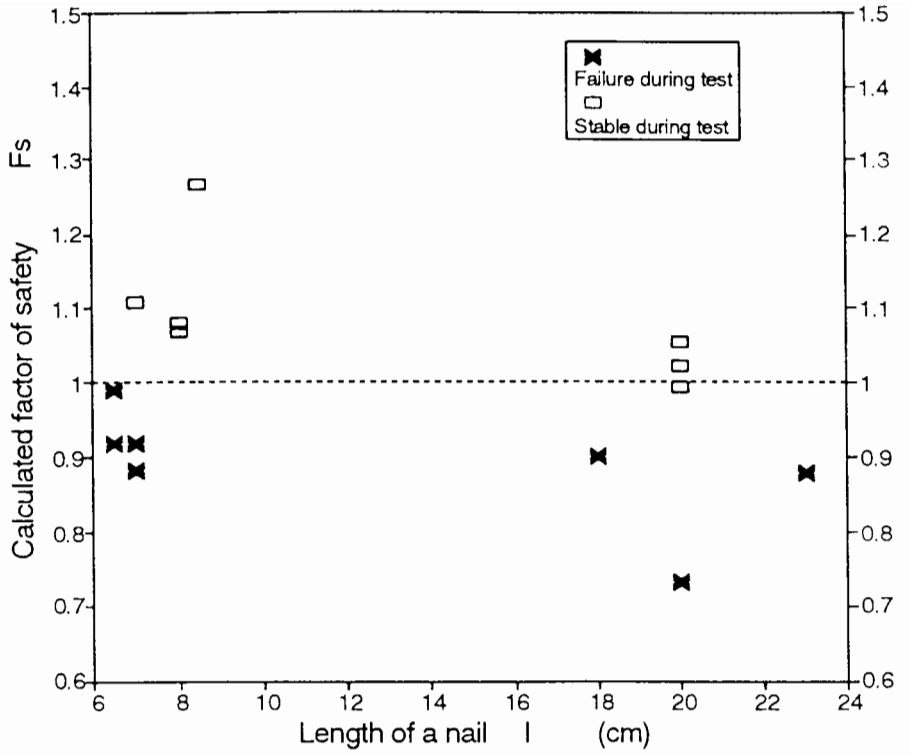

(c) N=50g acceleration

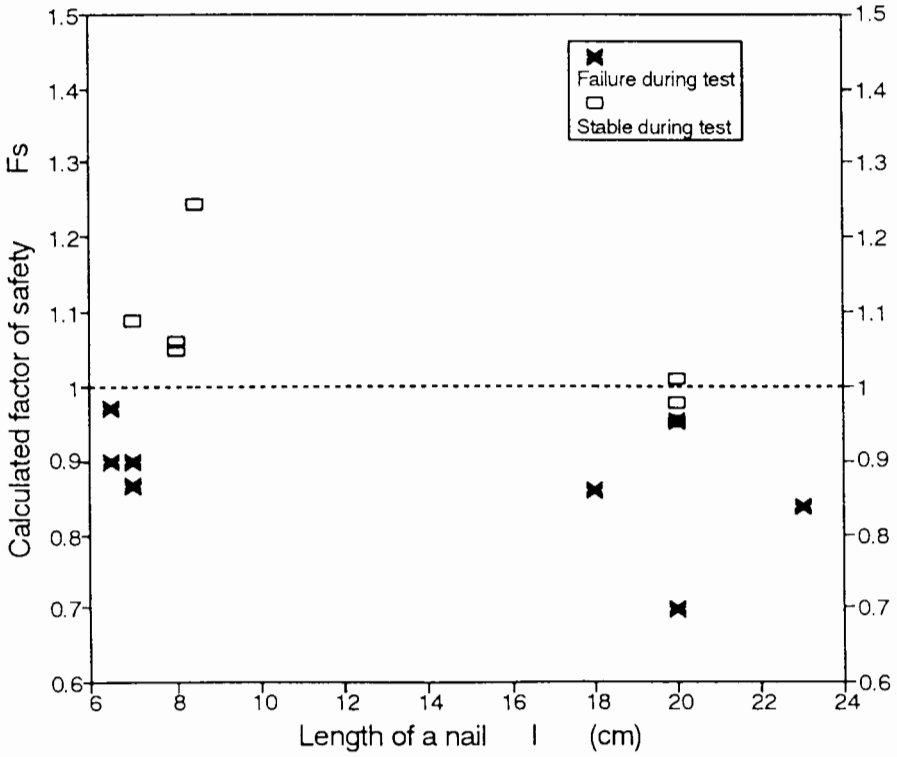

(e) N=60g acceleration

Fig.7.11 - Average factor of safety $(F_s)_{ave}$ and results of the centrifuge tests

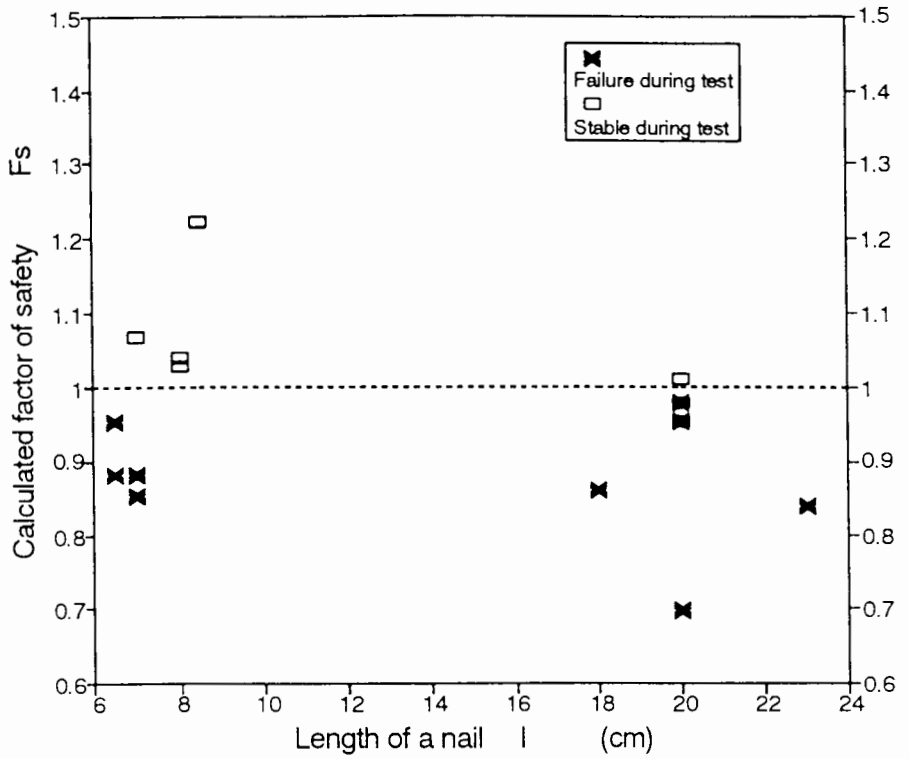

(f) N=70g acceleration

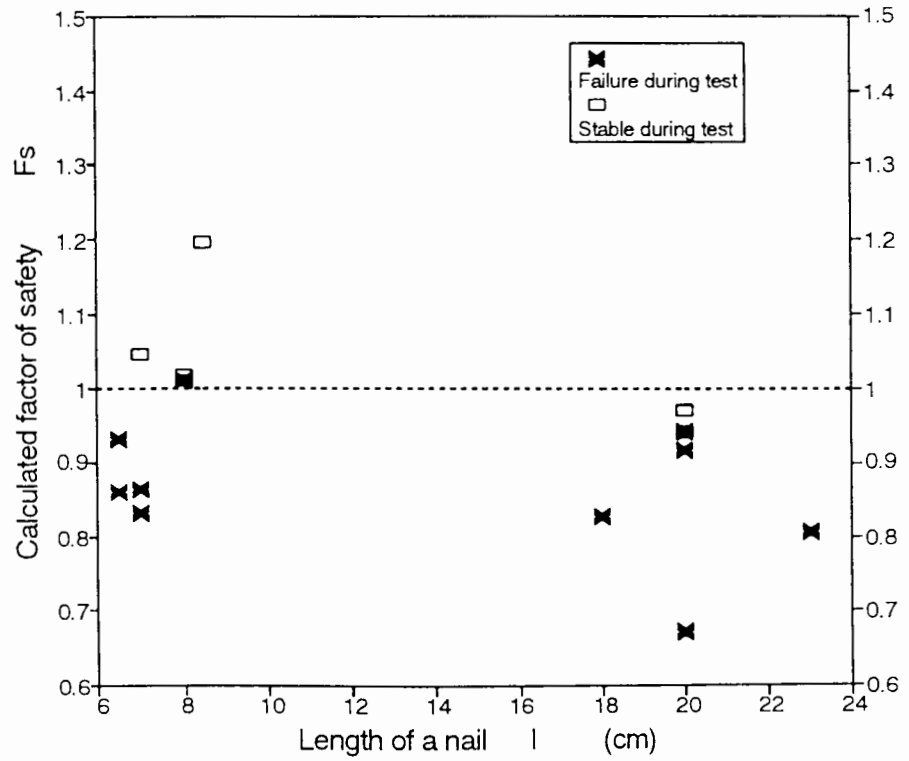

(g) N=80g acceleration

Fig.7.11 - Average factor of safety $(F_s)_{ave}$ and results of the centrifuge tests

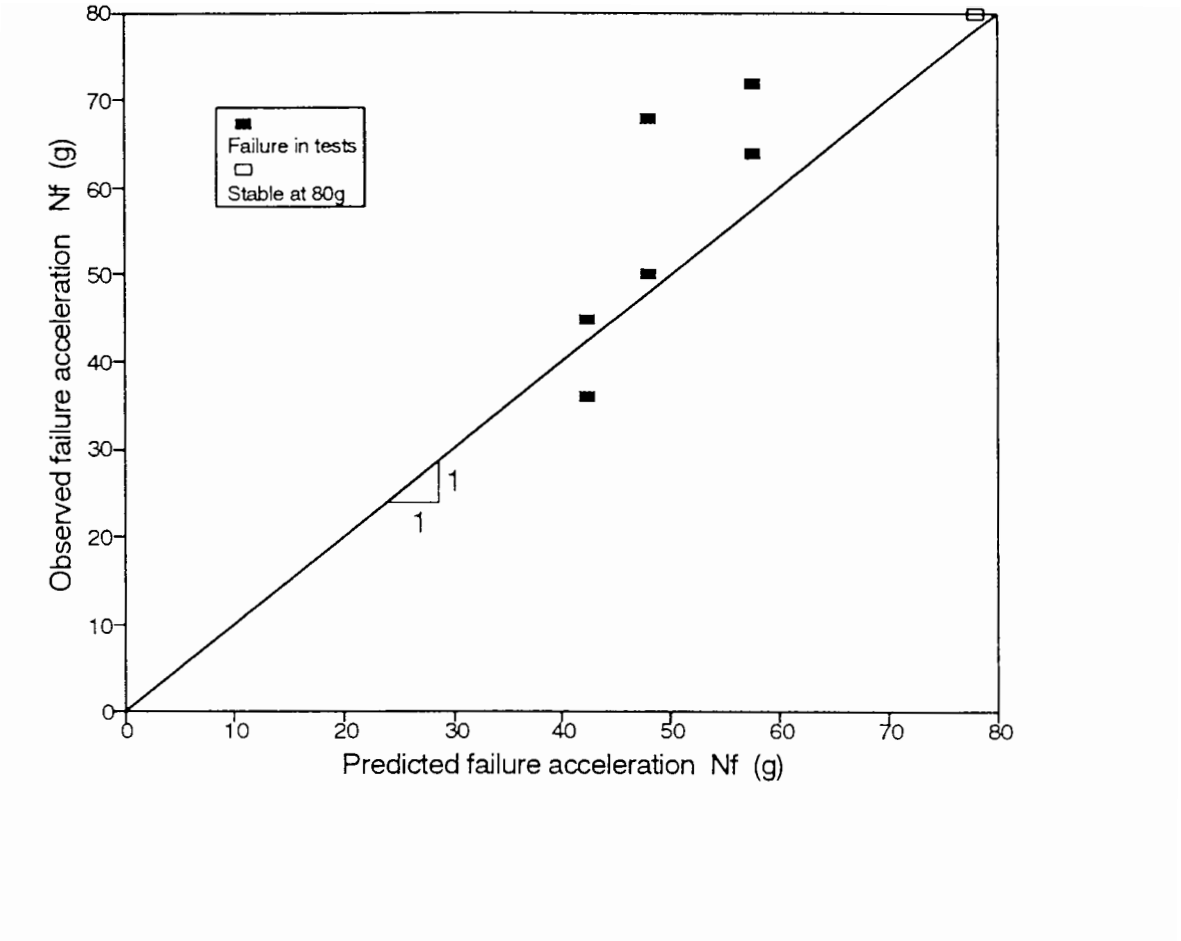

Fig.7.12 - Comparison of the failure accelerations N_f between the analysis and tests

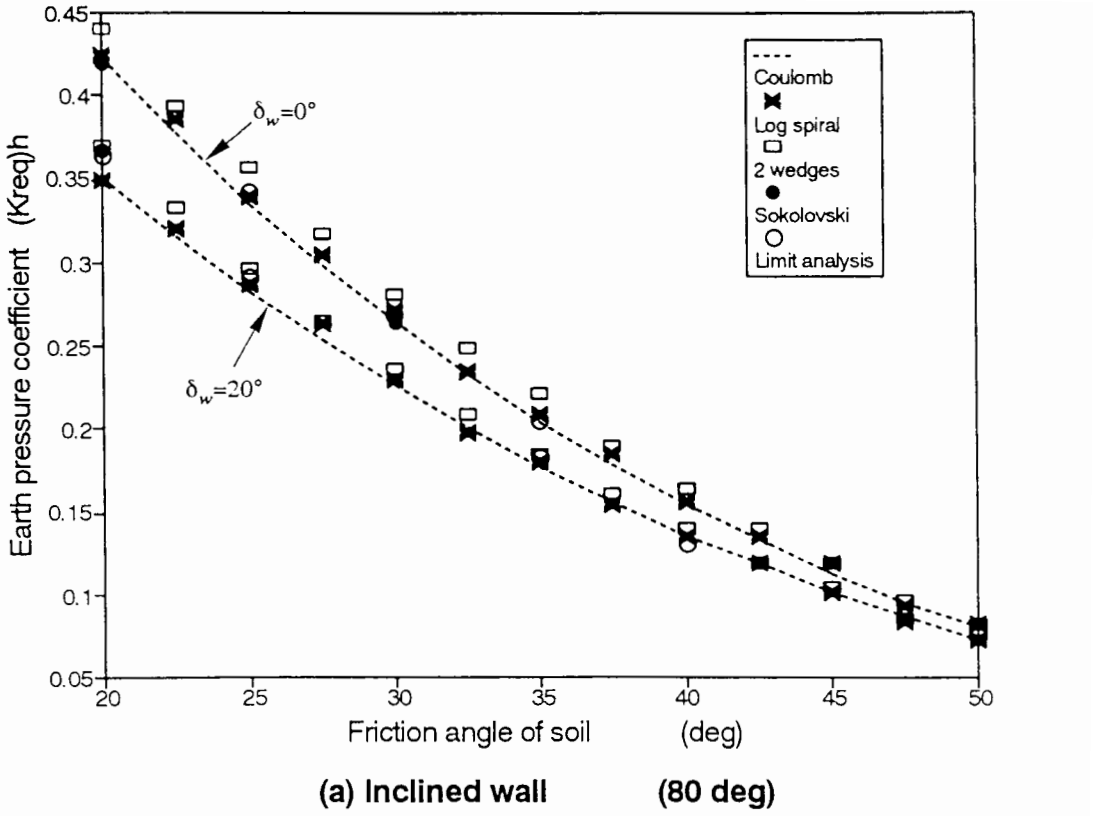

Fig.7.13 (a) - Comparison of the earth pressure coefficients $(K_{req})_h$ (Inclined wall β=80°)

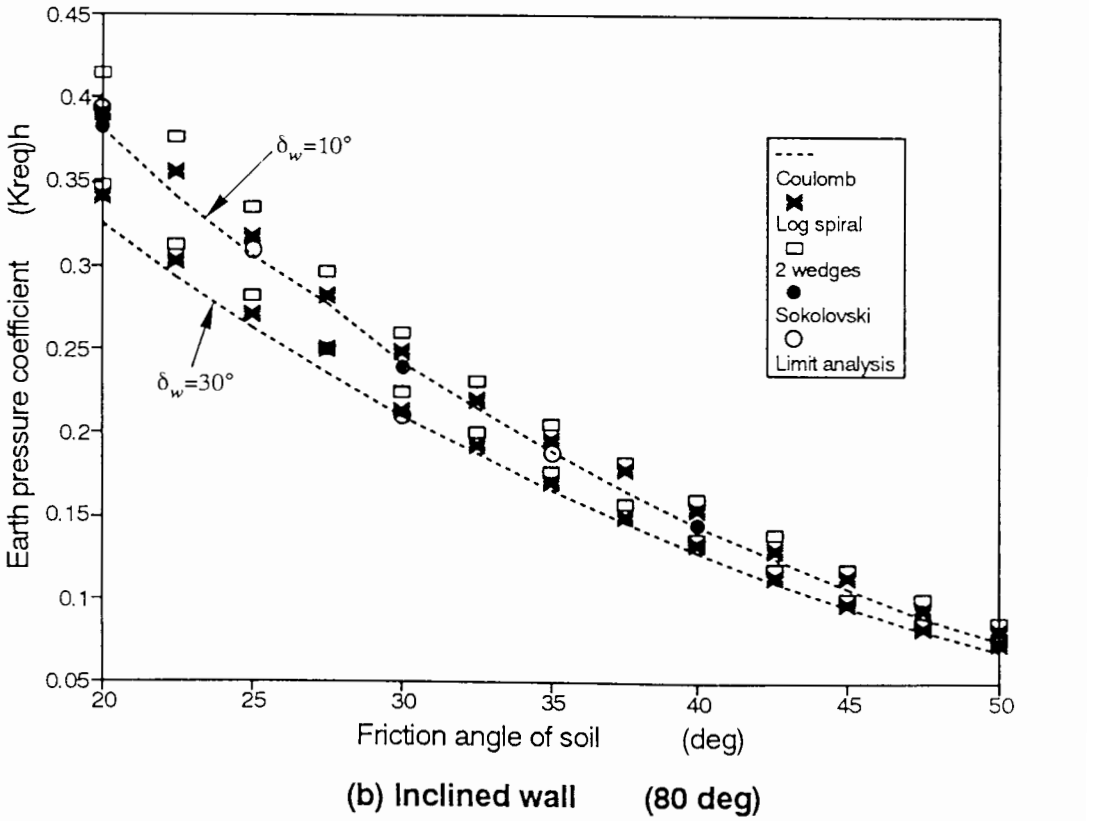

Fig.7.13 (b) - Comparison of the earth pressure coefficients $(K_{req})_h$ (Inclined wall β=80°)

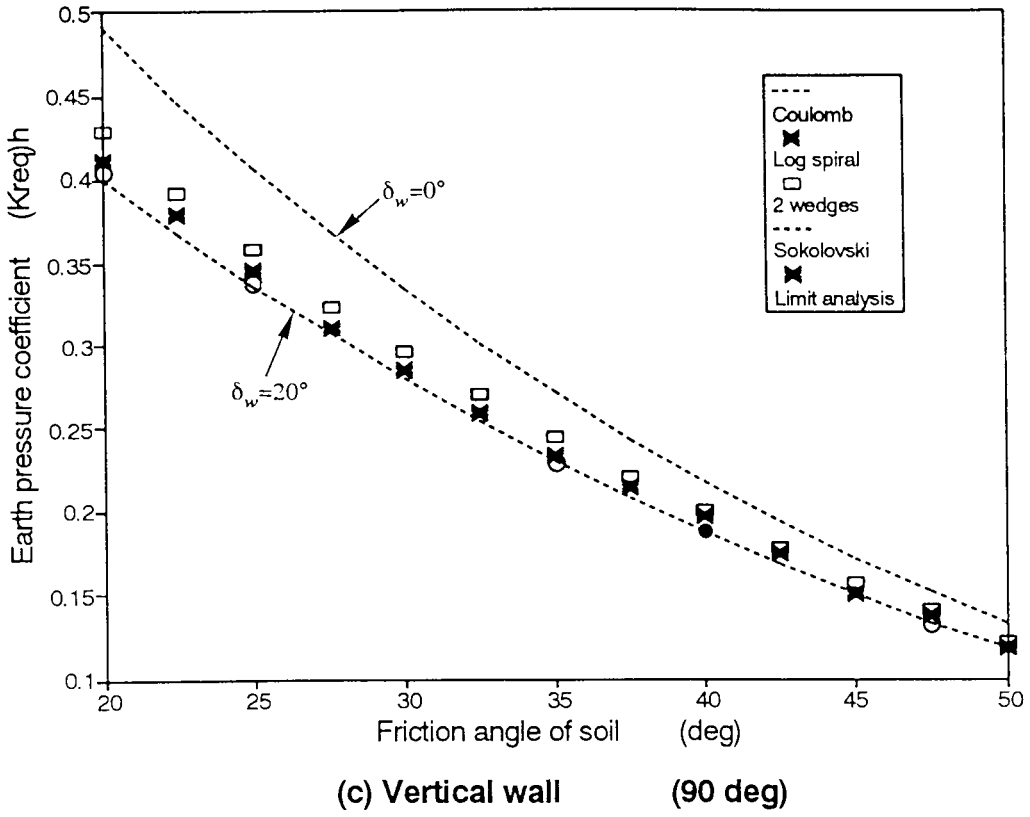

(c) Vertical wall (90 deg)

Fig.7.13 (c) - Comparison of the earth pressure coefficients $(K_{req})_h$ (Vertical wall β=90°)

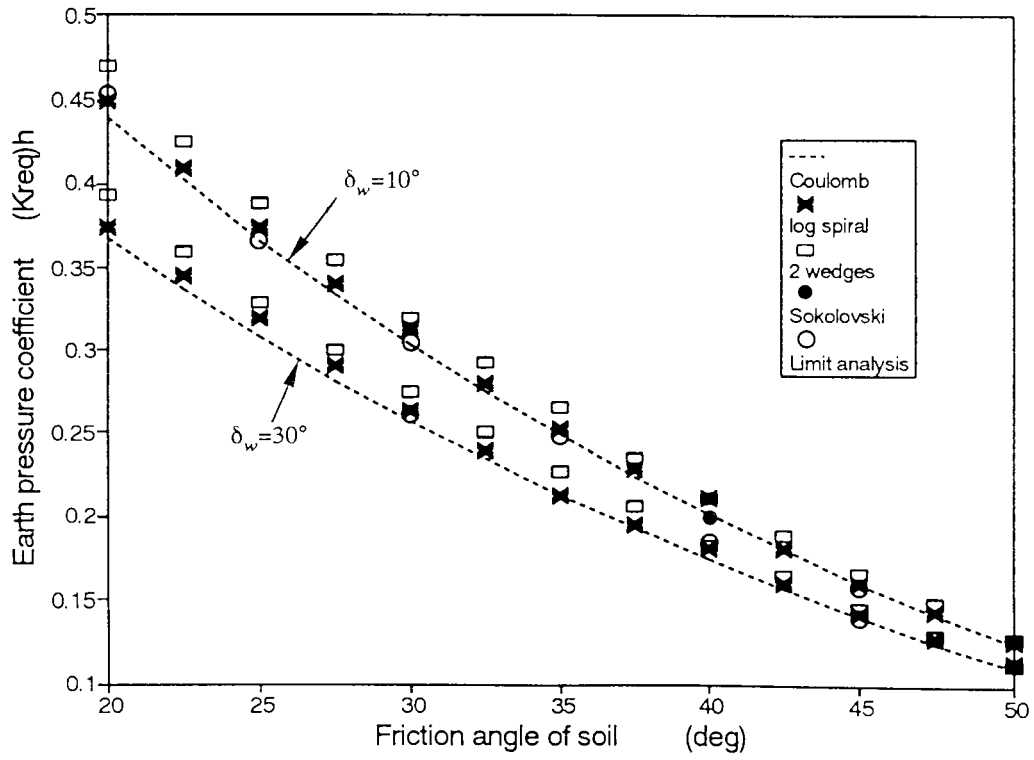

(d) Vertical wall (90 deg)

Fig.7.13 (d) - Comparison of the earth pressure coefficients $(K_{req})_h$ (Vertical wall β=90°)

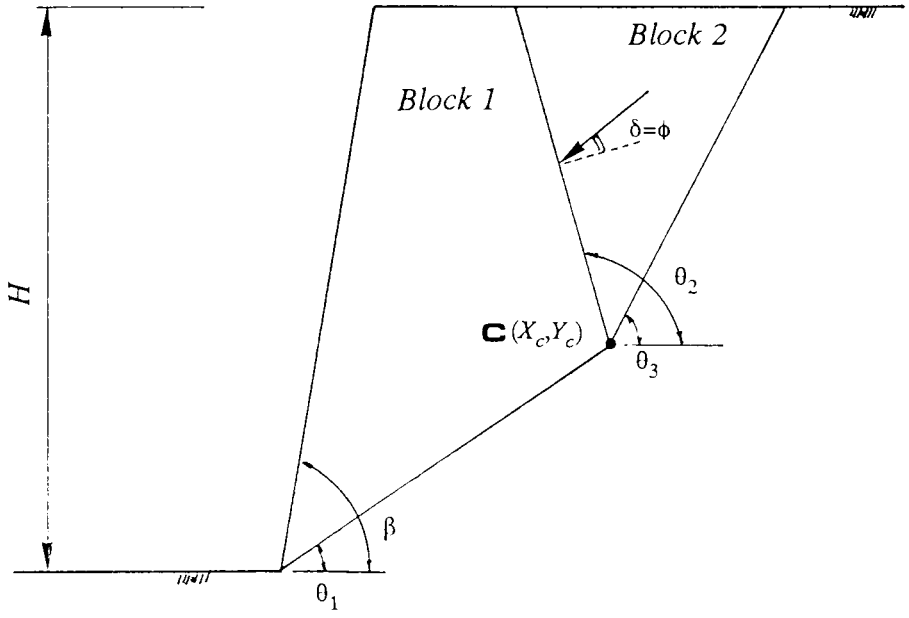

Fig.7.14 - Two part wedge analysis in nailed slope

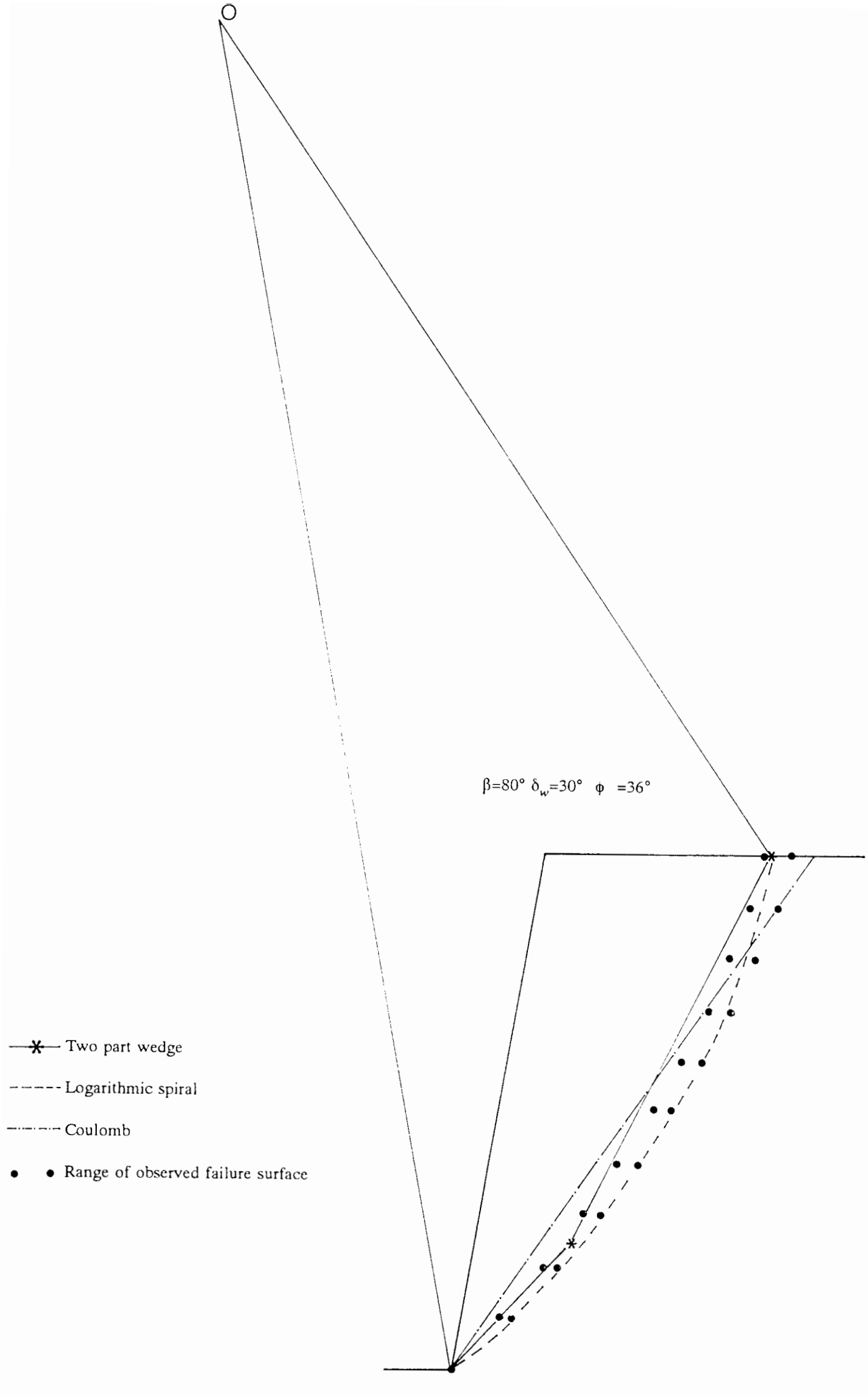

Fig.7.15 (a) - Comparisons of the failure surfaces between analyses and tests

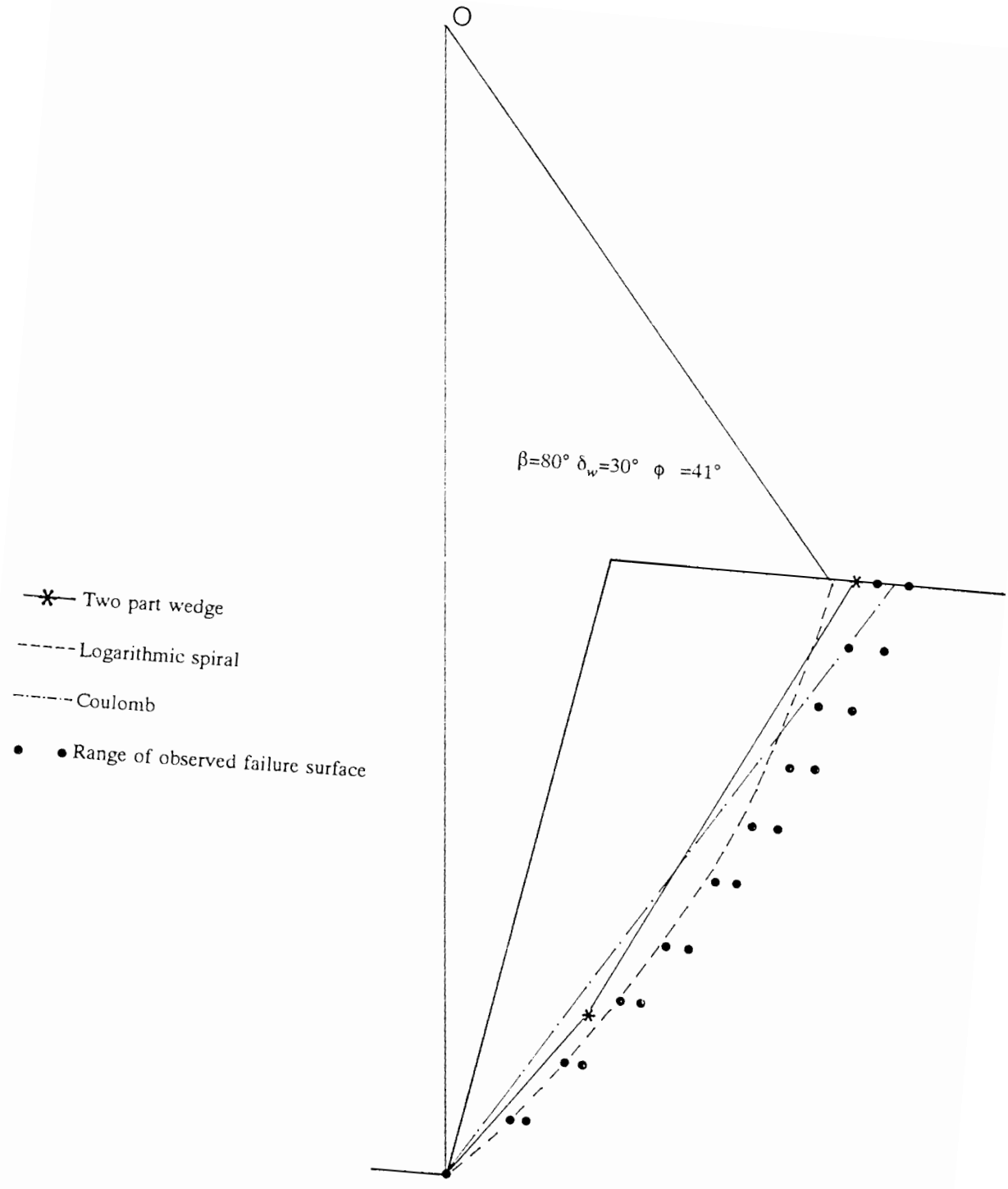

Fig.7.15 (b) - Comparisons of the failure surfaces between analyses and tests

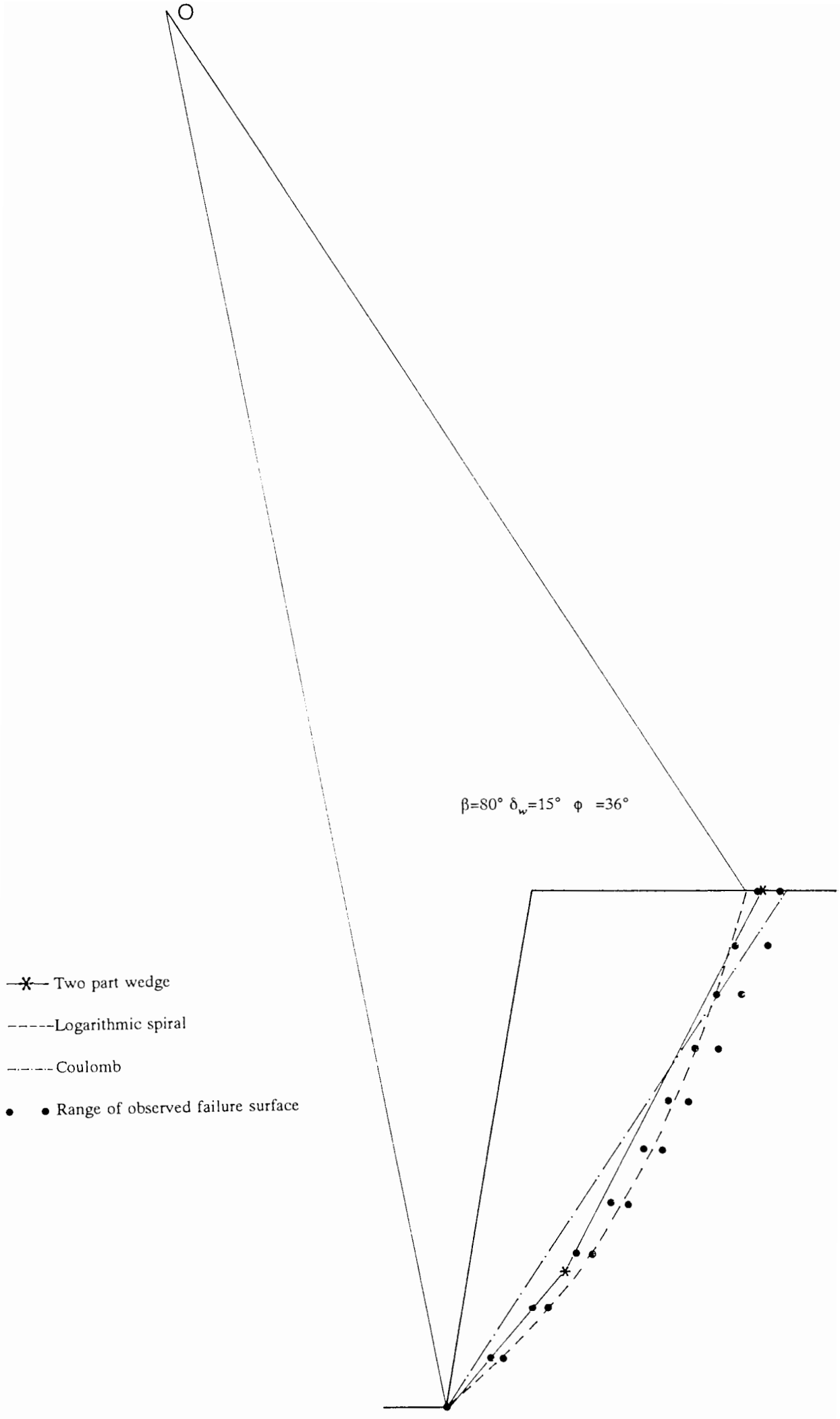

Fig.7.15 (c) - Comparisons of the failure surfaces between analyses and tests

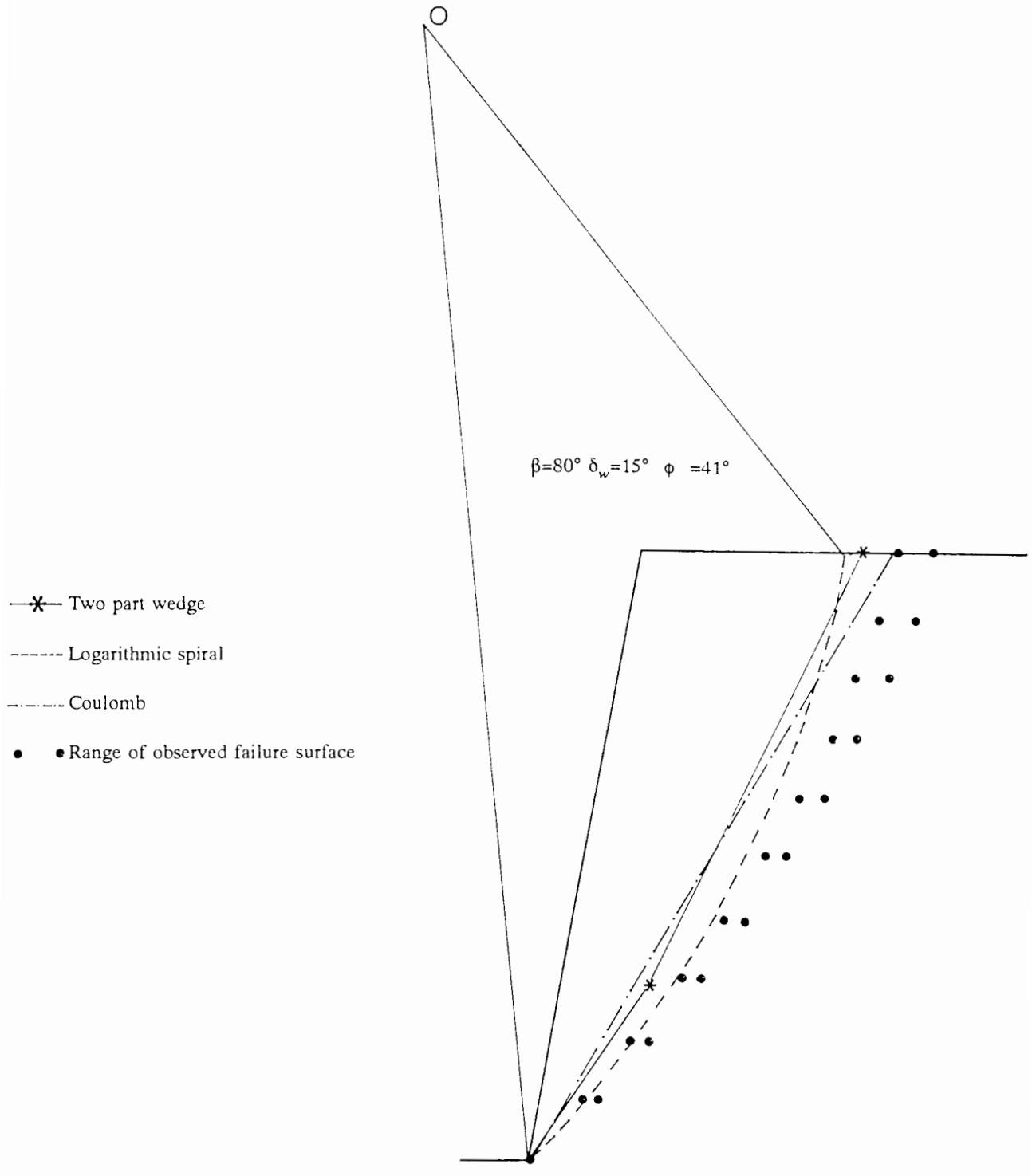

Fig.7.15 (d) - Comparisons of the failure surfaces between analyses and tests

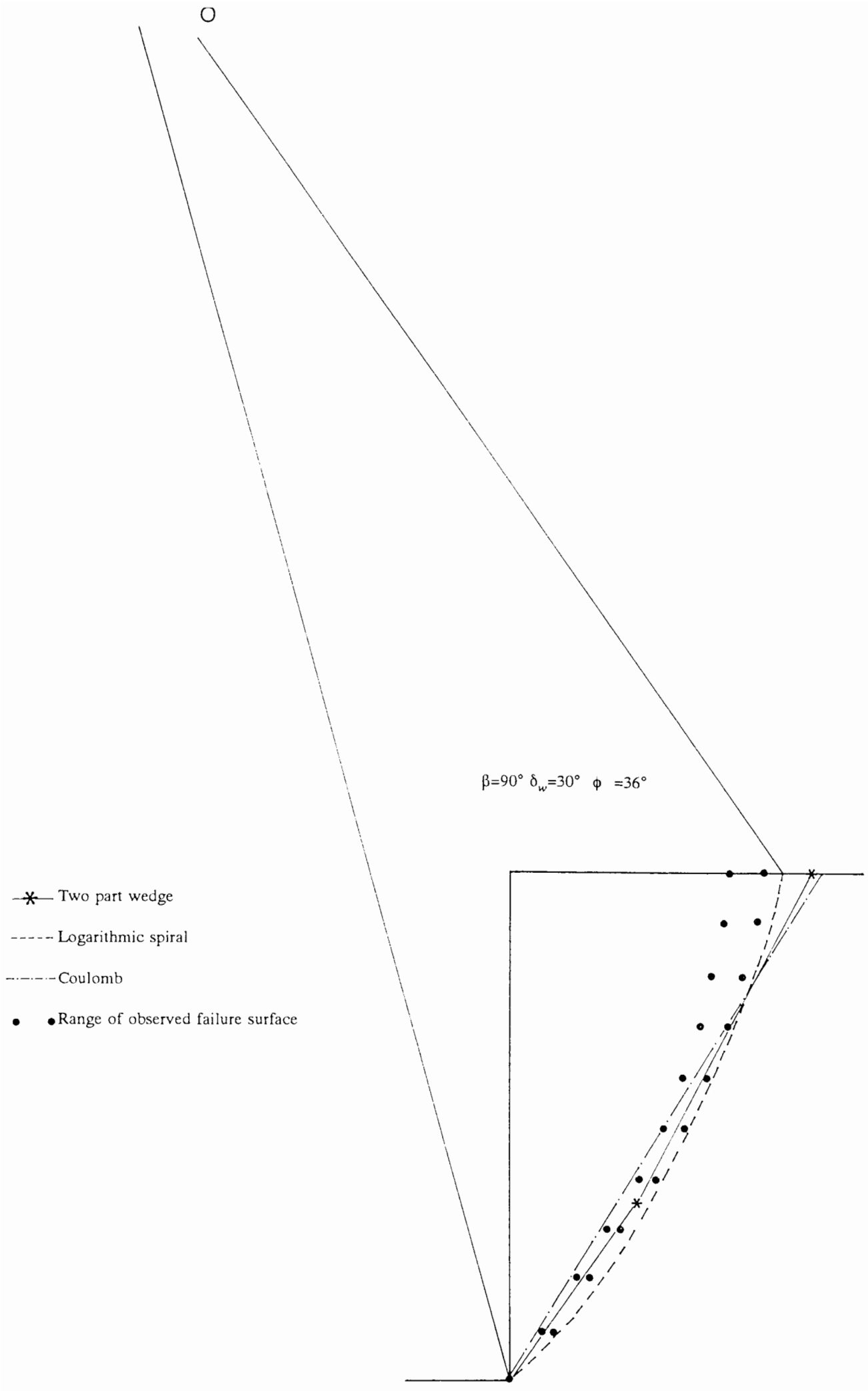

Fig.7.15 (e) - Comparisons of the failure surfaces between analyses and tests

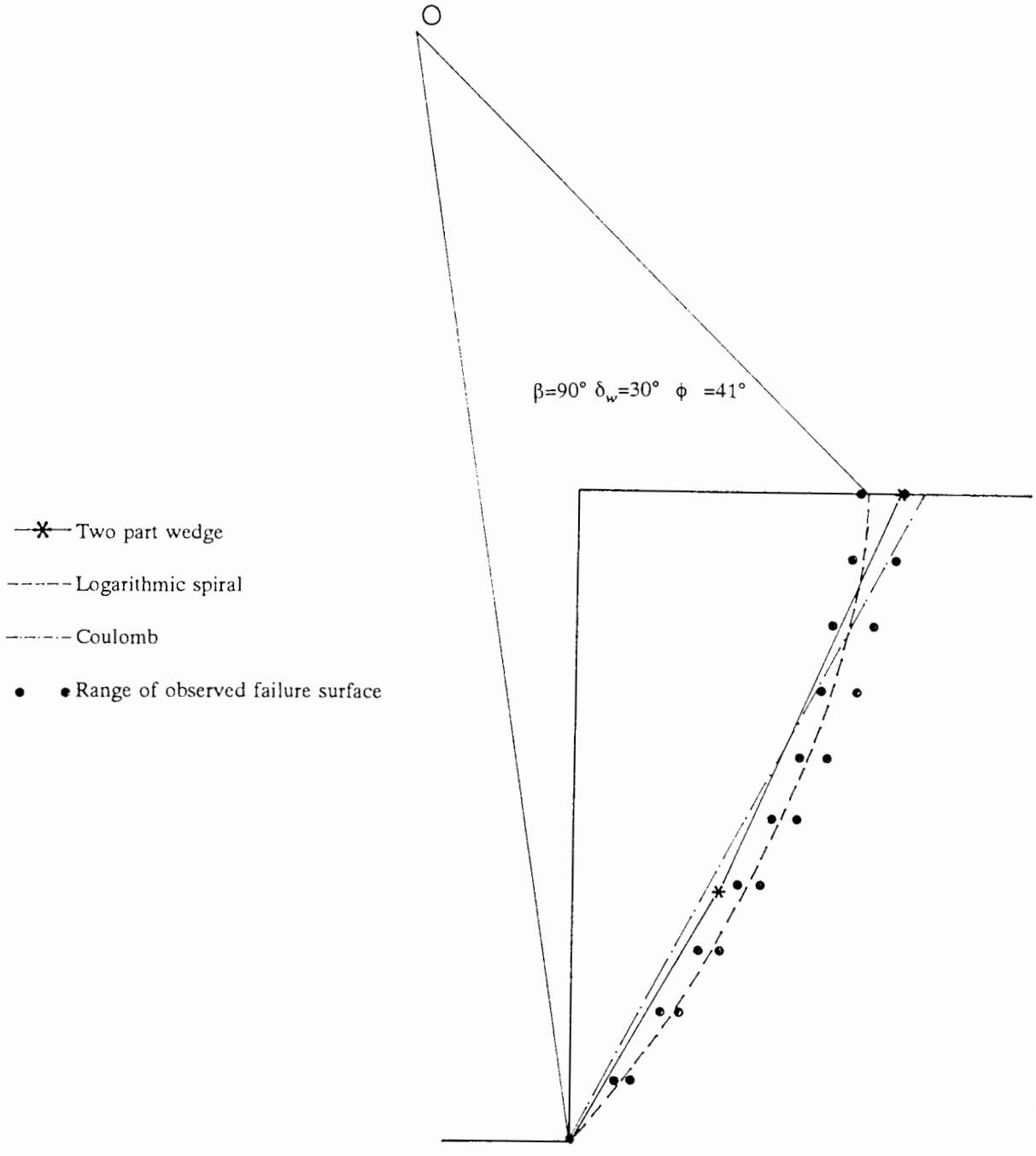

Fig.7.15 (f) - Comparisons of the failure surfaces between analyses and tests

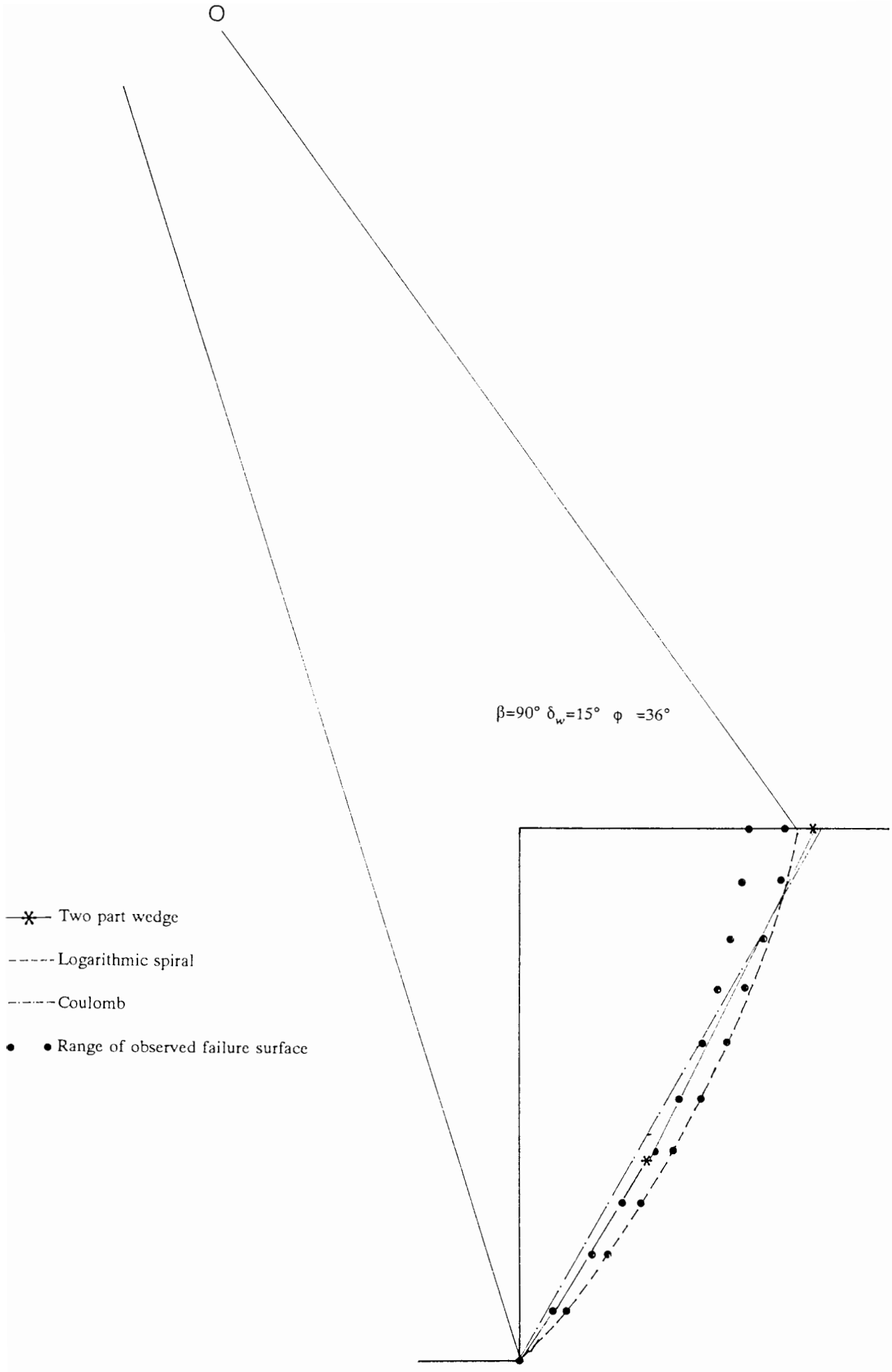

Fig.7.15 (g) - Comparisons of the failure surfaces between analyses and tests

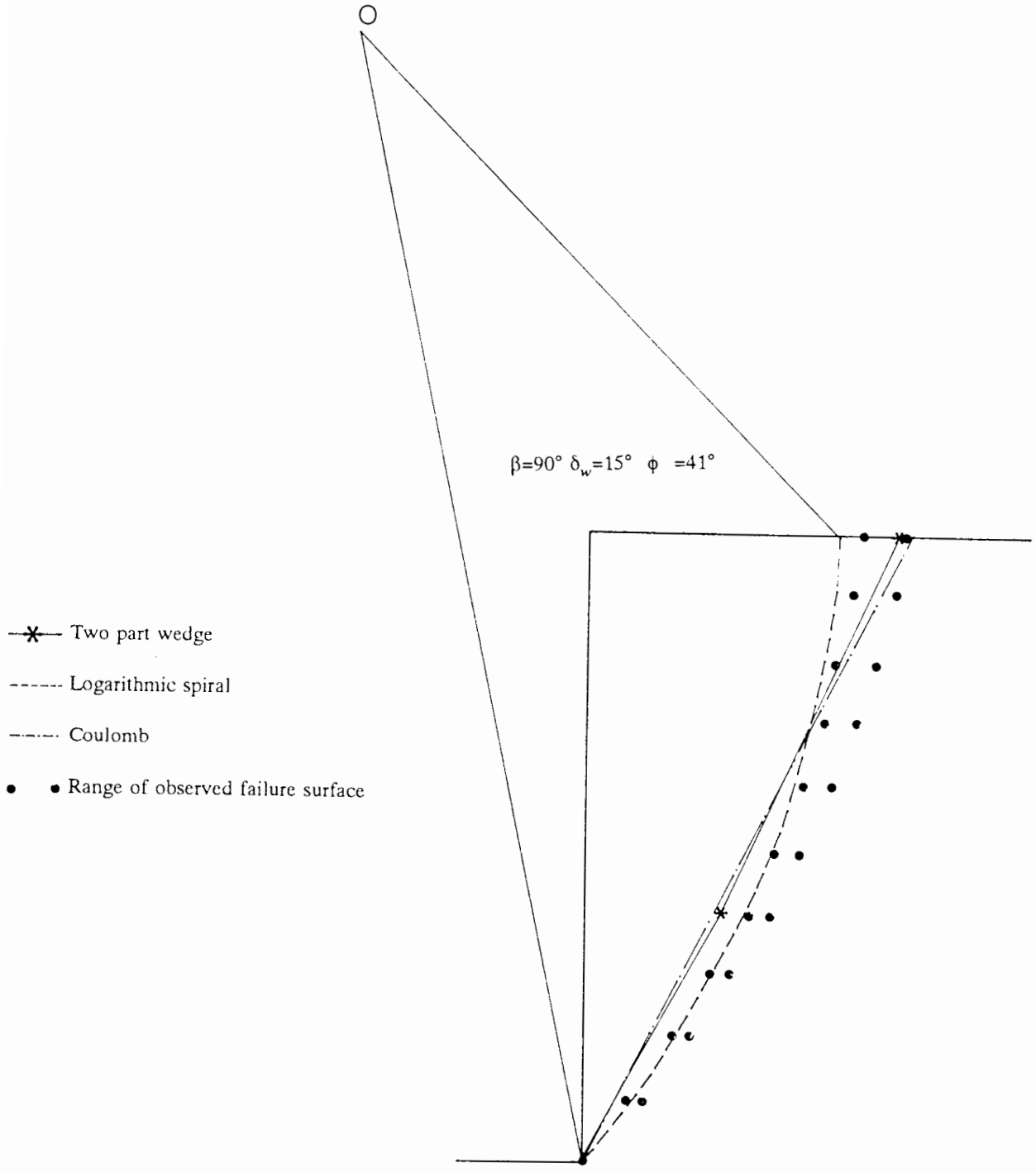

Fig.7.15 (h) - Comparisons of the failure surfaces between analyses and tests

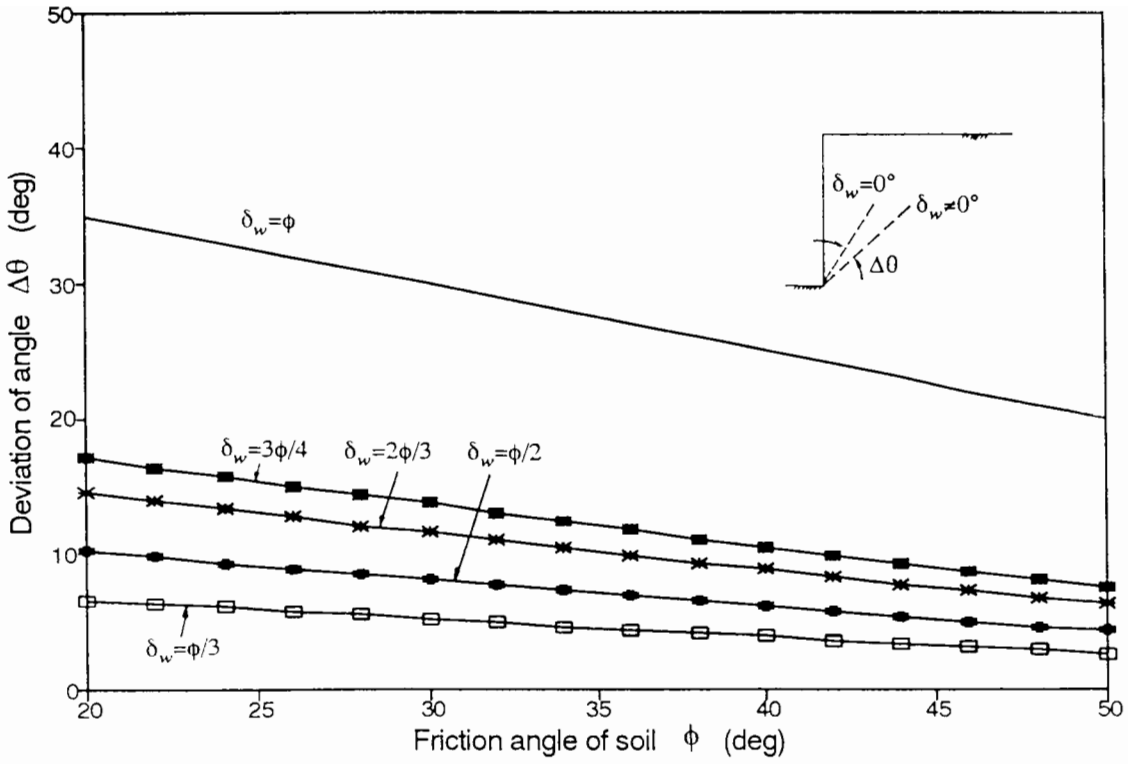

Fig.7.16 - Influence of wall friction δ_w on the direction of failure surface

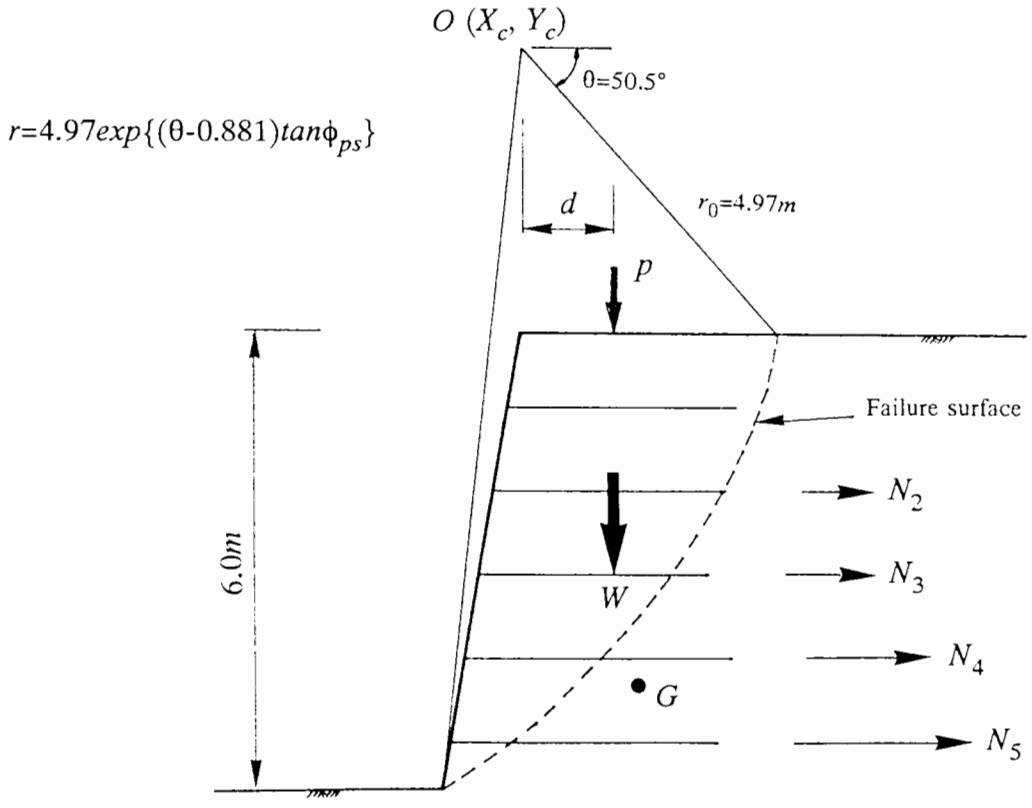

Fig.7.17 - Observed failure surface in the prototype test fitted by a logarithmic spiral